KU LEUVEN

ARENBERG DOCTORAL SCHOOL
Faculty of Engineering Science

Distributed Signal Processing Algorithms for Sensor and Actuator Networks

Applied to Wireless Acoustic Sensor and Actuator Networks and Cell-free Massive MIMO Systems

Robbe Van Rompaey

Supervisor:
Prof. dr. ir. M. Moonen

Dissertation presented in partial fulfillment of the requirements for the degree of Doctor of Engineering Science (PhD): Electrical Engineering

December 2022

Distributed Signal Processing Algorithms for Sensor and Actuator Networks

Applied to Wireless Acoustic Sensor and Actuator Networks and Cell-free Massive MIMO Systems

Robbe VAN ROMPAEY

Examination committee:
Prof. dr. ir. P. Moldenaers, chair
Prof. dr. ir. M. Moonen, supervisor
Prof. dr. ir. A. Bertrand
Prof. dr. ir. P. Patrinos
Prof. dr. ir. S. Pollin
Prof. dr. ir. G. Leus
(TU Delft)
Prof. dr. ir. G. Piñero
(UPV)

Dissertation presented in partial fulfillment of the requirements for the degree of Doctor of Engineering Science (PhD): Electrical Engineering

December 2022

© 2022 KU Leuven – Faculty of Engineering Science
Uitgegeven in eigen beheer, Robbe Van Rompaey, Kasteelpark Arenberg 10, bus 2446, B-3001 Leuven (Belgium)

Alle rechten voorbehouden. Niets uit deze uitgave mag worden vermenigvuldigd en/of openbaar gemaakt worden door middel van druk, fotokopie, microfilm, elektronisch of op welke andere wijze ook zonder voorafgaande schriftelijke toestemming van de uitgever.

All rights reserved. No part of the publication may be reproduced in any form by print, photoprint, microfilm, electronic or any other means without written permission from the publisher.

Preface

In de eerste maanden van mijn doctoraat gaf mijn toenmalige bureaugenoot me een zeer goede raad over het verloop van een doctoraat. In het begin lijkt het alsof je maar wat willekeurige resultaten bekomt, terwijl het verband ertussen ver te zoeken is. Als je echter lang genoeg doorgaat en niet opgeeft, zal later alles in zijn plooi vallen en zullen de connecties tussen alle resultaten duidelijk worden. Vanaf dan komt de rest van het onderzoek vanzelf. Nu, ongeveer vijf jaar later kan ik dit alleen maar bevestigen, met dit proefschrift als finale resultaat. Dit proefschrift was er nooit alleen gekomen, dus dit is het uitgerekende moment om alle volgende personen te bedanken.

Eerst en vooral wil ik mijn promotor Prof. Marc Moonen ten zeerste bedanken voor alles. Als professor heeft hij mij geïntroduceerd in de wondere wereld van de digitale signaalverwerking en wist me dan ook te overtuigen om in 2017 te starten met dit wiskundige avontuur. Zijn wetenschappelijke bijdragen aan de hoofdstukken in dit proefschrift en zijn uitgebreide reviews zijn uiteraard onovertrefbaar. Als promotor gaf hij me zeer veel vrijheid om te onderzoeken wat ik wou, maar wist hij me ook altijd nieuwe ideeën toe te reiken als ik vast zat of nood had aan variatie. Ik kwam altijd met een goed gevoel buiten na gezamenlijke meetings en de fles wijn die hij me gaf na een lange reviewperiode zal me zeker smaken en me met plezier doen terugdenken aan mijn doctoraatsperiode.

Naast mijn promotor wil ik alle leden van de examencommissie bedanken: Prof. Alexander Bertrand, Prof. Panos Patrinos, Prof. Sofie Pollin, Prof. Geert Leus, Prof. Gema Piñero and Prof. Paula Moldenaers. Dit voor hun tijd om mijn manuscript te lezen, hun waardevolle opmerkingen en suggesties en hun inspanningen om deel te nemen aan mijn doctoraatsverdedigingen. Ook dank aan Prof. Hugo Van hamme voor zijn aanwezigheid in mijn begeleidingscommissie.

An indispensable part of a Ph.D. are, of course, all the past and current colleagues sharing the same interest in signal processing. Therefore, I would like to thank

all the colleagues that already left the DSP group: Amin, Duowei, Fernando, Filippos, Giacomo, Giuliano, Hanne, Jeroen, Mina, Niccoló, Taewoong and Wouter, as well as all current colleagues: Aldona, Arina, Arnout, Bilgesu, Bram, Brent, Cem, Elisa, Hannes, Jesper, Julian, Kathy, Martin, Matthias, Milan, Mohit, Paul, Pourya, Randy, Rich, Santiago, Stefano, Thomas, Toon and Valerio. Thank you for all the nice (sometimes scientific) discussions in the office and around the coffee machine. Mohit and Elisa, a special thanks for hosting all the amazing BBQs (that I was able to join at least). Also Marc and Toon, I don't know how you do it, but you always manage to hire really nice and smart people, so keep this winning streak going! Also thanks for organizing all the original DSP-activities, like curling and the walk through Lier/Nijlen, which Anke and I enjoyed a lot.

Ook mijn toekomstige collega's bij Nokia Bell Labs (Wouter, Paschalis, Werner, ...), wil ik zeer graag bedanken voor de boeiende meetings tijdens het laatste deel van mijn doctoraat. Dit zorgde voor een fijne afwisseling om deze laatste periode goed door te komen. Ik kijk er naar uit om bij jullie te starten in januari.

Ik bedank ook graag al mijn vrienden en (schoon)familieleden voor alle leuke nevenactiviteiten naast het werk: familiefeesten, weekends, sportactiviteiten (o.a. lopen en padellen), etentjes, escape rooms, vakanties, gezelschapsspelavonden, verbouwingen, activiteiten en vergaderingen van ZeRo Skip, ... Deze gaven me telkens weer energie en terug zin om door te gaan. Ik voel me echt vereerd om door zo'n warme personen omringd te mogen zijn. In het bijzonder wil ik graag mijn beide ouders bedanken voor alle steun, goede raad en geduld die ze mij gegeven hebben. Nu wordt het mijn job om dit alles over te dragen naar de nieuwe generatie, maar hopelijk nog met veel hulp van al deze personen.

Als laatste, maar ook voornaamste, wil ik graag mijn grote liefde en levenspartner Anke bedanken. Niet alleen heeft ze geholpen bij het nalezen van grote delen van dit proefschrift, ze heeft mij ook altijd gesteund tijdens deze periode en wist me altijd op te beuren (o.a. met haar geweldige hoofdmassages) als het er eens tegen zat. Wij zijn een super goed team, zowel relationeel als professioneel, en ik kijk er echt naar uit om met jou een gezinnetje te vormen vanaf januari 2023!

Tot slot wil ik dit proefschrift opdragen aan al mijn grootouders (levend en overleden), die zeer hard hebben bijgedragen tot de persoon die ik vandaag ben geworden.

Robbe Van Rompaey

Mechelen, December 2022

Abstract

Technological progress in current analogue and digital devices together with the miniaturization of hardware have pushed sensing and actuating devices to new heights. Devices can perform more computationally intensive digital signal processing (DSP) tasks for a similar or even lower power budget and more devices can be placed on the same surface area, enriching DSP algorithms with more inputs/outputs and hence more degrees of freedom. When these devices have to perform a specific DSP task, such as the estimation or generation of a signal of interest, cooperation between devices with different locations can significantly enhance the overall performance, especially in adverse situations. The devices (or nodes) then need to be connected using either wired or wireless connections and form a sensor and actuator network (SAN). Compared to conventional fixed sensor or actuator arrays with a clearly localized position, SANs have access to more spatially distributed sensors and actuators, with more spatial degrees of freedom.

This thesis will focus specifically on estimating and generating signals using the multi-channel Wiener filter (MWF) within both wireless and wired SANs. When wireless connections are favored, e.g., for an ad-hoc placement of the devices, the term wireless sensor and actuator network (WSAN) is often used. Specifically in acoustic applications where the sensors and actuators consist of microphone and loudspeaker arrays respectively, the network is referred to as wireless acoustic sensor and actuator network (WASAN). However, when wired connections are already in place as is the case for cell-free massive multiple input multiple output (CFmMIMO) systems where a wired SAN can be formed using the fronthaul connections between access points (APs) with up to 100 antennas in currently deployed mobile networks, wired connections should be used. Both applications require high processing rates for sampling, processing and transmission, compared to traditional low-rate SANs. It is therefore critical to develop efficient algorithms under which these nodes can cooperate and enhance their estimation/generation tasks, under tight bandwidth, complexity and energy constraints.

Although aggregating and processing all uncompressed signals and parameters in one place (e.g., in a fusion center) seems straightforward, this demands a large communication bandwidth, consumes a lot of power and forms a single point of failure. This thesis therefore proposes novel distributed DSP algorithms, where nodes (microphone/loudspeaker arrays or APs) only exchange compressed signals and/or parameters and share the heavy computational burden of the centralized processing using in-network processing. The performance of centralized processing will be seen as an absolute benchmark for these distributed algorithm, and is often reached when the distributed algorithms have time to converge iteratively on stationary data.

The first part of the thesis presents distributed algorithms designed for application in a WAS(A)N. In this part node-specific MWF-based speech enhancement in a WASN and sound zoning in a WASAN are considered as DSP techniques. The algorithms are node-specific, since the speech signals to be estimated are different for each node (but still originating from the same sources), the local sound zones can be chosen independently at each node or local loudspeaker arrays have node-specific power constraints. The DSP tasks define centralized solutions using all available sensors/actuators and they are compared to stand-alone solutions, i.e., as if the nodes are not aware of the signals received/transmitted by other nodes. The design of all the distributed algorithms in this part follows a top-down strategy, under which it will be shown that the nodes iteratively (in a time-recursive fashion) converge to the centralized solution, by exchanging certain signals or parameters using the available wireless links.

The second part of this thesis focuses on developing distributed algorithms designed for application in CFmMIMO systems. The considered DSP tasks are MWF-based channel estimation, uplink receive combining, downlink transmit precoding and power allocation, taking into account channel estimation errors and different channel models. The presented distributed algorithms either use a network center as central processing unit to transmit the compressed data to and make final decoding/precoding decisions, or consider user-centric processing, whereby the decoding decisions are taken in the network by a user-specific AP. Similarly, convergence of the distributed algorithms to optimal solutions is shown, while strongly reducing the communication overhead over the available fronthaul links.

Finally, the last chapter provides the conclusions, summarizes the contributions of this thesis and further discusses possible future research directions.

Beknopte samenvatting

Door de technologische vooruitgang in de huidige analoge en digitale apparatuur en de miniaturisering van de hardware hebben sensoren en actuatoren nieuwe hoogten bereikt. Apparaten kunnen meer rekenintensieve digitale signaalverwerkingstaken (DSV-taken) uitvoeren voor een vergelijkbaar of zelfs lager energiebudget en er kunnen meer apparaten op hetzelfde oppervlak worden geplaatst, waardoor signaalverwerkingsalgoritmen worden verrijkt met meer inputs/outputs en dus meer vrijheidsgraden. Wanneer deze apparaten een specifieke DSV-taak moeten uitvoeren, zoals het schatten of genereren van een gewenst signaal, kan samenwerking tussen apparaten met verschillende locaties de algemene prestaties aanzienlijk verbeteren, vooral in ongunstige situaties. De apparaten (of knooppunten) moeten dan met elkaar worden verbonden via bekabelde of draadloze verbindingen en een sensor- en actuatornetwerk (SAN) vormen. Vergeleken met conventionele vaste sensor- of actuatorroosters met een duidelijk gelokaliseerde positie, hebben SANen toegang tot meer ruimtelijk verspreide sensoren en actuatoren, met meer ruimtelijke vrijheidsgraden.

Dit proefschrift zal zich specifiek richten op het schatten en genereren van signalen met behulp van de meerkanaals Wiener filter (MWF) binnen zowel draadloze als bekabelde SANen. Wanneer de voorkeur wordt gegeven aan draadloze verbindingen, bijvoorbeeld voor een ad-hoc plaatsing van de apparaten, wordt vaak de term draadloos sensor- en actuatornetwerk ('*wireless sensor and actuator network*' of WSAN) gebruikt. Met name bij akoestische toepassingen, waarbij de sensoren en actuatoren bestaan uit respectievelijk microfoon- en luidsprekerroosters, worden de netwerken ook wel draadlooze akoestische sensor- en actuatornetwerken ('*wireless acoustic sensor and actuator networks*' of WASANs) genoemd. Wanneer er echter reeds bekabelde verbindingen bestaan, zoals het geval is bij celvrije masieve meerdere-invoer-meerdere-uitvoer ('*cell-free massive multiple input multiple output*' of CFmMIMO) systemen waarbij een bekabeld SAN kan worden gevormd met behulp van de frontlijnverbindingen tussen toegangspunten ('*access points*' of AP's) met tot wel 100 antennes in de huidige mobiele netwerken, dienen bekabelde verbindingen te worden gebruikt.

Beide toepassingen vereisen hoge verwerkingssnelheden voor bemonstering, verwerking en transmissie, in vergelijking met traditionele SANen met lage verwerkingssnelheden. Daarom is het van cruciaal belang efficiënte algoritmen te ontwikkelen waarmee deze knooppunten kunnen samenwerken en hun schattings-/generatietaken kunnen verbeteren, onder strakke bandbreedte-, complexiteits- en energiebeperkingen.

Hoewel het samenvoegen en verwerken van alle ongecomprimeerde signalen en parameters op één plaats (bv. in een fusiecentrum) eenvoudig lijkt, vergt dit een grote communicatiebandbreedte, verbruikt het veel energie en vormt het een zwak punt (single point of failure). In dit proefschrift worden daarom nieuwe gedistribueerde DSV-algoritmen voorgesteld, waarbij de knooppunten (microfoon-/luidsprekerroosters of AP's) alleen gecomprimeerde signalen en/of parameters uitwisselen en de zware rekenlast van de gecentraliseerde verwerking delen door de verwerking te spreiden over het netwerk. De prestaties van gecentraliseerde verwerking zullen worden gezien als een absolute referentiemaat voor deze gedistribueerde verwerking, en worden vaak bereikt wanneer de gedistribueerde algoritmen tijd hebben om iteratief te convergeren op stationaire data.

Het eerste deel van het proefschrift presenteert gedistribueerde algoritmen die zijn ontworpen voor toepassing in een WAS(A)N. In dit deel worden knooppuntspecifieke MWF-gebaseerde spraakverbetering in een WASN en geluidszonering in een WASAN beschouwd als DSV-technieken. De algoritmen zijn knooppuntspecifiek, aangezien de te schatten spraaksignalen voor elk knooppunt verschillend zijn (maar wel afkomstig van dezelfde bronnen), de lokale geluidszones op elk knooppunt onafhankelijk kunnen worden gekozen of omdat de lokale luidsprekerrooster knooppuntspecifieke vermogensbeperkingen hebben. De DSV-taken definiëren gecentraliseerde oplossingen die gebruik maken van alle beschikbare sensoren/actuatoren en deze worden vergeleken met alleenstaande oplossingen, d.w.z. alsof de knooppunten niet op de hoogte zijn van de door andere knooppunten ontvangen/uitgezonden signalen. Het ontwerp van alle gedistribueerde algoritmen in dit deel volgt een top-down strategie, waarbij zal worden aangetoond dat de knooppunten iteratief (op een tijd-recursieve manier) convergeren naar de gecentraliseerde oplossing, door bepaalde signalen of parameters uit te wisselen met behulp van de beschikbare draadloze verbindingen.

Het tweede deel van deze thesis richt zich op de ontwikkeling van gedistribueerde algoritmen voor toepassing in CFmMIMO-systemen. De beschouwde SP-taken zijn MWF-gebaseerde kanaalschatting, uplink ontvangstcombinatie, downlink zendvoorcodering en vermogenstoewijzing, rekening houdend met kanaalschattingsfouten en verschillende kanaalmodellen. De gepresenteerde gedistribueerde algoritmen gebruiken ofwel een netwerkcentrum als centrale

verwerkingseenheid om de gecomprimeerde gegevens naar toe te zenden en de uiteindelijke decodeer-/voorcodeerbeslissingen te nemen, ofwel gebruikersgerichte verwerking, waarbij de decodeerbeslissingen in het netwerk worden genomen door een gebruikersspecifiek AP. Ook wordt aangetoond dat de gedistribueerde algoritmen naar optimale oplossingen convergeren, terwijl de communicatieoverhead over de beschikbare frontlijnverbindingen sterk wordt verminderd.

Het laatste hoofdstuk tenslotte bevat de conclusies, vat de bijdragen van dit proefschrift samen en bespreekt verder mogelijke toekomstige onderzoeksrichtingen.

Glossary

Acronyms and abbreviations

a.k.a	also known as
ACC	acoustic contrast control
AD	activity detection
ADMM	alternating direction method of multipliers
ANC	active noise canceling
AO	alternating optimization
AP	access point
ATF	acoustic transfer function
BER	bit error ratio
BS	base station
CDF	cumulative densitiy function
CE	channel estimation
CFmMIMO	cell-free massive multiple input multiple output
cfr.	conferatur, compare with, see also
CI	cochlear implant
CSI	channel state information
DACGEE	distributed adaptive covariance-matrix generalized eigenvector estimation

DANSE	distributed adaptive node-specific signal estimation
dB	decibel
DB-MWF	distributed multi-channel Wiener filter
DFT	discrete Fourier transform
DL	downlink
DOA	direction of arrival
DSP	digital signal processor/processing
e.g.	*exempli gratia*, for example
EVD	eigenvalue decomposition
FC	fusion center
GEVD	generalized eigenvalue decomposition
GSC	generalized sidelobe canceller
HA	hearing aid
Hz	hertz
i.e.	*id est*, that is
i.i.d.	independent and identically distributed
IoT	internet of things
KKT	Karush-Kuhn-Tucker
LCMV	linearly constrained minimum variance
LMMSE	local or linear minimum mean squared error
LMS	least mean squares
LoS	line-of-sight
MC	Monte Carlo
MIMO	multiple input multiple output
mMIMO	massive multiple input multiple output
MMSE	minimum mean squared error

MR	maximum ratio
MSE	mean squared error
MWF	multi-channel Wiener filter
NC	network center
NLoS	non line-of-sight
NSPE	node-specific parameter estimation
NSSE	node-specific signal estimation
OFDM	Orthogonal Frequency Division Multiplexing
PA	power allocation
PDMM	primal-dual method of multipliers
PM	pressure matching
QCQP	quadratically constrained quadratic program
r.h.s.	right hand side
RC	receive combining
RLS	recursive least squares
RZF	regularized zero-forcing
s.t.	subject to
SAN	sensor and actuator network
SDR	signal to distortion ratio
SE	spectral efficieny [bits/s/Hz]
SER	signal to error ratio
SINR	signal to interference and plus noise ratio
SNR	signal to noise ratio
SP	signal processing
SRO	sampling rate offset
STFT	short-time Fourier transform

TDD	time division duplexing
TOA	time-of-arrival
TP	transmit precoding
UE	user equipment
UL	uplink
ULA	uniform linear array
VAD	voice activity detection
w.l.o.g.	without loss of generality
WASAN	wireless acoustic sensor actuator network
WASN	wireless acoustic sensor network
WSN	wireless sensor network

Mathematical notation

a	scalar
$\mathbf{a}$	vector
$\mathbf{A}$	matrix
$\mathcal{A}$	set
$\mathbf{I}_R$	identity matrix of size $R \times R$
$\mathbf{1}_R$	one vector of size R
$\mathbf{0}$	all-zero matrix or vector
$\mathbf{e}_i$	vector of zeros with a '1' in position i
$tr\{\cdot\}$	trace of a matrix
$\{\cdot\}^*$	complex conjugate operation
$\{\cdot\}^H$	conjugate transpose operation
$\{\cdot\}^T$	transpose operation

$\{\cdot\}^{-1}$	matrix inverse
$E\{\cdot\}$	expectation operation
$\text{rank}(\mathbf{A})$	rank of matrix $\mathbf{A}$
$\approx$	approximately equal to
$\exists$	there exists
$\forall$	for all
$\lim_{x \leftarrow a} f(x)$	limit of function f as x approaches a
$\lvert \cdot \rvert$	cardinality of a set or absolute value
$\lvert\lvert \cdot \rvert\rvert$	norm
$\lvert\lvert \cdot \rvert\rvert_F$	Frobenius norm
$\text{Blkdiag}\{\cdot\}$	block diagonal matrix with arguments on block diagonal
$\text{diag}\{\cdot\}$	diagonal matrix with arguments on diagonal
$[\cdot]_0$	maximum value of $\{\cdot, 0\}$
$\triangleq$	is defined as
$\arg\min_x$	argument of the minimum
$\min_x$	minimize over x
mod	modular operator
$\mathcal{O}(\cdot)$	order
$\setminus$	set-theoretic complement
$\cup$	set-theoretic union
$\in$	is member of
$\text{ppk}(\mathbf{A})$	possible prior knowledge on the steering matrix $\mathbf{A}$
$\mathcal{NC}(\mathbf{x}, \mathbf{R})$	complex normal distribution with mean $\mathbf{x}$ and covariance $\mathbf{R}$

Contents

Abstract iii

Beknopte samenvatting v

Contents xv

1 Introduction and overview 1
- 1.1 Sensor and actuator networks . . . 2
  - 1.1.1 Definition and motivation . . . 2
  - 1.1.2 Wireless acoustic sensor and actuator networks . . . 4
  - 1.1.3 Cell-free massive MIMO . . . 5
- 1.2 Distributed signal processing algorithms for sensor and actuator networks . . . 8
  - 1.2.1 Centralized vs distributed processing . . . 8
  - 1.2.2 Time-adaptive signal and/or parameter estimation . . . 10
- 1.3 Challenges of distributed algorithms for sensor and actuator networks . . . 12
  - 1.3.1 Communication cost . . . 12
  - 1.3.2 Computational complexity . . . 13
  - 1.3.3 Adaptivity and convergence speed . . . 13
  - 1.3.4 Network topology . . . 14
  - 1.3.5 Scalability . . . 14
- 1.4 Overview . . . 15
  - 1.4.1 General overview . . . 15
  - 1.4.2 Technical assumptions . . . 16
  - 1.4.3 Thesis outline . . . 17

2 Multi-channel Wiener filter 21
- 2.1 Multi-channel Wiener filter basics . . . 21
- 2.2 Speech enhancement . . . 22
- 2.3 Sound zoning . . . 23

2.4 Channel estimation in (CF)mMIMO 26
2.5 Receive combining in (CF)mMIMO 28
2.6 GEVD-based distributed adaptive node-specific signal estimation 29

I Distributed signal processing algorithms for WAS(A)Ns 33

3 Distributed MWF-based speech enhancement with partial prior knowledge of desired source steering matrix 35
3.1 Introduction 37
3.2 Problem formulation and rank R PK-GEVD-MWF 40
3.2.1 Node-specific signal estimation 40
3.2.2 Centralized rank R $\bar{\mathbf{R}}_{\mathbf{ss}}$ estimation 41
3.2.3 Centralized rank R PK-GEVD-MWF 44
3.3 Lagrangian perspective on rank R PK-GEVD-MWF 46
3.4 Rank R PK-GEVD-DANSE 48
3.4.1 Algorithm description 48
3.4.2 Sufficient statistic 50
3.4.3 Communication cost and computational complexity . . 53
3.4.4 Topology independent rank R PK-GEVD-DANSE . . . 53
3.5 Rank R PK-GEVD-DANSE with rank deficiencies 55
3.5.1 $L_k < R$, $M_k - L_k < R$ 55
3.5.2 $L_k > R$, $M_k - L_k < R$ 55
3.5.3 $L_k < R$, $M_k - L_k > R$ 55
3.6 Numerical simulations 56
3.6.1 Distributed node-specific signal estimation in a WSN . . 56
3.6.2 Distributed speech enhancement in a WASN 57
3.7 Conclusion 61

4 Distributed sound zoning using acoustic contrast control 63
4.1 Introduction 65
4.2 Problem formulation: sound zoning in a WASAN 66
4.3 Centralized ACC method 68
4.4 Gradient based GEVD algorithm 69
4.5 DAG-ACC algorithm 70
4.6 Distributed adaptive gradient based ACC algorithm with reduced memory requirements 73
4.7 Simulations 74
4.8 Conclusion 76

5 Distributed sound zoning using pressure matching 77
5.1 Introduction 79

5.2 Signal model and problem formulation 80
5.3 Centralized algorithm 82
5.4 Distributed algorithm 83
5.5 Simulations 89
5.6 Conclusion 90

II Distributed signal processing algorithms for CFm-MIMO systems 91

6 Scalable and distributed MMSE-based uplink receive combining 93
6.1 Introduction 95
6.2 Signal model 95
6.2.1 Channel estimation 96
6.2.2 Uplink signal model 96
6.2.3 Uplink receive combining 97
6.3 Distributed MMSE receive combining 98
6.4 Scalable distributed MMSE receive combining 100
6.4.1 Scalability issue and solution 100
6.4.2 Scalable network-wide distributed MMSE receive combining 101
6.4.3 Scalable partial distributed MMSE receive combining . 102
6.5 Simulations 103
6.6 Conclusion 104

7 Distributed MMSE-Based uplink receive combining, downlink transmit precoding and optimal power allocation for CFmMIMO systems 105
7.1 Introduction 107
7.1.1 Related works 108
7.1.2 Contributions 109
7.1.3 Paper outline and notation 110
7.2 Signal model 110
7.2.1 UL channel estimation 111
7.2.2 UL data transmission 113
7.2.3 DL data transmission 114
7.3 UL receive combing and power allocation 115
7.3.1 UL receive combining 115
7.3.2 UL power allocation preliminaries 117
7.3.3 UL receive combining and power allocation 119
7.4 DL transmit precoding and power allocation 123
7.4.1 DL power allocation preliminaries 123
7.4.2 UL - DL duality 124
7.4.3 DL transmit precoding and power allocation 126

7.5 Further considerations . . . 128
7.5.1 Examples of power allocation strategies . . . 128
7.5.2 Scalability . . . 131
7.5.3 Network topologies . . . 131
7.6 Numerical simulations . . . 132
7.6.1 Numerical simulations UL . . . 132
7.6.2 Numerical simulations DL . . . 137
7.7 Conclusion . . . 140

8 Distributed combined channel estimation and receive combining for user-centric CFmMIMO systems 141
8.1 Introduction . . . 143
8.1.1 Novelty and paper outline . . . 144
8.1.2 Notations . . . 145
8.2 Channel and signal model . . . 146
8.2.1 Channel model . . . 147
8.2.2 Channel estimation . . . 148
8.2.3 Receive combining . . . 150
8.3 Centralized GEVD-based CE and RC . . . 151
8.3.1 Block diagonal $\overline{\mathbf{R}}_k$ with a local rank R^B . . . 152
8.3.2 Low rank $\overline{\mathbf{R}}_k$ with rank R^L . . . 154
8.3.3 Superposition of R^B-block diagonal and R^L-low rank $\overline{\mathbf{R}}_k$ 155
8.4 Distributed GEVD-based CE and RC . . . 160
8.4.1 Algorithm description . . . 162
8.4.2 Convergence analysis . . . 163
8.4.3 Communication cost . . . 165
8.5 Distributed multi-user RC . . . 166
8.6 Simulations . . . 167
8.6.1 Results for centralized GEVD-based CE and RC . . . 169
8.6.2 Results for rank $\{R^B, R^L\}$ GEVD-based DUCERC . . . 170
8.7 Conclusion . . . 170

9 Conclusion 173
9.1 Summary and conclusions . . . 173
9.2 Suggestions for future research . . . 179

III Appendices 183

A GEVD-based speech and noise correlation matrix estimation for MWF-based noise reduction 185
A.1 Introduction . . . 187
A.2 Problem statement . . . 188

A.2.1 MWF based noise reduction . . . 188
A.2.2 EVD based speech and noise correlation matrix estimation 189
A.2.3 GEVD-based speech and noise correlation matrix estimation 189
A.3 Modified GEVD-based speech and noise correlation matrix estimation . . . 190

B Appendix to Chapter 3 **197**
B.1 Useful identities . . . 197
B.2 Equivalence between (3.9) and (3.10) . . . 198
B.3 Derivation of rank R PK-GEVD-MWF . . . 199
B.4 Proof of Theorem 3.4.2 . . . 200
B.5 Proof of Lemma B.4.1 . . . 202

C Appendix to Chapter 7 **203**
C.1 Proof of Theorem 7.3.2 . . . 203

D Appendix to Chapter 8 **205**
D.1 Proof of (8.56) . . . 205
D.2 Proof of Theorem 8.4.1 . . . 206

E GEVD-based low-rank MMSE channel estimation for uplink cellular mMIMO systems **211**
E.1 Introduction . . . 213
E.2 Channel and signal model . . . 213
E.2.1 Channel model . . . 213
E.2.2 Signal model . . . 214
E.3 Optimal MMSE channel estimation . . . 216
E.4 Low-rank channel estimation . . . 217
E.4.1 Low-rank covariance matrix estimator . . . 217
E.4.2 Low-rank approximate MMSE estimator . . . 219
E.4.3 Improved low-rank approximate MMSE estimator . . . 219
E.5 Numerical simulations . . . 220
E.6 Conclusion . . . 223

Bibliography **225**

Curriculum Vitae **241**

List of publications **243**

Chapter 1

Introduction and overview

Technological progress in current analogue and digital devices together with the miniaturization of hardware have pushed sensing and actuating devices to new heights. Devices can perform more computationally intensive digital signal processing (DSP) tasks for a similar or even lower power budget and more devices can be placed on the same surface area, enriching signal processing algorithms with more inputs/outputs and hence more degrees of freedom. When these devices have to perform a specific DSP task, such as the estimation or generation of a signal of interest, cooperation between devices with different locations can significantly enhance the overall performance, especially in adverse situations. The devices (or nodes) then need to be connected using either wired or wireless connections and form a sensor and actuator network (SAN). When wireless connections are favored, e.g., for an ad-hoc placement of the devices, the term wireless sensor and actuator network (WSAN) [1] is often used. In acoustical applications where the senors and actuators consists of microphone and loudspeaker arrays respectively, the network is specifically referred to as wireless acoustic sensor and actuator network (WASAN). However, when wired connections are already in place, as is the case for cell-free massive multi input multiple output (CFmMIMO) systems where a wired SAN is formed using the fronthaul connections between access points (APs) in currently enrolled mobile networks, they should be used, albeit it under tight bandwidth and energy constraints.

In general SANs, it is therefore critical to develop and apply efficient DSP algorithms under which nodes[1] can cooperate to enhance the output performance of their corresponding DSP task, controlled by constraints in bandwidth, computational complexity or energy/hardware consumption. This thesis aims at developing novel efficient distributed DSP algorithms for SANs in which the nodes are tasked with estimating/generating of a signal of interest.

The rest of the chapter is organized as follows. In Section 1.1, SANs, WASANs and CFmMIMO systems are introduced in detail and their advantages in real-life situations are discussed. In Section 1.2, different signal processing strategies will be explained, together with the advantages of having the entire computational load of the SAN spread between different nodes inside the network (rather than in a central point) will be highlighted. Section 1.3 will discuss and review some of the important challenges for designing distributed algorithms for SANs. Finally, in Section 1.4, a chapter-by-chapter outline and the contributions of the thesis will be presented.

1.1 Sensor and actuator networks

1.1.1 Definition and motivation

Sensors consists of hardware that record a certain analogue signal and convert it to a digital signal using analogue-to-digital conversion. Examples are microphones, image sensors, light sensors or motion sensors. They have been successfully utilized in various practical DSP applications, like speech processing with portable devices (e.g., smartphones, laptops) or wearable devices (e.g., hearing aids, smartwatches) [2,3]. Actuators, on the other hand, are devices that generate a certain analogue signals from a digital signal using digital-to-analogue conversion. Examples are loudspeakers, displays or servo motors. Some devices, like transceivers with antennas, can perform both tasks, allowing them to both generate (=transmit) and record (=receive) electromagnetic waves.

By using the spatial properties of these digitally captured/reproduced signals, multi-channel DSP techniques can deliver a significantly improved performance when compared to single-channel DSP techniques which are constrained by the temporal characteristics of the captured/reproduced signals [4, 5]. For instance, multi-channel sensors can extract information on the relative position of the captured signals, which is a major advantage in signal enhancement

[1] The term node will be used to denote a collection of sensors/actuators forming one unit. In CFmMIMO literature, this term is basically the same as an AP, but this introduction will stick to the generic term 'node'.

with directional noise. The use of more antennas in mMIMO systems [6, 7] makes the radiation pattern of antenna array in the APs highly adaptable and more directional, such that less interference occurs at the undesired locations and a greater portion of the transmitted power reaches the area around the desired source. Increasing the number of sensors/actuators improves the performance of multi-channel DSP techniques since more devices provide more spatial information.

However, conventional sensor/actuator array are typically placed at specific locations with respect to some reference point and designed with a specific compact geometry. This has as unavoidable limitation that adding more sensors/actuators is not always feasible due to the compact design (e.g., antennas or microphones in smartphones), or that when sensors can be added, they are forced to be placed in close proximity, resulting in a clearly localized position in the spatial field. In situations where the desired source and the interfering sources are located in a similar direction seen from the array, or when the array is located far from the desired source, it has been shown that including nearby sensors/actuators, located closer to the desired source, can significantly increase the performance, as it is able to spatially separate the sources. For example, when used in audio and speech enhancement applications, binaural (two-sided) hearing aids (HAs) perform better than monaural (single-sided) HAs in terms of speech intelligibility, localization and listening quality [8]. Furthermore, adding an external microphone, located close to the desired speaker, to a binaural hearing aid noise reduction system can enhance the output signal to noise ratio (SNR) of each device simultaneously and even result in a better preservation of the binaural noise cues [9–11]. Additional performance gains can be made by including even more of these external microphones into a binaural hearing aid noise reduction system [12, 13]. Similar improvements are seen when the antenna signals received at different spatially distributed APs are combined, compared to the operation of one AP alone [14–17].

A so-called wired SAN may thus be generated by simply connecting these spatially distributed sensor/actuator arrays together using wires. In currently enrolled cellular mobile network for the Fifth Generation (5G) technology [18,19], the available fronthaul links between the APs can be used to interconnect the APs and form a wired SAN. Cell-free massive MIMO (CFmMIMO) is the concept describing the cooperation between the different APs and will further be elaborated upon in Subsection 1.1.3.

However, if the sensor arrays were mobile, the resulting wired SAN would not be appropriate, since the locations where the sensor arrays can be put are limited, and installation and maintenance costs are typically very high [20], particularly in applications where such a wired SAN needs to be formed in a large enclosure, such as in applications in [21–23]. Alternatively, data sharing between these

physically distributed sensor/actuator arrays can be accomplished by wireless connections. Each device must have a wireless transmitter, a wireless receiver and a power source for this (often a battery). A network made up of several of these collaborating nodes [24, 25] is typically referred to as a WSAN. WSANs can also be organized using a hierarchical structure where multiple master nodes can be defined, which collect/define signals of multiple slave nodes in their neighborhood. Even though WSANs alleviate many of the practical problems associated with wired SANs, the design of appropriate algorithms must still take bandwidth limits into consideration under even tighter power constraints. Section 1.3 provides a discussion about the design challenges of algorithms for wired/wireless SANs.

The envisaged SANs in this thesis contain several nodes where each one includes a sensor/actuator array of which the position and orientation is unknown. In addition, different nodes can have different local sensor/actuator arrangements or can be defined as a collection of several sensor/actuator arrays.

1.1.2 Wireless acoustic sensor and actuator networks

Wireless sensor networks (WSNs) have been employed in a wide range of applications [26–29], e.g., event detection [30, 31], navigation systems [32, 33] or under water applications [34]. Different subclasses of WSNs, such as wireless body area networks [35, 36] or wireless multimedia sensor networks [37, 38], have emerged over the past several years depending on the context in which they are employed. Wireless multimedia sensor networks deal with the acquisition and processing of multimedia content and have been used in applications such as image enhancement [39] and acoustical applications, where in the latter the term wireless acoustic sensor networks (WASNs) [40–42] is used. When loudspeakers are also available in the network, this term is extended to WASAN [43–45]. DSP applications in WASANs include acoustic multi-channel noise reduction [40, 46–51], echo cancellation [43, 52], signal dereverberation [53, 54], estimation and equalization of room acoustics [55], source localization and beamforming [56–58], source separation [59], or active noise control and equalization [60–62]. In real-life scenarios, WASANs can be formed by connecting devices with microphones and loudspeakers such as hearing aids, smartphones, smartwatches, laptops, headphones, etc. An example of a WASAN is illustrated in Figure 1.1.

The main goal of this thesis is to develop distributed algorithms for signal estimation/generation and parameter estimation in ad-hoc WASANs. The term ‘distributed’ here means that the WASAN’s entire processing task is divided across the nodes rather than concentrated in one place (see also Section 1.2.1).

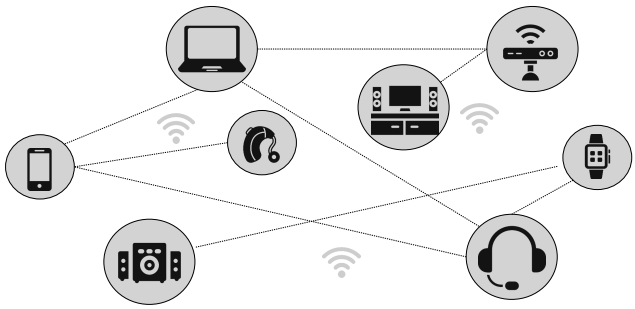

Figure 1.1: Example of a WASAN consisting of different devices, such as a smartphone, a smartwatch, a laptop, a headphone, a Kinect sensor, ...

Signal estimation in WASNs is investigated in Chapter 3. Signal generation or sound zoning [5, 63] is investigated in Chapter 4 and Chapter 5, for different setups with different definitions of a node, as shown in Figure 1.2. More information on the used symbols will be provided in Chapter 2.

1.1.3 Cell-free massive MIMO

MIMO technology plays an important role in present-day wireless communication standards and networks. It uses multiple antennas to transmit and receive multiple data signals simultaneously over one and the same radio channel and hence increase spectral efficiency. Massive MIMO (mMIMO) systems use a large(r) number of antennas, to reap additional benefits in rich scattering environments. While mMIMO was initially viewed as a promising concept for future cellular wireless communication networks, it already became a reality in 2018 with commercial deployment in several countries [19]. The signal processing methods required to achieve large spectral efficiency gains compared to conventional multi-user MIMO systems [64] are available and well understood [6]. The spectral efficiency gains associated with mMIMO emerge from the higher spatial resolution, its robustness against small-scale fading due to the so-called 'channel hardening' effect, and its ability to suppress interference even with imperfect channel state information (CSI). The use of massive MIMO systems for mm-wave frequencies [65] is also currently being considered.

One of the major shortcomings of current cellular wireless communication networks, where a user equipment (UE) is served only by the one AP of the cell it resides in, is that UEs on the cell borders experience a low channel

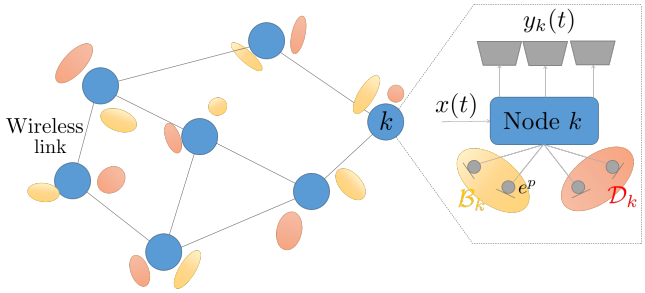

(a) WASAN setup 1: error microphone signals are part of the WASAN and are distributed over the different nodes. This is the setup that is considered in Chapter 4.

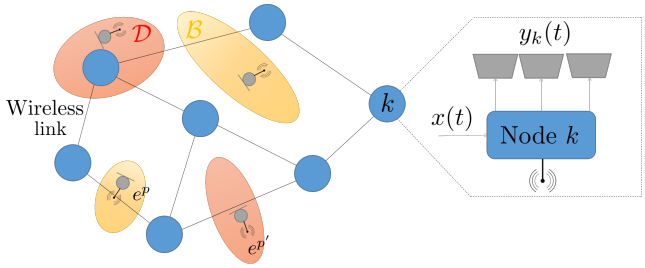

(b) WASAN setup 2: error microphone signals are recorded by dedicated microphone arrays that can transmit their recordings to all loudspeaker nodes. This is the setup that is considered in Chapter 5.

Figure 1.2: Different WASAN setups considered in this thesis.

gain from their serving AP and a high interference power from nearby cells, as presented in Figure 1.3a. Current receive combining and transmit precoding algorithms do not effectively mitigate such interference. To address this issue, the concept of CFmMIMO [66–68] has been proposed. In CFmMIMO systems, a UE may alternatively be served by all APs in the network instead of only one AP, as shown in Figure 1.3b. The joint operation of all APs then allows for implementing interference-rejecting equalization and precoding algorithms effective for all UEs in the network. CFmMIMO thus effectively eliminates cell borders while still reusing the network layout as rolled out previously, which offers the potential to spectacularly increase performance as compared to current cellular mMIMO systems. Realizing this potential will be one of the main challenges tackled by this thesis, and is addressed in Chapters 6-8.

CFmMIMO has its roots in works on distributed MIMO [14, 15] and coordinated

multipoint [16, 17]. An important aspect is that mMIMO systems experience small-scale fading resulting in highly time-varying channels that can be considered fixed only for a few milliseconds. While cellular mMIMO systems benefit from channel hardening, as antennas at the same AP experience similar channel gains and hence the small-scale fading averages out, the same cannot be expected from CFmMIMO systems, as well-separated APs experience large channel gain differences. On the other hand, the great spatial resolution will likely make channels to different UEs nearly orthogonal [69] which is known as 'favorable propagation'.

In CFmMIMO systems, the joint operation of all APs can be coordinated by a network center (NC), possibly located at the edge or in the cloud [70]. In a setup where all signal processing tasks are to be performed by the NC, raw baseband signals are transmitted between all the APs and the NC. However, due to geographic and topological constraints, this processing quickly becomes intractable as the number of APs increases. Also the computational complexity of current state-of-the-art receive combining and transmit precoding algorithms typically relates to the total number of antennas (summed over APs) and UEs in the network and furthermore may require channel state information (CSI) between all antennas and UEs. This clearly introduces scalability issues for growing network sizes. This unavoidable problem is addressed in this thesis by adhering to a user-centric approach [71–74]. In this approach, a UE is no longer served by all APs in the network (including APs far away from the UE), but rather by a selected set of (nearby) APs, as shown in Figure 1.3c. This is still in contrast to a cellular system where a UE is served by only one AP. Developing scalable user-centric signal processing algorithms is also a main challenge and investigated in Chapter 6 and Chapter 7.

The user-centric approach also limits the transmission of raw baseband signals between the APs and the NC. Nevertheless, the NC will still form a communication bottleneck and a single point of failure. To eliminate the need for a NC, a scalable distributed processing framework has to be developed. The network-wide task of the NC then has to be divided into user-related subtasks to be executed by ad-hoc local networks, where each local network is formed by the APs serving a particular UE, as shown in Figure 1.3d. The user-related subtasks will still be coupled, e.g., a resource allocation and precoding for one UE will result in stronger interference to other UEs. Therefore, inter-AP communication will have to be exploited to share parameters and signals between the APs. Dividing network-wide tasks into subtasks that can be executed by different network nodes fits in the framework of wired SANs. However, the envisaged user-centric approach leads to a specific scenario with partially overlapping 'interests' [75] between nearby APs (nodes), which is still an open problem. Developing distributed signal processing algorithms for this specific scenario,

with minimal inter-AP communication and yet close to optimal performance, are developed in Chapter 8, albeit only for channel estimation and receive combining.

1.2 Distributed signal processing algorithms for sensor and actuator networks

One way of performing the required SP task is that the nodes of a SAN send their sensor signal observations or parameters to a specialized (remote) facility, frequently referred to as a fusion center (FC). Then, in order to estimate the desired signals or parameters of interest, this FC gathers, combines, and processes all sensor signal observations and parameters over the whole SAN. The result can then be transferred back to the nodes in case they need this locally. However, it frequently happens that such an FC is either not available or located too far from some nodes, which causes a substantial increase in energy consumption at each node and is harmful to SANs, especially if they operate at high sampling rates. Additionally, using one FC forms a single point of failure, meaning that if the FC fails, the SAN's entire information processing will also fail. As an alternative, in-network processing is often preferred since nodes within the network then handle all of the SAN's signal processing in this configuration, as opposed to a FC. This section describes various forms of in-network processing.

1.2.1 Centralized vs distributed processing

One possible way of optimally performing the estimation tasks in a SAN, is by letting each node transmit all its sensor signals and/or parameters to all other nodes. In this way, every node serves as an FC, and this method of processing is referred to as centralized processing. The estimation performance is optimal, since each node can exploit the coherence between all signals in the network. A schematic example with two nodes is provided in Figure 1.4a. As nodes must communicate all of their sensor signal and parameters, centralized processing, despite producing the best estimation performance, presents the worst case performance in terms of communication cost efficiency and computational complexity, as it grows with the number of nodes in the SAN.

As an alternative, distributed processing can be used to accomplish in-network processing, which is preferable because it greatly reduces the communication cost and enables the physically distributed nodes of a SAN to share the heavy computational burden of the centralized processing, as illustrated in

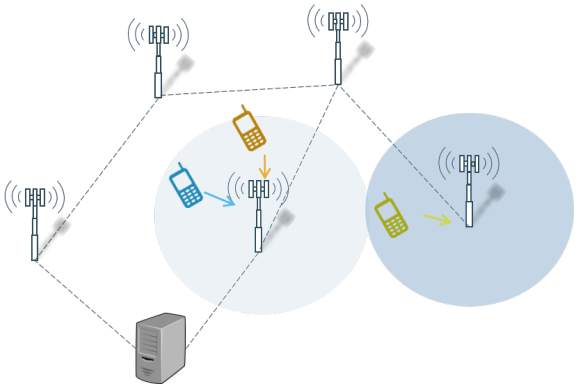

(a) Cellular mMIMO.

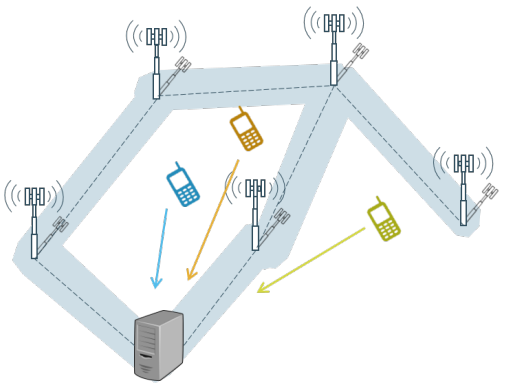

(b) CFmMIMO with NC.

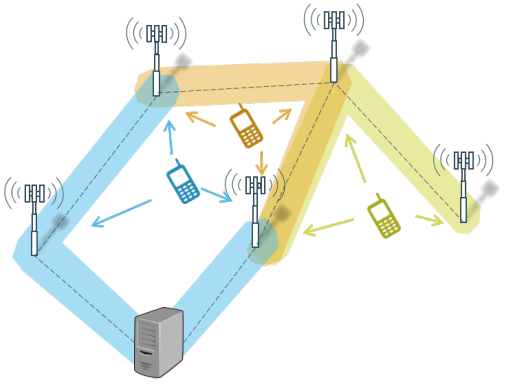

(c) User-centric CFmMIMO with NC.

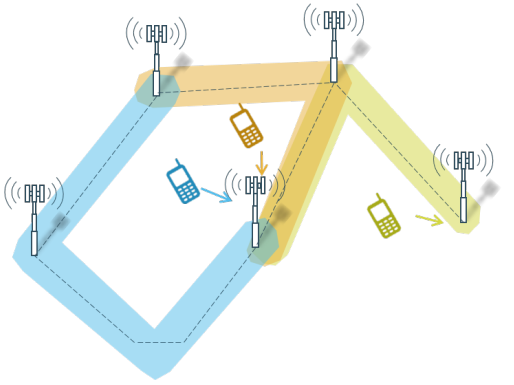

(d) User-centric CFmMIMO with master AP.

Figure 1.3: Difference between cellular mMIMO and different implementations of CFmMIMO.

Figure 1.4b. Each node locally processes its own sensor signal and parameters by including (compressed) signals and parameters received from its neighboring nodes. Since the exchanged signals are compressed during local processing and only communicated between close-by nodes, less bandwidth and energy is needed for the communication, making this approach of distributed processing scalable in terms of communication and computational complexity. The performance of centralized processing will be seen as an absolute benchmark for these types of distributed processing.

1.2.2 Time-adaptive signal and/or parameter estimation

In general, there exist two relevant classes of DSP problems in SAN: signal estimation and parameter estimation. In problems involving parameter estimation, a target vector (e.g., precoding vector or sound zoning filter) with a limited number of parameters must typically be estimated and changes must be tracked over time. By contrast in problems involving signal estimation, an additional block of samples from the desired signals must be estimated for each corresponding block of data collected at the sensors. As a result, the number of variables to be estimated in signal estimation issues increases linearly with sampling time.

This thesis proposes novel distributed algorithms for both signal and parameter estimation. This is done by exchanging compressed sensor signals or parameters in an efficient way. In the distributed algorithms developed here, this is achieved by restricting the actual compressed sensor signals that are exchanged between the nodes to being transmitted only once for each newly acquired block of sensor signals. Compressed parameters are only retransmitted if they are estimated based on the data of a newly acquired block. The distributed algorithms are thus iterating over time and not over the same block of sensor signal observations. The latter often happens in parameter estimation problems where algorithms have to iterate over the same block of sensor signal observations, requiring repeated re-transmissions and re-estimations of the parameters until they converge to an equilibrium. Therefore, local processing techniques that are often used in the context of distributed parameter estimation, such as consensus [76, 77], incremental [78], or diffusion [79–82] based algorithms, are often inefficient for signal estimation due to their inherent iterative re-estimation of the target vector. Therefore, this thesis focuses on distributed estimation techniques that update local filter coefficients and local compression rules over time, without iterating over the same block of sensor observations.

The fact that these compression rules are dependent on the local filters creates a catch-22 situation because computing the local filters also necessitates computing

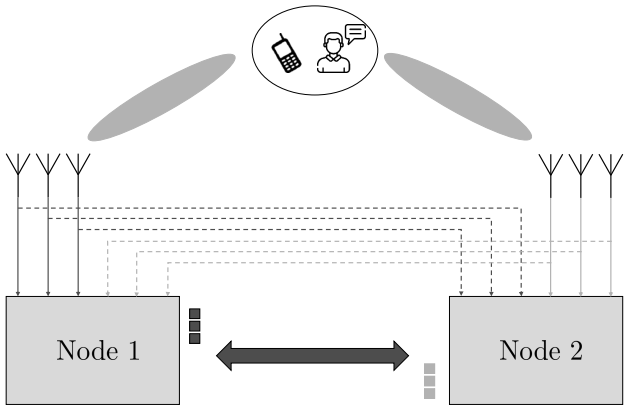

(a) Example of centralized processing with full exchange of signals and parameters. This leads to the best possible performance, but with the highest communication cost.

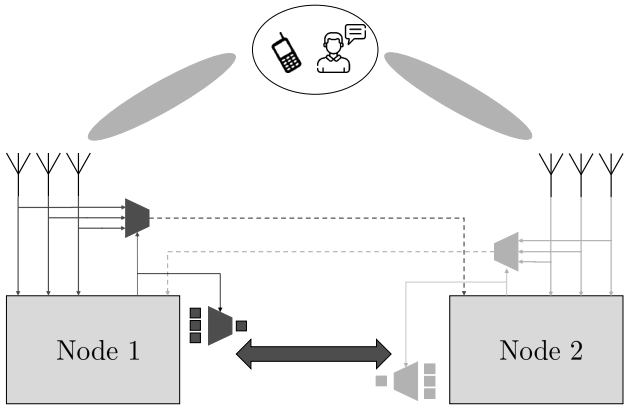

(b) Example of distributed processing using compressing filter-and-sum operations, reducing the communication cost strongly.

Figure 1.4: Centralized processing vs processing with a distributed algorithm.

the per-node compression rules. As a result, in order to enable improved future predictions, the compression rules of the developed algorithms must first be initialized with random entries and then repeatedly changed (adapted) in a time-recursive manner. The revised filters are only used for upcoming observations, so further updates of the local spatial filters (and subsequently the compression rules) use different blocks of sensor observations. These updates may take place sequentially at one node at a time (as in [83, 84]), or they may take place at all nodes simultaneously (as in [85]).

1.3 Challenges of distributed algorithms for sensor and actuator networks

This section highlights the specific challenges that are handled in the developed distributed algorithms of this thesis in order to avoid offering an exhaustive list. However, it is noted that numerous implementation challenges such as sampling frequency synchronization, sampling rate offsets, communication link failures and delays, quantization and transmission errors, voice activity detection (VAD) issues, and privacy constraints are also often present in practical scenarios.

1.3.1 Communication cost

Even when using state-of-the-art low-power technology, the wireless transmission of the signals is recognized to be the most power-hungry operation at each node [86–88]. Similarly, wired transmissions should be limited to minimize the queuing delays [89]. Therefore, it is crucial to create distributed algorithms that effectively lower the necessary communication cost while having little to no negative effects on the estimation performance of the per-node tasks.

Several general-purpose compressive techniques based on encoding (compression) and decoding (decompression) have been proposed to minimize transmitted data over wireless channels of a SAN [90–92]. However, when these strategies are used in distributed algorithms that rely on spatial filtering techniques, crucial information and cues for the DSP task may get lost. This could result in decreased estimate performance and, ultimately, unsatisfactory solutions [93–96]. Additionally, nodes that use such compressive techniques must perform a decompression when they get the compressed sensor signal observations from other nodes. This frequently raises the computational complexity per-node and necessitates additional computing and energy resources, which is not ideal for power-efficient SANs.

This thesis uses an alternate compression approach that reduces the necessary communication cost by using application-dependent compressive filter-and-sum operations. By essentially fusing many sensor signals, this linear compression approach produces a signal with fewer channels than the initial set of sensors. The compression rule at each node is chosen simultaneously with the computation of the local filter, as it is often related to parts of this local filter or intermediate variables computed during the node-specific DSP task.

1.3.2 Computational complexity

Each node of a SAN can only process and manage a reduced-dimensional version of the centralized task since it is often assumed that the processing capability of each node of a SAN is limited. To prevent buffer overruns or real-time performance failure, the total processing load should be evenly divided among the nodes.

The complexity reductions in the distributed algorithms developed in this thesis are a direct outcome of the filter-and-sum compression that is applied to the exchanged signals. In contrast to the dimension of matrices in the centralized scenario, the nodes have only access to a subset of the full sensor signals or parameters and hence perform their operations using reduced-dimensional inputs.

1.3.3 Adaptivity and convergence speed

In dynamic scenarios, environmental parameters and physical characteristics of a SAN may change over time. Hence distributed algorithms should be able to track and adapt to such changes. For instance, the distributed method should be able to adjust when the position of the sources (speakers/UEs) and the statistics of the channels alter over time.

In this thesis, the adaptation is accomplished by efficiently updating the spatial filters at various nodes (and thereby the compression rules) iteratively in a data-driven manner, with the iterations being spread out over time in a time-recursive block-wise manner. To be able to track and respond to changes in dynamic environments, the nodes' parameters must be updated at a frequency high enough for this to be possible, e.g., by allowing simultaneous updating [85].

1.3.4 Network topology

The network topology of a SAN is imposed by the set of wired or wireless communication links available. Although wireless links can be formed between any pair of nodes, in practice the node pairs which avoid communicating over long distances or through obstacles are more efficient in terms of link quality and energy consumption. There exist four basic topologies of SANs, namely ring, tree, star and fully-connected. Some topologies allow for more local degrees of freedom, increasing the convergence speed, but also the computational cost. Distributed algorithms may therefore operate on a combination of such basic topologies [97].

In practice, nearest-neighbor topologies are frequently preferred because they allow nodes to communicate over a short distance. However, these nearest-neighbor topologies may contain numerous cycles in their network graph, or paths that begin and terminate in the same node, when they are implemented in an unmanaged ad-hoc SAN. The distributed algorithms in this thesis cannot handle such cycles, in contrast to the majority of (ad-hoc) distributed parameter estimation algorithms that call for the exchange of parameters between nodes [76, 77, 80]. Cycles introduce feedback channels and causality issues, which may hamper the convergence of these distributed signal estimating algorithms from converging [98]. Such feedback paths can be avoided by means of topology control, e.g., based on a tree topology [99], a hierarchical tree-like topology [97], or based on a topology-independent scheme [100] in which a different tree can be used in each iteration. Most of the algorithms developed in this thesis will be presented in a topology-independent (tree-based) SAN, since all other topologies can be mapped to this general topology (without cycles).

Additionally, the communication channels are assumed to be optimal throughout this thesis, that is, noise-free and without any random failures. In real-world applications, appropriate measures must be taken to prevent instantaneous performance reductions in real-time signal estimation for scenarios involving potential network failures or packet loss (e.g., as in [98]).

1.3.5 Scalability

When the networks area grows, the number of nodes and desired sources increases as well. Even though reducing communication cost is essential, the communication cost for distributed algorithms is often proportional to the number of desired sources [83, 101]. Nodes might not even observe some of the desired sources or only with a very low SNR, but are still required to perform local processing tasks related to these desired sources [102]. This might

particularly pose a problem with large CFmMIMO networks, although user-centric CFmMIMO systems [71–74] are already proposed to overcome this issue. Scalable versions of the non-scalable distributed algorithms for CFmMIMO systems presented in this thesis will always be provided.

1.4 Overview

1.4.1 General overview

Chapter 2 will briefly discuss the multi-channel Wiener filter (MWF) in a centralized configuration, since this forms the common thread throughout the DSP tasks in all chapters. It will also review the GEVD-based distributed adaptive node-specific signal estimation (GEVD-DANSE) algorithm which allows to efficiently obtain the output of a MWF in a SANs.

The thesis then consist of the following two main parts:

The **first part** (Chapters 3-5) presents **distributed algorithms designed for application in WAS(A)Ns**. In this part node-specific MWF-based speech enhancement in WASN and sound zoning in WASAN are considered as basic SP techniques. The algorithms are node-specific, since the speech signals to be estimated are different for each node (but still originating from the same sources) and the local sound zones can be chosen independently at each node or local loudspeaker arrays have node-specific power constraints. The DSP tasks define centralized solutions using all available sensors/actuators and they are compared to stand-alone solutions, i.e., as if the nodes are not aware of the signals received by/transmitted to other nodes. The design of all the distributed algorithms in this part follows a top-down strategy, under which it will be shown that the nodes iteratively (in a time-recursive fashion) converge to the centralized solution, by exchanging certain signals or parameters using the available wireless links.

The **second part** (Chapters 6-8) presents **distributed algorithms designed for application in CFmMIMO systems**. The considered DSP tasks are MWF-based channel estimation, uplink receive combining, downlink transmit precoding and power allocation, taking into account channel estimation errors and different channel models. In Chapters 6-7, the presented distributed algorithms are using an NC as central unit to transmit the compressed data towards and make final decoding/precoding decisions. In Chapters 8, user-centric processing is considered, where the decoding decisions are taken within the network by a UE-specific AP, albeit only for channel estimation and receive combining. Similarly, convergence of the distributed algorithms to an optimal

user-centric solution is shown, while strongly reducing the communication overhead over the available fronthaul links.

The outline of Chapters 3 to 8 as well as their contributions is outlined in Section 1.4.3.

1.4.2 Technical assumptions

The distributed algorithms developed in this thesis rely on the following technical assumptions:

1. The sampling rates and sampling times between the sensors/actuators of different nodes are synchronized. More on this can be found as a suggestion for future research in Chapter 9.
2. The SANs have ideal communication links, i.e., signals are transmitted between different nodes with zero time and processing delay. In reality, this can bypassed by introducing some processing delay and using buffers to temporarily store the necessary signals until all signals are available for the DSP task.
3. Nodes have access to ideal information on their desired speakers (multi-source VAD, prior knowledge) or serving UEs (training sequences).
4. All the nodes in the SANs are able to observe the desired speakers or serving UEs with at least some of its sensors.
5. The network topology is fully-connected (Chapter 3) or can be turned into a tree-topology to efficiently construct the required in-network sums (all chapters).
6. For theoretical convergence statements, it is assumed that the signal models are perfectly satisfied and that the required signal correlation matrices are perfectly estimated using infinite observation windows. These statements only hold asymptoticly in practice and will be more valid when larger observation windows are used.

Furthermore, it is important to stress that the (relative) positions of the sensors/actuators of the nodes are unknown (ad-hoc) and different nodes can have different local arrangements. However, some prior knowledge cases in Chapter 3 require knowledge of the local sensor arrangement which is then assumed to be known.

1.4.3 Thesis outline

Chapter 3 presents a novel GEVD-based MWF for speech enhancement, where local partial prior knowledge of the desired sources steering matrix is included as a hard constraint. Partial prior knowledge can for example arise when direction-of-arrival (DOA)-information is present or when a node has access to sensors/signals that only contain noise. Each node estimates its own node-specific desired signal as received by its own sensors (to preserve the spatial characteristics of its sensor signals), using all the sensors and prior knowledge available in the WASN. Including prior knowledge has extra benefits, compared to the data-dependent GEVD-MWF: it provides more robust estimates in the presence of second-order statistics errors, e.g., due to non-stationarity of noise, low-SNR conditions or erroneous VADs. It is shown that the centralized MWF output can also be obtained in a distributed way, by altering the GEVD-based DANSE algorithm (reviewed in Subsection 2.6) by including prior knowledge GEVD-based low-rank approximations in the per-node local MWFs and by also transmitting compressed versions of local noise references. The newly proposed distributed algorithm is referred to as PK-GEVD-DANSE.
Chapter 3 has been published as:

- **Van Rompaey, R.**, Moonen, M., "Distributed Adaptive Signal Estimation in Wireless Sensor Networks with Partial Prior Knowledge of the Desired Sources Steering Matrix", IEEE Transactions on Signal and Information Processing over Networks, vol. 7, 2021, pp. 478-492.

Chapter 4 presents a distributed algorithm for acoustic contrast control based sound zoning in a WASAN organized as in setup 1 shown in Figure 1.2a. Each node is allowed to choose to which zone (bright or dark) each of their error microphones belongs. The centralized solution requires gathering impulse responses between all loudspeakers and microphones in one central place, to be able to compute the sound zoning filter using a GEVD. A gradient-based algorithm is presented to obtain the same centralized solution and that can be performed distributed using in-network sums of certain parameters. Performance is compared to the performance of a non-cooperative WASAN.
Chapter 4 has been published as:

- **Van Rompaey, R.**, Moonen, M., "Distributed Adaptive Acoustic Contrast Control for Node-specific Sound Zoning in a Wireless Acoustic Sensor and Actuator Network", Proceedings of 2020 28th European Signal Processing Conference (EUSIPCO), Amsterdam, The Netherlands, 2021, pp. 481-485.

Chapter 5 presents a distributed algorithm for pressure matching based sound zoning in a WASAN organized as in setup 2 in Figure 1.2b. The local

loudspeaker array has node-specific power constraints that can be chosen based on the available hardware. The centralized solution requires again gathering impulse responses between all loudspeaker and microphones in one central place, to be able to compute the sound zoning filter using a quadratically constrained quadratic program (QCQP). A Gauss-Seidel type algorithm is proposed, to be able to obtain the same filter in a distributed way, without requiring communication between the different nodes. The distributed sound zoning filter is shown to converge iteratively to the centralized sound zoning filter with the same power constraint.
Chapter 5 has been published as:

- **Van Rompaey, R.**, Moonen, M., "Sound Zoning in an Ad-hoc Wireless Acoustic Sensor and Actuator Network", Proceedings of 2021 29th European Signal Processing Conference (EUSIPCO), Dublin, Ireland, 2021, pp. 101-105.

Chapter 6 presents scalable distributed algorithms that can be used for uplink receive combining in CFmMIMO systems. It presents the baseline network-wide distributed MMSE receive combining (N-DRC) algorithm that is later extended in Chapter 7 by including optimal power allocation and downlink transmit precoding algorithms. The N-DRC algorithm is designed such that the CSI of an AP is required only locally and it is shown that optimal MMSE-based receive combining can still be obtained by exchanging only a small number of parameters between the APs and the NC. Scalable versions of the N-DRC algorithm are also proposed to fit in the user-centric approach of CFmMIMO.
Chapter 6 has been published as:

- **Van Rompaey, R.**, Moonen, M., "Scalable and Distributed MMSE algorithms for Uplink Receive Combining in Cell-free Massive MIMO Systems", Proceedings of 2021 IEEE International Conference on Acoustics, Speech and Signal Processing (ICASSP), Toronto, Canada, 2021, pp. 4445-4449.

Chapter 7 first extends the N-DRC algorithm by including optimal uplink power allocation techniques, where the power allocation is adjusted to the locally estimated large-scale fading properties of the channels. The necessary communications between the APs and the NC are reduced to a minimum and rely on in-network summations that can be performed efficiently if the network topology is arranged into a tree-topology. Using uplink/downlink duality [74, 103] a similar algorithm is derived for combined downlink transmit precoding and optimal power allocation. The used utility functions for the power allocation are the non-weighted max-sum SE and max-min SE, but the algorithms are not limited to these cases. Simulations are provided showing that the proposed algorithms outperform heuristic power allocation methods

and this both for the vanilla CFmMIMO system in Figure 1.3b as well as for the scalable user-centric CFmMIMO system in Figure 1.3c.
Chapter 7 has been published (without the scalable results) as:

- **Van Rompaey, R.**, Moonen, M., "Distributed MMSE-Based Uplink Receive Combining, Downlink Transmit Precoding and Optimal Power Allocation in Cell-Free Massive MIMO Systems", accepted for publication in EURASIP Journal on Wireless Communications and Networking.

Chapter 8 deals with channel estimation and uplink receive combining in user-centric CFmMIMO where the data of a UE is gathered at some master AP in the network as in Figure 1.3d. The channels satisfying a more general Rician fading model, existing of a combination of line-of-sight (LoS) and non-LoS components. The LoS component introduces correlation between the channels at different APs that can be exploited to improve the channel estimation and the receive combining. The channel estimates can then be obtained by processing the local antenna channels, together with compressed versions of all the antenna channels serving the UE. To make the proposed method scalable, a distributed user-centric channel estimation and receive combining (DUCERC) algorithm is presented that reduces the necessary communications between the APs.
Chapter 8 will be submitted for publication as:

- **Van Rompaey, R.**, Moonen, M., "Distributed Combined Channel Estimation and Optimal Uplink Receive Combining for User-centric Cell-free Massive MIMO systems", submitted for publication.

Chapters 3 and 8 also mention **Appendix A** which elaborates on the used optimization criterion for the estimation of the desired source correlation matrix (i.e., speech correlation matrix or channel covariance matrix). In generalized eigenvalue decomposition (GEVD) based MWF, this optimization criterion typically involves a prewhitening with the sample 'noise-only' or 'noise + interference' matrix. However, a more accurate form would include a prewhitening with the estimated noise correlation matrix instead of with the sample 'noise-only' or 'noise + interference' correlation matrix. Unfortunately this leads to a more difficult optimization problem, where the prewhitening indeed involves one of the optimization variables. It is therefore demonstrated that the modified optimization criterion, remarkably, leads to only minor modifications in the estimated correlation matrices and eventually the same MWF, which justifies the use of the original optimization criterion as a simpler substitute.
Appendix A has been published as:

- **Van Rompaey R.**, Moonen M., "GEVD Based Speech and Noise Correlation Matrix Estimation for Multichannel Wiener Filter Based

Noise Reduction", Proceedings of 2018 26th European Signal Processing Conference (EUSIPCO), Rome, Italy, 2018, pp. 2544-2548.

Chapter 8 also uses the novel channel estimation procedure developed for a cellular massive MIMO system explained in **Appendix E**. It proposes a data-driven channel covariance matrix estimator for low-rank channel covariance matrices using a GEVD of two covariance matrices that can be estimated from the available uplink data. The method requires a different way of assigning pilots to UEs, but except for synchronization, there is no need for communication between the different cells and no prior knowledge on the background noise is required. Approximate MMSE estimators are also derived based on the newly proposed channel covariance matrix estimator. The performance is evaluated in a simulated cellular massive MIMO setup.
Appendix E has been published as:

- **Van Rompaey, R.**, Moonen, M., "GEVD-based Low-Rank Channel Covariance Matrix Estimation and MMSE Channel Estimation for Uplink Cellular Massive MIMO Systems", Proceedings of 2020 30th European Signal Processing Conference (EUSIPCO), Belgrade, Serbia, 2022.

Finally, **Chapter 9** concludes the thesis and provides some suggestions for further research.

Chapter 2

Multi-channel Wiener filter

This section reviews the basic concepts of the multi-channel Wiener filter (MWF), forming a common thread throughout the centralized DSP tasks applied in this thesis. The MWF is first explained in a general context in Section 2.1. Then the applications of the MWF are discussed for the different DSP tasks considered in this thesis, being speech enhancement (Section 2.2), sound zoning (Section 2.3), channel estimation (Section 2.4) and receive combining (Section 2.5). At the end of this chapter, the GEVD-based distributed adaptive node-specific signal estimation (GEVD-DANSE) algorithm which allows to efficiently obtain the output of an MWF in a SANs, is reviewed shortly. The GEVD-DANSE algorithm forms the baseline algorithm for the algorithms developed in Chapter 3 and Chapter 8. The idea of performing Gauss-Seidel based updates to solve a network-wide objective distributively also returns in Chapter 5.

2.1 Multi-channel Wiener filter basics

The signal obtained at all M sensors in the SAN can be written as

$$\mathbf{y} = \mathbf{s} + \mathbf{n} \tag{2.1}$$

where $\mathbf{s} \in \mathbb{C}^M$ is the desired source component in the different sensor signals. $\mathbf{n} \in \mathbb{C}^M$ represents an additive noise signal that can be correlated between different sensors signals. It can also include interfering sources, like non-desired speech sources or signals from other UEs. The goal is to optimally estimate $\mathbf{s}$ by using a linear combination of all the sensor signals in $\mathbf{y}$, where the linear combination can be obtained by minimizing the following mean squared error

(MSE) criterion:

$$\hat{\mathbf{W}} = \arg\min_{\boldsymbol{W}} E\{\|\mathbf{s} - \boldsymbol{W}^H \mathbf{y}\|^2\}. \tag{2.2}$$

Here $E\{\cdot\}$ denotes the expected value operator and $\cdot^H$ is the hermitian transpose operator. The resulting filter is also known as the MWF. When $\bar{\mathbf{R}}_{\mathbf{yy}} = E\{\mathbf{y}\mathbf{y}^H\}$ is invertible, the unique solution of (2.2) is [104]

$$\hat{\mathbf{W}} = \bar{\mathbf{R}}_{\mathbf{yy}}^{-1} E\{\mathbf{y}\mathbf{s}^H\} = \bar{\mathbf{R}}_{\mathbf{yy}}^{-1} E\{\mathbf{s}\mathbf{s}^H\} \triangleq \bar{\mathbf{R}}_{\mathbf{yy}}^{-1} \bar{\mathbf{R}}_{\mathbf{ss}}. \tag{2.3}$$

The second step in (2.3) uses the (often valid) assumption that the additive noise signal $\mathbf{n}$ and the desired source signal $\mathbf{s}$ are uncorrelated. Note that this also implies that

$$\bar{\mathbf{R}}_{\mathbf{yy}} = \bar{\mathbf{R}}_{\mathbf{ss}} + \bar{\mathbf{R}}_{\mathbf{nn}} \Longrightarrow \bar{\mathbf{R}}_{\mathbf{ss}} = \bar{\mathbf{R}}_{\mathbf{yy}} - \bar{\mathbf{R}}_{\mathbf{nn}} \tag{2.4}$$

where $\bar{\mathbf{R}}_{\mathbf{nn}} = E\{\mathbf{n}\mathbf{n}^H\}$. Depending on the used application, the system can either have access to a data-dependent estimate of $\bar{\mathbf{R}}_{\mathbf{yy}}$ and $\bar{\mathbf{R}}_{\mathbf{nn}}$ and uses them to obtain an estimate for $\bar{\mathbf{R}}_{\mathbf{ss}}$ and/or have prior knowledge on $\bar{\mathbf{R}}_{\mathbf{yy}}$ or $\bar{\mathbf{R}}_{\mathbf{ss}}$ that can be exploited to get an estimate of the optimal MWF in (2.3).

2.2 Speech enhancement

Speech enhancement is often performed in the (short-term) Fourier transform domain [105], since convolutive time-domain mixtures can efficiently be described as instantaneous single-tap per-frequency mixtures. The complex-valued microphone signal $\mathbf{y}$ obtained in one frequency bin can then be written as given in (2.1). In the case of a single desired speaker, the desired speech component can further be written as

$$\mathbf{s} = \mathbf{a}\check{s} \tag{2.5}$$

where $\check{s}$ is the desired source signal and $\mathbf{a} \in \mathbb{C}^M$ is the unknown frequency-dependent steering vector.

In this thesis, node-specific speech enhancement in a WASN is considered. The node-specific task of node k is to find an estimate of the desired signal component $\hat{d}_k = \mathbf{e}_{d_k}^T \mathbf{a}\check{s}$, defined without loss of generality as the desired source signal in the first microphone signal of node k, where $\mathbf{e}_{d_k}$ selects the correct microphone signal in $\mathbf{y}$. The node-specific MWF can then be written as

$$\hat{\mathbf{w}}_k = \bar{\mathbf{R}}_{\mathbf{yy}}^{-1} \bar{\mathbf{R}}_{\mathbf{ss}} \mathbf{e}_{d_k} = \bar{\mathbf{R}}_{\mathbf{yy}}^{-1} \mathbf{a} E\{|\check{s}|^2\} \mathbf{a}^H \mathbf{e}_{d_k} \tag{2.6}$$

where $\bar{\mathbf{R}}_{\mathbf{ss}}$ is a rank-1 matrix.

Speech signals typically experience an on-off behavior. A voice activity detector (VAD) can determine whether a certain signal segment contains 'speech+noise' or 'noise-only' [106–109]. An estimate of $\bar{\mathbf{R}}_{\mathbf{yy}}$, denoted by $\mathbf{R}_{\mathbf{yy}}$ can then be computed as the (recursive) time average over different 'speech+noise' segments. Similarly an estimate $\mathbf{R}_{\mathbf{nn}}$ can be obtained by averaging over different 'noise-only' segments. It is then common to estimate $\mathbf{R}_{\mathbf{ss}}$, which typically experiences a low rank as shown in (2.6), using a GEVD of the matrix pencil $\{\mathbf{R}_{\mathbf{yy}}, \mathbf{R}_{\mathbf{nn}}\}$ given by [110]

$$\begin{aligned} \mathbf{R}_{\mathbf{yy}} &= \mathbf{Q}\mathbf{\Sigma}\mathbf{Q}^H \\ \mathbf{R}_{\mathbf{nn}} &= \mathbf{Q}\mathbf{Q}^H. \end{aligned} \tag{2.7}$$

Here, $\mathbf{Q} = \mathbf{X}^{-H}$ is an invertible matrix, the columns of $\mathbf{X}$ are unique (up to a sign-ambiguity) and define the generalized eigenvectors. $\mathbf{\Sigma}$ is a real-valued diagonal matrix where $\mathbf{\Sigma} = \text{diag}\{\hat{\sigma}_1, ..., \hat{\sigma}_M\}$ defines the generalized eigenvalues sorted from large to small.

A rank-1 estimate $\mathbf{R}_{\mathbf{ss}}$ is then given by keeping only the components in the eigenspace of the largest generalized eigenvalue [111] during the subtraction in (2.4) as

$$\mathbf{R}_{\mathbf{ss}} = \hat{\mathbf{q}}(\hat{\sigma} - 1)\hat{\mathbf{q}}^H \tag{2.8}$$

where $\hat{\mathbf{q}}$ contains the first column of $\mathbf{Q}$ and $\hat{\sigma} = \hat{\sigma}_1$. Using a GEVD has advantages compared to other methods, like simply performing the subtraction $\mathbf{R}_{\mathbf{yy}} - \mathbf{R}_{\mathbf{nn}}$ or incorporating the low rank using an EVD of this subtraction. More information can be found in [110] or in Appendix A. Sometimes prior knowledge on (parts of) $\mathbf{a}$ is available. Chapter 3 explains how this can be incorporated in this framework and generalizes it to situations with more than one desired speaker.

The final MWF (2.6) can then be written using the generalized eigenvectors and eigenvalues as

$$\hat{\mathbf{w}}_k = \hat{\mathbf{x}}\frac{\hat{\sigma} - 1}{\hat{\sigma}}\hat{\mathbf{q}}^H\mathbf{e}_{d_k} \tag{2.9}$$

where $\hat{\mathbf{x}}$ contains the first column of $\mathbf{X}$.

2.3 Sound zoning

There is a link[1] between the MWF and the used sound zoning filters throughout this thesis. Although the link is not clearly stated in Chapter 4 and Chapter 5,

[1] For more information, the interested reader is referred to [112]

it is still worth mentioning it for arguments of completeness. The sound zoning filters provided in Chapters 4 and 5 are defined in the time domain and require more extended formulas. To keep this introduction simple, this exposition is provided for frequency-based sound zoning, where the sound zoning filters are just a single tap filter in the frequency domain. Note that this theoretically corresponds to a convolution in the time domain when the number of frequency bins is large.

The purpose of sound zoning is generating L loudspeaker signals such that a certain desired signal x is clearly audible in certain zones, called the bright zones ($\mathcal{B}$), and almost not audible in other zones, called the dark zones ($\mathcal{D}$). As seen from Figure 1.2a and Figure 1.2b, there are error microphone scattered over the considered area in the different bright and dark zones. The sound pressure is measured at these error microphones, to provide feedback to the system. The signal measured by error microphone m (either belonging to the bright zone or the dark zone) can be written in a certain frequency bin as

$$p_m = \sum_{l=1}^{L} h_{ml}\ y_l = \sum_{l=1}^{L} h_{ml}\ w_l^*\ x = \mathbf{w}^H \mathbf{h}_m\ x \tag{2.10}$$

where y_l is the signal played by loudspeaker l, h_{ml} is the frequency-dependent channel between loudspeaker l and error microphone m and w_l is the single tap sound zoning filter applied to the desired signal x at loudspeaker l. $\mathbf{h}_m$ is the concatenation of the channels between all loudspeakers and microphone m and $\mathbf{w}$ is the concatenation of all sound zoning filters.

To determine the optimal sound zoning filter $\hat{\mathbf{w}}$, two objectives are typically proposed. The first objective, defined for all the error microphones in the bright zone, is determined by the deviation of the received signal to a certain predefined reference signal d_m. d_m is here defined as the signal obtained when one reference loudspeaker (defined w.l.o.g. as the first loudspeaker) plays the desired signal x, i.e., $d_m = h_{m1}x = \mathbf{e}_1^H \mathbf{h}_m x$:

$$\mathcal{J}_{\mathcal{B}}(\mathbf{w}) = \sum_{m\in\mathcal{B}} E\{|p_m - d_m|^2\} \tag{2.11}$$

$$= \mathbf{w}^H \underbrace{\sum_{m\in\mathcal{B}} \mathbf{h}_m E\{|x|^2\}\mathbf{h}_m^H}_{\bar{\mathbf{R}}_{\mathcal{B}}} \mathbf{w} - \mathbf{w}^H \underbrace{\sum_{m\in\mathcal{B}} \mathbf{h}_m E\{|x|^2\}\mathbf{h}_m^H \mathbf{e}_1}_{\bar{\mathbf{R}}_{\mathcal{B}}\mathbf{e}_1} - \mathbf{e}_1^H \bar{\mathbf{R}}_{\mathcal{B}} \mathbf{w} + \sum_{m\in\mathcal{B}} E\{|d_m|^2\}.$$

The desired signal for the dark zone is defined as 0 (no signal), so a similar objective can be defined as

$$\mathcal{J}_{\mathcal{D}}(\mathbf{w}) = \sum_{m\in\mathcal{D}} E\{|p_m - 0|^2\} = \mathbf{w}^H \underbrace{\sum_{m\in\mathcal{D}} \mathbf{h}_m E\{|x|^2\}\mathbf{h}_m^H}_{\bar{\mathbf{R}}_{\mathcal{D}}} \mathbf{w}. \tag{2.12}$$

Combining both objectives then results in one general objective to determine the optimal sound zoning filter $\hat{\mathbf{w}}$:

$$\hat{\mathbf{w}} = \arg\min_{\mathbf{w}} \mathcal{J}_{\mathcal{B}}(\mathbf{w}) + \mu\mathcal{J}_{\mathcal{D}}(\mathbf{w}) = (\bar{\mathbf{R}}_{\mathcal{B}} + \mu\bar{\mathbf{R}}_{\mathcal{D}})^{-1}\bar{\mathbf{R}}_{\mathcal{B}}\mathbf{e}_1 \tag{2.13}$$

where μ is a control parameter. (2.13) resembles the MWF formula in (2.3) if $\bar{\mathbf{R}}_{\mathcal{B}}$ replaces $\bar{\mathbf{R}}_{\mathbf{ss}}$ and $\mu\bar{\mathbf{R}}_{\mathcal{D}}$ replaces $\bar{\mathbf{R}}_{\mathbf{nn}}$. This shows that sound zoning and MWF are tightly coupled.

To compute this filter, estimates of the channels $\{\mathbf{h}_m\}$ for all m are necessary. It is typically assumed that the channels change slowly over time, such that the sound zoning filter can be considered as almost time-invariant [113]. Based on available estimates of the channels, e.g., estimated during a calibration phase and tracked during the operation, estimates of $\mathbf{R}_{\mathcal{B}}$ and $\mathbf{R}_{\mathcal{D}}$ can be obtained as provided in (2.11) and (2.12). Using a GEVD of the matrix pencil $\{\mathbf{R}_{\mathcal{B}}, \mathbf{R}_{\mathcal{D}}\}$, similar to the GEVD in (2.7), results in two well known types of sound zoning filters:

- If the full generalized eigenspace is used, the **pressure matching** (PM) [63, 114] solution is obtained, and the sound zoning filter is then obtained as
$$\hat{\mathbf{w}} = \mathbf{X}\left(\mathbf{\Sigma} + \mu\mathbf{I}_M\right)^{-1}\mathbf{\Sigma}\mathbf{Q}^H\mathbf{e}_1 \tag{2.14}$$
where $\mathbf{I}_M$ denotes the M-dimensional identity matrix. Chapter 5 defines an algorithm that converges to this filter in an efficient distributed way. It also generalized this discussion by including more desired signals (with different bright/dark zones) and local power constraints for each WASAN node.

- If only the mode with highest generalized eigenvalue is used[2], the **acoustic contrast control** (ACC) [115–117] solution is obtained. The sound zoning

[2]Practically it does not make sense to approximate $\bar{\mathbf{R}}_{\mathcal{B}}$ as a rank-1 one matrix, since this is generally not the case if there is more than one error microphone in the bright zone or when the system is defined in the time domain. However, the ACC solution is commonly used in sound zoning, but is often argued based on maximization of the power ratio in (2.16), instead of the current MWF-approach.

filter can then be written as

$$\hat{\mathbf{w}} = \hat{\mathbf{x}} \frac{\hat{\sigma}}{\hat{\sigma} + \mu} \hat{\mathbf{q}}^H \mathbf{e}_1. \tag{2.15}$$

Note that this is basically a scaled version of the generalized eigenvector and this solution also maximizes the ratio of the total power in the bright zone, divided by the total power in the dark zone (a.k.a. the acoustic contrast):

$$\frac{\mathbf{w}^H \mathbf{R}_{\mathcal{B}} \mathbf{w}}{\mathbf{w}^H \mathbf{R}_{\mathcal{D}} \mathbf{w}}. \tag{2.16}$$

Chapter 4 defines an algorithm for a WASAN that converges to this filter in an efficient distributed way.

Intermediate solutions that include more than one mode in the eigenspace, but not all modes, are also possible, defining a full spectrum of solutions between the ACC method and the PM method. However, these solutions are not investigated in this thesis.

2.4 Channel estimation in (CF)mMIMO

(CF)mMIMO operates in either Time-Division Duplex (TDD) mode or Frequency-Division Duplex mode [118, 119]. The latter is not considered in this thesis. The channels vary strongly over time and frequency. Therefore, in TDD mode, the time-frequency resources are divided into coherence blocks of τ_c samples for which the channel can be assumed constant and frequency flat as shown in Figure 2.1. A coherence block is then divided into three phases: τ_p samples are used for uplink channel estimation and τ_u and τ_d samples for uplink and downlink data respectively. The τ_p samples are used to define τ_p orthogonal pilots and a UE is typically assigned to use a certain pilot. The following statistic can be obtained by despreading the antenna signals using the pilot of a certain UE k in one coherence block:

$$\mathbf{y}_t = \sqrt{\tau_p p_k} \mathbf{h}_k + \sum_{i \in \mathcal{S}_t \setminus \{k\}} \sqrt{\tau_p p_i} \mathbf{h}_i + \mathbf{n} \tag{2.17}$$

where $\mathbf{h}_k$ denotes the channel between UE k and all the antenna signals of all the APs, $\mathcal{S}_t$ denotes the subset of UEs using the same training sequence t and p_i is the uplink transmit power of UE i.

An MMSE-based estimate of the channel for UE k can then be defined as

$$\min_{\boldsymbol{W}} E\{||\mathbf{h}_k - \boldsymbol{W}^H \mathbf{y}_t||^2\} \tag{2.18}$$

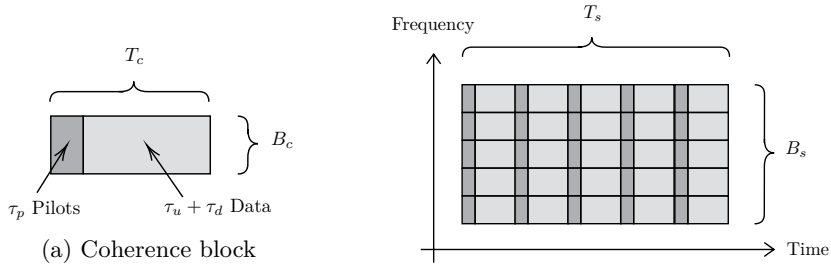

(a) Coherence block

(b) Grid with fixed statistics

Figure 2.1: Block fading model

where the expectation is defined with respect to different channel realizations. Again the MWF forms the optimal solution:

$$\hat{\mathbf{W}}_k = \sqrt{\tau_p p_k} \left(\tau_p p_k \bar{\mathbf{R}}_k + \sum_{i \in \mathcal{S}_t} \tau_p p_i \bar{\mathbf{R}}_i + \bar{\mathbf{R}}_{\mathbf{nn}} \right)^{-1} \bar{\mathbf{R}}_k \tag{2.19}$$

where $\bar{\mathbf{R}}_k = E\{\mathbf{h}_k \mathbf{h}_k^H\}$ is the channel covariance matrix. Comparing (2.19) to (2.3) shows that $\tau_p p_k \bar{\mathbf{R}}_k$ replaces $\bar{\mathbf{R}}_{\mathbf{ss}}$ and $\sum_{i \in \mathcal{S}_t} \tau_p p_i \bar{\mathbf{R}}_i + \bar{\mathbf{R}}_{\mathbf{nn}}$ serves as the interference+noise matrix. The MMSE-based channel estimate of $\mathbf{h}_k$, denoted by $\hat{\mathbf{h}}_k = \mathbf{W}_k^H \mathbf{y}_t$, is an unbiased estimate with estimation error $\tilde{\mathbf{h}}_k = \mathbf{h}_k - \hat{\mathbf{h}}_k$ that is uncorrelated with the estimate $\hat{\mathbf{h}}_k$ [7]. The estimation error covariance $\mathbf{C}_k = E\{\tilde{\mathbf{h}}_k \tilde{\mathbf{h}}_k^H\}$ can then also be computed as $\bar{\mathbf{R}}_k - \sqrt{\tau_p p_k} \mathbf{W}_k^H \bar{\mathbf{R}}_k$.

The structure of the channel covariance matrix $\bar{\mathbf{R}}_k$ depends on the used fading realization for the channel. The most commonly used fading realizations are Rayleigh fading [66, 72, 120–124] and Rician fading [121, 122, 125]. Rayleigh fading models channels without a Line-of-Sight (LoS) component and $\bar{\mathbf{R}}_k$ is modeled as a block diagonal matrix, without correlation between different APs. The channel estimation can then be performed locally at each AP (as shown in Chapter 6 and Chapter 7). Rician fading, on the other hand, is used to model channels with both LoS and non-LoS components. $\bar{\mathbf{R}}_k$ can then no longer be modeled as a block diagonal matrix, so the channel estimation requires access to the antenna signals of all APs in the network. Rician fading in CFmMIMO systems is further investigated in Chapter 8. Most literature assumes that the channel covariance matrices of all UEs are known a priori, which is a strong assumption since the matrix dimension grows with the number of antennas and furthermore the statistics are changing over time. Therefore, a new method for estimating channel covariance matrices is proposed in Appendix E for cellular mMIMO systems with Rayleigh fading and in Chapter 8 for CFmMIMO systems with Rician fading. It again uses a GEVD to obtain a robust estimate

of the channel covariance matrix. Chapter 8 also proposes efficient distributed solutions to obtain Rician fading-based channel estimates in CFmMIMO.

2.5 Receive combining in (CF)mMIMO

The antenna signals received during uplink (UL) data transmission can be written as

$$\mathbf{y} = \sqrt{p_k}\mathbf{h}_k s_k + \sum_{i \neq k} \sqrt{p_i}\mathbf{h}_i s_i + \mathbf{n} \tag{2.20}$$

where s_i is the unitary signal transmitted by UE i. The antenna signals can then be linearly combined using a receive combiner $\mathbf{v}_k \in \mathbb{C}^M$ to estimate the transmitted signal s_k as $\mathbf{v}_k^H \mathbf{y}$ at the network level. The performance of a receive combiner is typically evaluated using a standard lower bound for the ergodic capacity for UL data transmission of UE k, given by the achievable UL spectral efficiency (SE)

$$\mathrm{SE}_k^{\mathrm{UL}} = \frac{\tau_u}{\tau_c} E\left\{ \log_2(1 + \mathrm{SINR}_k^{\mathrm{UL}}) \right\} \text{ [bits/s/Hz]} \tag{2.21}$$

with the instantaneous effective signal-to-interference-and-noise ratio $\mathrm{SINR}_k^{\mathrm{UL}}$ given as

$$\frac{p_k |\mathbf{v}_k^H \hat{\mathbf{h}}_k|^2}{\sum_{i \neq k} p_i |\mathbf{v}_k^H \hat{\mathbf{h}}_i|^2 + \sum_i p_i \mathbf{v}_k^H \mathbf{C}_i \mathbf{v}_k + \mathbf{v}_k^H \bar{\mathbf{R}}_{\mathbf{nn}} \mathbf{v}_k}. \tag{2.22}$$

Here $\hat{\mathbf{h}}_i$ and $\mathbf{C}_i$ are the optimal MMSE-based channel estimate and estimation covariance matrix as defined in the previous section.

Maximum-ratio (MR) combining [66, 71, 126] with $\mathbf{v}_k = \hat{\mathbf{h}}_i$ has been identified as a convenient receive combiner in CFmMIMO systems with Rayleigh fading since there is no need to share CSI between the APs. However, this benefit comes at a significant performance loss compared to using minimum-mean-squared-error (MMSE) processing, where the generalized Rayleigh quotient in (2.22) is maximized in each coherence block by

$$\hat{\mathbf{v}}_k = \alpha \left(p_k \hat{\mathbf{h}}_k \hat{\mathbf{h}}_k^H + \sum_{i \neq k} p_i \hat{\mathbf{h}}_i \hat{\mathbf{h}}_i^H + \sum_i p_i \mathbf{C}_i + \bar{\mathbf{R}}_{\mathbf{nn}} \right)^{-1} \hat{\mathbf{h}}_k \tag{2.23}$$

where α can be any scalar. If α is chosen as $\sqrt{p_k}$, this is again an instance of the MWF where the desired signal is defined as s_k and the interfering/noise component in the sensor signals is given by $\sum_{i \neq k} \sqrt{p_i}\hat{\mathbf{h}}_i s_i + \sum_i \sqrt{p_i}\tilde{\mathbf{h}}_i s_i + \mathbf{n}$. Note that channel estimates are required for all UEs in the network, which is

not scalable. Therefore, different receive combiners, where only some channel estimates are available at certain APs, are presented in Chapters 6-8.

Chapter 7 also discusses optimal power allocation strategies. Optimization techniques are used to assign uplink powers p_i to all UE, based on an optimization criterion, typically involving the SE_k of all UEs. This is done using an alternating optimization framework, where the MWF is still used as an important substep. The downlink transmit precoding and power allocation problem can then be linked to the uplink receive combining and power allocation problem using uplink/downlink duality, and the MWF-based substep will in this case provide the necessary parameters for the transmit precoders of the APs.

2.6 GEVD-based distributed adaptive node-specific signal estimation

GEVD-based distributed adaptive node-specific signal estimation (GEVD-DANSE) [101] is a distributed algorithm developed for a WSN satisfying the signal model in (2.1). It assumes a low-rank constraint on the covariance matrix $\bar{\mathbf{R}}_{\mathbf{ss}}$ and uses the GEVD-based technique proposed in Section 2.2 to estimate $\mathbf{R}_{\mathbf{ss}}$ based on data-based estimates $\mathbf{R}_{\mathbf{yy}}$ and $\mathbf{R}_{\mathbf{nn}}$. The algorithm can more generally be applied to include higher ranks on $\bar{\mathbf{R}}_{\mathbf{ss}}$, which is for instance the case when there are more desired speakers in the WASN or when higher rank are necessary to model the channel covariance matrix $\bar{\mathbf{R}}_k$. Nevertheless, the rank-1 version is explained here for simplicity. The algorithm also assumes a fully-connected WSN, but it can be implemented in a tree-topology using similar techniques as in [100].

It is assumed that a node compresses each new block of its local M_k-dimensional sensor signals $\mathbf{y}_k$ using a local compression vector [3] $\mathbf{w}_{kk}^i$ to the single compressed sensor signal $z_k^i = \mathbf{w}_{kk}^{i,H}\mathbf{y}_k$. i will denote the iteration index of the distributed algorithm and $\mathbf{y}$, as defined in (2.1), is the stacked version of the local sensor signals $\mathbf{y}_k$ of all K nodes in the network with $M = \sum_{k=1}^{K} M_k$. The compressions z_k^i of all nodes are broadcast immediately to all other nodes in the network, such that each node has access to an extended sensor signals vector defined as

$$\tilde{\mathbf{y}}_k = [\mathbf{y}_k^T \; z_1^i \; \dots \; z_{k-1}^i \; z_{k+1}^i \; \dots \; z_K^i]^T. \tag{2.24}$$

Local versions of $\mathbf{R}^i_{\tilde{\mathbf{y}}_k\tilde{\mathbf{y}}_k}$ and $\mathbf{R}^i_{\tilde{\mathbf{n}}_k\tilde{\mathbf{n}}_k}$ can then be estimated using a VAD and the data in the new block. A local GEVD-based MWF can then be computed

[3] The local compression vector should ideally be chosen as the part of the optimal node-specific MWF $\hat{\mathbf{w}}_k$ in (2.9) belonging to the microphones of node k, which is indicated by the double subscript notation $\cdot_{kk}$.

based on the GEVD of $\mathbf{R}^i_{\tilde{\mathbf{y}}_k\tilde{\mathbf{y}}_k}$ and $\mathbf{R}^i_{\tilde{\mathbf{n}}_k\tilde{\mathbf{n}}_k}$ similar as was done in Section 2.2:

$$\tilde{\mathbf{w}}^i_k = \tilde{\mathbf{x}}^i_k \frac{\tilde{\sigma}^i_k - 1}{\tilde{\sigma}^i_1} \tilde{\mathbf{q}}^{i,H}_k \tilde{\mathbf{e}}_1 \tag{2.25}$$

where $\tilde{.}$ and subscript $_k$ are used to denote node-specific local quantities. The local filter output can then be obtained as $d^i_k = \tilde{\mathbf{w}}^{i,H}_k \tilde{\mathbf{y}}_k$ for all observations.

It is then shown in [101] that when the compression filter $\mathbf{w}^i_{kk}$ is updated in a round-robin cyclic fashion, i.e., only the updating node q (with a token) is allowed to update it in one iteration and passes the token to the next updating afterwards, and when $\mathbf{R}^i_{\tilde{\mathbf{y}}_k\tilde{\mathbf{y}}_k}$ and $\mathbf{R}^i_{\tilde{\mathbf{n}}_k\tilde{\mathbf{n}}_k}$ are estimated perfectly in each iteration, the filter output d^i_k converges to the same filter output d_k as it would obtain using centralized processing. The update basically consists of changing $\mathbf{w}^i_{kk}$ to the first M_k channels in $\tilde{\mathbf{w}}^i_k$. An overview of the GEVD-DANSE algorithm[4] is provided in Algorithm 1.

Algorithm 1: rank 1 GEVD-DANSE

1 - All nodes k initialize $\mathbf{w}^0_{kk}$ as random matrices.
- $i \leftarrow 0$ and $q \leftarrow 1$.

2 - All nodes k broadcast B observations of $z_k = \mathbf{w}^{i,H}_{kk}\mathbf{y}_k$ and construct $\tilde{\mathbf{y}}_k$ locally using the signals obtained from the other nodes.

3 - All nodes k estimate $\mathbf{R}^i_{\tilde{\mathbf{y}}_k\tilde{\mathbf{y}}_k}$ and $\mathbf{R}^i_{\tilde{\mathbf{n}}_k\tilde{\mathbf{n}}_k}$ based on the B observations and construct $\tilde{\mathbf{w}}^{i+1}_k$ as in (2.25) using the GEVD of $\{\mathbf{R}^i_{\tilde{\mathbf{y}}_k\tilde{\mathbf{y}}_k}, \mathbf{R}^i_{\tilde{\mathbf{n}}_k\tilde{\mathbf{n}}_k}\}$.

4 - Updating node q updates its local variables:

$$\mathbf{w}^{i+1}_{qq} = [\mathbf{I}_{M_k} \quad \mathbf{0}]^H \tilde{\mathbf{w}}^i_q. \tag{2.26}$$

- All other nodes do not change their variables:

$$\mathbf{w}^{i+1}_{kk} = \mathbf{w}^i_{kk}. \tag{2.27}$$

5 - All nodes k generate B observations of the estimated desired signal

$$d^{i+1}_k = \tilde{\mathbf{w}}^{i+1,H}_k \tilde{\mathbf{y}}^i_k. \tag{2.28}$$

6 - $i \leftarrow i+1$, $q \leftarrow (q \mod K) + 1$ and return to step 2.

Convergence of Algorithm 1 is proven by linking it to the distributed adaptive covariance-matrix generalized eigenvector estimation (DACGEE) algorithm in [128] and using the scale-invariant property of the GEVD, implying that

[4] In the original GEVD-DANSE algorithm in [101], only the updating node is recomputing the local GEVD-based MWF and the other nodes maintain their estimate from the previous iteration. However, letting each node update their local filter leads to an improved noise reduction performance as demonstrated in [127].

when it is partly compressed with a (scaled) version of the generalized eigenvector belonging to the highest eigenvalue, the value of highest generalized eigenvalue is not altered and its eigenspace can still be recovered. Although the node-specific MWFs are different at each node, they are still related using a linear transformation to the same generalized eigenvector as shown in (2.9). The DACGEE algorithm is using a Gauss-Seidel like updating scheme to find the highest eigenvector of the matrix pencil $\{\mathbf{R_{yy}}, \mathbf{R_{nn}}\}$ given by

$$\hat{\mathbf{x}} = \arg\max_{\mathbf{x}} \ \mathbf{x}^H \mathbf{R_{yy}} \mathbf{x} \tag{2.29}$$

$$s.t. \ \mathbf{x}^H \mathbf{R_{nn}} \mathbf{x} = 1. \tag{2.30}$$

The generalized eigenvector belonging to the highest generalized eigenvalue provides the unique solution (up to a sign ambiguity) and can be divided as $\mathbf{x} = [\mathbf{x}_1^H \ ... \ \mathbf{x}_K^H]^H$ over the different nodes (with $\mathbf{x}_k \in \mathbb{C}^{M_k}$). The DACGEE algorithm then basically proposes to solve the problem in an iterative way, where in each iteration the following problem is solved:

$$\begin{aligned} [\mathbf{x}_q^{i+1}, \{\alpha_k^{i+1}\}_{k \neq q}] = \underset{\mathbf{x}_q, \{\alpha_k\}_{k\neq q}}{\arg\max} \quad & \mathbf{x}^H \mathbf{R_{yy}} \mathbf{x} \\ s.t. \quad & \mathbf{x}^H \mathbf{R_{nn}} \mathbf{x} = 1 \\ & \mathbf{x}_k = \mathbf{x}_k^i \alpha_k \quad \forall k \neq q \end{aligned} \tag{2.31}$$

$$\mathbf{x}_k^{i+1} = \mathbf{x}_k^i \alpha_k^{i+1} \quad \forall k \neq q \tag{2.32}$$

where again q defines the updating node in a round-robin fashion. This is more than a normal Gauss-Seidel block coordinate-ascent update, since it allows to change the other blocks with a scalar multiplication. It is then shown in [101] that $\mathbf{x}_k^i \to \hat{\mathbf{x}}_k$ as $i \to \infty$. It is also shown that $\mathbf{q}_k^i \triangleq [\mathbf{I}_{M_k} \ \ \mathbf{0}]^H \tilde{\mathbf{q}}_k^i \to \hat{\mathbf{q}}_k$ and $\tilde{\sigma}_k^i \to \hat{\sigma}$ for all nodes k.

The general discussion of the basic concepts and applications of the MWF is hereby finalized. The next parts will focus on using the MWF on specific WASANs and CFmMIMO scenarios, and will each time provide novel distributed algorithms to obtain the centralized solution in an efficient distributed way.

Part I

Distributed signal processing algorithms for WAS(A)Ns

Chapter 3

Distributed MWF-based speech enhancement with partial prior knowledge of desired source steering matrix

Distributed Adaptive Signal Estimation in Wireless Sensor Networks with Partial Prior Knowledge of the Desired Sources Steering Matrix.

Robbe Van Rompaey and Marc Moonen

Published in
IEEE Transactions on Signal and Information Processing over Networks, vol. 7, 2021, pp. 478-492.

©2021 IEEE Reprint, with permission from:
R. Van Rompaey and M. Moonen, "Distributed Adaptive Signal Estimation in Wireless Sensor Networks with Partial Prior Knowledge of the Desired Sources Steering Matrix." in *IEEE Transactions on Signal and Information Processing over Networks*, vol. 7, pp. 478-492, 2021.
Changes include layout, representation and minor editing aspects.
The candidate's contributions as first author include all performed research and writing of the article under guidance of the co-author.

Abstract

In the past two decades, wireless sensor networks (WSNs) and their applications have been the topic of many studies. Different multi-sensor nodes are used to collect, process and distribute data over wireless links to perform different tasks such as smart detection, target tracking, node localization, etc. In this paper, the problem of distributed adaptive estimation of node-specific signals for signal enhancement or noise reduction is addressed. First the centralized rank R generalized eigenvalue decomposition (GEVD) based multichannel Wiener filter (MWF) with prior knowledge for node-specific signal estimation in a WSN is introduced, where (some of) the nodes have partial prior knowledge of the desired sources steering matrix. A distributed adaptive estimation algorithm for a fully-connected WSN is then proposed demonstrating that this MWF can be obtained by letting the nodes work on compressed (i.e., reduced-dimensional) sensor signals compared to the centralized algorithm. The distributed algorithm can be used in applications such as speech enhancement in a wireless acoustic sensor network (WASN), where (some of) the nodes have prior knowledge on the location of the desired speech sources and on their local microphone array geometry or have access to clean noise reference signals. Foundations for a proof of convergence using a Lagrangian framework, are given, since convergence is observed in batch-mode simulations. Finally, numerical simulation results are provided for a speech enhancement scenario.

Keywords Wireless Sensor Networks (WSN), distributed estimation, Multichannel Wiener Filter (MWF), generalized eigenvalue decomposition (GEVD), prior knowledge.

3.1 Introduction

In a wireless sensor network (WSN) [24, 26, 129], nodes aim to combine their sensor signals with (possibly compressed) sensor signals of other nodes in some optimal way to perform a task at hand, such as the estimation of a node-specific desired signal [130], smart detection [131], target tracking [132], node localization [133], etc... This generally leads to superior estimation performance compared to the stand-alone performance, where each node uses only local sensor signals. The goal for every node could be to obtain the same estimation performance as if all the sensor signals were collected in a fusion center (FC) [78, 95], but then in a distributed fashion while minimizing the local computations and communications with the other nodes [83, 101, 134].

Node-specific signal estimation is considered here, where the different node-specific desired signals are assumed to be dependent on the same desired sources. The so-called distributed adaptive node-specific signal estimation algorithm (DANSE) and GEVD-DANSE in [83, 101] exploit this common signal subspace, to significantly compress the sensor signals that are communicated between the nodes, without compromising performance. To construct the corresponding signal correlation matrix, the algorithms assume to have access to the activity (on-off) pattern of the desired sources. However, in low SNR scenarios, this might result in a poor estimation of the signal correlation matrix, deteriorating the node-specific signal estimation performance [110]. Inspired by Ali et all. [12, 13], a scenario is considered in this paper where (some of) the nodes have partial prior knowledge of the desired sources steering matrix, which can, for instance, in an acoustic scenario be obtained if nodes have prior knowledge on the location of the desired speech sources and on their local microphone array geometry [135] or have access to clean noise reference signals [136]. In previous work [137], the case where the nodes' desired signals are dependent on only one desired source is investigated and the so-called prior-knowledge GEVD-DANSE (PK-GEVD-DANSE) is proposed. Here this algorithm is extended to multiple desired sources and further theoretical analysis and numerical simulations are provided.

Algorithms in [83, 101] are using either an oracle to find the signal correlation matrix or a fully data-driven approach based on a GEVD and the on-off behavior of the sources to estimate the signal correlation matrix. The introduction of local partial prior knowledge on the signal correlation matrix, which has beneficial effects on the estimation performance as illustrated by [12, 13, 138], has only been done in a centralized fashion (e.g., using a fusion center), since the partial prior knowledge is measured with respect to the noise correlation matrix and the noise is typically correlated between the nodes. However, the PK-GEVD-DANSE shows that the local partial prior knowledge can still be included in the algorithm by allowing the nodes to broadcast twice the number of compressed

signals compared to [83, 101]. Still the performance is improved by exploiting this prior knowledge, justifying this extra communication.

The introduction of prior information to a WSN has already been done for different applications, like inverse source problems in acoustic wave propagation [139,140], distributed optimization [138] and failure detection [141]. Distributed node-specific signal enhancement algorithms with constraints on the node-specific filters, which is mostly posed as a linearly constrained minimum variance (LCMV) beamforming problem [142], has already been investigated [134, 143–145]. However, to construct the constraints in these approaches, it is assumed to either have access to the network-wide steering matrix or an estimate thereof. Here a different approach is considered where it is assumed that (some of) the nodes have partial prior knowledge on the local steering matrix and the relation to the network-wide steering matrix is estimated by the algorithm.

In the rest of the paper, bold lower case letters are used to denote complex vectors, bold upper case letters are used to represent complex matrices and italic upper/lower case letters are used to denote optimization variables. $\mathbf{I}_R$ is the $R \times R$ identity matrix and $\mathbf{0}$ denotes the all zeros matrix whose dimensions will be provided using subscript or will be clear from the context. $||.||$, $||.||_F$ and $E\{.\}$ denote the Euclidean norm, Frobenius norm and expected value operator respectively. Lastly $\text{tr}\{.\}$,$.^*$ and $.^H$ are used to denote the trace, conjugate and conjugate transpose operation. The paper will introduce many different symbols, so a non-exhaustive overview of the most relevant notation is given in Table 3.1. Each symbol in the table will be further explained in the text.

The paper is organized as follows. Section 3.2 introduces the problem formulation of node-specific signal estimation and the centralized rank R generalized eigenvalue decomposition (GEVD) based multichannel Wiener filter (MWF) with prior knowledge for node-specific signal estimation in a WSN, where (some of) the nodes have partial prior knowledge of the desired sources steering matrix are presented . In Section 3.3 an alternative derivation of the centralized algorithm is provided using a Lagrangian framework, where the Lagrange parameters will turn out to play an important role in the distributed algorithm. A distributed adaptive estimation algorithm for a fully-connected WSN is then proposed in Section 3.4 demonstrating that this MWF can be obtained by letting the nodes work on compressed (i.e., reduced-dimensional) sensor signals compared to the centralized algorithm. It turns out that the number of compressed sensor signals communicated by a node that has prior knowledge, will be twice the number of communicated signals needed in previous algorithms [83,101], since extra compressed sensor signals are needed to propagate the prior knowledge to all the other nodes. An argument for convergence is also provided in Section 3.4 as well as the extension to a topology-independent algorithm. Some special cases for which changes to the distributed algorithm are required,

Table 3.1: Overview of used notation.

Notation	Examples of usage	Description
$\bar{\cdot}$	$\bar{\mathbf{R}}_{\mathbf{yy}}, \bar{\mathbf{W}}_k, \bar{\mathbf{d}}_k$	Quantities related to the true (unknown) signals.
$\hat{\cdot}$	$\hat{\mathbf{y}}, \hat{\mathbf{R}}_{\hat{\mathbf{n}}\hat{\mathbf{n}}}, \hat{\mathbf{Q}}, \hat{\mathbf{W}}, \hat{\mathbb{X}}$	Quantities related to the reduced dimensional signals after centralized LCMV-filtering.
$\cdot_k$	$\mathbf{y}_k, \mathbf{H}_k, \mathbf{W}_{kk}, \mathbf{\Lambda}_{kk}, \mathbb{X}_{kk}, \mathbb{\Lambda}_{kk}, \mathbf{z}_k$	Local quantities related to the sensor signals of node k.
$\tilde{\cdot}_k$	$\tilde{\mathbf{y}}_k, \mathbf{R}_{\tilde{\mathbf{n}}_k\tilde{\mathbf{n}}_k}, \tilde{\mathbf{H}}_k, \tilde{\mathbf{C}}_k, \tilde{\mathbf{F}}_k, \tilde{\mathbf{W}}_k, \tilde{\mathbf{\Lambda}}_{kk}, \tilde{\mathbb{X}}_k, \tilde{\mathbb{\Lambda}}_k$	Local quantities related to all the available signals at node k including compressed signals form other nodes.
$\hat{\cdot}_k$	$\hat{\mathbf{y}}_k, \mathbf{R}_{\hat{\mathbf{n}}_k\hat{\mathbf{n}}_k}, \hat{\mathbf{W}}_k, \hat{\mathbb{X}}$	Local quantities related to the reduced dimensional signals after local LCMV-filtering at node k.
$\underline{\cdot}$	$\underline{\mathbf{z}}_k$	Compressed signals related to the local noise references at node k.

are listed in Section 3.5. Section 3.6 provides numerical simulations to show convergence of the proposed distributed algorithm and the performance gains obtained from the availability of prior knowledge. Also the effect of estimation errors in the correlation matrices is experimentally verified. An application of the distributed algorithm to speech enhancement in a wireless acoustic sensor network (WASN) is provided.

3.2 Problem formulation and rank R PK-GEVD-MWF

3.2.1 Node-specific signal estimation

A fully-connected WSN is considered with K nodes, where node $k \in \mathcal{K} = \{1, ..., K\}$ has access to observations of an M_k-dimensional complex-valued sensor signal $\mathbf{y}_k$:

$$\mathbf{y}_k = \mathbf{s}_k + \mathbf{n}_k = \mathbf{A}_k \check{\mathbf{s}} + \mathbf{n}_k \tag{3.1}$$

where $\check{\mathbf{s}}$ is a vector containing the R complex-valued desired source signals, $\mathbf{A}_k$ is a (for the time being) unknown $M_k \times R$-dimensional complex-valued steering matrix and $\mathbf{n}_k$ is an additive noise signal that can be correlated with other noise signals in the WSN. Define also the centralized M-dimensional signals $\mathbf{y}, \mathbf{s}, \mathbf{n}$ and the centralized $M \times R$-dimensional steering matrix $\mathbf{A}$ as the stacked version of $\mathbf{y}_k, \mathbf{s}_k, \mathbf{n}_k$ and $\mathbf{A}_k$ respectively, where $M = \sum_{k=1}^{K} M_k$. Then (3.1) can be extended to

$$\mathbf{y} = \mathbf{s} + \mathbf{n} = \mathbf{A}\check{\mathbf{s}} + \mathbf{n}. \tag{3.2}$$

The node-specific task of node k is to find an estimate of the R-dimensional desired signal $\check{\mathbf{d}}_k$, defined w.l.o.g. as the mixture of desired source signals in the node's first R channels[1]:

$$\bar{\mathbf{d}}_k = [\mathbf{I}_R \ \mathbf{0}_{R\times(M_k-R)}] \ \mathbf{s}_k = \mathbf{E}_k^T \mathbf{s}_k = \mathbf{E}_{\mathbf{d}_k}^T \mathbf{s} \tag{3.3}$$

where $\mathbf{E}_{\mathbf{d}_k} = [\mathbf{0}_{R\times(M_1+...+M_{k-1})} \ \mathbf{E}_k^T \ \mathbf{0}_{R\times(M_{k+1}+...+M_K)}]^T$ selects the correct mixture of desired source signals in $\mathbf{s}$. Each node estimates its desired signal $\bar{\mathbf{d}}_k$ as a linear combination of all the sensor signals in $\mathbf{y}$ by minimizing the following mean squared error (MSE) criterion:

$$\boxed{\bar{\mathbf{W}}_k = \arg\min_{\boldsymbol{W}_k} E\{\|\bar{\mathbf{d}}_k - \boldsymbol{W}_k^H \mathbf{y}\|^2\}.} \tag{3.4}$$

[1]The reason why at least R desired signals are estimated will become clear later on. Special cases such as when $M_k < R$ or $\text{rank}([\mathbf{I}_R \ \mathbf{0}]\mathbf{A}_k) < R$ are discussed in Section 3.5.

The resulting filter is referred to as the multichannel Wiener filter (MWF)[2]. If $\bar{\mathbf{R}}_{\mathbf{yy}} = E\{\mathbf{y}\mathbf{y}^H\}$ has full rank, the unique solution of (3.4) is [104]:

$$\boxed{\begin{aligned}\bar{\mathbf{W}}_k &= \bar{\mathbf{R}}_{\mathbf{yy}}^{-1}\bar{\mathbf{R}}_{\mathbf{yd}_k} = \bar{\mathbf{R}}_{\mathbf{yy}}^{-1}\bar{\mathbf{R}}_{\mathbf{ys}}\mathbf{E}_{\mathbf{d}_k} \\ &= \left(\bar{\mathbf{R}}_{\mathbf{nn}} + \bar{\mathbf{R}}_{\mathbf{ss}}\right)^{-1}\bar{\mathbf{R}}_{\mathbf{ss}}\mathbf{E}_{\mathbf{d}_k}\end{aligned}} \tag{3.5}$$

with $\bar{\mathbf{R}}_{\mathbf{yd}_k} = E\{\mathbf{y}\bar{\mathbf{d}}_k^H\}$, $\bar{\mathbf{R}}_{\mathbf{ys}} = E\{\mathbf{y}\mathbf{s}^H\}$, $\bar{\mathbf{R}}_{\mathbf{nn}} = E\{\mathbf{n}\mathbf{n}^H\}$ and $\bar{\mathbf{R}}_{\mathbf{ss}} = E\{\mathbf{s}\mathbf{s}^H\}$. The last step in (3.5) is allowed due to the (often valid) assumption that the additive noise signal $\mathbf{n}$ and the desired source signals in $\check{\mathbf{s}}$ are uncorrelated. The signal correlation matrix $\bar{\mathbf{R}}_{\mathbf{ss}}$ is then given by $\mathbf{A}E\{\check{\mathbf{s}}\check{\mathbf{s}}^H\}\mathbf{A}^H$, where $E\{\check{\mathbf{s}}\check{\mathbf{s}}^H\}$ is a diagonal matrix containing the desired source signal powers. Notice that $\bar{\mathbf{R}}_{\mathbf{ss}}$ is not directly observable, since nodes do not have access to the clean desired source signal component $\mathbf{s}_k$. A robust way to estimate the signal correlation matrix $\bar{\mathbf{R}}_{\mathbf{ss}}$ is given in the next subsection, based on the exploitation of the on-off behavior of the desired source signals to first estimate $\bar{\mathbf{R}}_{\mathbf{yy}}$ and $\bar{\mathbf{R}}_{\mathbf{nn}}$ and on partial prior knowledge of the desired sources steering matrix $\mathbf{A}$. A bird's eye view on the system model is given in Figure 3.1.

3.2.2 Centralized rank R $\bar{\mathbf{R}}_{\mathbf{ss}}$ estimation

If the desired source signals have a simultaneous on-off behavior and the on-off detection is available, e.g., via a centralized [106, 108] or distributed [107] multi-speaker voice activity detector in speech applications, a distinction can be made between the *signal+noise* and *noise-only* periods to estimate the correlation matrix $\bar{\mathbf{R}}_{\mathbf{yy}}$ and $\bar{\mathbf{R}}_{\mathbf{nn}}$ respectively. The estimation can be done by (recursive) time-averaging during *signal+noise* and *noise-only* periods if $\mathbf{y}$ is assumed to satisfy (short-term) stationarity and ergodicity conditions and the estimates will be denoted by $\mathbf{R}_{\mathbf{yy}}$ and $\mathbf{R}_{\mathbf{nn}}$ respectively.

$\bar{\mathbf{R}}_{\mathbf{ss}}$ can then be estimated[3] as $\mathbf{R}_{\mathbf{ss}} = \mathbf{R}_{\mathbf{yy}} - \mathbf{R}_{\mathbf{nn}}$. However, such an estimate has mostly a rank larger than R and might not even be positive definite, especially in low SNR scenarios [110], so that a better correlation matrix estimation method is needed.

[2]Notice that all above signals and filters are defined as complex-valued signals, permitting the model to include, e.g., convolutive time-domain mixtures, described as instantaneous per-frequency mixtures in the (short-term) Fourier transform domain, making it also applicable for speech enhancement.

[3]Note that the true signal correlation matrices are denoted by $\bar{\mathbf{R}}_{\mathbf{yy}}, \bar{\mathbf{R}}_{\mathbf{nn}}$ and $\bar{\mathbf{R}}_{\mathbf{ss}}$, the measured correlation matrices are denoted by $\mathbf{R}_{\mathbf{yy}}$ and $\mathbf{R}_{\mathbf{nn}}$ and the estimated signal correlation matrices using the measured correlation matrices is denoted by $\mathbf{R}_{\mathbf{ss}}$.

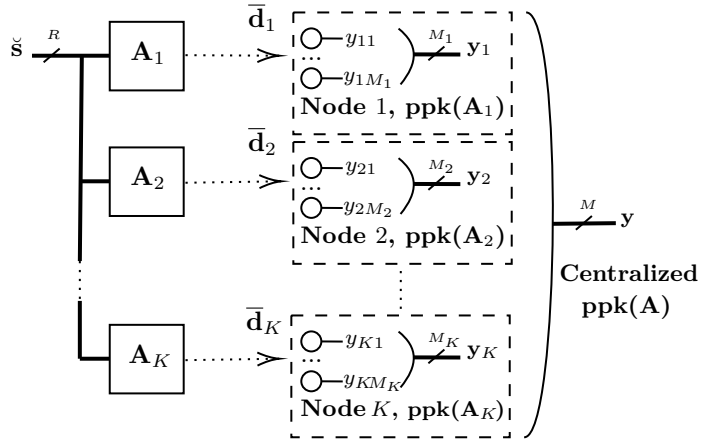

Figure 3.1: Bird's eye view on system model. The network contains K nodes, where node k collects M_k sensor signals and estimates a node-specific R-dimensional desired signal $\bar{\mathbf{d}}_k$, which is a mixture of the R source signals and where ppk($\mathbf{A}_k$) denotes possible partial prior knowledge on the steering matrix $\mathbf{A}_k$ available at node k.

A better method to estimate the signal correlation matrix, used in the so-called GEVD-MWF, is given by solving the following optimization problem [110, 146]:

$$\mathbf{R}_{\mathbf{ss}} = \underset{\text{rank}(\boldsymbol{R}_{\mathbf{ss}})=R}{\arg\min} \| \mathbf{R}_{\mathbf{nn}}^{-1/2} (\mathbf{R}_{\mathbf{yy}} - \mathbf{R}_{\mathbf{nn}} - \boldsymbol{R}_{\mathbf{ss}}) \mathbf{R}_{\mathbf{nn}}^{-H/2} \|_F^2 \tag{3.6}$$

of which the solution is based on the GEVD of the matrix pencil $\{\mathbf{R}_{\mathbf{yy}}, \mathbf{R}_{\mathbf{nn}}\}$ and will be defined later on. Here $\mathbf{R}_{\mathbf{ss}}$ is constrained to be rank R and approximation errors are considered relative to the estimated noise correlation matrix $\mathbf{R}_{\mathbf{nn}}$ (cfr. the pre- and post-multiplication with the Cholesky factor of $\mathbf{R}_{\mathbf{nn}}^{-1} = \mathbf{R}_{\mathbf{nn}}^{-H/2} \mathbf{R}_{\mathbf{nn}}^{-1/2}$).

Recently [12,13,137] extended optimization problem (3.6) by introducing partial prior knowledge of the desired source steering vector for a single desired source signal scenario. Partial prior knowledge is here imposed by constraining the row- and column space of $\mathbf{R}_{\mathbf{ss}}$ to a given subspace.

Extending this method in the WSN context and to multiple desired source signals, one can consider a scenario where a node k has prior knowledge on the columnspace of the local steering matrix $\mathbf{A}_k$, represented by a unitary $M_k \times L_k$ subspace matrix $\mathbf{H}_k$. An example scenario is presented in Section 3.6. The orthogonal complement to the column space of $\mathbf{H}_k$ is then represented by a unitary $M_k \times (M_k - L_k)$ blocking matrix $\mathbf{B}_k$, such that $\mathbf{H}_k^H \mathbf{B}_k = \mathbf{0}$. Stacking

these subspace and blocking matrices in one centralized subspace and blocking matrix respectively results in

$$\mathbf{H} = \begin{bmatrix} \mathbf{H}_1 & \cdots & \mathbf{0} \\ \vdots & \ddots & \vdots \\ \mathbf{0} & \cdots & \mathbf{H}_K \end{bmatrix}, \mathbf{B} = \begin{bmatrix} \mathbf{B}_1 & \cdots & \mathbf{0} \\ \vdots & \ddots & \vdots \\ \mathbf{0} & \cdots & \mathbf{B}_K \end{bmatrix} \tag{3.7}$$

where $\mathbf{H}$ is a block diagonal $M \times L$ matrix and $\mathbf{B}$ a block diagonal $M \times (M-L)$ matrix with $L = \sum_{k=1}^{K} L_k$. Here $M - L$ is representing the amount of prior knowledge available, summed over all the nodes, with $L \geq R$ since $\mathbf{A}$ is assumed to be rank R. An extreme case is when node k does not have any prior knowledge, then $\mathbf{H}_k = \mathbf{I}_{M_k}$ and $\mathbf{B}_k = \begin{bmatrix} \end{bmatrix}$ and so $M_k - L_k = 0$ ('zero prior knowledge'). Another extreme case is when node k knows its local steering matrix $\mathbf{A}_k$ (up to a random $R \times R$ invertible matrix $\mathbf{G}$) , then $\mathbf{H}_k = \mathbf{A}_k\mathbf{G}$ and so $M_k - L_k = M_k - R$. An in-between case is where some of the sensor signals in node k are known to be clean noise reference signals. For instance, when the first sensor signal in node k is a clean noise reference signal, then

$$\mathbf{H}_k = \begin{bmatrix} \mathbf{0} \\ \mathbf{I}_{M_{k-1}} \end{bmatrix}; \mathbf{B}_k = \begin{bmatrix} 1 \\ \mathbf{0} \end{bmatrix} \tag{3.8}$$

and so $M_k - L_k = 1$.

Note that this representation of the prior knowledge is very relevant for an ad-hoc WSN, since a node only has to be aware of the locations of its local sensors, but not of the location of the sensors of other nodes. So if one node changes the position of its sensors, the prior knowledge of the other nodes remains unchanged.

The following centralized optimization criterion is then defined to provide an improved estimate for $\bar{\mathbf{R}}_{\mathbf{ss}}$:

$$\mathbf{R}_{\mathbf{ss}} = \underset{\substack{\text{rank}(\boldsymbol{R}_{\mathbf{ss}})=R \\ \mathbf{B}^H \boldsymbol{R}_{\mathbf{ss}} \mathbf{B} = \mathbf{0}}}{\arg\min} \| \mathbf{R}_{\mathbf{nn}}^{-1/2} (\mathbf{R}_{\mathbf{yy}} - \mathbf{R}_{\mathbf{nn}} - \boldsymbol{R}_{\mathbf{ss}}) \mathbf{R}_{\mathbf{nn}}^{-H/2} \|_F^2 . \tag{3.9}$$

where the column and row space of $\mathbf{R}_{\mathbf{ss}}$ are now also constrained to lie in the column space of $\mathbf{H}$.

As shown in Appendix B.2, the solution of (3.9) can equivalently be obtained by solving

$$\mathbf{R}_{\hat{\mathbf{s}}\hat{\mathbf{s}}} = \underset{\text{rank}(\boldsymbol{R}_{\hat{\mathbf{s}}\hat{\mathbf{s}}})=R}{\arg\min} \| \mathbf{R}_{\hat{\mathbf{n}}\hat{\mathbf{n}}}^{-1/2} (\mathbf{R}_{\hat{\mathbf{y}}\hat{\mathbf{y}}} - \mathbf{R}_{\hat{\mathbf{n}}\hat{\mathbf{n}}} - \boldsymbol{R}_{\hat{\mathbf{s}}\hat{\mathbf{s}}}) \mathbf{R}_{\hat{\mathbf{n}}\hat{\mathbf{n}}}^{-H/2} \|_F^2 . \tag{3.10}$$

The reduced $L \times L$-dimensional correlation matrices $\{\mathbf{R}_{\hat{\mathbf{y}}\hat{\mathbf{y}}}, \mathbf{R}_{\hat{\mathbf{n}}\hat{\mathbf{n}}}\}$ defined as

$$\begin{aligned} \mathbf{R}_{\hat{\mathbf{y}}\hat{\mathbf{y}}} &= \mathbf{C}^H \mathbf{R}_{\mathbf{yy}} \mathbf{C} \\ \mathbf{R}_{\hat{\mathbf{n}}\hat{\mathbf{n}}} &= \mathbf{C}^H \mathbf{R}_{\mathbf{nn}} \mathbf{C} \end{aligned} \tag{3.11}$$

are determined as the correlation matrices corresponding to the compressed signal $\hat{\mathbf{y}} = \mathbf{C}^H\mathbf{y}$, where $\mathbf{C} \in \mathbb{C}^{M\times L}$ can be defined using the following LCMV-criterion:

$$\mathbf{C} = \underset{\mathbf{H}^H\boldsymbol{C}=\mathbf{I}_L}{\arg\min}\ \mathrm{tr}\{\boldsymbol{C}^H\mathbf{R}_{\mathbf{nn}}\boldsymbol{C}\} \tag{3.12}$$

where every column of $\mathbf{C}$ represents a specific LCMV-beamformer. The solution, here based on a generalized sidelobe canceller (GSC)-implementation [147], is given by

$$\mathbf{C} = \mathbf{H} - \mathbf{B}\mathbf{F} \tag{3.13}$$

$$\mathbf{F} = (\mathbf{B}^H\mathbf{R}_{\mathbf{nn}}\mathbf{B})^{-1}\mathbf{B}^H\mathbf{R}_{\mathbf{nn}}\mathbf{H}. \tag{3.14}$$

where $\mathbf{F} \in \mathbb{C}^{M-L\times L}$ is the filter estimating the noise component in the fixed beamformer branch $\mathbf{H}^H\mathbf{n}$ from the noise references $\mathbf{B}^H\mathbf{n}$:

$$\mathbf{F} = \underset{\boldsymbol{F}}{\arg\min}\, E\{\|\mathbf{H}^H\mathbf{n} - \boldsymbol{F}^H\mathbf{B}^H\mathbf{n}\|^2\}. \tag{3.15}$$

$\mathbf{C}$ can be verified to satisfy (B.7) since $\mathbf{C}^H\mathbf{H} = \mathbf{I}_L$ and $\mathbf{C}^H\mathbf{R}_{\mathbf{nn}}\mathbf{B} = \mathbf{0}$.

The solution to (3.10) is based on the GEVD [104, 148] of the reduced $L \times L$-dimensional matrix pencil $\{\mathbf{R}_{\hat{\mathbf{y}}\hat{\mathbf{y}}}, \mathbf{R}_{\hat{\mathbf{n}}\hat{\mathbf{n}}}\}$:

$$\begin{aligned}\mathbf{R}_{\hat{\mathbf{y}}\hat{\mathbf{y}}} &= \hat{\mathbf{Q}}\hat{\mathbf{\Sigma}}\hat{\mathbf{Q}}^H \\ \mathbf{R}_{\hat{\mathbf{n}}\hat{\mathbf{n}}} &= \hat{\mathbf{Q}}\hat{\mathbf{Q}}^H\end{aligned} \tag{3.16}$$

Here, $\hat{\mathbf{Q}} = \hat{\mathbf{X}}^{-H}$ is an invertible matrix, the columns of $\hat{\mathbf{X}}$ are unique (up to a sign-ambiguity) and define the generalized eigenvectors. $\hat{\mathbf{\Sigma}}$ is a real-valued diagonal matrix where $\hat{\mathbf{\Sigma}} = \mathrm{diag}\{\hat{\sigma}_1, ..., \hat{\sigma}_L\}$ defines the generalized eigenvalues sorted from large to small.

Finally the estimate $\mathbf{R}_{\mathbf{ss}}$ of (3.9) is given by [111]

$$\begin{aligned}\mathbf{R}_{\mathbf{ss}} &= \mathbf{H}\hat{\mathbf{Q}}\mathrm{diag}\{\hat{\sigma}_1 - 1, ..., \hat{\sigma}_R - 1, 0, ..., 0\}\hat{\mathbf{Q}}^H\mathbf{H}^H \\ &= \mathbf{H}\hat{\mathbb{Q}}\Sigma_{\hat{\mathbf{s}}\hat{\mathbf{s}}}\hat{\mathbb{Q}}^H\mathbf{H}^H\end{aligned} \tag{3.17}$$

where $\hat{\mathbb{Q}}$ contains the first R columns of $\hat{\mathbf{Q}}$ and $\Sigma_{\hat{\mathbf{s}}\hat{\mathbf{s}}} = \mathrm{diag}\{\hat{\sigma}_1 - 1, ..., \hat{\sigma}_R - 1\}$.

3.2.3 Centralized rank R PK-GEVD-MWF

Substituting estimate $\mathbf{R}_{\mathbf{ss}}$ of (3.17) and $\mathbf{R}_{\mathbf{nn}}$ as $\bar{\mathbf{R}}_{\mathbf{ss}}$ and $\bar{\mathbf{R}}_{\mathbf{nn}}$ respectively in (3.5), after some manipulations provided in Appendix B.3, results in the following estimate of the MWF in (3.4):

$$\boxed{\mathbf{W}_k = \mathbf{C}\hat{\mathbf{W}}\mathbf{H}^H\mathbf{E}_{\mathbf{d}_k}} \tag{3.18}$$

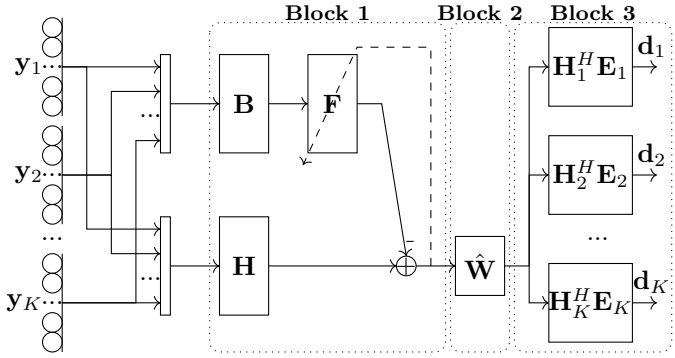

Figure 3.2: Schematic overview of the rank R PK-GEVD-MWF

where

$$\begin{aligned}\hat{\mathbf{W}} &= \hat{\mathbf{X}}\text{diag}\{\frac{\hat{\sigma}_1 - 1}{\hat{\sigma}_1}, ..., \frac{\hat{\sigma}_R - 1}{\hat{\sigma}_R}, 0, ..., 0\}\hat{\mathbf{Q}}^H \\ &= \hat{\mathbb{X}}\text{diag}\{\frac{\hat{\sigma}_1 - 1}{\hat{\sigma}_1}, ..., \frac{\hat{\sigma}_R - 1}{\hat{\sigma}_R}\}\hat{\mathbb{Q}}^H\end{aligned} \tag{3.19}$$

is the GEVD-based MWF [101, 110] that estimates $\hat{\mathbf{s}} = \mathbf{C}^H\mathbf{s}$ from $\hat{\mathbf{y}} = \mathbf{C}^H\mathbf{y}$. Here $\hat{\mathbb{X}}$ contains the first R columns of $\hat{\mathbf{X}}$.

The filter obtained in (3.18) is referred to as the rank R prior-knowledge GEVD-based MWF (rank R PK-GEVD-MWF) and the formula shows that the resulting filter is a concatenation of three different blocks. The first block corresponds to the LCMV-beamformer (3.12), the second block is a rank R GEVD-based MWF and the last block is a selection and scaling part, specific to node k, to produce an estimate $\mathbf{d}_k$ of the desired signal $\bar{\mathbf{d}}_k$. A schematic overview of the rank R PK-GEVD-MWF is given in Figure 3.2.

To determine the centralized rank R PK-GEVD-MWF, the correlation matrices $\mathbf{R}_{\mathbf{yy}}$ and $\mathbf{R}_{\mathbf{nn}}$ have to be constructed first. This would require each node k to send all of its M_k sensor signals in $\mathbf{y}_k$ to a FC, which will require a large communication bandwidth. Furthermore, as these correlation matrices are large, the inversion of $\mathbf{B}^H\mathbf{R}_{\mathbf{nn}}\mathbf{B}$ in (3.14) and the GEVD in (3.19) will require significant computational power at the FC.

To overcome this complexity problem, a distributed adaptive estimation algorithm is presented in this paper. However, in the next section the centralized rank R PK-GEVD-MWF is first derived alternatively using a Lagrangian framework, since the expression for the Lagrange parameters will turn out to play an important in the distributed filter.

3.3 Lagrangian perspective on rank R PK-GEVD-MWF

In this section expression (3.18) for the rank R PK-GEVD-MWF is derived via a different optimization problem. First notice that all the node-specific rank R PK-GEVD-MWFs have a common column space, which can be observed from

$$\mathbf{W}_k = \underbrace{\mathbf{C}\hat{\mathbb{X}}}_{\mathbb{X}} \underbrace{\text{diag}\{\frac{\hat{\sigma}_1 - 1}{\hat{\sigma}_1}, ..., \frac{\hat{\sigma}_R - 1}{\hat{\sigma}_R}\}\hat{\mathbb{Q}}^H \mathbf{H}^H \mathbf{E}_{\mathbf{d}_k}}_{\mathbf{G}_k} \tag{3.20}$$

where $\mathbf{G}_k$ is a node-specific non-singular $R \times R$ matrix and $\mathbb{X}$ is common for all filters $\mathbf{W}_k$. In the following, the optimization problem is proposed for the node-independent variable $\mathbb{X} \in \mathbb{C}^{M \times R}$ and by later using the substitution

$$\mathbb{X} = \mathbf{W}_k \mathbf{G}_k^{-1} \tag{3.21}$$

expression (3.18) and the corresponding Lagrange parameters will be obtained.

A different optimization problem that, as shown in the following derivation, will result in the same expression for $\mathbb{X}$, is given as follows:

$$\mathbb{X} = \underset{\substack{\mathbb{X}^H \mathbf{R}_{\mathbf{nn}} \mathbb{X} = \mathbf{I}_R \\ \mathbf{B}^H \mathbf{R}_{\mathbf{nn}} \mathbb{X} = \mathbf{0}}}{\arg\max} \ \text{tr}\{\mathbb{X}^H \mathbf{R}_{\mathbf{yy}} \mathbb{X}\}. \tag{3.22}$$

Without the last equality constraint ($\mathbf{B}^H \mathbf{R}_{\mathbf{nn}} \mathbb{X} = \mathbf{0}$), $\mathbb{X}$ would contain the R principal generalized eigenvectors of the matrix pencil $\{\mathbf{R}_{\mathbf{yy}}, \mathbf{R}_{\mathbf{nn}}\}$ corresponding to the largest generalized eigenvalues. Note that the optimal solution of (3.22) will never be unique, since $\mathbb{X}\mathbf{U}$ with $\mathbf{U}\mathbf{U}^H = \mathbf{I}_R$ gives the same objective function while satisfying all the constraint. This non-uniqueness problem is averted by constraining $\mathbb{X}^H \mathbf{R}_{\mathbf{yy}} \mathbb{X}$ to be a diagonal matrix with its (real) diagonal elements sorted from large to small.[4]

Since problem (3.22) is a constrained optimization problem, it can be solved using a Langrangian framework implying that the solution of (3.22) is given by saddle points (or in this case stationary points) of the Lagrangian function [149]:

$$\begin{aligned} L(\mathbb{X}, \boldsymbol{M}, \mathbb{\Lambda}) = \text{tr}\{\mathbb{X}^H \mathbf{R}_{\mathbf{yy}} \mathbb{X}\} + \text{tr}\{\boldsymbol{M}^H (\mathbb{X}^H \mathbf{R}_{\mathbf{nn}} \mathbb{X} - \mathbf{I}_R) \\ + (\mathbb{X}^H \mathbf{R}_{\mathbf{nn}} \mathbb{X} - \mathbf{I}_R) \boldsymbol{M}\} \\ - \text{tr}\{\mathbb{\Lambda}^H \mathbf{B}^H \mathbf{R}_{\mathbf{nn}} \mathbb{X} + \mathbb{X}^H \mathbf{R}_{\mathbf{nn}} \mathbf{B} \mathbb{\Lambda}\}. \end{aligned} \tag{3.23}$$

[4] There is still a sign ambiguity for each column of $\check{\mathbb{X}}$, but this sign ambiguity is compensated by $\mathbf{G}_k$ to obtain a unique PK-GEVD-MWF $\mathbf{W}_k$.

The stationary points are given by the following set of equations

$$\begin{aligned}\nabla_{\mathbb{X}^*} L(.) &= \mathbf{R_{yy}}\mathbb{X} + \mathbf{R_{nn}}\mathbb{X}(\boldsymbol{M} + \boldsymbol{M}^H) - \mathbf{R_{nn}}\mathbf{B}\mathbb{\Lambda} = \mathbf{0} \\ \nabla_{\boldsymbol{M}^*} L(.) &= \mathbb{X}^H\mathbf{R_{nn}}\mathbb{X} - \mathbf{I}_R = \mathbf{0} \\ \nabla_{\mathbb{\Lambda}^*} L(.) &= \mathbf{B}^H\mathbf{R_{nn}}\mathbb{X} = \mathbf{0}.\end{aligned} \tag{3.24}$$

The uniqueness constraint of $\mathbb{X}$ can then be imposed by forcing $(\boldsymbol{M} + \boldsymbol{M}^H)$ to be a (real) diagonal matrix with its (real) diagonal elements sorted from large to small. Substituting $\mathbb{X} = \mathbf{C}\hat{\mathbb{X}}$ in (3.24), where $\mathbf{C}$ is defined in (B.7), results in

$$\begin{aligned}&\mathbf{R_{yy}}\mathbf{C}\hat{\mathbb{X}} + \mathbf{R_{nn}}\mathbf{C}\hat{\mathbb{X}}(\boldsymbol{M} + \boldsymbol{M}^H) - \mathbf{R_{nn}}\mathbf{B}\mathbb{\Lambda} = \mathbf{0} \\ &\hat{\mathbb{X}}^H\mathbf{C}^H\mathbf{R_{nn}}\mathbf{C}\hat{\mathbb{X}} - \mathbf{I}_R = \mathbf{0} \\ &\mathbf{B}^H\mathbf{R_{nn}}\mathbf{C}\hat{\mathbb{X}} = \mathbf{0}\hat{\mathbb{X}} = \mathbf{0}.\end{aligned} \tag{3.25}$$

The last equation is then automatically fulfilled for every $\hat{\mathbb{X}}$. Multiplying the first equation first with $\mathbf{C}^H$ and then with $\mathbf{B}^H$, results in (using (3.16))

$$\begin{aligned}&\mathbf{R}_{\hat{\mathbf{y}}\hat{\mathbf{y}}}\hat{\mathbb{X}} + \mathbf{R}_{\hat{\mathbf{n}}\hat{\mathbf{n}}}\hat{\mathbb{X}}(\boldsymbol{M} + \boldsymbol{M}^H) = \mathbf{0} \\ &\mathbf{B}^H\mathbf{R_{yy}}\mathbf{C}\hat{\mathbb{X}} - \mathbf{B}^H\mathbf{R_{nn}}\mathbf{B}\mathbb{\Lambda} = \mathbf{0} \\ &\hat{\mathbb{X}}^H\mathbf{R}_{\hat{\mathbf{n}}\hat{\mathbf{n}}}\hat{\mathbb{X}} - \mathbf{I}_R = \mathbf{0}.\end{aligned} \tag{3.26}$$

Looking at the first and last equation and taking the objective ($\mathrm{tr}\{\mathbb{X}^H\mathbf{R_{yy}}\mathbb{X}\} = \mathrm{tr}\{\hat{\mathbb{X}}^H\mathbf{R}_{\hat{\mathbf{y}}\hat{\mathbf{y}}}\hat{\mathbb{X}}\}$) into account, one can see that the optimal $\hat{\mathbb{X}}$ contains the R generalized eigenvectors of the matrix pair $\{\mathbf{R}_{\hat{\mathbf{y}}\hat{\mathbf{y}}}, \mathbf{R}_{\hat{\mathbf{n}}\hat{\mathbf{n}}}\}$ corresponding to the largest generalized eigenvalues. The optimal $\mathbb{X}$ can then be found using $\mathbb{X} = \mathbf{C}\hat{\mathbb{X}}$ which is exactly the same expression for $\mathbb{X}$ as in (3.20). The optimal value of $\mathbb{\Lambda}$ is given by

$$\mathbb{\Lambda} = (\mathbf{B}^H\mathbf{R_{nn}}\mathbf{B})^{-1}\mathbf{B}^H\mathbf{R_{yy}}\mathbb{X}. \tag{3.27}$$

Both $\mathbb{X}$ and $\mathbb{\Lambda}$ will play an important role as compression matrices for the distributed algorithm presented in the next section.

Using the substitution defined in (3.21), the node-specific Lagrange parameter is given by

$$\begin{aligned}\mathbf{\Lambda}_k &= (\mathbf{B}^H\mathbf{R_{nn}}\mathbf{B})^{-1}\mathbf{B}^H\mathbf{R_{yy}}\mathbb{X}\mathbf{G}_k \\ &= (\mathbf{B}^H\mathbf{R_{nn}}\mathbf{B})^{-1}\mathbf{B}^H\mathbf{R_{yy}}\mathbf{W}_k.\end{aligned} \tag{3.28}$$

Before presenting the distributed PK-GEVD-DANSE, some extra definitions are introduced. A partitioning of the filter $\mathbf{W}_k$ is defined as $\mathbf{W}_k = [\mathbf{W}_{k1}^T \ ... \ \mathbf{W}_{kN}^T]^T$ where $\mathbf{W}_{kq}$ denotes the $M_k \times R$ submatrix of $\mathbf{W}_k$ that is applied to $\mathbf{y}_q$ in (3.4). Similarly a partitioning of $\mathbf{\Lambda}_k$ is defined as $\mathbf{\Lambda}_k = [\mathbf{\Lambda}_{k1}^T \ ... \ \mathbf{\Lambda}_{kN}^T]^T$ where $\mathbf{\Lambda}_{kq}$ denotes the $(M_k - L_k) \times R$ submatrix of $\mathbf{\Lambda}_k$ that is multiplied with $\mathbf{B}_q$ in (3.23). Note that for the optimal filters $\mathbf{W}_k$ and Lagrange parameters $\mathbf{\Lambda}_k$, the following relations hold:

$$\begin{aligned} \mathbf{W}_{kq} &= \mathbb{X}_{kk}\mathbf{G}_q \\ \mathbf{\Lambda}_{kq} &= \mathbb{\Lambda}_{kk}\mathbf{G}_q \end{aligned} \tag{3.29}$$

with $\mathbb{X} = [\mathbb{X}_{11}^T \ ... \ \mathbb{X}_{NN}^T]^T$ and $\mathbb{\Lambda} = [\mathbb{\Lambda}_{11}^T \ ... \ \mathbb{\Lambda}_{NN}^T]^T$ defined similarly.

3.4 Rank R PK-GEVD-DANSE

To overcome the complexity problem that emerges when all M sensor signals in $\mathbf{y}$ are sent to a FC, a distributed adaptive estimation algorithm is presented in this section. In a fully-connected WSN each node then broadcasts only $2R$ compressed sensor signals and the computations in each node are performed on a smaller number of signals[5], i.e., only the local sensor signals and the received compressed sensor signals from the other nodes. It will turn out that each node will (upon convergence) still obtain the same desired signal estimates as if the node had access to all the sensor signals in the WSN and so could directly compute the centralized rank R PK-GEVD-MWF. The distributed algorithm is referred to as the rank R Prior Knowledge GEVD-based Distributed Adaptive Node-Specific Signal Estimation (rank R PK-GEVD-DANSE) after DANSE and GEVD-DANSE of [83] and [101]. A drawback of the rank R PK-GEVD-DANSE is the slower adaptation and tracking speed compared to the centralized rank R PK-GEVD-MWF, since the rank R PK-GEVD-DANSE needs multiple iterations on the same data to converge to the optimal centralized rank R PK-GEVD-MWF.

3.4.1 Algorithm description

In the rank R PK-GEVD-DANSE, in one iteration i, each node k broadcasts, instead of observations of the full M_k sensor signal $\mathbf{y}_k$, observations of $2R$ compressed sensor signals:

[5] In an iteration of Algorithm 2, the inversion of a reduced-dimensional matrix $\tilde{\mathbf{B}}_q^H \mathbf{R}_{\tilde{\mathbf{n}}_q \tilde{\mathbf{n}}_q} \tilde{\mathbf{B}}_q$ and the GEVD of a reduced dimensional matrix pencil $\{\mathbf{R}_{\hat{\mathbf{y}}_q \hat{\mathbf{y}}_q}, \mathbf{R}_{\hat{\mathbf{n}}_q \hat{\mathbf{n}}_q}\}$ are needed.

- the signal $\mathbf{z}_k^i = \mathbf{W}_{kk}^{i,H}\mathbf{y}_k$ where the $M_k \times R$-dimensional compression matrix $\mathbf{W}_{kk}^i$ is obtained by partitioning $\mathbf{W}_k^i$, which is an estimate of $\mathbf{W}_k$ in iteration i;
- the signal $\underline{\mathbf{z}}_k^i = \mathbf{\Lambda}_{kk}^{i,H}\mathbf{B}_k^H\mathbf{y}_k$ corresponding to compressed versions of the local noise references $\mathbf{B}_k^H\mathbf{y}_k$, where the $(M_k - L_k) \times R$ compression matrix $\mathbf{\Lambda}_{kk}^i$ is obtained by partitioning $\mathbf{\Lambda}_k^i$, which is an estimate of $\mathbf{\Lambda}_k$ in iteration i.

Consequently, each node k has access to observations of the reduced-dimensional sensor signal $\tilde{\mathbf{y}}_k^i = [\mathbf{y}_k^T \ \mathbf{z}_{-k}^{i,T} \ \underline{\mathbf{z}}_{-k}^{i,T}]^T$ where the subscript $_{-k}$ refers to the concatenation of the compressed sensor signals of the other nodes, i.e.,

$$\mathbf{z}_{-k}^i = [\mathbf{z}_1^{i,T} ... \ \mathbf{z}_{k-1}^{i,T} \ \mathbf{z}_{k+1}^{i,T} \ ... \ \mathbf{z}_K^{i,T}]^T \tag{3.30}$$

$$\underline{\mathbf{z}}_{-k}^i = [\underline{\mathbf{z}}_1^{i,T} ... \ \underline{\mathbf{z}}_{k-1}^{i,T} \ \underline{\mathbf{z}}_{k+1}^{i,T} \ ... \ \underline{\mathbf{z}}_K^{i,T}]^T. \tag{3.31}$$

To be able to perform the same operations as in the centralized rank R PK-GEVD-MWF on these reduced-dimensional sensor signals, the following subspace matrix $\tilde{\mathbf{H}}_k$ and corresponding blocking matrix $\tilde{\mathbf{B}}_k$ are defined for node k:

$$\tilde{\mathbf{H}}_k = \begin{bmatrix} \mathbf{H}_k & \mathbf{0} \\ \mathbf{0} & \mathbf{I}_{R(K-1)} \\ \mathbf{0} & \mathbf{0} \end{bmatrix}; \quad \tilde{\mathbf{B}}_k = \begin{bmatrix} \mathbf{B}_k & \mathbf{0} \\ \mathbf{0} & \mathbf{0} \\ \mathbf{0} & \mathbf{I}_{R(K-1)} \end{bmatrix}. \tag{3.32}$$

The steering matrix subspace for $\mathbf{y}_k$ is defined by $\mathbf{H}_k$ and so represented by $\mathbf{H}_k$ and $\mathbf{B}_k$ in $\tilde{\mathbf{H}}_k$ and $\tilde{\mathbf{B}}_k$ respectively. The steering matrix subspace for $\mathbf{z}_{-k}^i$ is unknown and thus represented by $\mathbf{I}_{R(K-1)}$ in $\tilde{\mathbf{H}}_k$ and by $[\ ]$ in $\tilde{\mathbf{B}}_k$. The steering matrix subspace for $\underline{\mathbf{z}}_{-k}^i$ is empty because this signal is a compressed version of the local noise references ($\mathbf{B}_k^H\mathbf{y}_k = \mathbf{B}_k^H\mathbf{a}_k\check{s} + \mathbf{B}_k^H\mathbf{n}_k = \mathbf{B}_k^H\mathbf{n}_k$), where the signal component is already locally canceled and is represented by $[\ ]$ in $\tilde{\mathbf{H}}_k$ and hence by $\mathbf{I}_{R(K-1)}$ in $\tilde{\mathbf{B}}_k$.

The rank R PK-GEVD-DANSE is presented in Algorithm 2. This is a block-iterative round-robin algorithm[6], where the updating node performs the same operations as in the centralized rank R PK-GEVD-MWF, but here with locally defined reduced-dimensional variables $\tilde{\mathbf{F}}_k, \tilde{\mathbf{C}}_k, \hat{\tilde{\mathbf{W}}}_k$ and $\tilde{\mathbf{W}}_k$. A schematic overview of the local rank R PK-GEVD-MWF is given in Figure 3.3.

[6]Instead of round-robin updates, simultaneous and asynchronous updating as discussed in [85], requiring relaxed updates in (3.38) and (3.39), can also be performed, but this is not discussed here for ease of exposition.

Algorithm 2: rank R PK-GEVD-DANSE

1 - All nodes $k \in \mathcal{K}$ construct $\tilde{\mathbf{H}}_k$ and $\tilde{\mathbf{B}}_k$ using node k's prior knowledge, initialize $\mathbf{W}_{kk}^0$ and $\mathbf{\Lambda}_{kk}^0$ as random matrices
- $i \leftarrow 0$ and $q \leftarrow 1$.
2 - All nodes $k \in \mathcal{K}$ broadcast B observations of $\mathbf{z}_k = \mathbf{W}_{kk}^{i,H}\mathbf{y}_k$ and $\underline{\mathbf{z}}_k = \mathbf{\Lambda}_{kk}^{i,H}\mathbf{B}_k^H\mathbf{y}_k$ and construct locally

$$\tilde{\mathbf{y}}_k^i = [\mathbf{y}_k^T \ \mathbf{z}_{-k}^{i,T} \ \underline{\mathbf{z}}_{-k}^{i,T}]^T. \tag{3.33}$$

3 - Updating node q estimates $\mathbf{R}_{\tilde{\mathbf{n}}_q\tilde{\mathbf{n}}_q}$ based on the B observations and updates its local LCMV-beamformer:

$$\tilde{\mathbf{F}}_q^{i+1} = \left(\tilde{\mathbf{B}}_q^H\mathbf{R}_{\tilde{\mathbf{n}}_q\tilde{\mathbf{n}}_q}\tilde{\mathbf{B}}_q\right)^{-1}\tilde{\mathbf{B}}_q^H\mathbf{R}_{\tilde{\mathbf{n}}_q\tilde{\mathbf{n}}_q}\tilde{\mathbf{H}}_q \tag{3.34}$$

$$\tilde{\mathbf{C}}_q^{i+1} = \tilde{\mathbf{H}}_q - \tilde{\mathbf{B}}_q\tilde{\mathbf{F}}_q^{i+1}, \quad \hat{\mathbf{y}}_q = \tilde{\mathbf{C}}_q^{i+1^H}\tilde{\mathbf{y}}_q. \tag{3.35}$$

- Updating node q estimates $\mathbf{R}_{\hat{\mathbf{y}}_q\hat{\mathbf{y}}_q}$ and $\mathbf{R}_{\hat{\mathbf{n}}_q\hat{\mathbf{n}}_q}$ based on the B observations and constructs $\hat{\mathbf{W}}_q^{i+1}$ as in (3.19) using the GEVD of $\{\mathbf{R}_{\hat{\mathbf{y}}_q\hat{\mathbf{y}}_q}, \mathbf{R}_{\hat{\mathbf{n}}_q\hat{\mathbf{n}}_q}\}$ and updates its local variables:

$$\tilde{\mathbf{W}}_q^{i+1} = \tilde{\mathbf{C}}_q^{i+1}\hat{\mathbf{W}}_q^{i+1}\tilde{\mathbf{H}}_q^H[\mathbf{I}_R \ \ \mathbf{0}]^H \tag{3.36}$$

$$\tilde{\mathbf{\Lambda}}_q^{i+1} = \left(\tilde{\mathbf{B}}_q^H\mathbf{R}_{\tilde{\mathbf{n}}_q\tilde{\mathbf{n}}_q}\tilde{\mathbf{B}}_q\right)^{-1}\tilde{\mathbf{B}}_q^H\mathbf{R}_{\tilde{\mathbf{y}}_q\tilde{\mathbf{y}}_q}\tilde{\mathbf{W}}_q^{i+1} \tag{3.37}$$

$$\mathbf{W}_{qq}^{i+1} = \left[\mathbf{I}_{M_q} \quad \mathbf{0}\right]\tilde{\mathbf{W}}_q^{i+1} \tag{3.38}$$

$$\mathbf{\Lambda}_{qq}^{i+1} = \left[\mathbf{I}_{M_q-L_q} \quad \mathbf{0}\right]\tilde{\mathbf{\Lambda}}_q^{i+1}. \tag{3.39}$$

- All other nodes do not change their variables:

$$\tilde{\mathbf{W}}_k^{i+1} = \tilde{\mathbf{W}}_k^i, \mathbf{\Lambda}_{kk}^{i+1} = \mathbf{\Lambda}_{kk}^i, \mathbf{W}_{kk}^{i+1} = \mathbf{W}_{kk}^i. \tag{3.40}$$

4 - All nodes $k \in \mathcal{K}$ generate B observations of the estimated desired signal $\mathbf{d}_k^{i+1} \approx \tilde{\mathbf{W}}_k^{i+1,H}\tilde{\mathbf{y}}_k^i$.
5 - $i \leftarrow i+1$, $q \leftarrow (q \mod K)+1$ and return to step 2.

3.4.2 Sufficient statistic

A formal convergence proof for PK-GEVD-DANSE is not available, but convergence is conjectured as follows:

Conjecture 3.4.1. *Assume that* $\mathbf{R}_{\mathbf{yy}}$ *and* $\mathbf{R}_{\mathbf{nn}}$ *are positive definite matrices. The rank* R *PK-GEVD-DANSE converges for any initialization of its compression matrices* $\mathbf{W}_{kk}^0$ *and* $\mathbf{\Lambda}_{kk}^0$ *to the network-wide PK-GEVD-MWF* (3.18) *for any* k*, i.e., when* $i \to \infty$ *then* $\mathbf{W}_{kk}^i = \mathbf{W}_{kk}, \mathbf{\Lambda}_{kk}^i = \mathbf{\Lambda}_{kk}$ *and* $\mathbf{d}_k^i = \mathbf{W}_k^H\mathbf{y} \ \forall k$.

In Section 3.6 extensive simulations are provided in which convergence of the rank R PK-GEVD-DANSE is consistently observed, supporting this conjecture. In addition, in this section a formal explanation for the seemingly arbitrary choice

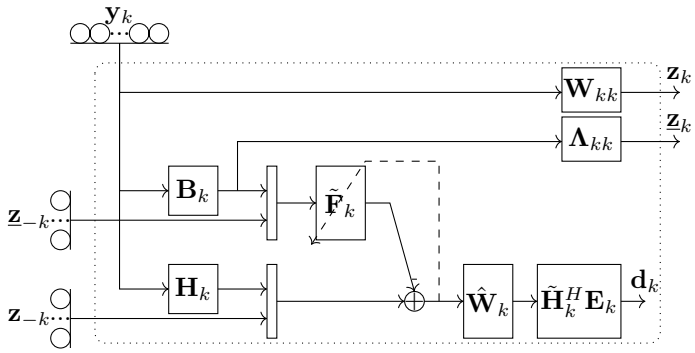

Figure 3.3: Schematic overview of the per-node operations in the rank R PK-GEVD-DANSE. The signals outside the dotted box are the signals that the node receives and sends to the other nodes.

of the expressions for the compression matrices $\mathbf{W}_{kk}^i$ and $\mathbf{\Lambda}_{kk}^i$ in Algorithm 2 is provided. It is shown that when the compression matrices reach a certain state where $\mathbf{W}_{kk}^i = \mathbf{W}_{kk}$ and $\Lambda_{kk}^i = \breve{\mathbf{\Lambda}}_{kk}$ for all k, this state is an equilibrium state of Algorithm 2 and the desired signal estimates are the same as the the desired signal estimates of the rank R PK-GEVD-MWF for all nodes. This property of Algorithm 2 is referred to here as the sufficient statistic property of the compressions $\mathbf{W}_{kk}$ and $\mathbf{\Lambda}_{kk}$ for all nodes. To next main theorem provides a sufficient statistic property of the compression $\mathbf{W}_{kk}, \mathbf{\Lambda}_{kk}$, for each node k. It is noted that, similar to [83, 101], the proof for the sufficient statistic property assumes that the local correlation matrices are perfectly estimated using infinitely many observations, to make the theoretical analysis mathematically tractable. In practice, a finite observation window is used to estimate local correlation matrices, and therefore, this analysis should be viewed as an asymptotic analysis for which the approximation accuracy improves when a larger observation window is used.

Theorem 3.4.2. *If the rank R PK-GEVD-DANSE has reached a state in iteration $i^\star$ where $\mathbf{W}_{kk}^{i^\star}$ and $\mathbf{\Lambda}_{kk}^{i^\star}$ have the same column space as $\mathbb{X}_{kk}$ and $\mathbb{\Lambda}_{kk}$ respectively, i.e., there exist transformation matrices $\mathbf{G}_k^{i^\star,1}$ and $\mathbf{G}_k^{i^\star,2}$ such that*

$$\mathbf{W}_{kk}^{i^\star} = \mathbb{X}_{kk}\mathbf{G}_k^{i^\star,1}, \;\; \mathbf{\Lambda}_{kk}^{i^\star} = \mathbb{\Lambda}_{kk}\mathbf{G}_k^{i^\star,2} \tag{3.41}$$

for all k, then this state corresponds to an equilibrium point, i.e., $\tilde{\mathbf{W}}_k^{i+1} = \tilde{\mathbf{W}}_k^i$ and $\tilde{\mathbf{\Lambda}}_k^{i+1} = \tilde{\mathbf{\Lambda}}_k^i, \forall k$ where $i \geq i^\star$, and this equilibrium point is given by

$$\tilde{\mathbf{W}}_k^{i^\star} = \begin{bmatrix} \mathbb{X}_{kk}\mathbf{G}_k \\ \mathbf{G}_1^{-1}\mathbf{G}_k \\ \vdots \\ \mathbf{G}_K^{-1}\mathbf{G}_k \\ \mathbf{0} \\ \vdots \\ \mathbf{0} \end{bmatrix}, \tilde{\mathbf{\Lambda}}_k^{i^\star} = \begin{bmatrix} \mathbb{\Lambda}_{kk}\mathbf{G}_k \\ \mathbf{G}_1^{-1}\mathbf{G}_k \\ \vdots \\ \mathbf{G}_K^{-1}\mathbf{G}_k \end{bmatrix} \tag{3.42}$$

such that $\mathbf{G}_k^{i^\star,1}$ and $\mathbf{G}_k^{i^\star,2}$ are equal to $\mathbf{G}_k$ and the final filter for every node k is given by the node-specific rank R PK-GEVD-MWF $\mathbf{W}_k = \mathbb{X}\mathbf{G}_k$.

Proof. See Appendix B.4. □

A similar sufficient statistic property is also valid for the DANSE and GEVD-DANSE of [83, 101], showing that the optimal node-specific filters are stable solutions under the update rules of the considered round-robin updates. To prove convergence of DANSE and GEVD-DANSE, the updates of the algorithm (using transformation matrices) are linked to a centralized objective function that follows a monotonically nondecreasing path over the different updates. For GEVD-DANSE this is optimization problem (3.22) without the constraint $\mathbf{B}^H\mathbf{R}_{\mathbf{nn}}\mathbb{X} = \mathbf{0}$. Since these centralized objective functions are bounded below/above, this shows that the updates result in filters converging to a fixed point. The sufficient statistic property is then used to show that the optimal centralized filter is the only stable solution.

Conjecture 3.4.1 is based on the convergence theorems of DANSE and GEVD-DANSE. However, linking the updates of PK-GEVD-DANSE to a centralized objective function, for example based on (3.22), that experience a nonincreasing/nondecreasing path over the different updates, is seen to be particularly hard. The constraint $\mathbf{B}^H\mathbf{R}_{\mathbf{nn}}\mathbb{X} = \mathbf{0}$ is only satisfied upon convergence of PK-GEVD-DANSE, allowing the objective function $\text{tr}\{\mathbb{X}^H\mathbf{R}_{\mathbf{yy}}\mathbb{X}\}$ to reach values higher than the optimal one during intermediate updates. Therefore, Conjecture 3.4.1 can only be given as a statement, a complete proof is still missing.

3.4.3 Communication cost and computational complexity

In each iteration of the rank R PK-GEVD-DANSE, each node transmits $2RB$ and receives $2(K-1)RB$ complex scalars, where B is the number of observations in one iteration. Assuming the same communication cost for the transmitter and the receiver modules, the total communication cost for node k in each iteration will be $2KRB$, leading to a network communication cost of $2K^2RB$. However, in a setup where each node functions as a FC, the communication cost of each individual node and the communication cost of the whole network would be KM_kB and KMB, respectively. If $2R < M_k$, then obviously the rank R PK-GEVD-DANSE reduces the communication cost for this node with a factor $M_k/2R$. This dimensionality reduction then also results in a reduced per-node computational complexity. The network-wide PK-GEVD-MWF has a complexity of $O(L^3)$ for the GEVD-computation and $O((M-L)^3)$ for the matrix inversion in (3.15), whereas the rank R PK-GEVD-DANSE has a complexity of $O((L_q+R(K-1))^3)$ and $O((M_q-L_q+R(K-1))^3)$ respectively at the updating node q. When compared to the the setup where each node functions as a FC, this reduction comes at the cost of having a slower adaptation speed or tracking performance due to the iterative nature of the rank R PK-GEVD-DANSE. A overview of the discussed communication costs and computational complexities is given in Table 3.2.

Table 3.2: Comparison of communication cost and computational complexity at updating node q.

	Transmitted signals	Received signals	Computational Complexity
Centralized PK-GEVD-MWF	M_qB	$(M-M_q)B$	$O(L^3+(M-L)^3)$
PK-GEVD-DANSE	$2RB$	$2R(K-1)B$	$O\big((L_q+R(K-1))^3+(M_q-L_q+R(K-1))^3\big)$

3.4.4 Topology independent rank R PK-GEVD-DANSE

Algorithm 2 operates in a fully-connected network, i.e., each node communicates with all of the other nodes in the network via a wireless link. As the number of wireless links scales with $O(K^2)$, which becomes intractable for large K, other topologies are investigated in which the number of links is smaller. In [97, 100]

simple changes are made to let the original DANSE [83] operate in different topologies, such as tree topologies.

To show that similar changes will also work for the proposed rank R PK-GEVD-DANSE, a topology-independent variant is considered. For this topology independent rank R PK-GEVD-DANSE, it is assumed that a node q has access to the sum of the $\mathbf{z}_k^i$ and $\underline{\mathbf{z}}_k^i$ of all other nodes, denoted by $\mathbf{z}_{\circ q}^i$ and $\underline{\mathbf{z}}_{\circ q}^i$ respectively given as

$$\mathbf{z}_{\circ q}^i = \sum_{k \neq q} \mathbf{z}_k^i = \sum_{k \neq q} \mathbb{X}_{kk}^{i,H} \mathbf{y}_k \tag{3.43}$$

$$\underline{\mathbf{z}}_{\circ q}^i = \sum_{k \neq q} \underline{\mathbf{z}}_k^i = \sum_{k \neq q} \lambda_{kk}^{i,H} \mathbf{B}_k^H \mathbf{y}_k. \tag{3.44}$$

Efficient methods for constructing these network-wide sums in (3.43) and (3.44) are presented in [100]. This is compared to the case where updating node q has access to the $(K-1)R$-dimensional signals $\mathbf{z}_{-q}^i$ and $\underline{\mathbf{z}}_{-q}^i$. The local operations of this topology independent rank R PK-GEVD-DANSE are similar to those of Algorithm 2, except for the fact that the subspace matrix and corresponding blocking matrix have to be redefined as

$$\tilde{\mathbf{H}}_k = \begin{bmatrix} \mathbf{H}_k & \mathbf{0} \\ \mathbf{0} & \mathbf{I}_R \\ \mathbf{0} & \mathbf{0} \end{bmatrix}; \quad \tilde{\mathbf{B}}_k = \begin{bmatrix} \mathbf{B}_k & \mathbf{0} \\ \mathbf{0} & \mathbf{0} \\ \mathbf{0} & \mathbf{I}_R \end{bmatrix} \tag{3.45}$$

and that the compression matrices are redefined as $\mathbb{X}_{qq}^i$ and $\mathbb{\Lambda}_{qq}^i$ compared to $\mathbf{W}_{qq}^i$ and $\mathbf{\Lambda}_{qq}^i$ in Algorithm 2. Since each node has to compute a (reduced dimensional) GEVD as presented in (3.19) from which it obtains $\hat{\mathbb{X}}_q^i$ as a byproduct, $\mathbb{X}_{qq}^i$ and $\mathbb{\Lambda}_{qq}^i$ can be computed as

$$\mathbb{X}_{qq}^i = \begin{bmatrix} \mathbf{I}_{M_q} & \mathbf{0} \end{bmatrix} \tilde{\mathbf{C}}_q^i \hat{\mathbb{X}}_q^i \tag{3.46}$$

$$\mathbb{\Lambda}_{qq}^i = \begin{bmatrix} \mathbf{I}_{M_q - L_q} & \mathbf{0} \end{bmatrix} \left(\tilde{\mathbf{B}}_q^H \mathbf{R}_{\tilde{\mathbf{n}}_q \tilde{\mathbf{n}}_q} \tilde{\mathbf{B}}_q \right)^{-1} \tilde{\mathbf{B}}_q^H \mathbf{R}_{\tilde{\mathbf{y}}_q \tilde{\mathbf{y}}_q} \tilde{\mathbf{C}}_q^i \hat{\mathbb{X}}_q^i \tag{3.47}$$

It is important that these compression matrices are redefined, such that the different compressed signals add coherently. A similar sufficient statistic property as in Section 3.4.2 can than be derived since it is clear that at convergence

$$\mathbb{X}^H \mathbf{y} = \mathbb{X}_{qq}^H \mathbf{y}_q + \sum_{k \neq q} \mathbb{X}_{kk}^H \mathbf{y}_k = [\mathbb{X}_{qq}^H \mathbf{I}_R] \begin{bmatrix} \mathbf{y}_q \\ \mathbf{z}_{\circ q} \end{bmatrix} \tag{3.48}$$

and

$$\mathbb{\Lambda}^H \mathbf{B}^H \mathbf{y} = \mathbb{\Lambda}_{qq}^H \mathbf{B}_q^H \mathbf{y}_q + \sum_{k \neq q} \mathbb{\Lambda}_{kk}^H \mathbf{B}_k^H \mathbf{y}_k = [\mathbb{\Lambda}_{qq}^H \mathbf{B}_q^H \ \mathbf{I}_R] \begin{bmatrix} \mathbf{y}_q \\ \mathbf{z}_{\circ q}^i \end{bmatrix}. \tag{3.49}$$

The local desired signal estimate can then be computed as $\mathbf{W}_q^H \mathbf{y} = \mathbf{G}_q^H \mathbb{X}^H \mathbf{y}$.

3.5 Rank R PK-GEVD-DANSE with rank deficiencies

Algorithm 2 assumes that $L_k > R$ and $M_k - L_k > R \; \forall k$ in order to obtain the communication cost and computational complexity reductions as discussed in Subsection 3.4.3. However, if this does not hold for certain nodes, Algorithm 2 needs to be adapted as follows:

3.5.1 $L_k < R$, $M_k - L_k < R$

In this case, it is more efficient that node k defines its compressed sensor signals as $\mathbf{z}_k = \mathbf{H}_k^H \mathbf{y}_k$ and $\underline{\mathbf{z}}_k = \mathbf{B}_k^H \mathbf{y}_k$, such that the total number of broadcast signals is equal to M_k instead of $2R$ when the (rank-deficient) compressions matrices defined in Algorithm 2 are used. There is no communication cost reduction compared to the setup where each node functions as a FC in this case.

3.5.2 $L_k > R$, $M_k - L_k < R$

In this case, it is more efficient that node k redefines $\underline{\mathbf{z}}_k$ in as $\underline{\mathbf{z}}_k = \mathbf{B}_k^H \mathbf{y}_k$. The definition for $\mathbf{z}_k^i$ remains the same as in Algorithm 2. A specific case is when $M_k = L_k$. This corresponds to the case where $B_k = [\,]$. This means that node k has no partial prior knowledge on the local steering matrix. Since this node does not have any noise-references, this leads to $\underline{\mathbf{z}}_k = [\,]$, thus this node only transmits $\mathbf{z}_k$ and has a further communication cost reduction (R broadcast signals i.s.o $2R$). When this is the case for all nodes in the WSN, Algorithm 2 reduces to the GEVD-DANSE of [101].

3.5.3 $L_k < R$, $M_k - L_k > R$

This case can only happen when $\text{rank}(A_k) < R$, i.e., when node k is not observing all the R desired sources. The rank of $\tilde{\mathbf{W}}_k^{i+1}$ in (3.36) is then equal to $L_k < R$, and the resulting compression matrices $\mathbf{W}_{kk}^{i+1}$ and $\mathbf{\Lambda}_{kk}^{i+1}$ have also the same rank. However, for the sufficient statistic property, it is required that the column space of the compression matrices should contain the R-dimensional column space of $\mathbb{X}_{kk}$ and $\mathbb{\Lambda}_{kk}$. This can be fixed by redefining the compression matrices as in the topology-independent PK-GEVD-DANSE, i.e., by using (3.46) and (3.47).

3.6 Numerical simulations

3.6.1 Distributed node-specific signal estimation in a WSN

To demonstrate the convergence and optimality of the rank R PK-GEVD-DANSE, the following scenario is used. The scenario consists of 4 nodes with each $M_k = 15$ sensor signals, 3 desired source $\check{\mathbf{s}}[t]$ and 10 undesired noise sources $\check{\mathbf{n}}[t]$. Node 1 and node 2 have access to an exact (normalized) estimate of their steering matrix $\mathbf{A}_1$ and $\mathbf{A}_2$, which are then equal to $\mathbf{H}_1$ and $\mathbf{H}_2$ respectively. The first 5 sensor signals of node 3 correspond directly to 5 of the 10 undesired noise sources. Finally, node 4 has the prior knowledge that its first 5 sensors do not observe the desired sources. The prior knowledge of node 3 and 4 can thus be captured by the following matrices:

$$\mathbf{H_3} = \mathbf{H_4} = \begin{bmatrix} \mathbf{0} \\ \mathbf{I}_{10} \end{bmatrix}. \tag{3.50}$$

The rank 3 PK-GEVD-DANSE is run in batch-mode[7]. Monte-Carlo (MC) simulations are conducted and compared with the convergence of rank 3 GEVD-DANSE and rank 6 GEVD-DANSE (same number of broadcast signals as rank 3 PK-GEVD-DANSE). Also the results of the centralized GEVD-MWF and the centralized PK-GEVD-MWF are shown. In every MC run and $\forall k \in \{1, 2, 3, 4\}$, a new random desired sources steering matrix $\mathbf{A}_k$ and new random undesired noise steering matrix $\mathbf{D}_k$ are generated from a 0-mean complex Gaussian distribution with variance 1, with the following constraints to satisfy the scenario. The first 5 rows of $\mathbf{A}_3$ and $\mathbf{A}_4$ are always equal to zero and the first 3 rows of $\mathbf{D}_3$ are $\begin{bmatrix} \mathbf{I}_5 & \mathbf{0} \end{bmatrix}$. Also $B = 1000$ samples of $\check{\mathbf{s}}[t]$ (being active for 50% of the time), $\check{\mathbf{n}}[t]$ and a random noise component $\mathbf{n}_k[t]$ (to model sensor noise) are generated to create the sensor signals

$$\mathbf{y}_k[t] = \mathbf{A}_k\check{\mathbf{s}}[t] + \mathbf{D}_k\check{\mathbf{n}}[t] + \mathbf{n}_k[t] \quad \forall k \in \{1, 2, 3, 4\} \tag{3.51}$$

by drawing them from a 0-mean complex Gaussian distribution. The variances are chosen such that the average SNR over all the sensors observing the desired sources, is equal to 0 dB. To algorithms are run with a perfect activity detection (AD-error = 0%), and when 5% or 10% of the samples are wrongly classified, introducing estimation error in $\mathbf{R_{yy}}$ and $\mathbf{R_{nn}}$.

[7] In batch-mode, iterations are performed over the same block of observations. Note that in reality the algorithm is executed in an adaptive, time-recursive manner, where each iteration is performed over a different signal segment and the same block of samples will never be broadcast multiple times.

The upper part of Fig. 3.4 shows the average (over 200 MC runs) of the decrease in the $L2$-objective function:

$$\sum_{t,k} \frac{1}{BK} \|\bar{\mathbf{d}}_k[t] - \mathbf{d}_k^i[t]\|_2^2 \tag{3.52}$$

as a function of the number of iterations of the rank 3 PK-GEVD-DANSE and shows the result when the centralized rank 3 GEVD-MWF and PK-GEVD-MWF are used to estimate $\bar{\mathbf{d}}_k[t]$. The rank 3 GEVD-DANSE is able to reduce the objective function compared to the rank 6 GEVD-DANSE showing that increasing the rank in the GEVD is only beneficial when it matches the considered setup, but the addition of the prior knowledge as done in rank 3 PK-GEVD-DANSE, reduces the objective even further. It is also clear that prior knowledge makes the algorithm more robust to AD-errors compared to GEVD-DANSE with the same estimation errors. This happens because PK-GEVD-DANSE is only influenced by mistakes in the lower dimensional subspace (determined by the prior knowledge), while the performance of GEVD-DANSE is influenced by all mistakes in the measured correlation matrices. The bottom part of Fig. 3.4 shows the average (over 200 MC runs) of the squared error between the centralized filter $\mathbf{W}_k$ and the local filter $\tilde{\mathbf{W}}_k^i$ (converted to a centralized filter via the compression matrices $\mathbf{W}_{kk}^i$ and $\mathbf{\Lambda}_{kk}^i$) averaged over all the nodes. This same is done for the rank 3 GEVD-DANSE. The PK-GEVD-DANSE is also run in a rank 1 and rank 2 version on the same data (with the same partial prior knowledge). Convergence to machine precision is observed for each algorithm, independent of the rank. This supports the statement that Algorithm 2 converges for every positive definite matrix pencil $\{\mathbf{R_{yy}}, \mathbf{R_{nn}}\}$. The convergence speed of rank 3 PK-GEVD-DANSE is higher then the convergence of the rank 3 GEVD-DANSE, due to the fact that nodes in rank 3 PK-GEVD-DANSE receive more compressed signals from the other nodes and have by consequence more degrees of freedom to solve their local optimization problem.

3.6.2 Distributed speech enhancement in a WASN

To evaluate the performance of the proposed distributed PK-GEVD-DANSE and the effect of adding prior knowledge in a realistic environment, an acoustic scenario is simulated using the image method [150]. Note that the signal model (3.1) is approximately valid for convolutive mixtures that are evaluated in the short-time Fourier transform domain. A WASN with 3 nodes is located in a square room with reflective walls. Figure 3.5 shows a schematic illustration of the scenario and the positioning of the nodes. Table 3.3 describes the parameters used to generate the acoustic scenario. There is one desired speaker in the center

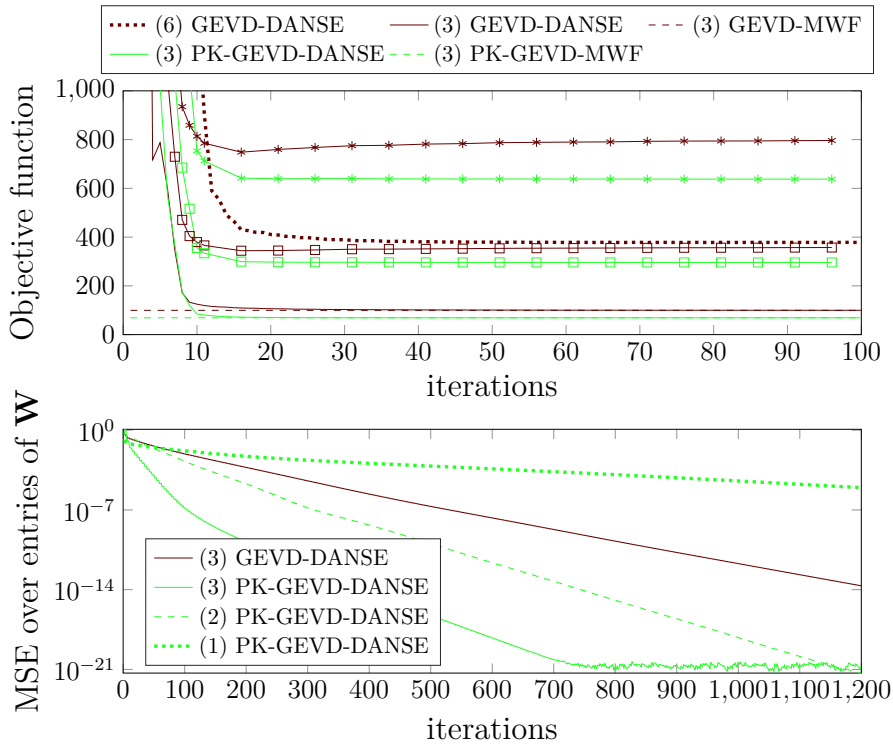

Figure 3.4: Convergence properties of PK-GEVD-DANSE.
(Upper figure) Comparison between rank 3 PK-GEVD-DANSE, rank 3 GEVD-DANSE, rank 6 GEVD-DANSE and the centralized rank 3 GEVD-MWF and PK-GEVD-MWF by considering the objective function (3.52). Lines without marks have no AD-errors, lines with square marks (□) have 5% AD-errors and lines with asterisk marks (∗) have 10% AD-errors.
(Lower figure) Comparison between rank 3 PK-GEVD-DANSE, rank 2 PK-GEVD-DANSE, rank 1 PK-GEVD-DANSE and rank 3 GEVD-DANSE in terms of convergence speed to the corresponding centralized filter. The number between brackets denotes the rank used for the considered algorithm or considered rank approximation problem.

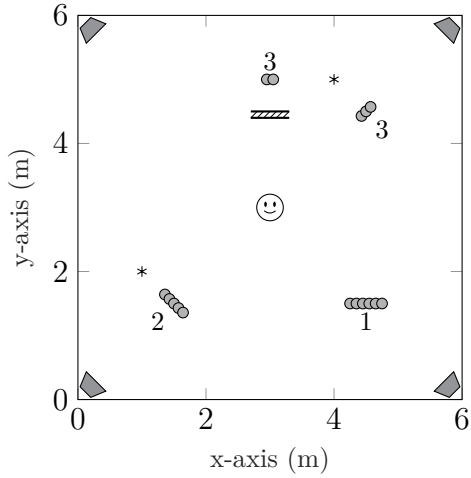

Figure 3.5: The acoustic scenario considered in the simulations. The desired speech source is located in the center of the room, surrounded by microphone arrays belonging to specific nodes. The two other noise sources are depicted by $(*)$ and the four loudspeakers are in the corners of the room. A sound absorbing wall prevents that 2 microphones of node 3 observe the desired speaker, while still observing all the other sources in the scenario.

of the room surrounded by microphone arrays with omnidirectional microphones. Two noise sources (one white noise source and one babble noise source) are also present. Four loudspeakers are playing four different undesired signals (2 speech signals and 2 white noise signals) and are each located in a different corner of the room. All speech signals are sentences from the HINT database [151]. In addition to the aforementioned noise sources, the microphone signals have an uncorrelated noise component consisting of white noise with power that is 10%-of the power of the desired signal in the first microphone of node 1. The power of the other noise sources is equal and normalized to obtain an input broadband SNR of approximately -10 dB in the reference microphone of each node. All nodes and all sound sources are in the same horizontal plane, 1m above ground level. A sound absorbing wall prevents that 2 microphones of node 3 observe the desired speaker, but the microphones are still observing all the other sources in the scenario. A fourth node is considered that consists of all the signals played by the four loudspeaker.

The prior knowledge for each considered frequency bin in the short-time Fourier transform domain, is determined as follows. Node 1 is assumed to have an estimate of the impulse response between the desired speaker and each of its

Table 3.3: Parameters used to generate the acoustic scenario.

Room dimension	6m × 6m × 3m
T_{60}	0.24s
Microphone spacing	10 cm
Sampling frequency	16kHz
DFT size Hann-window (50% overlap)	256

microphones. As a consequence the prior knowledge matrix $\mathbf{H}_1$ is computed by computing the Fourier transform of this impulse responses and combining the corresponding frequency bins to obtain the steering vector $\mathbf{h}_1[n]$ (where n is the bin index). $\mathbf{H}_1[n]$ is then given by normalizing $\mathbf{h}_1[n]$ for each bin. Node 2 knows that the desired speaker is in its broadside direction and approximates its prior knowledge matrix $\mathbf{H}_2[n]$ (using the planar wave assumption [135]) as $[\frac{1}{\sqrt{M_2}} ... \frac{1}{\sqrt{M_2}}]^T$ for each frequency bin n. No prior knowledge is assumed for the microphones of node 3, but since the 2 (last) microphones are not observing the desired source, the subspace matrix $\mathbf{H}_3$ and blocking matrix $\mathbf{B}_3$ can be represented by

$$\mathbf{H}_3 = \begin{bmatrix} 1 & 0 & 0 \\ 0 & 1 & 0 \\ 0 & 0 & 1 \\ 0 & 0 & 0 \\ 0 & 0 & 0 \end{bmatrix}, \ \mathbf{B}_3 = \begin{bmatrix} 0 & 0 \\ 0 & 0 \\ 0 & 0 \\ 1 & 0 \\ 0 & 1 \end{bmatrix} \tag{3.53}$$

for each frequency bin n. Since node 4 is not observing the desired signal, the prior knowledge in each frequency bin is represented by $\mathbf{H}_4 = [\,]$ and $\mathbf{B}_4 = \mathbf{I}_4$.

Three performance measures are used to assess the quality of the noise reduction and the convergence of the algorithm, namely the broadband signal to noise ratio (SNR), the signal to distortion ratio (SDR) and the signal to error ratio (SER). These performance measures are defined at node k as

$$\mathrm{SNR}_k[i] = \frac{E\{|s_k^i|^2\}}{E\{|n_k^i|^2\}}, \quad \mathrm{SDR}_k[i] = \frac{E\{|s_k^i|^2\}}{E\{|s_k^i - s_{k1}|^2\}} \quad \mathrm{SER}_k[i] = \frac{E\{|s_{k1}|^2\}}{E\{|s_{k1} - d_k^i|^2\}} \tag{3.54}$$

with d_k^i the output at node k in iteration i and s_k^i, n_k^i the corresponding time domain desired speech component and noise component respectively. Finally s_{k1} is the desired time domain speech in the first microphone signal of node k. Since the performance of the noise reduction in all the microphone signals of the WASN is similar, the performance measures are only provided for the first microphone signal of node 1. The desired signal component of this reference microphone serves also as reference for the perfect VAD.

Batch-mode simulations

At first, the algorithm is run in batch-mode on the first 5s of the signals. In each iteration the local correlation matrices are re-estimated over the full 5s using a simple time-averaging procedure. The performance measures for both the rank 1 GEVD-DANSE iterations and the rank 1 PK-GEVD-DANSE iterations are provided in Figure 3.6a, where the performance of centralized (PK-)GEVD-MWF are also provided to observe the convergence. It is clear that the performance of both algorithms converges to the performance of the centralized (PK-)GEVD-MWF and that the performance is almost the same after 10 iterations. The 3 performance measures for the PK-GEVD-MWF are higher than the performance measures for the GEVD-MWF (without prior knowledge), but the strongest benefit is obtained when looking at the speech distortion and the estimation error.

Block-mode simulations

The algorithm is also run as presented in Algorithm 2, where blocks of observations equivalent to 5s are used to compute the signal correlation matrices and update the compression matrices. The performance measures for both the rank 1 GEVD-DANSE iterations and the rank 1 PK-GEVD-DANSE iterations are provided in Figure 3.6b, where the performance of the centralized (PK-)GEVD-MWF are also provided as a reference. It is clear that the performance of PK-GEVD-DANSE is mostly superior to the GEVD-DANSE performance except in terms of speech distortion where the performance is similar.

3.7 Conclusion

In this paper, the centralized rank R PK-GEVD-MWF has been derived as an extension to the centralized rank R GEVD-based MWF by introducing partial prior knowledge on the desired sources steering matrix. The centralized rank R PK-GEVD-MWF is also considered in a Lagrangian framework to facilitate the step towards the distributed algorithm. The so-called PK-GEVD-DANSE, has then been presented to show that the output of this filter can be computed in a fully-connected WSN in a distributed way. Instead of broadcasting all its sensor signals, each node broadcasts only a compressed versions of its sensor signals, reducing the communication cost and computational complexity, compared to a setup where each node functions as a fusion center. The algorithm has been validated by means of numerical simulations, showing the benefits of including prior knowledge, even in situations with estimation error in the correlation matrices. The algorithm is also applied to a speech enhancement scenario in a WASN, where it is observed that the addition of partial prior knowledge indeed has beneficial effect on the noise reduction performance.

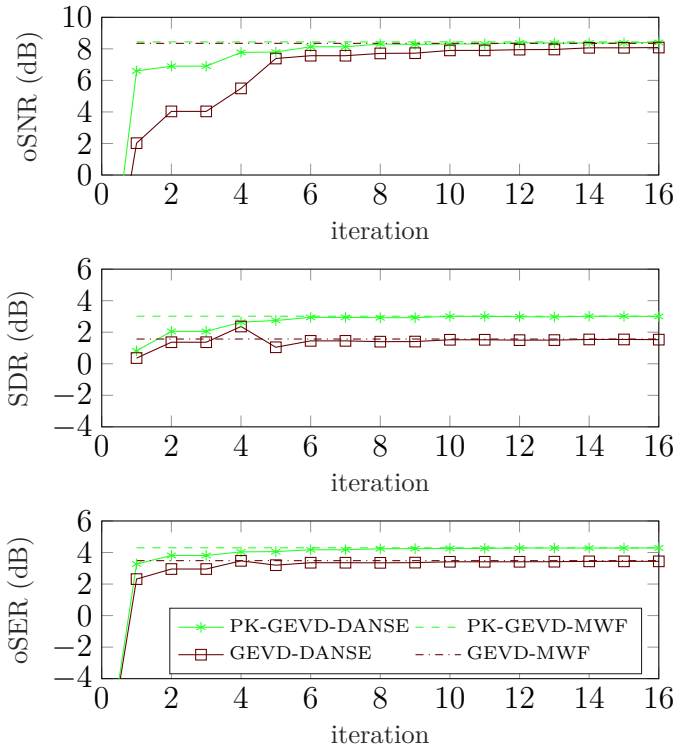

(a) Performance measures of the GEVD-DANSE and PK-GEVD-DANSE run in batch-mode compared to the centralized GEVD-MWF en PK-GEVD-MWF.

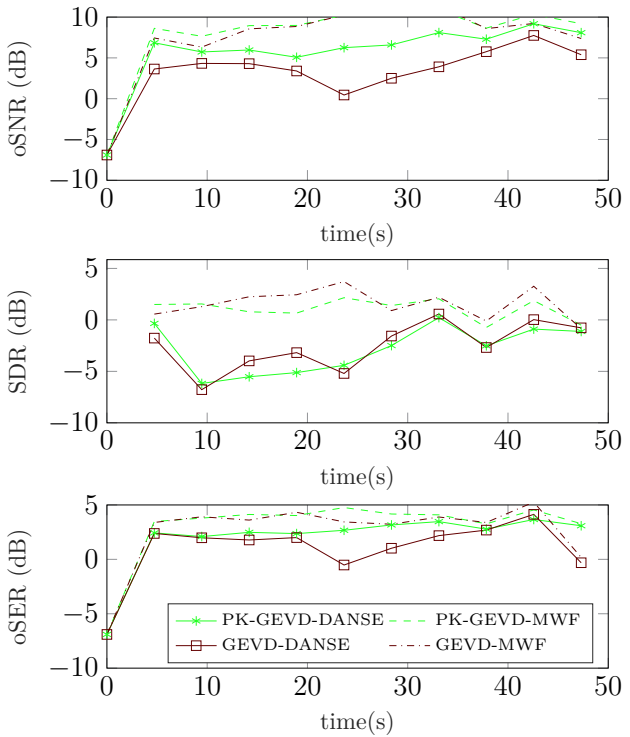

(b) Performance measures of the GEVD-DANSE and PK-GEVD-DANSE run in block-mode compared to the centralized GEVD-MWF and PK-GEVD-MWF.

Chapter 4

Distributed sound zoning using acoustic contrast control

Distributed Adaptive Acoustic Contrast Control for Node-specific Sound Zoning in a Wireless Acoustic Sensor and Actuator Network.

Robbe Van Rompaey and Marc Moonen

Published in
Proceedings of the *2020 28th European Signal Processing Conference (EUSIPCO)*, Amsterdam, The Netherlands, 2021, pp. 481-485.

©2021 IEEE Reprint, with permission from:
R. Van Rompaey and M. Moonen, "Distributed Adaptive Acoustic Contrast Control for Node-specific Sound Zoning in a Wireless Acoustic Sensor and Actuator Network" in *2020 28th European Signal Processing Conference (EUSIPCO)*, Amsterdam, The Netherlands, pp. 481-485, 2021.
Changes include layout, representation and minor editing aspects. Section 4.6 is also added as an extension of the presented distributed algorithm in Section 4.5. The candidate's contributions as first author include all performed research and writing of the article under guidance of the co-author.

Abstract

This paper presents a distributed adaptive algorithm for node-specific sound zoning in a wireless acoustic sensor and actuator network (WASAN), based on a network-wide acoustic contrast control (ACC) method. The goal of the ACC method is to simultaneously create node-specific zones with high signal power (bright zones) while minimizing power leakage in other node-specific zones (dark zones). To obtain this, a network-wide objective involving the acoustic coupling between all the loudspeakers and microphones in the WASAN is proposed where the optimal solution is based on a centralized generalized eigenvalue decomposition (GEVD). To allow for distributed processing, a gradient based GEVD algorithm is first proposed that minimizes the same objective. This algorithm can then be modified to allow for a fully distributed implementation, involving in-network summations and simple local processing. The algorithm is referred to as the distributed adaptive gradient based ACC algorithm (DAG-ACC). The proposed algorithm outperforms the non-cooperative distributed solution after only a few iterations and converges to the centralized solution, as illustrated by computer simulations.

Keywords Acoustic Contrast Control, Sound Zoning, Wireless Sensor Network, Wireless Sensor and Actuator Network (WASAN), Generalized Eigenvalue Decomposition (GEVD).

4.1 Introduction

A wireless acoustic sensor and actuator network (WASAN) [24] consists of multiple (collections of) devices that are equipped with microphones and loudspeakers and connected via wireless links. When the devices, also referred to as nodes, are able to manipulate their loudspeaker signals, new applications like active noise cancellation (ANC) [61, 152] and sound zone control [63, 112, 153] emerge. This paper focuses on sound zoning in a WASAN.

The goal of sound zoning is to simultaneously create zones with high signal power, i.e., bright zones, while minimizing power leakage in other zones, i.e., dark zones, and this is controlled by measuring the pressure in these zones by means of microphones. In a WASAN, each node can decide independently which of their local microphones belongs to a bright zone and which to a dark zone, hence these zones can indeed be termed node-specific. To create the desired sound zones, optimal FIR filters are designed to pre-filter all the loudspeaker signals in the WASAN. Design criteria to obtain these optimal filters, involve the resulting signal power and the signal distortion in the bright zones, and the power leakage in the dark zones. In the acoustic contrast control (ACC) method, the ratio between the power leakage in the dark zones and the signal power in the bright zones is minimized. In the pressure matching (PM) method [116], the signal distortion is explicitly taken into account, generally resulting in a much higher dark zone leakage compared to the ACC method. Hybrid methods [154] combining the trade-offs between ACC and PM are therefore also available.

This paper focuses on the ACC method where the optimal loudspeaker pre-filters are found by minimizing a network-wide objective involving the acoustic coupling between all the loudspeakers and microphones in the WASAN and where the optimal solution is based on a centralized generalized eigenvalue decomposition (GEVD). To allow for distributed processing, a gradient based GEVD algorithm is first proposed. This algorithm can then be modified to allow for a fully distributed implementation, involving in-network summations [49, 100, 155] and simple local processing. The algorithm is referred to as the distributed adaptive gradient based ACC algorithm (DAG-ACC). The algorithm belongs to the class of distributed algorithms that elicit cooperation between nodes in a network to simultaneously solve different but related parameter estimation problems [61, 156, 157].

The paper is organized as follows. The problem formulation and the centralized ACC method are presented in Section 4.2 and 4.3 respectively. In Section 4.4 the gradient based GEVD algorithm is presented and Section 4.5 introduces the DAG-ACC which transforms the gradient based GEVD algorithm to allow for in-network distributed processing. An extension of the DAG-ACC algorithm,

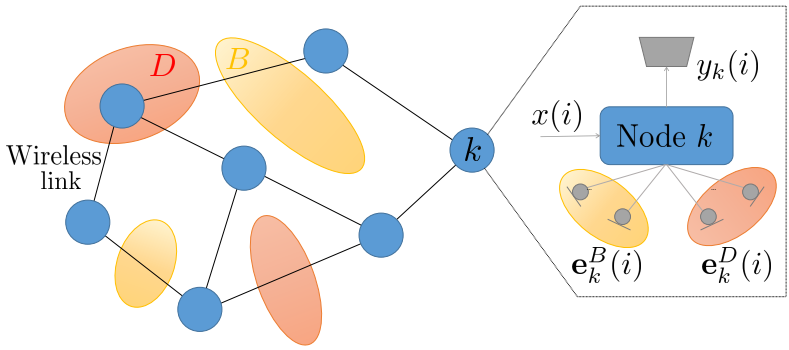

Figure 4.1: WASAN with node-specific bright and dark zones.

reducing the local storage cost, is described in Section 4.6. Computer simulations to illustrate the convergence, are provided in Section 4.7. Conclusions are given in Section 4.8.

4.2 Problem formulation: sound zoning in a WASAN

Consider a WASAN consisting of K nodes deployed in a region where different bright zones and dark zones are defined. As depicted in Fig. 4.1, each node consists of a loudspeaker[1] and a collection of microphones defining the node-specific bright zone signal vector $\mathbf{e}_k^B(i) \in \mathbb{R}^{N_k^B}$ and dark zone signal vector $\mathbf{e}_k^D(i) \in \mathbb{R}^{N_k^D}$, with i the time index. The letters B and D refer to the bright and dark zone respectively. Node-specific means that nodes can decide independently which of their local microphones belongs to the bright zone and which to the dark zone. Moreover, each node has access to the same reference signal $x(i)$.[2]

[1]The derivations can easily be extended to multiple loudspeakers per node, as long as the number of loudspeakers is smaller than the number of bright microphones as well as the number of dark zone microphones of the node.

[2]An extension to multiple reference signals where the node-specific sound zones can be different for each reference signal, is possible. The resulting local loudspeaker signal is then simply the sum of the obtained loudspeaker signals when considering only one reference signal at the time.

The goal of the ACC method implemented at node k is to define the loudspeaker signal as a filtered version of the reference signal $x(i)$ such that the power in the bright zone microphones is as high as possible whereas the dark zone microphones should ideally measure a power of 0.[3] Considering that the acoustic coupling between the loudspeaker of any node $\bar{k}$ and the microphones of node k are modeled as N_k^m L-th order FIR filters $\forall m \in \{B, D\}$, i.e., each time domain impulse response is stacked as one row in $\mathbf{H}_{\bar{k},k}^m = [\mathbf{H}_{\bar{k},k}^m(1) \ ... \ \mathbf{H}_{\bar{k},k}^m(L)] \in \mathbb{R}^{N_k^m \times L}$, the microphone signal vector $\mathbf{e}_k^m(i)$ of node k is described as

$$\begin{aligned}\mathbf{e}_k^m(i) &= \sum_{\bar{k}=1}^{K} \sum_{l=1}^{L} \mathbf{H}_{\bar{k},k}^m(l) y_{\bar{k}}(i-l+1) \\ &= \sum_{\bar{k}=1}^{K} \sum_{l=1}^{L} \mathbf{H}_{\bar{k},k}^m(l) \mathbf{x}(i-l+1)^T \mathbf{w}_{\bar{k}} \\ &= \sum_{\bar{k}=1}^{K} \mathbf{H}_{\bar{k},k}^m \mathbf{X}(i)^T \mathbf{w}_{\bar{k}} \qquad \forall m \in \{B, D\}\end{aligned} \tag{4.1}$$

where

- $y_{\bar{k}}(i)$ is the loudspeaker signal at node $\bar{k}$ at time instant i constructed as $\mathbf{x}(i)^T \mathbf{w}_{\bar{k}}$ with $(.)^T$ the transpose operator,
- $\mathbf{w}_{\bar{k}} \in \mathbb{R}^M$ denotes the ACC filter of M coefficients applied by node $\bar{k}$ to the reference signal,
- $\mathbf{x}(i) = [x(i) \ ... \ x(i-M+1)]^T \in \mathbb{R}^M$,
- $\mathbf{X}(i) = [\mathbf{x}(i) \ ... \ \mathbf{x}(i-L+1)] \in \mathbb{R}^{M \times L}$.

In equation (4.1), the ACC filters $\{\mathbf{w}_k\}_{k=1}^K$ are considered to be time-invariant [113]. Note that this assumption is approximately satisfied if the coefficients of the ACC filters change slowly compared to the timescale of the system to be controlled, i.e., the impulse responses $\{\mathbf{H}_{\bar{k},k}^m\}_{\bar{k}=1}^K$.

Assume that the impulse responses $\{\mathbf{H}_{\bar{k},k}^m\}_{\bar{k}=1}^K$ are known by node k or can be estimated by node k in a calibration phase [158] and tracked during the operation [159]. Since the loudspeaker signal played by a node is also observed

[3] This will however introduce a high signal distortion in the bright zone microphones, which is a typical side-effect of the ACC method.

by the other nodes, the objective of the nodes is to cooperate in order to produce the optimal loudspeaker outputs $\{y_k(i)\}_{k=1}^K$ by finding the ACC filters $\{\mathbf{w}_k\}_{k=1}^K$ that minimize[4]

$$J_{ACC}(\{\mathbf{w}_k\}_{k=1}^K) = \frac{\sum_{k=1}^K E\{\mathbf{e}_k^D(i)^T\mathbf{e}_k^D(i)\}}{\sum_{k=1}^K E\{\mathbf{e}_k^B(i)^T\mathbf{e}_k^B(i)\}} \tag{4.2}$$

where $E\{.\}$ is the expected value operator.

Note that $E\{\mathbf{e}_k^D(i)^T\mathbf{e}_k^D(i)\}$ and $E\{\mathbf{e}_k^B(i)^T\mathbf{e}_k^B(i)\}$ denote the sum of the microphone signal powers in the dark zone and bright zone of node k respectively. The global objective is therefore the ratio between the sum of the powers of all the dark zone microphone signals and the sum of the powers of all the bright zone microphone signals in the WASAN.

4.3 Centralized ACC method

Stacking all the ACC filters $\{\mathbf{w}_k\}_{k=1}^K$ into one augmented $\tilde{M}$-dimensional vector

$$\mathbf{w} = [\mathbf{w}_1^T \ ... \ \mathbf{w}_K^T]^T \tag{4.3}$$

where $\tilde{M} = KM$, equation (4.1) can be rewritten as

$$\mathbf{e}_k^m(i) = \mathbf{U}_k^m(i)\mathbf{w} \tag{4.4}$$

where

$$\mathbf{U}_k^m(i) = [\mathbf{H}_{1,k}^m\mathbf{X}(i)^T \ ... \ \mathbf{H}_{K,k}^m\mathbf{X}(i)^T] \quad \forall m \in \{B, D\}. \tag{4.5}$$

By substituting (4.4) in (4.2), the optimal time-invariant centralized ACC filters correspond to the $\mathbf{w}^*$ that minimizes

$$\begin{aligned} J_{ACC}(\mathbf{w}) &= \frac{\sum_{k=1}^K E\{\mathbf{w}^T\mathbf{U}_k^D(i)^T\mathbf{U}_k^D(i)\mathbf{w}\}}{\sum_{k=1}^K E\{\mathbf{w}^T\mathbf{U}_k^B(i)^T\mathbf{U}_k^B(i)\mathbf{w}\}} \\ &= \frac{\mathbf{w}^T\sum_{k=1}^K \mathbf{R}_k^D\mathbf{w}}{\mathbf{w}^T\sum_{k=1}^K \mathbf{R}_k^B\mathbf{w}} \\ &= \frac{\mathbf{w}^T\mathbf{R}^D\mathbf{w}}{\mathbf{w}^T\mathbf{R}^B\mathbf{w}} \end{aligned} \tag{4.6}$$

[4] In (2.16) of Chapters 2, the ACC is defined as the inverse of this ratio, that needs to be maximized. Note that this is fully equivalent as minimizing the inverse ratio.

where $\mathbf{R}_k^m \triangleq E\{\mathbf{U}_k^m(i)^T\mathbf{U}_k^m(i)\}$ and $\mathbf{R}^m \triangleq \sum_{k=1}^K \mathbf{R}_k^m$. Node k can estimate the correlation matrices $\{\mathbf{R}_k^m\}_{m\in\{B,D\}}$ locally by time-averaging over a certain time-period, if the signal $x(i)$ is considered to be (quasi-)stationary and ergodic.

The objective in (4.6) is a Rayleigh quotient of symmetric positive definite matrices $\{\mathbf{R}^D, \mathbf{R}^B\}$ and so the optimal solution $\mathbf{w}^*$ is (up to a scalar multiplication) given by the generalized eigenvector corresponding to smallest generalized eigenvalue of the matrix pencil $\{\mathbf{R}^D, \mathbf{R}^B\}$ [160]. However, to compute a centralized solution, each node has to transmit the $(\tilde{M}\times\tilde{M})$-dimensional matrices $\{\mathbf{R}_k^m\}_{m\in\{B,D\}}$ to a fusion center where the ACC filters $\{\mathbf{w}_k\}_{k=1}^K$ are computed via a generalized eigenvalue decomposition (GEVD) and then transmitted back to the nodes. This is not a robust method, as it introduces a single point of failure, and furthermore, requires a high computational capacity of the fusion center to compute the GEVD of a matrix pencil whose dimension grows linearly with the number of nodes K in the WASAN. To alleviate these high computational and communication requirements, a gradient based GEVD algorithm is first proposed in Section 4.4 and then it will be shown in Section 4.5 that this algorithm allows for an efficient distributed implementation.

4.4 Gradient based GEVD algorithm

The gradient of (4.6) is given by

$$\begin{aligned}\nabla_{\mathbf{w}} J_{ACC} &= \frac{\mathbf{R}^D\mathbf{w}}{\mathbf{w}^T\mathbf{R}^B\mathbf{w}} - \frac{\left(\mathbf{w}^T\mathbf{R}^D\mathbf{w}\right)\mathbf{R}^B\mathbf{w}}{\left(\mathbf{w}^T\mathbf{R}^B\mathbf{w}\right)^2} \\ &= \alpha\left(\mathbf{R}^D\mathbf{w} - \frac{\left(\mathbf{w}^T\mathbf{R}^D\mathbf{w}\right)}{\left(\mathbf{w}^T\mathbf{R}^B\mathbf{w}\right)}\mathbf{R}^B\mathbf{w}\right)\end{aligned} \tag{4.7}$$

where α is a scalar. Note that the gradient is equal to zero in every generalized eigenvector of the matrix pencil $\{\mathbf{R}^D, \mathbf{R}^B\}$. The gradient provides a direction of ascent, so if the optimization variable $\mathbf{w}$ takes small steps in the direction of the negative gradient, a decrease in the objective J_{ACC} is guaranteed. Therefore, Algorithm 3 is proposed to solve (4.6) iteratively. Here n denotes the iteration index.

A procedure similar to [161] can be followed to show that Algorithm 3 converges to the unique (up to a scalar multiplication) generalized eigenvector $\mathbf{w}^*$ corresponding to the smallest generalized eigenvalue of the matrix pencil $\{\mathbf{R}^D, \mathbf{R}^B\}$. Necessary requirements are:

Algorithm 3: Gradient based GEVD algorithm

1 - Initialize $\mathbf{w}(0)$ randomly.
- $n \leftarrow 0$.

2 Perform a gradient update with stepsize μ:

$$\sigma(n) = \frac{\mathbf{w}(n)^T \mathbf{R}^D \mathbf{w}(n)}{\mathbf{w}(n)^T \mathbf{R}^B \mathbf{w}(n)} \tag{4.8}$$

$$\mathbf{p}(n) = \mathbf{R}^D \mathbf{w}(n) - \sigma(n) \mathbf{R}^B \mathbf{w}(n) \tag{4.9}$$

$$\mathbf{w}(n+1) = \mathbf{w}(n) - \mu \mathbf{p}(n). \tag{4.10}$$

3 - $n \leftarrow n+1$ and return to step 2 until some stopping criterion is met.

- the stepsize μ should be smaller than $2/(\lambda_{max}^{\mathbf{R}^B} S)$, with $\lambda_{max}^{\mathbf{R}^B}$ the largest eigenvalue of $\mathbf{R}^B$ and S the difference between the largest and smallest generalized eigenvalue of the matrix pencil $\{\mathbf{R}^D, \mathbf{R}^B\}$,
- $\mathbf{w}(0)^T \mathbf{w}^*$ is not equal to zero,
- $\mathbf{R}^B$ and $\mathbf{R}^D$ are symmetric positive definite matrices.

Note that $\sigma(n)$ tracks the evolution in the objective J_{ACC} for the current estimate $\mathbf{w}(n)$. Determining an optimal stepsize

$$\mu^*(n) = \arg\min_{\mu} J_{ACC}(\mathbf{w}(n) - \mu \mathbf{p}(n)) \tag{4.11}$$

for faster convergence as in [160, 162] requires computing the smallest Ritz value and corresponding Ritz vector of the matrix pencil $\{\mathbf{R}^D, \mathbf{R}^B\}$ with respect to $\{\mathbf{w}(n), \mathbf{p}(n)\}$, which complicates the distributed implementation of the next section and will only be briefly touched upon further in the paper.

4.5 DAG-ACC algorithm

Algorithm 3 allows for a distributed implementation. To see this, note that the matrix vector products of (4.8) and (4.9) in Algorithm 3 can be written as:

$$\begin{aligned} \mathbf{R}^m \mathbf{w}(n) &= \sum_{k=1}^{K} E\{\mathbf{U}_k^{mT}(i) \mathbf{U}_k^m(i) \mathbf{w}(n)\} \\ &= \sum_{k=1}^{K} E\{\mathbf{U}_k^{mT}(i) \mathbf{e}_k^m(i)\} = \sum_{k=1}^{K} \mathbf{r}_k^m = \mathbf{r}^m \end{aligned} \tag{4.12}$$

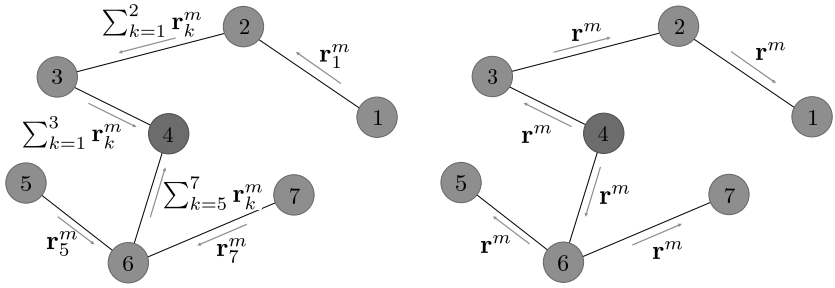

(a) Phase 1 (b) Phase 2

Figure 4.2: Tree based in-network summation

where $\mathbf{r}_k^m = E\{\mathbf{U}_k^{m\,T}(i)\mathbf{e}_k^m(i)\}$ can be estimated locally by node k when $\mathbf{w}(n)$ is used as ACC filters in the WASAN, since node k has access to both $\mathbf{U}_k^m(i)$ and $\mathbf{e}_k^m(i)$.[5] If the nodes are able to construct the in-network sum $\sum_{k=1}^{K} \mathbf{r}_k^m$ to obtain $\{\mathbf{r}^m\}_{m\in\{B,D\}}$ and if each node has a local copy of the current ACC filters $\mathbf{w}^k(n)$, where superscript k refers to the local copy at node k, then Algorithm 3 can be executed in a fully distributed fashion.

Algorithms to obtain in-network summations with minimal communication requirement are abundantly available in literature, e.g., relying on gossip or consensus methods [49, 155]. However, these methods typically need many iterations to converge, as well as multiple broadcasts of intermediary summed variables. Therefore, based on [100], a method is proposed to calculate the in-network summation which relies on a tree topology that is formed from the set of available links in the network, and that has a minimal communication requirement (only 2 transmissions for each link). Fig. 4.2 shows the network flow. In a first phase, a tree is formed using the available links in the network [163], consisting of one root node and $K-1$ non-root nodes. A non-root node k with only one neighbor (=leaf node) starts by transmitting $\{\mathbf{r}_k^m\}_{m\in\{B,D\}}$ to its neighbor. A node k with more than one neighbor waits until it receives signals from all its neighbors except one denoted by k' and transmits $\{\mathbf{r}_k^m + \sum_{\bar{k}\in\{\mathcal{N}_k\setminus k'\}} \mathbf{r}_{\bar{k}}^m\}_{m\in\{B,D\}}$ to node k', where $\mathcal{N}_k$ denotes the set of neighbors of node k. This continues until the root node receives signals from all its neighbors. The root node then computes $\{\mathbf{r}^m = \mathbf{r}_k^m + \sum_{\bar{k}\in\mathcal{N}_k} \mathbf{r}_{\bar{k}}^m\}_{m\in\{B,D\}}$ in the next phase and broadcasts this back to all the nodes using the available communication tree.

[5] Note that $\mathbf{r}_k^m$ can also be estimated as $E\{\mathbf{U}_k^{m\,T}(i)\mathbf{U}_k^m(i)\mathbf{w}(n)\}$, however, using $E\{\mathbf{U}_k^{m\,T}(i)\mathbf{e}_k^m(i)\}$ should be more robust to possible modeling errors in $\mathbf{U}_k^m(i)$. Extra simulations are needed to confirm this statement.

The resulting distributed adaptive gradient based ACC algorithm (DAG-ACC) is presented in Algorithm 4. It is adaptive in the sense that in between two consecutive gradient steps, the nodes re-estimate their correlation vectors $\{\mathbf{r}_k^m\}_{m\in\{B,D\}}$ using a frame of I samples, so that any change in the signal statistics of $x(i)$ or $\{\mathbf{H}_{k,k}^m\}_{m\in\{B,D\}}$ can indeed be tracked. In this way, n now corresponds both to the iteration index as well as the frame index.

Algorithm 4: Distributed Adaptive Gradient based ACC algorithm (DAG-ACC)

1 - Initialize $\mathbf{w}^k(0)$ with the same random vector $\forall k$.
- $n \leftarrow 0$.

2 - Each node k selects the part $\mathbf{w}_k^k(n)$ corresponding to its local ACC filter of $\mathbf{w}^k(n)$ to produce the loudspeaker signals:

$$y_k(nI+i) = \mathbf{x}^T(nI+i)\mathbf{w}_k^k(n), \quad i = 1..I. \tag{4.13}$$

3 - Each node k collects I observations of their bright and dark zone microphones and estimates $\mathbf{r}_k^B(n)$ and $\mathbf{r}_k^D(n)$ via time averaging in the frame:

$$\mathbf{r}_k^m(n) = \frac{1}{I}\sum_{i=1}^{I} \mathbf{U}_k^{mT}(nI+i)\mathbf{e}_k^m(nI+i) \quad \forall m \in \{B,D\}. \tag{4.14}$$

4 - The nodes interchange $\mathbf{r}_k^B(n)$ and $\mathbf{r}_k^D(n)$ such that each node obtains locally the in-network sum vectors:

$$\mathbf{r}^m(n) = \sum_{k=1}^{K} \mathbf{r}_k^m(n) \quad \forall m \in \{B,D\}. \tag{4.15}$$

5 Each node k performs a gradient update of its local estimation of the centralized ACC filter with the same stepsize μ:

$$\sigma^k(n) = \frac{\mathbf{w}^k(n)^T\mathbf{r}^D(n)}{\mathbf{w}^k(n)^T\mathbf{r}^B(n)} \tag{4.16}$$

$$\mathbf{p}^k(n) = \mathbf{r}^D(n) - \sigma^k(n)\mathbf{r}^B(n) \tag{4.17}$$

$$\mathbf{w}^k(n+1) = \mathbf{w}^k(n) - \mu\mathbf{p}^k(n). \tag{4.18}$$

6 - $n \leftarrow n+1$ and return to step 2.

As each iteration of the algorithm needs only two in-network summations to compute vectors $\{\mathbf{r}^m\}_{m\in\{B,D\}}$, the communication requirement is much lower than when the full network correlation matrices $\{\mathbf{R}^m\}_{m\in\{B,D\}}$ need to be formed. Also the local memory requirement are reduced since the

matrices $\{\mathbf{R}_k^m \in \mathbb{R}^{\bar{M}\times\bar{M}}\}_{m\in\{B,D\}}$ do not need to be stored. The local processing requirement is also very low, compared to performing a GEVD of the matrix pencil $\{\mathbf{R}^D, \mathbf{R}^B\}$. The important drawback is that the algorithm needs some iterations to converge to the optimal filter $\mathbf{w}^*$.

It is also possible to perform T gradient iterations with the same batch of data in frame n. In this case, however, every node needs to keep track of the full local correlation matrix $\mathbf{R}_k^m(n)$ defined as

$$\mathbf{R}_k^m(n) = \frac{1}{I}\sum_{i=1}^{I} \mathbf{U}_k^m(nI+i)^T \mathbf{U}_k^m(nI+i) \quad \forall m \in \{B, D\} \tag{4.19}$$

which significantly increases the memory requirement in the node. For each frame n, the nodes then compute an in-network summation of $\mathbf{r}_k^m(n,t) = \mathbf{R}_k^m(n)\mathbf{w}^k(n,t)$ denoted by $\mathbf{r}^m(n,t)$ for $m \in \{B, D\}$, update the gradient as

$$\mathbf{w}^k(n,t+1) = \mathbf{w}^k(n,t) - \mu\left(\mathbf{r}^D(n,t) - \frac{\mathbf{w}^k(n,t)^T\mathbf{r}^D(n,t)}{\mathbf{w}^k(n,t)^T\mathbf{r}^B(n,t)}\mathbf{r}^B(n,t)\right) \tag{4.20}$$

and do this for all $t = \{0, ..., T-1\}$. Using $\mathbf{w}^k(n+1,0) = \mathbf{w}^k(n,T)$, one can then proceed to the next frame. This procedure will increase the convergence speed, but also increases the communication requirement due to the extra in-network summations and increases the memory requirement for each node (cfr supra).

If one is able to compute $\mathbf{r}^m(n,t) = \sum_{k=1}^K \mathbf{R}_k^m(n)\mathbf{w}^k(n,t)$ in a distributed fashion, then one can also compute $\mathbf{R}^m(n)\mathbf{p}^k(n) = \sum_{k=1}^K \mathbf{R}_k^m(n)\mathbf{p}^k(n)$ for $m \in \{B, D\}$, which is needed to compute the Ritz vector for an optimal stepsize selection (4.11). This again increases the convergence speed but again at the cost of an increased memory and communication requirement.

4.6 Distributed adaptive gradient based ACC algorithm with reduced memory requirements

The DAG-ACC algorithm of the previous section requires that each node stores and updates a copy of all the sound zoning filters $\{\mathbf{w}_k\}_{k=1}^K\}$ locally. This can be avoided by noticing that $\sigma(n)$ in (4.8) and (4.16) can be computed using

$$\sigma(n) = \frac{\sum_{k=1}^K P_k^D(n)}{\sum_{k=1}^K P_k^B(n)} = \frac{P^D(n)}{P^B(n)} \tag{4.21}$$

where $\forall m \in \{B, D\}$

$$P_k^m(n) = E\{\mathbf{e}_k^{m\,T}\mathbf{e}_k^m\} \approx \frac{1}{I}\sum_{i=1}^{I}\mathbf{e}_k^{m\,T}(nI+i)\mathbf{e}_k^m(nI+i). \tag{4.22}$$

If a node has access to $P^D(n)$ and $P^B(n)$, it no longer requires all sound zoning filters in $\mathbf{w}(n)$ to compute $\sigma(n)$. Hence, it only has to store and update its local sound zoning filter $\mathbf{w}_k(n)$ to be able to produce the loudspeaker signals. However, computing $P^D(n)$ and $P^B(n)$ requires computing two extra in-network summations in each iteration, but this is negligible compared to computing the $2\tilde{M}$ in-network summations for $\mathbf{r}^B(n)$ and $\mathbf{r}^B(n)$. The extended DAG-ACC algorithm is presented in Algorithm 5. Note that the extended DAG-ACC algorithm is theoretically performing the same operations as the original DAG-ACC algorithm, except that $P^m(n)$ $\forall m \in \{B, D\}$ are estimated empirically[6].

4.7 Simulations

To demonstrate the effectiveness of the DAG-ACC, a WASAN scenario with $K = 5$ nodes is considered. Each node has one bright zone microphone, one dark zone microphone and one loudspeaker. The reference signal $x(i)$ is a Gaussian noise source with zero mean and unit variance of size 3000. The ACC filters $\{\mathbf{w}_k\}_{k=1}^K$ have length $M = 20$. The acoustic coupling between the loudspeakers and the microphones is modeled by means of random impulse responses with zero mean and unit variance of length $L = 10$. Moreover, at frame $n = 150$ and $n = 300$, a random Gaussian component with zero mean and variance 0.1 is added to the impulse responses to model a possible re-estimation of the local impulse responses. To demonstrate convergence, algorithm 4 is run in batch mode, meaning that the reference signal $x(i)$ is periodic with period 3000 and $I = 3000$. The stepsize μ is set to 0.01.

In the simulations, the proposed DAG-ACC is compared with the centralized ACC method presented in section 4.3. Also the result of a non-cooperative ACC method is provided, obtained when each node solves a local ACC problem based on:

$$J_{ACC,k}(\mathbf{w}_k) = \frac{E\{\mathbf{w}_k^T\mathbf{X}(i)\mathbf{H}_{k,k}^D\mathbf{H}_{k,k}^{D\,T}\mathbf{X}(i)^T\mathbf{w}_k\}}{E\{\mathbf{w}_k^T\mathbf{X}(i)\mathbf{H}_{k,k}^B\mathbf{H}_{k,k}^{B\,T}\mathbf{X}(i)^T\mathbf{w}_k\}}. \tag{4.30}$$

Note that this $J_{ACC,k}$ does not take into account the coupling between nodes, and will automatically generate suboptimal ACC filters. In Fig. 4.3, the objective

[6]This should again make it more robust to possible estimation errors, but extra simulations are needed to confirm this statement.

Algorithm 5: Extended Distributed Adaptive Gradient based ACC algorithm (extended DAG-ACC)

1 - Initialize $\mathbf{w}_k(0)$ randomly $\forall k$.
- $n \leftarrow 0$.

2 - Each node k produces the loudspeaker signals:

$$y_k(nI+i) = \mathbf{x}^T(nI+i)\mathbf{w}_k^k(n), \quad i = 1..I. \tag{4.23}$$

3 - Each node k collects I observations of their bright and dark zone microphones and estimates $\mathbf{r}_k^B(n)$, $\mathbf{r}_k^D(n)$, $P_k^B(n)$ and $P_k^D(n)$ via time averaging in the frame:

$$\mathbf{r}_k^m(n) = \frac{1}{I}\sum_{i=1}^{I} \mathbf{U}_k^{m\,T}(nI+i)\mathbf{e}_k^m(nI+i) \quad \forall m \in \{B, D\} \tag{4.24}$$

$$P_k^m(n) = \frac{1}{I}\sum_{i=1}^{I} \mathbf{e}_k^{m\,T}(nI+i)\mathbf{e}_k^m(nI+i) \quad \forall m \in \{B, D\}. \tag{4.25}$$

4 - The nodes interchange $\mathbf{r}_k^B(n)$, $\mathbf{r}_k^D(n)$, $P_k^B(n)$ and $P_k^D(n)$ such that each node obtains locally the in-network sum vectors:

$$\mathbf{r}^m(n) = \sum_{k=1}^{K} \mathbf{r}_k^m(n) \quad \forall m \in \{B, D\} \tag{4.26}$$

$$P^m(n) = \sum_{k=1}^{K} P_k^m(n) \quad \forall m \in \{B, D\}. \tag{4.27}$$

5 Each node k performs a gradient update of its local estimation of the centralized ACC filter with the same stepsize μ:

$$\mathbf{p}_k(n) = \mathbf{E}_k^T\mathbf{r}^D(n) - \frac{P_k^D(n)}{P_k^B(n)}\mathbf{E}_k^T\mathbf{r}^B(n) \tag{4.28}$$

$$\mathbf{w}_k(n+1) = \mathbf{w}_k(n) - \mu\mathbf{p}_k(n) \tag{4.29}$$

where $\mathbf{E}_k$ is a selection matrix that select the rows in $\mathbf{r}^m(n)$ corresponding to the local sound zoning filter.

6 - $n \leftarrow n+1$ and return to step 2.

J_{ACC} is plotted for each iteration of Algorithm 4 and J_{ACC} is also plotted for the centralized and non-cooperative ACC method. Here the median over 100 independent experiments is shown. The bumps in the 3 graphs are due to the abrupt changes of the impulse responses as described earlier. As expected, note that the DAG-ACC converges to the same optimal value $J_{ACC}(\mathbf{w}^*)$ as the centralized ACC method. The median MSE between the normalized $\mathbf{w}^*$

and normalized $\mathbf{w}(n)$ reaches the machine precision after 50000 iterations, which confirms convergence (not shown in Fig 4.3). Moreover, although the J_{ACC} for the non-cooperative ACC method is lower than the the J_{ACC} for the random initialization in Algorithm 4 initially, the DAG-ACC outperforms the non-cooperative ACC method already after a few iterations. As discussed, this degradation occurs due to the absence of cooperation among the nodes when they are solving ACC problems that are indeed coupled.

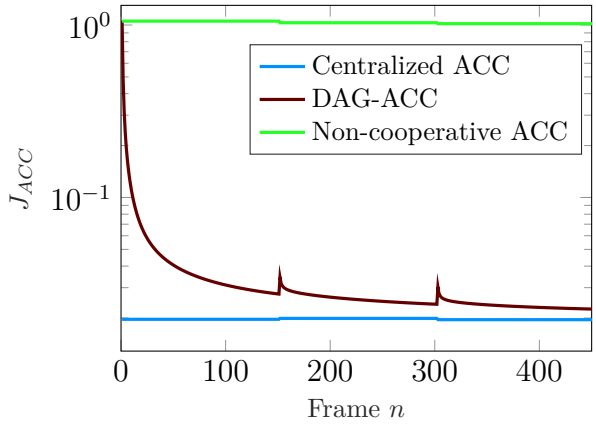

Figure 4.3: Evolution of the objective J_{ACC} for the DAG-ACC and the centralized and non-cooperative ACC method.

4.8 Conclusion

In this paper a node-specific ACC sound zoning has been considered in a WASAN. An (extended) distributed adaptive gradient-based ACC algorithm has been proposed, avoiding the high communication and computational requirements of a centralized ACC method. The algorithm has been shown to converge to the solution of the centralized method, by means of computer simulations.

Chapter 5

Distributed sound zoning using pressure matching

Sound Zoning in an Ad-hoc Wireless Acoustic Sensor and Actuator Network.

Robbe Van Rompaey and Marc Moonen

Published in
Proceedings of the *2021 29th European Signal Processing Conference (EUSIPCO)*, Dublin, Ireland, 2021, pp. 101-105.

©2021 IEEE Reprint, with permission from:
R. Van Rompaey and M. Moonen, "Sound Zoning in an Ad-hoc Wireless Acoustic Sensor and Actuator Network" in *2021 29th European Signal Processing Conference (EUSIPCO)*, Dublin, Ireland, pp. 101-105, 2021.
Changes include layout, representation and minor editing aspects.
The candidate's contributions as first author include all performed research and writing of the article under guidance of the co-author.

Abstract

In this paper, the pressure matching (PM) method to sound zoning is considered in an ad-hoc wireless acoustic sensor and actuator network (WASAN) consisting of multiple audio-devices with loudspeakers and microphones. The goal of sound zoning is to simultaneously create different zones with different dominant sounds. To obtain this, a network-wide objective involving the acoustic coupling between all the loudspeakers and microphones is presented where the optimal solution is obtained by solving a quadratically constraint quadratic program (QCQP). To allow for distributed processing, a Gauss-Seidel type algorithm is proposed. It requires only that all the nodes have access to the different microphone signals, but other than this there is no need for communication between different nodes or with a fusion center (FC). The algorithm is referred to as the distributed adaptive PM algorithm (DA-PM). The algorithm is proven to converge to the optimal solution, as also illustrated by Monte Carlo simulations and evaluated in a simulated acoustic environment.

Keywords Pressure Matching, Sound Zoning, Wireless Sensor and Actuator Network (WASAN), Quadratically Constraint Quadratic Program (QCQP).

5.1 Introduction

An ad-hoc wireless acoustic sensor and actuator network (WASAN) consists of multiple audio-devices, equipped with microphones and loudspeakers, where wireless links make it possible for the devices to communicate and cooperate to perform a certain audio processing task. Ad-hoc mean that the relative positions of the different audio-devices, also referred to as nodes, are undefined, unknown and can change during the operation. When the nodes are able to manipulate their loudspeaker signals, new applications like active noise cancellation [61,152] and sound zone control [63, 112, 153] emerge. This paper focuses on sound zoning in an ad-hoc WASAN.

The goal of sound zoning is to simultaneously create different zones with different dominant sounds. This is controlled by measuring the pressure in these zones by means of so-called error microphones. In a WASAN, each zone can decide independently which sound signals belong to its required sound signals and which sound signals are interfering sound signals that should be suppressed. To create the desired sound zones, FIR filters are designed to pre-filter all the loudspeaker signals in the WASAN. Design criteria for these filters involve the signal distortion for the required sound signals and the resulting interfering sound power. In the acoustic contrast control (ACC) method [44], the ratio between the power of the residual interfering sound signals and the power of the required sound signals is minimized. In the pressure matching (PM) method [116], the signal distortion of the required sound signals is explicitly taken into account. Hybrid methods [112, 154] combining the ACC and PM criteria are also available.

This paper focuses on the PM method where the FIR filters are designed by minimizing an objective involving the acoustic coupling between all the loudspeakers and error microphones in the WASAN, without exceeding the maximum power of each loudspeaker. The optimal solution can be found by solving a quadratically constraint quadratic program (QCQP). Solving the QCQP requires gathering all acoustic information in a fusion center (FC), which however might become intractable as the number of nodes grows large. To allow for distributed processing, a Gauss-Seidel type algorithm is proposed. It requires only that all the nodes have access to the different microphone signals, but other than this there is no need for communication between different nodes or with a FC. The algorithm is referred to as the distributed adaptive PM algorithm (DA-PM). The algorithm is proven to converge to the optimal solution, as also illustrated by Monte Carlo simulations and evaluated in a simulated acoustic environment.

The paper is organized as follows. The problem formulation and the centralized

PM method are presented in Section 5.2 and 5.3 respectively. In Section 5.4, the distributed algorithm is presented. Computer simulations to illustrate the convergence of the presented algorithm, are provided in Section 5.5. Conclusions are given in Section 5.6.

5.2 Signal model and problem formulation

A WASAN is considered where P localized error microphones are recording the sound pressure in P different sound zones. K nodes, equipped with L loudspeakers each, are also scattered over the considered region in an ad-hoc fashion. The nodes are assumed to have access to the different error microphone signals (e.g., the error microphones can broadcast their signals using wireless links), but other communications between the nodes will not be needed. Each node has also access to S different sound signals $x_s(t)$, with t the time index. Each sound signal belongs either to the required sound signals $\mathcal{R}_p$ or the interfering sound signals $\mathcal{I}_p$ of sound zone p.

The goal of the PM method is to produce a desired sound pressure $d_p(t)$ in sound zone p, defined as the sound pressure produced by a virtual source playing all required sound signals $x_s(t)$ in $\mathcal{R}_p$, i.e.,

$$d^p(t) = \sum_{n=0}^{N-1} h_{\mathrm{v}}^p(n) \sum_{s\in\mathcal{R}_p} x_s(t-n) = \sum_{s\in\mathcal{R}_p} \underbrace{\sum_{n=0}^{N-1} h_{\mathrm{v}}^p(n) x_s(t-n)}_{d_s^p(t)}. \tag{5.1}$$

Here $\mathbf{h}_{\mathrm{v}}^p = [h_{\mathrm{v}}^p(0) \ ... \ h_{\mathrm{v}}^p(N-1)]^T$ models the impulse response between the virtual source and error microphone p as an N-th order FIR filter and $(.)^T$ is the transpose operator.

To produce the desired pressures, loudspeaker l of node k in the WASAN will play a signal y_{kl} obtained as a convolution of the known S sound signals and S unknown M-th order PM filters $\{\mathbf{w}_{kl,s}\}_{s=1...S}$, i.e.,

$$y_{kl}(t) = \sum_{s=1}^{S} \sum_{m=0}^{M-1} w_{kl,s}(m) x_s(t-m) = \sum_{s=1}^{S} \mathbf{w}_{kl,s}^T \mathbf{x}_s(t) \tag{5.2}$$

with $\mathbf{w}_{kl,s} = [w_{kl,s}(0) \ ... \ w_{kl,s}(M-1)]^T$ and $\mathbf{x}_s = [x_s(t) \ ... \ x_s(t-M+1)]^T$. The sound pressure $e^p(t)$ received at error microphone p is then given by the sum of all loudspeaker signals convolved with the impulse responses between

the loudspeakers and the error microphones, i.e.,

$$e^p(t) = \sum_{k=1}^{K}\sum_{l=1}^{L}\sum_{n=0}^{N-1} h_{kl}^p(n) y_{kl}(t-n) + n^p(t) = \sum_{s=1}^{S}\sum_{k=1}^{K}\sum_{l=1}^{L} \mathbf{w}_{kl,s}^T \mathbf{H}_{kl}^p \tilde{\mathbf{x}}_s(t) + n^p(t)$$

$$= \sum_{s=1}^{S}\sum_{k=1}^{K} \mathbf{w}_{k,s}^T \mathbf{H}_k^p \tilde{\mathbf{x}}_s(t) + n^p(t) = \sum_{s=1}^{S} \underbrace{\mathbf{w}_s^T \mathbf{H}^p \tilde{\mathbf{x}}_s(t)}_{e_s^p(t)} + n^p(t). \tag{5.3}$$

where $n^p(t)$ denotes additive noise[1] uncorrelated with the sounds and $\mathbf{H}_{kl}^p$ is a Toeplitz matrix defined as

$$\mathbf{H}_{kl}^p = \begin{bmatrix} \boxed{\mathbf{h}_{kl}^{p,T}} & 0 & \dots & 0 \\ 0 & \boxed{\mathbf{h}_{kl}^{p,T}} & \dots & 0 \\ \vdots & \vdots & \ddots & \ddots & \ddots & \vdots \\ 0 & 0 & \dots & \boxed{\mathbf{h}_{kl}^{p,T}} \end{bmatrix} \in \mathbb{R}^{M\times(M+N-1)}. \tag{5.4}$$

where $\mathbf{h}_{kl}^p$ is the N-th order impulse response between loudspeaker l of node k and error microphone p. The other quantities used in (5.3) are defined as $\mathbf{H}_k^p = [\mathbf{H}_{k1}^{p,T} \ \dots \ \mathbf{H}_{kL}^{p,T}]^T$, $\mathbf{H}^p = [\mathbf{H}_1^{p,T} \ \dots \ \mathbf{H}_K^{p,T}]^T$, $\mathbf{w}_{k,s} = [\mathbf{w}_{k1,s}^T \ \dots \ \mathbf{w}_{kL,s}^T]^T$, $\mathbf{w}_s = [\mathbf{w}_{1,s}^T \ \dots \ \mathbf{w}_{K,s}^T]^T$ and $\tilde{\mathbf{x}}_s(t) = [x_s(t) \ \dots \ x_s(t-M-N+2)]^T$.

In equation (5.2) and (5.3), the PM filters are considered to be time-invariant [113]. Note that this assumption is approximately satisfied if the coefficients of the PM filters change slowly compared to the time scale of the system to be controlled, i.e., the impulse responses $\mathbf{h}_{kl}^p$.

It is also assumed that the sound signals are uncorrelated. Consequently $d_s^p(t)$ can only be obtained from $e_s^p(t)$. The optimal PM filters $\hat{\mathbf{W}} = [\hat{\mathbf{w}}_1 \ \dots \ \hat{\mathbf{w}}_S]$ can be found from the following optimization problem:

$$\min_{\mathbf{W}} \sum_{p=1}^{P} \left(\sum_{s\in\mathcal{R}_p} E\{||d_s^p(t) - e_s^p(t)||^2\} + \mu \sum_{s\in\mathcal{I}_p} E\{||e_s^p(t)||^2\} \right)$$

$$s.t. \sum_{s=1}^{S} \mathbf{w}_{kl,s}^T \underbrace{E\{\mathbf{x}_s(t)\mathbf{x}_s(t)^T\}}_{\mathbf{R}_{\mathbf{x}_s\mathbf{x}_s}} \mathbf{w}_{kl,s} \leq P_{kl} \quad \forall k,l. \tag{5.5}$$

[1]The noise is the result of background noise, quantization and thermal noise of the error microphone and can also consist of training sequences transmitted by loudspeakers to estimate the impulse response.

Here $E\{.\}$ denotes the expected value operator and is implemented by (recursive) time-averaging over a time window. The power of each loudspeaker signal $y_{kl}(t)$ is also constrained by a maximal power P_{kl}, i.e., $E\{y_{kl}^2(t)\} \leq P_{kl}$. The parameter μ is included as a trade-off between the reproduction error for the required sound signals and the residual interfering sound power [112].

5.3 Centralized algorithm

The objective function of (5.5) , denoted by $J(\mathbf{W})$, can, after some matrix manipulations, be written as

$$J(\mathbf{W}) = \sum_{s=1}^{S} \left(\mathbf{w}_s^T \mathbf{R}_s \mathbf{w}_s - 2\mathbf{w}_s^T \mathbf{r}_s + E\{|d_s^p(t)|^2\} \right) \tag{5.6}$$

where

$$\mathbf{R}_s = \sum_{p \in \mathcal{B}_s} \mathbf{H}^p \mathbf{R}_{\tilde{\mathbf{x}}_s \tilde{\mathbf{x}}_s} \mathbf{H}^{p,T} + \mu \sum_{p \in \mathcal{D}_s} \mathbf{H}^p \mathbf{R}_{\tilde{\mathbf{x}}_s \tilde{\mathbf{x}}_s} \mathbf{H}^{p,T} \tag{5.7}$$

$$\mathbf{r}_s = \sum_{p \in \mathcal{B}_s} \mathbf{H}^p E\{\tilde{\mathbf{x}}_s(t) d_s^p(t)\}, \quad \mathbf{R}_{\tilde{\mathbf{x}}_s \tilde{\mathbf{x}}_s} = E\{\tilde{\mathbf{x}}_s(t) \tilde{\mathbf{x}}_s(t)^T\} \tag{5.8}$$

with $\mathcal{B}_s$ and $\mathcal{D}_s$ denoting the collection of error microphones with $s \in \mathcal{R}_p$ and $s \in \mathcal{I}_p$ respectively, often referred to as the bright and dark zone for sound s.

Note that (5.5) is a convex QCQP and has a unique optimal solution $\hat{\mathbf{W}}$ since $\mathbf{R}_s$ and $\mathbf{R}_{\mathbf{x}_s \mathbf{x}_s}$ are positive definite[2] for all sources. This solution can be found using well know methods, e.g., interior-point methods [149]. The optimal solution will fulfill the KKT conditions

$$\begin{aligned}
&\forall s, k : \mathbf{E}_k^T \left(\mathbf{R}_s + \sum_{l=1}^{L} \hat{\lambda}_{kl} \mathbf{E}_{kl} \mathbf{R}_{\mathbf{x}_s \mathbf{x}_s} \mathbf{E}_{kl}^T \hat{\mathbf{w}}_s \right) = \mathbf{E}_k^T \mathbf{r}_s \\
&\forall k, l : \sum_{s=1}^{S} \hat{\mathbf{w}}_{kl,s}^T \mathbf{R}_{\mathbf{x}_s \mathbf{x}_s} \hat{\mathbf{w}}_{kl,s} \leq P_{kl} \\
&\forall k, l : \hat{\lambda}_{kl} \left(\sum_{s=1}^{S} \hat{\mathbf{w}}_{kl,s}^T \mathbf{R}_{\mathbf{x}_s \mathbf{x}_s} \hat{\mathbf{w}}_{kl,s} - P_{kl} \right) = 0.
\end{aligned} \tag{5.9}$$

[2]The optimal solution will no longer be unique when $\mathbf{R}_s$ is positive semi-definite. The distributed algorithm presented in Section 5.4 will in this case converge to a particular minimizer of the problem, but it is not possible to define which one, therefore, positive definiteness is assumed.

The matrices $\mathbf{E}_{kl} = [\mathbf{0}\ \mathbf{I}_M\ \mathbf{0}]^T \in \mathbb{R}^{MKL \times M}$ and $\mathbf{E}_k = [\mathbf{0}\ \mathbf{I}_{ML}\ \mathbf{0}]^T \in \mathbb{R}^{MKL \times ML}$ are all zero matrices where the identity matrix is placed on the positions corresponding to indexes k and l and to indexes of all loudspeakers of node q respectively.

However, to compute these optimal PM filters $\hat{\mathbf{W}}$, all impulse responses $\mathbf{h}_{kl}^p$ have to be available at a central FC. This FC then has to solve the QCQP (5.5), which is an optimization problem with $KMLS$ variables. This introduces a single point of failure, and furthermore, requires a high computational capacity in the FC. To alleviate these problems, an efficient distributed algorithm is presented in the next section, which is then shown to converge to the same optimal PM filters.

5.4 Distributed algorithm

Before presenting the distributed algorithm, the following Gauss-Seidel procedure for solving the QCQP is discussed. Here i denotes the iteration index and q is the updating node:

1. Initialize $\mathbf{W}^0$ randomly without violating any constraint in (5.5), set $i \leftarrow 0$ and $q \leftarrow 1$.
2. Solve the reduced dimensional QCQP to obtain $\mathbf{w}_{k,s}^{i+1}$ for all the nodes:

$$\begin{aligned} &\min_{\mathbf{W}} \sum_{s=1}^{S} \mathbf{w}_s^T \mathbf{R}_s \mathbf{w}_s - 2\mathbf{w}_s^T \mathbf{r}_s + E\{|d_s^p(t)|^2\} \\ &s.t. \sum_{s=1}^{S} \mathbf{w}_{ql,s}^T \mathbf{R}_{\mathbf{x}_s \mathbf{x}_s} \mathbf{w}_{ql,s} \leq P_{ql} \quad \forall l \\ &\mathbf{w}_{k,s} = \mathbf{w}_{k,s}^i \quad \forall s, k \neq q. \end{aligned} \tag{5.10}$$

3. $i \leftarrow i+1$, $q \leftarrow \mathrm{mod}(q, K) + 1$ and return to step 2.

The following result holds for this Guass-Seidel procedure.

Theorem 5.4.1. *If $\mathbf{R}_s$ has full rank $\forall s$ and the sequence $\{\mathbf{W}^i\}_{i \in \mathbb{N}}$ is generated by the Gauss-Seidel procedure defined above, then*

$$\lim_{i \to \infty} \mathbf{W}^i = \hat{\mathbf{W}}. \tag{5.11}$$

Proof. The proof starts by defining $\mathbf{p}_s^i = \mathbf{w}_s^{i+1} - \mathbf{w}_s^i = \mathbf{E}_q(\mathbf{w}_{q,s}^{i+1} - \mathbf{w}_{q,s}^i)\ \forall s$. From the first KKT condition of (5.10) (Lagrangian stationarity), it is clear that there exist $\{\lambda_{ql}^{i+1} \geq 0\}_{l=1\ldots L}$ such that $\mathbf{W}^{i+1}$ fulfills $\forall s$

$$\mathbf{E}_q^T\left(\mathbf{R}_s\mathbf{w}_s^{i+1} - \mathbf{r}_s + \sum_{l=1}^{L}\lambda_{ql}^{i+1}\mathbf{E}_{ql}\mathbf{R}_{\mathbf{x}_s\mathbf{x}_s}\mathbf{E}_{ql}^T\mathbf{w}_s^{i+1}\right) = \tag{5.12}$$

$$\mathbf{E}_q^T\left(\mathbf{R}_s\mathbf{w}_s^{i+1} - \mathbf{r}_s + \sum_{l\in\mathcal{A}_q^{i+1}}\lambda_{ql}^{i+1}\mathbf{E}_{ql}\mathbf{R}_{\mathbf{x}_s\mathbf{x}_s}\mathbf{E}_{ql}^T\mathbf{w}_s^{i+1}\right) = \mathbf{0}$$

where $\mathcal{A}_q^{i+1}$ is the set of active constraints and $\lambda_{ql}^{i+1} = 0$ for $l \notin \mathcal{A}_q^{i+1}$. This leads to the following identities $\forall s$:

$$\mathbf{p}_s^{i,T}\left(\mathbf{R}_s\mathbf{w}_s^{i+1} - \mathbf{r}_s\right) = -\sum_{l\in\mathcal{A}_q^{i+1}}\lambda_{ql}^{i+1}\mathbf{p}_s^{i,T}\mathbf{E}_{ql}\mathbf{R}_{\mathbf{x}_s\mathbf{x}_s}\mathbf{E}_{ql}^T\mathbf{w}_s^{i+1}. \tag{5.13}$$

Since $\mathbf{W}^i$ is a feasible solution of (5.10), it can be written as

$$P_{ql} \geq \sum_{s=1}^{S}\mathbf{w}_s^{i,T}\mathbf{E}_{ql}\mathbf{R}_{\mathbf{x}_s\mathbf{x}_s}\mathbf{E}_{ql}^T\mathbf{w}_s^i = \sum_{s=1}^{S}\mathbf{w}_s^{i+1,T}\mathbf{E}_{ql}\mathbf{R}_{\mathbf{x}_s\mathbf{x}_s}\mathbf{E}_{ql}^T\mathbf{w}_s^{i+1} + \tag{5.14}$$

$$\mathbf{p}_s^{i,T}\mathbf{E}_{ql}\mathbf{R}_{\mathbf{x}_s\mathbf{x}_s}\mathbf{E}_{ql}^T\mathbf{p}_s^i - 2\mathbf{p}_s^{i,T}\mathbf{E}_{ql}\mathbf{R}_{\mathbf{x}_s\mathbf{x}_s}\mathbf{E}_{ql}^T\mathbf{w}_s^{i+1}\Big).$$

Here $l \in \mathcal{A}_q^{i+1}$ implies that $\sum_{s=1}^{S}\mathbf{w}_s^{i+1,T}\mathbf{E}_{ql}\mathbf{R}_{\mathbf{x}_s\mathbf{x}_s}\mathbf{E}_{ql}^T\mathbf{w}_s^{i+1} = P_{ql}$, resulting in the inequalities $\forall l \in \mathcal{A}_q^{i+1}$:

$$2\sum_{s=1}^{S}\mathbf{p}_s^i\mathbf{E}_{ql}\mathbf{R}_{\mathbf{x}_s\mathbf{x}_s}\mathbf{E}_{ql}^T\mathbf{w}_s^{i+1} \geq \sum_{s=1}^{S}\mathbf{p}_s^i\mathbf{E}_{ql}\mathbf{R}_{\mathbf{x}_s\mathbf{x}_s}\mathbf{E}_{ql}^T\mathbf{p}_s^i. \tag{5.15}$$

It can be verified using the definition of the cost function $J(\mathbf{W})$, (5.13) and (5.15) that

$$\begin{aligned} J(\mathbf{W}^i) - J(\mathbf{W}^{i+1}) &= \sum_{s=1}^{S}\left(\mathbf{p}_s^{i,T}\mathbf{R}_s\mathbf{p}_s^i - 2\mathbf{p}_s^{i,T}(\mathbf{R}_s\mathbf{w}_s^{i+1} - \mathbf{r}_s)\right) \\ &\geq \sum_{s=1}^{S}\left(\mathbf{p}_s^{i,T}\mathbf{R}_s\mathbf{p}_s^i + \sum_{l\in\mathcal{A}_q^{i+1}}\lambda_{ql}^{i+1}\mathbf{p}_s^{i,T}\mathbf{E}_{ql}\mathbf{R}_{\mathbf{x}_s\mathbf{x}_s}\mathbf{E}_{ql}^T\mathbf{p}_s^i\right) \\ &\geq \sum_{s=1}^{S}\lambda_{\min}(\mathbf{R}_s)||\mathbf{p}_s^i||^2 \geq \lambda_{\min}\sum_{s=1}^{S}||\mathbf{p}_s^i||^2 \geq 0 \end{aligned} \tag{5.16}$$

where $\lambda_{\min}(\mathbf{R}_s)$ denotes the smallest eigenvalue of $\mathbf{R}_s$ and $\lambda_{\min} = \min_s \lambda_{\min}(\mathbf{R}_s)$. Since $\mathbf{W}^{i+1}$ minimizes the cost function under the same constraints as $\mathbf{W}^i$, it must hold that $J(\mathbf{W}^{i+1}) \leq J(\mathbf{W}^i), \forall i > 0$. Therefore, and since the cost function $J(\mathbf{W})$ is bounded below by zero, it holds that

$$\sum_{i=0}^{\infty} \left(J(\mathbf{W}^i) - J(\mathbf{W}^{i+1}) \right) = J(\mathbf{W}^0) - \lim_{i \to \infty} J(\mathbf{W}^i) < \infty. \tag{5.17}$$

Using $\lambda_{\min} > 0$, this leads to the result

$$\sum_{i=0}^{\infty} \sum_{s=1}^{S} ||\mathbf{p}_s^i||^2 < \infty \Rightarrow \lim_{i \to \infty} ||\mathbf{W}^{i+1} - \mathbf{W}^i||^2 = 0. \tag{5.18}$$

At iteration $i+1$, updating node $q = \text{mod } (i, K) + 1$ computes $\mathbf{W}^{i+1}$ and the L local lagrange parameters $\boldsymbol{\lambda}_{ql}^{i+1}$ satisfying (5.12). K iterations before, similar solutions, denoted by $\mathbf{W}^{i-K+2}$ and the L local lagrange parameters $\boldsymbol{\lambda}_{ql}^{i-K+2}$, were computed by updating node q, this time satisfying

$$\mathbf{E}_q^T \left(\mathbf{R}_s \mathbf{w}_s^{i-K+2} - \mathbf{r}_s + \sum_{l=1}^{L} \lambda_{ql}^{i-K+2} \mathbf{E}_{ql} \mathbf{R}_{\mathbf{x}_s \mathbf{x}_s} \mathbf{E}_{ql}^T \mathbf{w}_s^{i-K+2} \right) = \mathbf{0} \quad \forall s. \tag{5.19}$$

Equating (5.12) and (5.19), results in the following relation $\forall s$

$$\mathbf{E}_q^T \sum_{l=1}^{L} \lambda_{ql}^{i+1} \mathbf{E}_{ql} \mathbf{R}_{\mathbf{x}_s \mathbf{x}_s} \mathbf{E}_{ql}^T \mathbf{w}_s^{i+1} \tag{5.20}$$

$$= \mathbf{E}_q^T \Big(\sum_{l=1}^{L} \lambda_{ql}^{i-K+2} \mathbf{E}_{ql} \mathbf{R}_{\mathbf{x}_s \mathbf{x}_s} \mathbf{E}_{ql}^T \mathbf{w}_s^{i-K+2} + \mathbf{R}_s \left(\mathbf{w}_s^{i-K+2} - \mathbf{w}_s^{i+1} \right) \Big).$$

Note that λ_{ql}^{i-K+2} and $\mathbf{E}_{ql}^T \mathbf{w}_s^{i-K+2} = \mathbf{w}_{ql,s}^{i-k+2}$ are the same as $\lambda_{ql}^{\bar{i}}$ and $\mathbf{E}_{ql}^T \mathbf{w}_s^{\bar{i}} = \mathbf{w}_{ql,s}^{\bar{i}}$ with $i - K + 2 \leq \bar{i} \leq i$ since these quantities are not modified between iterations $i - K + 1$ and i. Therefore (5.12) can finally be rewritten $\forall s$ as

$$\mathbf{E}_q^T \left(\mathbf{R}_s \mathbf{w}_s^{\bar{i}} - \mathbf{r}_s + \sum_{l=1}^{L} \lambda_{ql}^{\bar{i}} \mathbf{E}_{ql} \mathbf{R}_{\mathbf{x}_s \mathbf{x}_s} \mathbf{E}_{ql}^T \mathbf{w}_s^{\bar{i}} \right) = \mathbf{E}_q^T \mathbf{R}_s \left(\mathbf{w}_s^{\bar{i}} - \mathbf{w}_s^{i-K+2} \right). \tag{5.21}$$

Equation (5.18) shows that $||\mathbf{W}^{i+1} - \mathbf{W}^i||$ and by extension[3] $||\mathbf{W}^{\bar{i}} - \mathbf{W}^{i-K+2}||$ becomes infinitesimally small when $i \to \infty$, hence

$$\lim_{i \to \infty} \left\| \mathbf{E}_q^T \left(\mathbf{R}_s \mathbf{w}_s^i - \mathbf{r}_s + \sum_{l=1}^{L} \lambda_{ql}^i \mathbf{E}_{ql} \mathbf{R}_{\mathbf{x}_s \mathbf{x}_s} \mathbf{E}_{ql}^T \mathbf{w}_s^i \right) \right\| = 0 \quad \forall s. \tag{5.22}$$

[3]This can be shown by repeatedly applying the triangle inequality.

Note that this is valid for all i and not only for i with $q = \text{mod}\,(i, K) + 1$ since $\bar{i}$ can be any iteration between $i - K + 2$ and i. A similar result can be obtained for other updating nodes q, which shows that the lagrangian stationarity condition in (5.9) is satisfied upon convergence. All other KKT-conditions (primal feasibility and complementary slackness) in (5.9) are already satisfied in each iteration. Since it is assumed that $\hat{\mathbf{W}}$ is the unique solution of the KKT-conditions, this therefore shows that $\lim_{i\to\infty} \mathbf{W}^i = \hat{\mathbf{W}}$. □

The optimization problem in (5.10) can, after some manipulations and removing constants in the objective function, be written as

$$\min_{\mathbf{W}_q} \sum_{s=1}^{S} \mathbf{w}_{q,s}^T \mathbf{R}_{q,s} \mathbf{w}_{q,s} - 2\mathbf{w}_{q,s}^T \left(\mathbf{r}_{q,s} - \mathbf{H}_q^p \mathbf{r}_s^i + \mathbf{R}_{q,s} \mathbf{w}_{q,s}^i\right)$$

$$s.t. \sum_{s=1}^{S} \mathbf{w}_{ql,s}^T \mathbf{R}_{\mathbf{x}_s \mathbf{x}_s} \mathbf{w}_{ql,s} \leq P_{ql} \quad \forall l \tag{5.23}$$

with $\mathbf{W}_q = [\mathbf{w}_{q,1}\ ...\ \mathbf{w}_{q,S}]$ and

$$\mathbf{R}_{q,s} = \sum_{p\in\mathcal{B}_s} \mathbf{H}_q^p \mathbf{R}_{\tilde{\mathbf{x}}_s \tilde{\mathbf{x}}_s} \mathbf{H}_q^{p,T} + \mu \sum_{p\in\mathcal{D}_s} \mathbf{H}_q^p \mathbf{R}_{\tilde{\mathbf{x}}_s \tilde{\mathbf{x}}_s} \mathbf{H}_q^{p,T} \tag{5.24}$$

$$\mathbf{r}_{q,s} = \sum_{p\in\mathcal{B}_s} \mathbf{H}_q^p E\{\tilde{\mathbf{x}}_s(t) d_s^p(t)\} \tag{5.25}$$

$$\mathbf{r}_s^i = \sum_{p\in\mathcal{B}_s} \mathbf{R}_{\tilde{\mathbf{x}}_s \tilde{\mathbf{x}}_s} \mathbf{H}^{p,T} \mathbf{w}_s^i + \mu \sum_{p\in\mathcal{D}_s} \mathbf{R}_{\tilde{\mathbf{x}}_s \tilde{\mathbf{x}}_s} \mathbf{H}^{p,T} \mathbf{w}_s^i. \tag{5.26}$$

Although (5.23) is much easier to solve than (5.5) since it has only LSM optimization variables, (5.26) still requires the knowledge of all impulse responses $\mathbf{h}_{kl}^p$ and current PM filters in the WASAN. Luckily (5.26) can also be computed from the error microphone signals as

$$\mathbf{r}_s^i = \sum_{p\in\mathcal{B}_s} E\{\tilde{\mathbf{x}}(t) e^p(t)\} + \mu \sum_{p\in\mathcal{D}_s} E\{\tilde{\mathbf{x}}(t) e^p(t)\}. \tag{5.27}$$

Based on this observation, a distributed adaptive PM algorithm (DA-PM) can be proposed as defined in Algorithm 6. The steps that are presented in Algorithm 6 are more general than the steps performed in the Gauss-Seidel procedure. To avoid confusion, the iteration index is now put between brackets (i). The differences are that in each iteration (i) of Algorithm 6 a set of nodes

$\mathcal{S}^i$ is chosen to perform an update of their local PM filters. Also, instead of updating each local filter with the newly computed filter, a smooth combination between the newly computed filter and the filter from the previous iterations is used, using a predefined smoothing parameter α^i.

Proving convergence of Algorithm 6 can be done similarly as in [85], which is omitted here for conciseness. It requires that $\Delta\mathbf{W}^{(i+1)} = \mathbf{W}^{(i+1)} - \mathbf{W}^{(i)}$ is a direction of descent, which can be argued as follows. Both $\mathbf{W}^{i+1}$ and $\mathbf{W}^i$ are satisfying the convex constraints in (5.5) as well as any convex combinations $\mathbf{W} = \mathbf{W}^i + \alpha_i(\Delta\mathbf{W}^{i+1})$ with $\Delta\mathbf{W}^{i+1} = \mathbf{W}^{i+1} - \mathbf{W}^i = [\mathbf{0}\ \Delta\mathbf{W}_q^{i+1}\ \mathbf{0}]$ and $\alpha_i \in (0,1)$. Since $J(\mathbf{W}^{i+1}) \leq J(\mathbf{W}^i)$ and the objective function is strictly convex, this shows that $\Delta\mathbf{W}^{i+1}$ is a non-decreasing direction of descent for $J(\mathbf{W}^i)$, i.e.

$$\sum_{s=1}^{S} \nabla_{\mathbf{w}_s} J(\mathbf{w}_s^i)^T \Delta\mathbf{w}_s^{i+1} = \sum_{s=1}^{S} \nabla_{\mathbf{w}_{q,s}} J(\mathbf{w}_s^i)^T \Delta\mathbf{w}_{q,s}^{i+1} \leq 0 \tag{5.28}$$

with equality if $\mathbf{W}^{i+1} = \mathbf{W}^i$. In Algorithm 6 all nodes in the current update set $\mathcal{S}^i$ are performing a similar update, such that $\Delta\mathbf{W}_q^{(i+1)} = \Delta\mathbf{W}_q^{i+1}$ for all $q \in \mathcal{S}^i$ and is zero for all other positions. The directional derivative of $J(\mathbf{W}^i)$ in the direction $\Delta\mathbf{W}^{(i+1)}$ can then be written as

$$\sum_{s=1}^{S} \nabla_{\mathbf{w}_s} J(\mathbf{w}_s^i)^T \Delta\mathbf{w}_s^{(i+1)} = \sum_{q\in\mathcal{S}^i} \sum_{s=1}^{S} \nabla_{\mathbf{w}_{q,s}} J(\mathbf{w}_s^i)^T \Delta\mathbf{w}_{q,s}^{i+1} \tag{5.29}$$

which is lesser than or equal to zero when using (5.28). This shows that also $\Delta\mathbf{W}^{(i+1)}$ is a direction of descent.

The conditions for α_i to guarantee convergence are that

$$\alpha^i \in (0,1]; \quad \lim_{i\to\infty} \alpha^i; \quad \sum_{i=0}^{\infty} \alpha^i = \infty. \tag{5.30}$$

Simulations showed that this can be relaxed in practice to a condition $\alpha^i \leq \alpha^\star$, where $\alpha^\star$ is scenario-dependent. The condition for determining the sets $\mathcal{S}^i$ for $i = 0...\infty$ is that none of the nodes permanently stops the updating process of its parameters. This means that when the number of times a node k belongs to $\mathcal{S}^i$ is counted for $i = 0...\infty$, this number will be unbounded. It is noted that this requires no centralized controller, each node can on the fly decide when and how often it performs an update of its parameters.

The above Gauss-Seidel procedure is obtained by choosing $\mathcal{S}^i = \text{mod}(i, K) + 1$ and $\alpha_i = 1$ in Algorithm 6.

Algorithm 6: Distributed Adaptive PM algorithm (DA-PM)

1 - Initialize $\mathbf{w}_{k,s}^{(0)}$ $\forall k, s$ without violating any constraint in (5.5).
- $i \leftarrow 0$.

2 - Each node k produces the loudspeaker signals for $t = 1...T$:

$$y_{kl}(iT+t) = \sum_{s=1}^{S} \mathbf{w}_{kl,s}^{(i),T} \mathbf{x}(iT+t) \quad \forall l. \tag{5.31}$$

3 - The error microphone signals $e^p(iT+t)$ $\forall p$ are transmitted to all nodes $k \in \mathcal{S}^i$.

4 - Each node $q \in \mathcal{S}^i$ performs the following operations:

1. Collect T observations of $e^p(iT+t)$ $\forall p$ and estimate $\mathbf{r}_s^{(i)}$ using (5.27).
2. Compute new estimates of $\mathbf{h}_{ql}^p$ $\forall l, p$ or reuse previous estimates.
3. Estimate $\mathbf{R}_{q,s}$ and $\mathbf{r}_{q,s}$ using (5.24) and (5.25).
4. Solve QPCP (5.23) to obtain $\mathbf{w}_{q,s}^{\text{new}}$ $\forall s$.
5. Update the local PM filters as

$$\mathbf{w}_{q,s}^{(i+1)} = (1-\alpha^i)\mathbf{w}_{q,s}^{(i)} + \alpha^i \mathbf{w}_{q,s}^{\text{new}} \quad \forall s. \tag{5.32}$$

5 - All other nodes $k \notin \mathcal{S}^i$ do not update their PM filters:

$$\mathbf{w}_{k,s}^{(i+1)} = \mathbf{w}_{k,s}^{(i)} \quad \forall s. \tag{5.33}$$

6 - $i \leftarrow i+1$ and return to step 2.

The estimation of the impulse responses $\mathbf{h}_{kl}^p$ in step 4.2 is necessary to track possible changes in the impulse responses and can be done using training sequences. The updating node q then adds a training signal $\delta_{ql}(t)$[4] that is uncorrelated with the sounds, to its loudspeaker signals $\mathbf{y}_{ql}(iT+t)$ and estimates the impulse responses as:

$$\mathbf{h}_{ql}^p = E\{\boldsymbol{\delta}_{ql}(t)\boldsymbol{\delta}_{ql}(t)^T\}^{-1} \sum_{t=1}^{T} \boldsymbol{\delta}_{ql}(t) e^p(iT+t) \quad \forall l, p \tag{5.34}$$

with $\boldsymbol{\delta}_{ql}(t) = [\delta_{ql}(t) \ ... \ \delta_{ql}(t-N+1)]^T$.

The advantages of the DA-PM are that the local computational complexity is much more relaxed and that there is no need for commutation between the nodes or communication with a FC. The disadvantage is that it requires multiple

[4]Since this will distort the signal received at the error microphones, it can also be useful to use colored noise (e.g., a noise signal with the spectrum below the hearing threshold for all frequencies) to estimate the impulse responses.

iterations to converge to the optimal solution, and will hence experience a slower tracking speed compared to a centralized implementation.

5.5 Simulations

To demonstrate the convergence of the DA-PM, 50 Monte Carlo simulations are performed on a WASAN with $K = 6$ nodes, $L = 4$ loudspeakers per node and $P = 10$ error microphones. Each error microphone randomly picks 1 out of 3 sound signals as its required sound signal and defines its desired sound pressure as the clean required sound. The sounds are generated as Gaussian noise with zero mean and unit variance of $T = 1000$ samples. P_{kl} is set to 0.1 to activate the constraints and $\mu = 2$. The impulse responses are modeled as random impulse responses with zero mean and unit variance of order $N = 10$ and the PM filters have order $M = 10$ as well. In the simulations, the proposed DA-PM with $S^i = \{1, ..., K\}$ and $\alpha_i = 0.5$ for all iterations, is compared to the Gauss-Seidel procedure, the optimal PM filters and the stand-alone PM filters, obtained when each node locally solves (5.10) with the PM filters of the other nodes put to zero. Figure 5.1 shows $||\hat{\mathbf{W}} - \mathbf{W}^i||$ and $J(\mathbf{W})$ for the different filters in each iterations, averaged over 50 Monte Carlo runs. Convergence can be observed and it is clear that the proposed DA-PM method converges faster to the optimal solution than the Gauss-Seidel procedure.

To evaluate the performance of the DA-PM, an acoustic scenario is simulated using the image method [150] in a room of dimension $5m \times 5m \times 3m$ and with a reverberation time $T_{60} = 0.222$. There are 4 nodes, each having an array 4 loudspeakers, spaced $0.5m$ from each other, and each located at $0.5m$ from a wall. The virtual source is located in the center of the room and 3 error microphones are located in a radius of $0.5m$ from this center, each requiring a different sound signal. The 3 different sound signals are 5 seconds of speech from the HINT database. P_{kl} is also set to 0.1 and at iterations 40 and 80, all loudspeakers and error microphones are moved $0.2m$ in a random direction, realizing a change in the impulse responses. M is set to 50. The used performance measure is the distortion ratio, defined as

$$\text{DR} = \sum_{p=1}^{P} \frac{E\{||d_p(t)||^2\}}{E\{||d_p(t) - \sum_{s=1}^{S} \mathbf{w}_s^T \mathbf{H}^p \mathbf{x}_s(t)||^2\}}. \tag{5.35}$$

The results for the different algorithms are shown in Figure 5.2. It is clear that the Gauss-Seidel procedure and the DA-PM converge to the optimal solution and that they can track changes in the acoustic environment. The DA-PM also outperforms the stand-alone solution after 2 iterations.

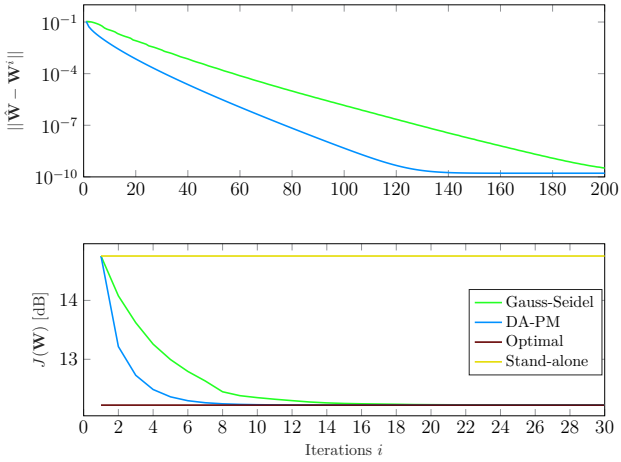

Figure 5.1: Evolution of $||\hat{\mathbf{W}} - \mathbf{W}^i||$ and $J(\mathbf{W})$ for the DA-PM and Gauss-Seidel procedure, compared to the optimal and stand-alone solution.

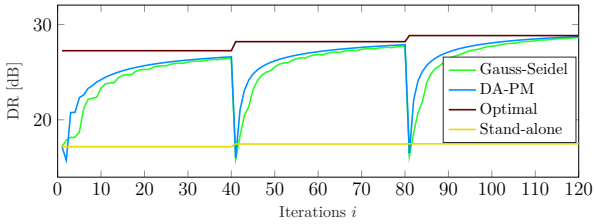

Figure 5.2: Evolution of DR for the DA-PM and Gauss-Seidel procedure, compared to the optimal and stand-alone solution.

5.6 Conclusion

In this paper, PM based sound zoning has been considered in a WASAN. A distributed adaptive PM algorithm has been proposed, avoiding the high communication and computational requirements of a centralized algorithm. The algorithm has been shown to converge to the solution of the centralized algorithm, by means of Monte Carlo simulations and evaluated in a simulated acoustic scenario.

Part II

Distributed signal processing algorithms for CFmMIMO systems

Chapter 6

Scalable and distributed MMSE-based uplink receive combining

Scalable and Distributed MMSE algorithms for Uplink Receive Combining in Cell-free Massive MIMO Systems.

Robbe Van Rompaey and Marc Moonen

Published in
Proceedings of the *2021 IEEE International Conference on Acoustics, Speech and Signal Processing (ICASSP)*, Toronto, Canada, 2021, pp. 4445-4449.

©2021 IEEE Reprint, with permission from:
R. Van Rompaey and M. Moonen, "Scalable and Distributed MMSE algorithms for Uplink Receive Combining in Cell-free Massive MIMO Systems" in *2021 IEEE International Conference on Acoustics, Speech and Signal Processing (ICASSP)*, Toronto, Canada, pp. 4445-4449, 2021.
Changes include layout, representation and minor editing aspects.
The candidate's contributions as first author include all performed research and writing of the article under guidance of the co-author.

Abstract

In cell-free Massive MIMO systems, a large number of distributed wireless access points (AP) are simultaneously serving a number of user equipments (UEs). This setup has the ability to offer a good quality of service, be it that there is still a need for low-complexity signal processing algorithms. In this paper, the problem of optimal uplink receive combining is tackled by providing an efficient distributed MMSE algorithm, with a minimal number of exchanged parameters between the APs and the network center. Scalable versions of this distributed MMSE algorithm are also proposed ensuring that the algorithm can be used in large networks with many UEs.

Keywords Cell-free Massive MIMO, uplink receive combining, distributed algorithms, user-centric networking

6.1 Introduction

Cell-free Massive MIMO systems have recently been introduced [66, 124] where a large number of access points (AP) jointly serve a smaller number of user equipments (UEs). The APs use channel estimates, possibly obtained from received uplink pilots, and apply receive combining and transmit beamforming to transfer data from and to the UEs. It has been shown that Massive MIMO systems provide better performance compared to small-cell systems, even with the simple local maximum-ratio (MR) combining scheme [66, 71, 126].

An improved performance is obtained when the simple MR combining scheme is replaced with minimum mean squared error (MMSE) combining schemes [74, 164, 165], where typically the channel state information (CSI) has to be transmitted to a network center (NC) in order to determine the receiver vectors. The NC can either be a physical processing unit that is responsible for processing the signals of all UEs, or can be seen as a virtual set of tasks that are performed somewhere in the network. Although a significant performance increase can be achieved, the drawbacks of network-wide MMSE combining schemes, namely the need for centralizing the CSI and the increased computational complexity when the number of UEs and APs grows large, make them not very practical.

In this paper, the problem of optimal uplink receive combining is tackled where these drawbacks are resolved. An efficient distributed MMSE algorithm is proposed where the CSI of an AP is required only locally and only a small number of parameters have to be exchanged between the APs and the NC. Scalable versions of this distributed MMSE algorithm based on a user-centric approach [71, 74] ensure that the algorithm can also be used for large networks with many UEs. The paper also includes simulations to show the performance of the proposed algorithms.

6.2 Signal model

Consider a cell-free Massive MIMO system consisting of K single-antenna UEs and L APs randomly deployed over the considered area, with M_l antennas in the l-th AP and with local processing capabilities in each AP. The APs are connected to a NC via a physical network. This setup allows for coherent reception of data from the UEs. In the cell-free Massive MIMO literature [67, 124] it is often assumed that $M \gg K$ and that both M and K are large, with $M = \sum_{l=1}^{L} M_l$ the total number of antennas in the considered area.

The UEs use τ_u time slots for uplink data transmission and τ_p time slots are

reserved for channel estimation[1]. The channel from UE k to AP l is denoted by $\mathbf{h}_{kl} \in \mathbb{C}^{M_l}$ such that the channel from UE k and all the APs is given by $\mathbf{h}_k = [\mathbf{h}_{k1}^T \ ... \ \mathbf{h}_{kL}^T]^T \in \mathbb{C}^M$. The channel $\mathbf{h}_{kl}$ is assumed to remain constant during a coherence block[2] $\tau_c = \tau_p + \tau_u$ and can be approximated as being drawn from an independent correlated Rayleigh fading realization $\mathcal{NC}(0, \mathbf{R}_{kl})$. $\mathbf{R}_{kl} \in \mathbb{C}^{M_l \times M_l}$ is a positive semi-definite spatial correlation matrix describing the large-scale fading, including geometric pathloss, shadowing, antenna gains, and spatial channel correlation [7]. The Complex Gaussian distribution models the small-scale fading. Due to the spatial distribution of the APs in the network, the channel vectors of different APs are independently distributed, i.e., $E\{\mathbf{h}_{kl}\mathbf{h}_{kn}^H\} = \mathbf{0}_{M_l \times M_n}$ for $l \neq n$, such that the channel estimation can be performed independently at each AP.

6.2.1 Channel estimation

It is assumed that AP l can obtain a local estimate $\hat{\mathbf{h}}_{kl}$ of $\mathbf{h}_{kl} = \hat{\mathbf{h}}_{kl} + \tilde{\mathbf{h}}_{kl}$ for UE k in each coherence block. Furthermore, the estimation is assumed to be unbiased with an estimation error $\tilde{\mathbf{h}}_{kl}$ that is uncorrelated with the estimation $\hat{\mathbf{h}}_{kl}$ and with known variance $\mathbf{C}_{kl}$:

$$\tilde{\mathbf{h}}_{kl} \sim \mathcal{NC}(0, \mathbf{C}_{kl}). \tag{6.1}$$

There exist multiple channel estimation techniques, that provide these quantities for example based on training sequences [74, 166] or Bayesian learning [167], where often an estimate of the spatial correlation matrix $\mathbf{R}_{kl}$ is required.

6.2.2 Uplink signal model

During uplink data transmission, the received signal $\mathbf{y}_l \in \mathbb{C}^{M_l}$ at AP l is given by

$$\mathbf{y}_l = \sum_{k=1}^{K} \mathbf{h}_{kl} s_k + \mathbf{n}_l = \mathbf{H}_l \mathbf{s} + \mathbf{n}_l \tag{6.2}$$

where $s_k \in \mathbb{C}$ is the signal transmitted by UE k with transmit power $p_k = E\{s_k s_k^H\}$ and $\mathbf{n}_l \sim \mathcal{NC}(0, \mathbf{R}_{\mathbf{n}_l \mathbf{n}_l})$ is an additive Gaussian noise component, modeling antenna noise and quantization noise. The noise components of

[1]The uplink receive combining schemes considered in this paper can also be used for downlink transmit beamforming when the APs and UEs operate using a TDD protocol exploiting the duality between uplink and downlink [7].

[2]Note that abstraction is made of the practical Orthogonal Frequency Division Multiplexing (OFDM) based multi-carrier modulation. See [6, Sec. 2] how this simplification can be done.

the different antennas of an AP are often assumed to be independent, i.e., $\mathbf{R}_{\mathbf{n}_l\mathbf{n}_l} = \sigma^2\mathbf{I}_{M_l}$, but here a more general case is considered with a general $\mathbf{R}_{\mathbf{n}_l\mathbf{n}_l}$. Furthermore, $\mathbf{H}_l = [\mathbf{h}_{1l} \ ... \ \mathbf{h}_{Kl}]$ is the concatenation of the channels from all the UEs to AP l and $\mathbf{s} = [s_1 \ ... \ s_K]^T$. Stacking the received signals of all APs in $\mathbf{y} = [\mathbf{y}_1^T \ ... \ \mathbf{y}_L^T]^T \in \mathbb{C}^M$ as well as the noise components in $\mathbf{n} = [\mathbf{n}_1^T \ ... \ \mathbf{n}_L^T]^T \in \mathbb{C}^M \sim \mathcal{NC}(0, \mathbf{R}_{\mathbf{nn}})$ where $\mathbf{R}_{\mathbf{nn}} = \text{Blkdiag}\{\mathbf{R}_{\mathbf{n}_1\mathbf{n}_1}, ..., \mathbf{R}_{\mathbf{n}_L\mathbf{n}_L}\}$, results in the network-wide signal model:

$$\mathbf{y} = \mathbf{H}\mathbf{s} + \mathbf{n} \tag{6.3}$$

with $\mathbf{H} = [\mathbf{H}_1^T \ ... \ \mathbf{H}_L^T]^T = [\mathbf{h}_1 \ ... \ \mathbf{h}_K]$.

6.2.3 Uplink receive combining

In network-wide receive combining the signals $\mathbf{s}$ are estimated by linearly combining the received signals $\mathbf{y}$ by means of a receiver matrix $\mathbf{V} \in \mathbb{C}^{M\times K}$. Note that this linear combining can be performed in the network if AP l selects the local receiver matrix $\mathbf{V}_l = [\mathbf{v}_{1l} \ ... \ \mathbf{v}_{Kl}] \in \mathbb{C}^{M_l\times K}$ in $\mathbf{V} = [\mathbf{V}_1^T \ ... \ \mathbf{V}_L^T]^T$ and computes the local estimate $\mathbf{z}_l = \mathbf{V}_l^H\mathbf{y}_l$. The NC then estimates $\mathbf{s}$ by combining the local estimates as

$$\hat{\mathbf{s}} = \sum_{l=1}^{L} \mathbf{z}_l = \sum_{l=1}^{L} \mathbf{V}_l^H\mathbf{y}_l = \mathbf{V}^H\mathbf{y}. \tag{6.4}$$

The goal is then to choose a local receiver matrix $\mathbf{V}_l$ that provides a good estimate $\hat{\mathbf{s}}$, but where the CSI of an AP is required only locally. In cell-free Massive MIMO literature a MR combing scheme is often used with $\mathbf{V}_l = \hat{\mathbf{H}}_l$ [66, 71, 126]. Other heuristic schemes that perform generally better, but require more processing power of the AP are local MMSE combining schemes [68]. In this paper, network-wide MMSE receive combining schemes [74] will be considered, requiring typically network-wide CSI. However, in Section 6.3 it is shown that if a small number of parameters can be exchanged between the NC and the APs, this network-wide MMSE receive combining can still be obtained efficiently at the NC where the CSI is used only locally leading to an efficient distributed MMSE algorithm. Since the number of combining vectors that an AP has to compute, grows with the number of UEs in the network, inspired by [74], scalable versions of this distributed MMSE algorithm are also derived, resulting in combining schemes that scale independently of the number of UEs in the network presented in Section 6.4.

6.3 Distributed MMSE receive combining

The network-wide MMSE receiver matrix $\mathbf{V}^{\text{N-RC}} = [\mathbf{v}_1^{\text{N-RC}} \ ... \ \mathbf{v}_K^{\text{N-RC}}]$ is obtained by minimizing the mean squared error between the transmitted signal $\mathbf{s}$ and the estimate obtained by linearly combining the received signals $\mathbf{y}$

$$\mathbf{V}^{\text{N-RC}} = \arg\min_{\mathbf{V}} E\{||\mathbf{s} - \mathbf{V}^H\mathbf{y}||^2\} \tag{6.5}$$

where $E\{.\}$ is the expected value operator and $||.||$ is the Euclidean norm. The optimal solution of this convex optimization problem has a closed form and is given by

$$\mathbf{V}^{\text{N-RC}} = E\{\mathbf{y}\mathbf{y}^H\}^{-1}E\{\mathbf{y}\mathbf{s}^H\} \tag{6.6}$$

with the uplink correlation matrix $E\{\mathbf{y}\mathbf{y}^H\}$ given as

$$\begin{aligned} E\{\mathbf{y}\mathbf{y}^H\} &= E\{\mathbf{H}\mathbf{s}\mathbf{s}^H\mathbf{H}^H\} + E\{\mathbf{n}\mathbf{n}^H\} \\ &= \hat{\mathbf{H}}E\{\mathbf{s}\mathbf{s}^H\}\hat{\mathbf{H}}^H + E\{\tilde{\mathbf{H}}\mathbf{s}\mathbf{s}^H\tilde{\mathbf{H}}^H\} + E\{\mathbf{n}\mathbf{n}^H\} \\ &= \hat{\mathbf{H}}\mathbf{P}\hat{\mathbf{H}}^H + \sum_{k=1}^{K} p_k\mathbf{C}_k + \mathbf{R}_{\mathbf{nn}} \end{aligned} \tag{6.7}$$

where $\mathbf{C}_k = \text{Blkdiag}\{\mathbf{C}_{k1}, ..., \mathbf{C}_{kL}\}$ and $E\{\mathbf{s}\mathbf{s}^H\} = \mathbf{P} = \text{diag}\{p_1, ..., p_K\}$. In the second step, $\mathbf{H}$ is replaced by $\hat{\mathbf{H}}+\tilde{\mathbf{H}}$ and the fact that $\hat{\mathbf{H}}$ and $\tilde{\mathbf{H}}$ are uncorrelated is also used. In the last step, independence between the signals and the channel estimation error is used. Furthermore, the cross-correlation matrix $E\{\mathbf{y}\mathbf{s}^H\}$ is given by

$$E\{\mathbf{y}\mathbf{s}^H\} = \hat{\mathbf{H}}\mathbf{P}. \tag{6.8}$$

The closed form expression for the network-wide MMSE receiver matrix $\mathbf{V}^{\text{N-RC}}$ is then obtained as

$$\mathbf{V}^{\text{N-RC}} = (\hat{\mathbf{H}}\mathbf{P}\hat{\mathbf{H}}^H + \underbrace{\sum_{k=1}^{K} p_k\mathbf{C}_k + \mathbf{R}_{\mathbf{nn}}}_{\mathbf{T}})^{-1}\hat{\mathbf{H}}\mathbf{P}. \tag{6.9}$$

It is shown [7] that the receiver vector $\mathbf{v}_k^{\text{N-RC}}$ maximizes the achievable spectral efficiency (SE) of UE k given by

$$\text{SE}_k = \frac{\tau_u}{\tau_c}E\{\log_2(1 + \text{SINR}_k)\} \tag{6.10}$$

where the expectation is with respect to the different channel realizations and where SINR_k is given by the ratio

$$\frac{p_k|\mathbf{v}_k^H\hat{\mathbf{h}}_k|^2}{\sum_{i=1,i\neq k}^{K} p_i|\mathbf{v}_k^H\hat{\mathbf{h}}_i|^2 + \mathbf{v}_k^H\mathbf{T}\mathbf{v}_k} \tag{6.11}$$

which will be used as a performance measure in the simulations.

To obtain this filter, all the APs have to send their local estimate $\hat{\mathbf{H}}_l \in \mathbb{C}^{M_l \times K}$, estimation error variance $\sum_{k=1}^{K} p_k \mathbf{C}_{kl} \in \mathbb{C}^{M_l \times M_l}$ and $\mathbf{R}_{\mathbf{n}_l \mathbf{n}_l}$ to the NC, which leads to a significant communication cost, especially when the number of antennas M_l of an AP l is large. The NC then has to invert an $M \times M$ matrix to obtain $\mathbf{V}^{\text{N-RC}}$. During receive combining, the NC needs to have access to all M received signals $\mathbf{y}$, which requires a larger network communication than when the local estimates can be combined in the network as in (6.4).

However, the expression for the network-wide MMSE receiver matrix $\mathbf{V}^{\text{N-RC}}$ can be rewritten as

$$\begin{aligned}
\mathbf{V}^{\text{N-RC}} &= \left[\mathbf{T}^{-1} - \mathbf{T}^{-1}\hat{\mathbf{H}}\left(\mathbf{P}^{-1} + \hat{\mathbf{H}}^H\mathbf{T}^{-1}\hat{\mathbf{H}}\right)^{-1}\hat{\mathbf{H}}^H\mathbf{T}^{-1}\right]\hat{\mathbf{H}}\mathbf{P} \\
&= \mathbf{T}^{-1}\hat{\mathbf{H}}\left(\mathbf{P}^{-1} + \hat{\mathbf{H}}^H\mathbf{T}^{-1}\hat{\mathbf{H}}\right)^{-1}\left[\left(\mathbf{P}^{-1} + \hat{\mathbf{H}}^H\mathbf{T}^{-1}\hat{\mathbf{H}}\right) - \hat{\mathbf{H}}^H\mathbf{T}^{-1}\hat{\mathbf{H}}\right]\mathbf{P} \\
&= \mathbf{T}^{-1}\hat{\mathbf{H}}\left(\mathbf{P}^{-1} + \hat{\mathbf{H}}^H\mathbf{T}^{-1}\hat{\mathbf{H}}\right)^{-1} \\
&= \begin{bmatrix}\mathbf{W}_1 \\ \vdots \\ \mathbf{W}_L\end{bmatrix}\left(\mathbf{P}^{-1} + \mathbf{X}\right)^{-1} \qquad (6.12)
\end{aligned}$$

with

$$\mathbf{W}_l = \left(\sum_{k=1}^{K} p_k \mathbf{C}_{kl} + \mathbf{R}_{\mathbf{n}_l \mathbf{n}_l}\right)^{-1}\hat{\mathbf{H}}_l \qquad (6.13)$$

and

$$\mathbf{X} = \sum_{l=1}^{L} \hat{\mathbf{H}}_l^H \mathbf{W}_l. \qquad (6.14)$$

The Sherman-Morrison-Woodbury formula and the fact that $\mathbf{T}$ is a block-diagonal matrices are used in (6.12).

Based on this equivalence, an efficient way of obtaining the network-wide MMSE estimate is presented in Algorithm 7 as the network-wide distributed MMSE receive combining (N-DRC) algorithm. Here the CSI is only used locally to construct $\mathbf{W}_l$ and $\hat{\mathbf{H}}_l^H \mathbf{W}_l$, but does not need to be transmitted to the NC.

A simple procedure to obtain the in-network sum in step 2 of Algorithm 7 is based on the formation of a tree topology using the available physical links

between the APs [163] with the NC as root node. A leaf node AP l with only one neighbor starts with transmitting its transformed signals to its neighbor. An AP l with more than one neighbor waits until it has received signals from all its neighbors, except one denoted by n and transmits $\mathbf{w}_l + \sum_{\bar{l}\in\{\mathcal{N}_l\setminus n\}} \mathbf{w}_{\bar{l}}$ to AP n, where $\mathcal{N}_l$ denotes the set of neighbors of node l. This continues until the root node NC has received signals from all its neighbors. The root node NC can then compute $\mathbf{w}$ straightforwardly. A similar procedure can be followed to construct $\mathbf{X}$, but since $\mathbf{X}$ is Hermitian symmetric, the transmission of only $\frac{K^2+K}{2}$ i.s.o. K^2 parameters is required.

Algorithm 7: Network-Wide Distributed MMSE Receive Combining (N-DRC)

Perform the following steps in each coherence block:

1 - Each AP l obtains a local estimate of $\hat{\mathbf{H}}_l$ and $\mathbf{R}_{\mathbf{n}_l\mathbf{n}_l}$ and computes $\mathbf{W}_l$ using (6.13).
- Each AP l transmits the parameter $\hat{\mathbf{H}}_l^H\mathbf{W}_l \in \mathbb{C}^{K\times K}$ and the transformed signals $\mathbf{w}_l = \mathbf{W}_l^H\mathbf{y}_l \in \mathbb{C}^K$ for all received signals in the coherence block to the NC.

2 The network is used to perform an in-network sum to obtain

$$\mathbf{w} = \sum_{l=1}^{L} \mathbf{w}_l, \ \mathbf{X} = \sum_{l=1}^{L} \hat{\mathbf{H}}_l^H\mathbf{W}_l. \tag{6.15}$$

3 The NC then computes the network-wide MMSE estimate as

$$\hat{\mathbf{s}} = \left(\mathbf{P}^{-1} + \mathbf{X}\right)^{-H} \mathbf{w}. \tag{6.16}$$

6.4 Scalable distributed MMSE receive combining

6.4.1 Scalability issue and solution

The N-DRC algorithm presented in the previous section scales with the number of UEs K in the network. Each AP needs to compute $\mathbf{W}_l$ for all UEs in the network. Therefore, an AP has to estimate all channels $\hat{\mathbf{H}}_l$ and transmits a $K \times K$ matrix in each coherence block. Since the received signal $\mathbf{h}_{kl}s_k$ at AP l becomes weaker when the distance between AP l and UE k increases, the estimate $\hat{\mathbf{h}}_{kl}$ will be worse due to background noise and interference from other UEs that are in the proximity of AP l. Also the number of parameters that need to be transmitted and received in each iteration, may become too large for the obtained benefit in performance.

As proposed in [74], this issue can be solved by moving to a user-centric approach, where a UE k is only served by a subset of APs for which a good channel estimate $\hat{\mathbf{h}}_{kl}$ can be obtained. This will be represented by defining the binary serving matrix $\mathbf{D}$ as

$$[\mathbf{D}]_{kl} = \begin{cases} 1 & \text{if AP } l \text{ is serving UE } k \\ 0 & \text{else.} \end{cases} \tag{6.17}$$

Defining the set of UEs that are served by AP l as $\mathcal{D}_l = \{k|D_{kl} = 1\}$, each AP l only needs to compute a local receiver vector $\mathbf{v}_{kl}$ $\forall k \in \mathcal{D}_l$ instead of for all UEs in the network. Heuristic approaches to obtain $\mathbf{D}$ such that $|\mathcal{D}_l|$ (where $|.|$ denotes the cardinality of a set) is constant or independent of the total number of UEs K, are presented in [74] and it is assumed that the NC knows the UE-assignment. By also bounding the number of interfering UEs in the MMSE estimation, fully scalable MMSE receive combining objectives can be proposed for which a distributed algorithm can be derived. Two scalable objectives are presented in the next subsections.

6.4.2 Scalable network-wide distributed MMSE receive combining

In this scalable version of N-DRC, each AP l only estimates $\mathbf{h}_{kl}$ if $k \in \mathcal{D}_l$ and ignores the effect of the other channels by setting them to 0, i.e., $\hat{\mathbf{h}}_{kl} = \mathbf{0}$ and $\mathbf{C}_{kl} = \mathbf{0}$ if $[\mathbf{D}]_{kl} = 0$. If these modifications are used in (6.5), a similar expression for the scalable network-wide MMSE receiver matrix $\mathbf{V}^{\text{SN-RC}}$ as (6.12) is obtained, but with a different expression for $\mathbf{W}_l$ and $\mathbf{X}$ given by

$$\mathbf{W}_l^{\text{S}} = \left(\sum_{k \in \mathcal{D}_l} p_k \mathbf{C}_{kl} + \mathbf{R}_{\mathbf{n}_l \mathbf{n}_l} \right)^{-1} \hat{\mathbf{H}}_l \mathbf{D}_l \tag{6.18}$$

and

$$\mathbf{X}^{\text{S}} = \sum_{l=1}^{L} \mathbf{D}_l \hat{\mathbf{H}}_l^H \mathbf{W}_l^{\text{S}} \tag{6.19}$$

where the diagonal matrix $\mathbf{D}_l$ has 1 on its k'th diagonal element if $[\mathbf{D}]_{kl} = 1$ and zero otherwise. The N-DRC algorithm can be transformed to the scalable network-wide distributed MMSE receive combining (SN-DRC) algorithm by replacing the matrices $\mathbf{W}_l$ and $\mathbf{X}$ with the scalable versions defined above. Since here only $|\mathcal{D}_l|$ elements of $\mathbf{w}_l$ and $|\mathcal{D}_l| \times |\mathcal{D}_l|$ elements of $\mathbf{D}_l \hat{\mathbf{H}}_l^H \mathbf{W}_l^{\text{S}}$ are non-zero, this will strongly reduce the transmitted data of an AP l. However, care should be taken when the in-network sums are constructed using a tree topology, since the different signals need to be added in a coherent way.

6.4.3 Scalable partial distributed MMSE receive combining

Table 6.1: Comparison of proposed algorithms.

Scheme	Parameters transmitted by each AP	Parameters received at NC	PC at each AP	PC at NC
N-RC	$M_l K + \frac{M_l^2+M_l}{2}$	$MK + \sum_{l=1}^{L} \frac{M_l^2+M_l}{2}$	-	$O(M^3)$
N-DRC	$\frac{K^2+K}{2}$	$\frac{K^2+K}{2}$	$O(M_l^3)$	$O(K^3)$
LSFD [164]	K^2	LK^2	$O(M_l^3)$	$O(KL^3)$
SN-DRC	$\frac{\lvert\mathcal{D}_l\rvert^2+\lvert\mathcal{D}_l\rvert}{2}$	$\frac{K^2+K}{2}$	$O(M_l^3)$	$O(K^3)$
SP-DRC	$\frac{\lvert\mathcal{D}_l\rvert^2+\lvert\mathcal{D}_l\rvert}{2}$	$\frac{K^2+K}{2}$	$O(M_l^3)$	$O(K\lvert\mathcal{P}_k\rvert^3)$

Even with the communication reduction proposed in the previous section, the NC still has to invert a $K \times K$ matrix to construct the estimate $\hat{\mathbf{s}}$ in (6.16), which still scales with the number of UEs K. In [164] it is stated that the interference affecting UE k is mainly generated by a small subset of other UEs. Therefore, the subset of UEs

$$\mathcal{P}_k = \{i | \exists l : D_{kl} D_{il} = 1\} \subset \{1, ..., K\} \tag{6.20}$$

is assumed to have a significant effect on the received signals used to estimate $\hat{s}_k$. The subset considers all the UEs that have at least one AP in common with UE k.

As such, a heuristic partial MMSE receiver vector $\mathbf{v}_k^{\text{P-RC}}$ is proposed to estimate s_k:

$$\mathbf{v}_k^{\text{P-RC}} = \left(\hat{\mathbf{H}} \mathbf{Q}_k \mathbf{Q}_k^H \mathbf{P} \mathbf{Q}_k \mathbf{Q}_k^H \hat{\mathbf{H}}^H + \sum_{k=1}^{K} p_k \mathbf{C}_k + \mathbf{R}_{\mathbf{nn}} \right)^{-1} \hat{\mathbf{h}}_k p_k \tag{6.21}$$

with $\mathbf{Q}_k = \mathbf{I}_{:,\mathcal{P}_k}$, selecting the $|\mathcal{P}_k|$ columns of $\mathbf{I}_K$ with index $i \in \mathcal{P}_k$. This heuristic partial MMSE receiver vector $\mathbf{v}_k^{\text{P-RC}}$ can be rewritten as

$$\mathbf{v}_k^{\text{P-RC}} = \begin{bmatrix} \mathbf{W}_1 \\ \vdots \\ \mathbf{W}_L \end{bmatrix} \mathbf{Q}_k \left(\left(\mathbf{Q}_k^H \mathbf{P} \mathbf{Q}_k \right)^{-1} + \mathbf{Q}_k^H \mathbf{X}^S \mathbf{Q}_k \right)^{-1} \mathbf{q}_k \tag{6.22}$$

with $\mathbf{q}_k = \mathbf{Q}_k^H \mathbf{e}_k$. Substituting $\mathbf{W}_l$ and $\mathbf{X}$ with $\mathbf{W}_l^S$ and $\mathbf{X}^S$ from (6.18) and (6.19) respectively results in a fully scalable filter, denoted by $\mathbf{v}_k^{\text{SP-RC}}$. The N-DRC algorithm can again be adapted to provide the output of the scalable partial MMSE receiver vector $\mathbf{v}_k^{\text{SP-RC}}$ by changing the final combining method in step 3 of Algorithm 7 to

$$\hat{s}_k = \mathbf{q}_k^H \left(\left(\mathbf{Q}_k^H \mathbf{P} \mathbf{Q}_k \right)^{-1} + \mathbf{Q}_k^H \mathbf{X} \mathbf{Q}_k \right)^{-H} \mathbf{Q}_k^H \mathbf{w} \tag{6.23}$$

for each UE k and by replacing $\mathbf{W}_l$ and $\mathbf{X}$ with its scalable versions (6.18) and (6.19) respectively. The obtained algorithm will be denoted with the scalable partial distributed MMSE receive combining (SP-DRC) algorithm. A major advantage of the SP-DRC algorithm is that in (6.23) only a $|\mathcal{P}_k| \times |\mathcal{P}_k|$ matrix needs to be inverted i.s.o. the $K \times K$ matrix of (6.16).

As a summary, Table 6.1 gives a comparison of the different proposed algorithms in terms of the number of parameters that need to be exchanged in each coherence block as well as in terms of the processing complexity (PC) of performing the required inversion operation. The Large-Scale Fading Decoding (LSFD) [165] approach is added as a reference. Note that heuristic (non-optimal) approaches like MR and (P)LMMSE [66,67,74] combining are not requiring the exchange of parameters between NC and APs. The proposed algorithms strongly reduce the communication requirement of the network and the PC at the NC compared to the centralized N-RC, but require that each AP has local processing capabilities. The SP-DRC scales best when the number of UEs grows large (since $|\mathcal{D}_l|, |\mathcal{P}_k|$ are independent of K), but its performance will be shown to be suboptimal to the other algorithms.

6.5 Simulations

Numerical results are provided in this section to demonstrate the performance of the proposed distributed algorithms. A similar setup as [74] with the MMSE-channel estimator [68] is considered ($K = 100$ UEs) but the number of APs is decreased to $L = 50$ with 16 antennas per AP . Figure 6.1 shows the cumulative distributed function (CDF) of the SE per UE, estimated using 25 network realizations and 1000 channel realizations for the different algorithms. Also the performance of the conventional MR combining scheme [66,71,126] and (scalable) local MMSE ((S)L-RC) combining schemes [74] are provided as benchmarks.

The results show that the proposed algorithms perform very well compared to the benchmarks. The performance decrease between the N-DRC algorithm and the scalable SN-DRC algorithm is very limited, while the reduction in channel estimations and in the transmission of parameters and transformed signals for

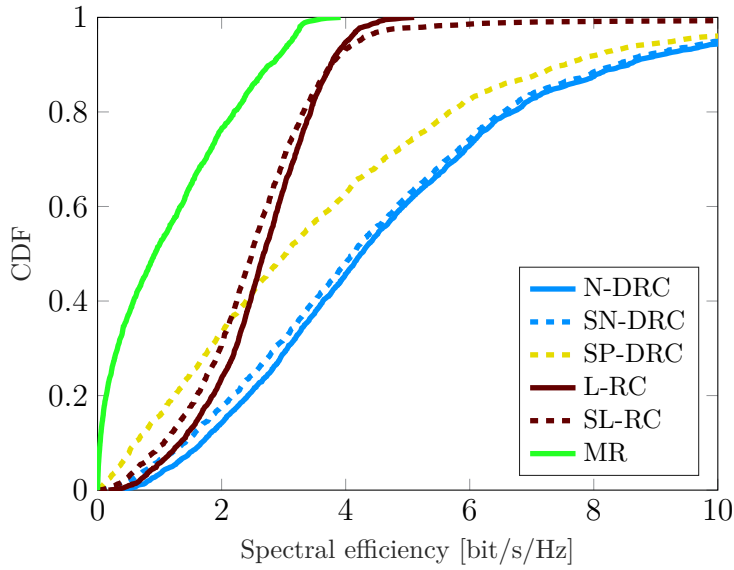

Figure 6.1: Uplink SE per UE for the proposed algorithms.

the algorithms is significant since $|\mathcal{D}_l| = 10 << 100$. The SP-DRC algorithm performs better than the (scalable) local MMSE combining schemes for 60% of the UEs and the maximal value for $|\mathcal{P}_k|$ is 54 in all the simulations, making this an interesting substitute for local MMSE receive combining.

6.6 Conclusion

This paper presented different MMSE receive combining algorithms for cell-free Massive MIMO systems, that allow for an efficient distributed implementation when a small number of parameters can be exchanged between the NC and APs. To avoid scalability issues when the number of UEs grows large, scalable version are proposed and simulations confirm that their performance is very similar to the performance of its non-scalable version.

Chapter 7

Distributed MMSE-Based uplink receive combining, downlink transmit precoding and optimal power allocation for CFmMIMO systems

Distributed MMSE-Based Uplink Receive Combining, Downlink Transmit Precoding and Optimal Power Allocation in Cell-Free Massive MIMO Systems.

Robbe Van Rompaey and Marc Moonen

Accepted for publication in
EURASIP Journal on Wireless Communications and Networking.

©2022 EURASIP Reprint, with permission from: R. Van Rompaey and M. Moonen, "Distributed MMSE-Based Uplink Receive Combining, Downlink Transmit Precoding and Optimal Power Allocation in Cell-Free Massive MIMO Systems", accepted for publication in EURASIP Journal on Wireless Communications and Networking.

Changes include layout, representation and minor editing aspects. A subsection on scalability is further added to Section 7.5 and extra results on scalability are added to the simulation section. The candidate's contributions include all performed research and writing of the article under guidance of the co-author.

Abstract

In cell-free massive MIMO (multiple-input multiple-output) systems, a large number of distributed wireless access points (AP) simultaneously serve a number of user equipments (UEs). This setup has recently been introduced as a promising alternative for the current 5G cellular networks. The setup has the ability to offer a good quality of service, especially for the UEs on the cell edges, be it that there is still a need for low-complexity signal processing algorithms. In this paper, the problem of optimal power allocation combined with uplink receive combining and downlink transmit precoding is tackled by providing efficient distributed MMSE-based algorithms. The necessary fronthaul communications to estimate the combining/precoding vectors and the necessary large-scale channel statistics are reduced to a minimum and rely on in-network summation that can be accomplished whenever the APs can be arranged into a tree-topology. Non-weighted max-sum and max-min are used as utilities for the power allocation, but the algorithms are not limited to these cases. Simulations show that the proposed algorithms outperform heuristic power allocation methods, both in uplink and downlink.

Keywords Cell-Free massive MIMO (CFmMIMO), uplink receive combining, downlink transmit precoding, optimal power allocation, distributed processing, Minimum-Mean-Squared-Error (MMSE).

7.1 Introduction

MIMO ('multiple-input multiple-output') technology plays an important role in present-day wireless communication standards and networks. It uses multiple antennas to transmit and receive multiple data signals simultaneously over one and the same radio channel and hence increase spectral efficiency. Massive MIMO (mMIMO) systems use a large(r) number of antennas, to reap additional benefits in rich scattering environments. While mMIMO was initially viewed as a promising concept for future cellular wireless communication networks, it already became a reality in 2018 with commercial deployment in several countries [19]. The signal processing methods required to achieve large spectral efficiency gains compared to conventional multi-user MIMO systems [64] are available and well understood [168]. The spectral efficiency gains associated with mMIMO emerge from the higher spatial resolution, its robustness against small-scale fading due to the so-called 'channel hardening' effect, and its ability to suppress interference even with imperfect channel state information (CSI).

One of the major shortcomings of current cellular wireless communication networks, where a user equipment (UE) is served only by the access point (AP) of the cell it resides in, is that UEs on the cell edges experience a low channel gain to their serving AP and a high interference power from nearby cells. Current uplink (UL) receive combining and downlink (DL) transmit precoding algorithms do not effectively mitigate such interference. To address this issue, the concept of cell-free massive MIMO (CFmMIMO) [66–68] has been proposed as a promising alternative for the current 5G cellular networks. In CFmMIMO systems a large number of APs are connected to a network center (NC) and cooperate via a fronthaul network to serve a large number of UEs in the network simultaneously as shown in Figure 7.1. The joint operation of the APs then allows for implementing interference-rejecting combining and precoding algorithms effective for all UEs in the network. CFmMIMO thus effectively eliminates cell borders while still reusing the network layout as rolled out previously, which offers the potential to spectacularly increase performance as compared to current cellular mMIMO systems.

CFmMIMO has its roots in works on distributed MIMO [14,15] and coordinated multipoint [16,17], but with the distinction that a UE can be served by several APs, instead of only by the one AP serving the cell in which the UE is located and that the transmission is coordinated by a NC. To allow for a scalable and low-complexity implementation, CFmMIMO has to operate under the following constraints [68]: (a) the time division duplex (TDD) protocol is used, exploiting channel reciprocity between UL and DL; (b) UL channel estimates are computed locally at each AP and will be used only locally, which means that they are not directly communicated to the NC over the fronthaul links;

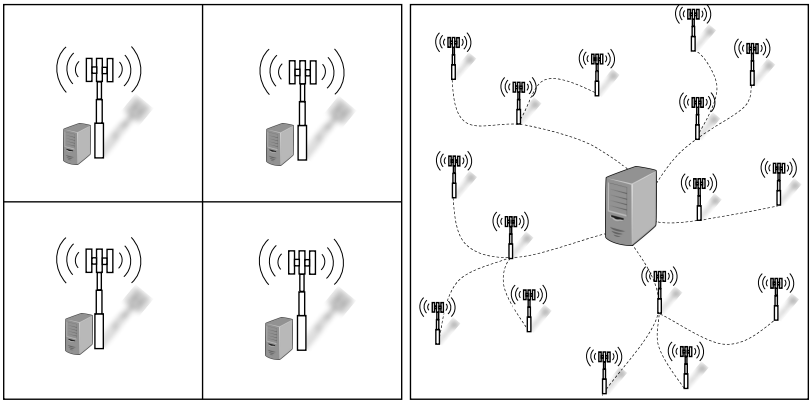

Figure 7.1: Comparison of a cellular massive MIMO system (left) with a CFmMIMO system (right). In a CFmMIMO system, a large number of APs with multiple antennas are connected to a NC, serving a large number of UEs in the coverage area.

(c) combining/precoding vectors are computed locally at the APs and not at the NC; (d) the fronthaul network is only used to send data symbols and the necessary channel statistics to perform centralized data decisions.

7.1.1 Related works

The authors in [66, 122] proposed to use maximum ratio combining and conjugate beamforming for UL and DL data transmission in CFmMIMO systems, presented closed-form expressions for the spectral efficiency in UL and DL for each UE and formulated max-min power control algorithms, which were shown to outperform a cellular setup. However, using more complicated combining and precoding algorithms combined with heuristic power allocation methods [17, 67, 68, 73, 169], are shown to lead to higher throughputs. Optimal UL power allocation and receive combining was investigated in [164, 170] using minimum-mean-squared error (MMSE) processing by formulating the original

max-min signal-to-interference-plus-noise ratio problem for the optimization of combining vectors at a central point (like the NC). Unfortunately centralized computations increase the fronthaul communication and are not complying with the scalable characteristics of CFmMIMO systems as defined before. Optimal DL power allocation was considered in [67] combined with zero-forcing transmit precoding: although the gains were significant, the zero-forcing transmit precoding again requires a fully centralized computation with significant fronthaul communications. In [171], optimal power allocation algorithms for local partial zero-forcing were proposed as a scalable counterpart and showed to achieve a performance close to the performance of zero-forcing transmit precoding and the centralized regularized zero-forcing transmit precoding, which is a benchmark in DL transmit precoding and can be related to MMSE combining in the UL via UL/DL duality [74, 103]. In [172], a max sum SE problem in an uplink CFmMIMO system was also investigated. Artificial neural networks were used, with the UE positions as input and the power control policy as the output. An UL CFmMIMO system with limited fronthaul was taken into consideration in [173], where zero-forcing was employed locally to heuristically estimate the max sum SE power control scheme. For single antenna APs, a deep neural network-based power allocation method was proposed in [174].

7.1.2 Contributions

The missing point in the research field is the fact that (optimal) MMSE-based combining/precoding in its original form can only be performed at the NC if all antenna signals are transmitted to it, which implies a large fronthaul communication overhead. Otherwise, heuristic combining/precoding schemes can be used at the APs, reducing the fronthaul communication overhead strongly, but optimal performance can no longer be guaranteed. The same can be stated for the UL and DL power allocation. Therefore, in this paper an MMSE-based distributed UL receive combing and power allocation algorithm (D-UL-RCPA) and DL transmit precoding and power allocation algorithm (D-DL-TPPA) are presented that are scalable and yet attain this optimal performance. The combining/precoding vectors are computed only at the APs, such that the computation are distributed over the network and are not only performed by the NC. The necessary fronthaul communications to estimate the combining/precoding vectors and the necessary large-scale channel statistics are reduced to a minimum and rely on in-network summation that can be accomplished whenever the APs can be arranged into a tree-topology. The reduction in fronthaul communications is especially large when the total number of antennas in the network is larger than the total number of UEs.

The algorithms are derived based on general lower bounds of the system achievable rate, taking into account the effect of channel estimation errors. Non-weighted max-sum and max-min are used as utilities for the power allocation, but the algorithms are not limited to these cases. The former power allocation strategy maximizes the proposed lower bound for the total system sum rate, while the latter, targeting fairness across users, maximizes the minimum spectral efficiency lower bound across all the UEs. Simulations show that the proposed algorithms outperform heuristic power allocation methods, both in UL and DL.

7.1.3 Paper outline and notation

The paper is organized as follows. The signal model is presented in Section 7.2. In Section 7.3 an optimal UL receive combining and power allocation strategy is developed and an efficient distributed algorithm for a CFmMIMO system is presented, A similar algorithm is developed in Section 7.4 for DL transmit precoding and power allocation, using UL/DL duality. Some further considerations about the power allocation strategies, scalability aspects and network topologies are presented in Section 7.5. The performance of the proposed algorithms is numerically evaluated and compared in Section 7.6. Conclusions and further research directions are provided in Section 7.7.

Superscripts $.^T$ and $.^H$ are used to denote the transpose and conjugate transpose operation. Bold lower case letters $\mathbf{b} = [b_1 \ ... \ b_K]^T$ are used to denote complex vectors and bold upper case letters are used to represent complex matrices $\mathbf{A} = [\mathbf{a}_1 \ ... \ \mathbf{a}_K]$. $\mathbf{I}_N$ is the $N \times N$ identity matrix and $\mathbf{0}$ denotes an all zeros vectors whose dimensions are clear from the context. The multi-variate circularly symmetric complex Gaussian distribution with correlation matrix $\mathbf{R}$ is denoted by $\mathcal{NC}(0, \mathbf{R})$, $\text{diag}\{a_1, ..., a_K\}$ is used to denote a diagonal matrix with $a_1, ..., a_K$ on its diagonal and $\text{Blkdiag}\{\mathbf{A}_1, ..., \mathbf{A}_K\}$ is used for a block diagonal matrix with the square matrices $\mathbf{A}_1, ..., \mathbf{A}_K$ on the diagonal. Finally $||.||$ and $E\{.\}$ denote the Euclidean norm and expected value operator respectively.

7.2 Signal model

Consider a CFmMIMO system consisting of K single-antenna UEs and L APs, each having N antennas and local processing capabilities, that are randomly deployed over the coverage area. The APs are connected to a NC via a fronthaul network. This setup allows for coherent transmission and reception of data to and from the UEs. In the CFmMIMO literature [67, 124] it is often assumed

that the number of antennas NL is much larger than the number of UEs K and that both L and K are large.

The time-frequency resources are divided into coherence blocks of τ_c samples during which the channels are assumed to remain constant [103]. APs and UEs operate using a TDD protocol and a channel coherence interval is divided into three phases: UL channel estimation, UL data transmission and DL data transmission. These phases consist of τ_p, τ_u and τ_d samples respectively, such that $\tau_c = \tau_p + \tau_u + \tau_d$. Since the TDD protocol is used, the UL channel and the DL channel are assumed to be each other's conjugate due to channel reciprocity, so that indeed only UL channel estimation has to be performed. The channel from UE k to AP l is given by $\mathbf{h}_{kl} \in \mathbb{C}^N$ and the channel from UE k to all the APs is denoted by $\mathbf{h}_k = [\mathbf{h}_{k1}^T \ ... \ \mathbf{h}_{kL}^T]^T \in \mathbb{C}^{NL}$. The channels $\mathbf{h}_{kl}$ are assumed to remain constant during a coherence block[1] and drawn from an independent correlated Rayleigh fading realization $\mathcal{NC}(\mathbf{0}, \mathbf{R}_{kl})$ in each coherence block[2]. $\mathbf{R}_{kl} \in \mathbb{C}^{N \times N}$ is the positive semi-definite spatial correlation matrix describing the large-scale fading, including geometric pathloss, shadowing, antenna gains, and spatial channel correlation [7]. The large-scale fading is assumed to remain constant over different coherence blocks. The Gaussian distribution models the small-scale fading. Due to the spatial distribution of the APs in the network, the channel vectors of different APs are independently distributed, i.e., $E\{\mathbf{h}_{kl}\mathbf{h}_{kn}^H\} = \mathbf{0}_{N \times N}$ for $l \neq n$, such that channel estimation can be performed independently at each AP. A schematic overview of the signal model is provided in Figure 7.2.

7.2.1 UL channel estimation

In the UL channel estimation phase, the UEs send UL pilots to allow for simultaneous channel estimation at the APs. There are τ_p mutually orthogonal pilot signals of τ_p samples, normalized to have unit power. Each UE is assigned to a pilot signal $\phi_k \in \mathbb{C}^{\tau_p}$ when it gains access to the network (see [66, 74] for pilot assignment protocols). As K is often much larger than τ_p, the same pilot signal will be assigned to multiple UEs, leading to pilot contamination and the associated negative effects on the channel estimation [168, 175, 176]. The received signal $\mathbf{y}_l^{\text{pilot}} \in \mathbb{C}^{N \times \tau_p}$ at AP l is given as:

$$\mathbf{y}_l^{\text{pilot}} = \sum_{k=1}^{K} \sqrt{p_k^{\text{pilot}}} \mathbf{h}_{kl} \phi_k^H + \mathbf{n}_l^{\text{pilot}} \tag{7.1}$$

[1] Note that abstraction is made of the practical Orthogonal Frequency Division Multiplexing (OFDM) based multi-carrier modulation. See [6, Sec. 2] how this simplification can be done.

[2] One can consider the more general Rician fading channel [125], but this is not considered here for simplicity.

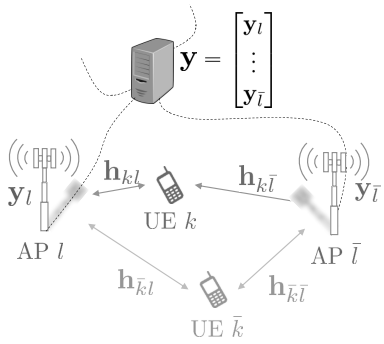

Figure 7.2: Schematic overview of the signal model for 2 different UE $(k, \bar{k})$ and 2 different AP $(l, \bar{l})$ with the used symbols.

where p_k^{pilot} is the pilot transmit power of UE k and $\mathbf{n}_l^{\text{pilot}} \in \mathbb{C}^{N \times \tau_p}$ is thermal noise. Let $\mathcal{S}_t \subset \{1, ..., K\}$ denote the subset of UEs assigned to the same pilot signal ϕ_t for $t \in \{1, ..., \tau_p\}$. After despreading, i.e., multiplying the signal coherently with $\phi_t / ||\phi_t||$, the received signal $\mathbf{y}_{tl}^{\text{pilot}} \in \mathbb{C}^N$ at AP l is given as

$$\mathbf{y}_{tl}^{\text{pilot}} = \sum_{i \in \mathcal{S}_t} \sqrt{\tau_p p_i^{\text{pilot}}} \mathbf{h}_{il} + \mathbf{n}_{tl}^{\text{pilot}} \tag{7.2}$$

where the thermal noise $\mathbf{n}_{tl}^{\text{pilot}}$ for each pilot signal t is distributed as $\mathcal{NC}(\mathbf{0}, \mathbf{R}_{\mathbf{n}_l \mathbf{n}_l}^{\text{pilot}})$. Assuming that AP l is aware of the local large-scale fading correlation matrix $\mathbf{R}_{kl}$ (see e.g., [166, 177–179] for correlation matrix estimation methods) of all the UEs, the MMSE estimate of $\mathbf{h}_{kl}$ for $k \in \mathcal{S}_t$ is

$$\hat{\mathbf{h}}_{kl} = \sqrt{\tau_p p_k^{\text{pilot}}} \mathbf{R}_{kl} \boldsymbol{\Psi}_{tl}^{-1} \mathbf{y}_{tl}^{\text{pilot}} \tag{7.3}$$

where

$$\boldsymbol{\Psi}_{tl} = E\{\mathbf{y}_{tl}^{\text{pilot}} \mathbf{y}_{tl}^{\text{pilot},H}\} = \sum_{i \in \mathcal{S}_t} \tau_p p_i^{\text{pilot}} \mathbf{R}_{il} + \mathbf{R}_{\mathbf{n}_l \mathbf{n}_l}^{\text{pilot}}. \tag{7.4}$$

The MMSE estimate $\hat{\mathbf{h}}_{kl}$ of $\mathbf{h}_{kl}$ is an unbiased estimate with estimation error $\tilde{\mathbf{h}}_{kl} = \mathbf{h}_{kl} - \hat{\mathbf{h}}_{kl}$. The distribution of both random variables is given by

$$\hat{\mathbf{h}}_{kl} \sim \mathcal{NC}(\mathbf{0}, \tau_p p_k^{\text{pilot}} \mathbf{R}_{kl} \boldsymbol{\Psi}_{tl}^{-1} \mathbf{R}_{kl}) \tag{7.5}$$

$$\tilde{\mathbf{h}}_{kl} \sim \mathcal{NC}(\mathbf{0}, \mathbf{R}_{kl} - \tau_p p_k^{\text{pilot}} \mathbf{R}_{kl} \boldsymbol{\Psi}_{tl}^{-1} \mathbf{R}_{kl}) \triangleq \mathcal{NC}(\mathbf{0}, \mathbf{C}_{kl}). \tag{7.6}$$

It is noted that the $N \times N$ matrices $\sqrt{\tau_p p_k^{\text{pilot}}}\mathbf{R}_{kl}\boldsymbol{\Psi}_{tl}^{-1}$ and $\mathbf{C}_{kl}$ can be precomputed for complexity reduction at AP k, since they only depend on the channel statistics, which are changing slowly throughout the communication[3].

7.2.2 UL data transmission

In the UL data transmission phase, the received signal $\mathbf{y}_l^{\text{UL}} \in \mathbb{C}^N$ at AP l is given by

$$\mathbf{y}_l^{\text{UL}} = \sum_{k=1}^{K} \mathbf{h}_{kl} s_k + \mathbf{n}_l^{\text{UL}} = \mathbf{H}_l \mathbf{s} + \mathbf{n}_l^{\text{UL}} \tag{7.7}$$

where $s_k \in \mathbb{C}$ is the signal transmitted by UE k with UL transmit power $p_k = E\{s_k s_k^H\}$ and $\mathbf{n}_l^{\text{UL}} \in \mathbb{C}^N \sim \mathcal{NC}(\mathbf{0}, \mathbf{R}_{\mathbf{n}_l\mathbf{n}_l}^{\text{UL}})$ is an additive Gaussian noise component, including thermal antenna noise and quantization noise during UL transmission. Furthermore, $\mathbf{H}_l = [\mathbf{h}_{1l} \ ... \ \mathbf{h}_{Kl}] \in \mathbb{C}^{N\times K}$, $\mathbf{s} = [s_1 \ ... \ s_K]^T \in \mathbb{C}^K$ and $\mathbf{p} = [p_1 \ ... \ p_K]^T \in \mathbb{R}^K$ are the concatenation of the channels from all the UEs to AP l, the signals transmitted by all the UEs and the UL transmit powers respectively. Stacking the received signals of all APs in $\mathbf{y}^{\text{UL}} = [\mathbf{y}_1^{\text{UL},T} \ ... \ \mathbf{y}_L^{\text{UL},T}]^T \in \mathbb{C}^{NL}$ as well as the noise components in $\mathbf{n}^{\text{UL}} = [\mathbf{n}_1^{\text{UL},T} \ ... \ \mathbf{n}_L^{\text{UL},T}]^T \in \mathbb{C}^{NL} \sim \mathcal{NC}(0, \mathbf{R}_{\mathbf{nn}}^{\text{UL}})$ where $\mathbf{R}_{\mathbf{nn}}^{\text{UL}} = \text{Blkdiag}\{\mathbf{R}_{\mathbf{n}_1\mathbf{n}_1}^{\text{UL}}, ..., \mathbf{R}_{\mathbf{n}_L\mathbf{n}_L}^{\text{UL}}\}$, results in the network-wide signal model:

$$\mathbf{y}^{\text{UL}} = \mathbf{H}\mathbf{s} + \mathbf{n}^{\text{UL}} \tag{7.8}$$

with $\mathbf{H} = [\mathbf{h}_1 \ ... \ \mathbf{h}_K] = [\mathbf{H}_1^T \ ... \ \mathbf{H}_L^T]^T \in \mathbb{C}^{NL\times K}$.

In network-wide UL receive combining the signal s_k is estimated by linearly combining the received signal $\mathbf{y}^{\text{UL}}$ with a combining vector $\mathbf{v}_k \in \mathbb{C}^{NL}$, i.e., $\hat{s}_k = \mathbf{v}_k^H \mathbf{y}^{\text{UL}}$. Note that this linear combining can be performed in the network if AP l selects the local combining vector $\mathbf{v}_{kl} \in \mathbb{C}^N$ in $\mathbf{v}_k = [\mathbf{v}_{k1}^T \ ... \ \mathbf{v}_{kL}^T]^T$ and computes the local estimate $\mathbf{v}_{kl}^H \mathbf{y}_l$. The NC then estimates s_k by combining the local estimates as:

$$\hat{s}_k = \sum_{l=1}^{L} \mathbf{v}_{kl}^H \mathbf{y}_l^{\text{UL}} = \mathbf{v}_k^H \mathbf{h}_k s_k + \sum_{i\neq k} \mathbf{v}_k^H \mathbf{h}_i s_i + \mathbf{v}_k^H \mathbf{n}^{\text{UL}}. \tag{7.9}$$

The goal is then to choose the combining vector $\mathbf{v}_k$ that provides a good estimate $\hat{s}_k$, but where the APs use only local CSI. A popular choice in CFmMIMO

[3]Changes are due to UE mobility or new scheduling decisions, but these channel statistics changes are typically 50 times slower than the small scale fading statistics changes, so are assumed negligible for several coherence blocks.

literature is maximum-ratio (MR) combing with $\mathbf{v}_{kl} = \hat{\mathbf{h}}_{kl}$ [66, 71, 126]. An alternative heuristic scheme, which performs generally better but requires more processing power of the AP is local MMSE combining [68]. Network-wide UL power allocation algorithms for MR combining can be found in [124, 164, 170]. In this paper, network-wide MMSE combining [74] and associated power allocation algorithms will be considered, requiring typically network-wide CSI. However, this paper shows that if a limited number of parameters can be exchanged between the NC and the APs, this network-wide MMSE combining and associated power allocation can still be obtained locally at each AP.

7.2.3 DL data transmission

In the DL data transmission phase, the received signal y_k^{DL} at UE k is given by

$$\begin{aligned} y_k^{\mathrm{DL}} &= \sum_{l=1}^{L} \mathbf{h}_{kl}^H \sum_{i=1}^{K} \mathbf{w}_{il} \sqrt{\rho_i} \zeta_i + n_k^{\mathrm{DL}} \\ &= \mathbf{h}_k^H \mathbf{w}_k \sqrt{\rho_k} \zeta_k + \sum_{i \neq k} \mathbf{h}_k^H \mathbf{w}_i \sqrt{\rho_i} \zeta_i + n_k^{\mathrm{DL}} \end{aligned} \tag{7.10}$$

where $\zeta_k \in \mathbb{C}$ is the signal transmitted to UE k with unit DL transmit power, ρ_k is the network-wide DL transmit power allocated to UE k, $n_k^{\mathrm{DL}} \sim \mathcal{NC}\left(0, \sigma_k^{2,\mathrm{DL}}\right)$ is an additive Gaussian noise component, $\mathbf{w}_k = [\mathbf{w}_{k1}^T ... \mathbf{w}_{kL}^T]^T \in \mathbb{C}^{NL}$ is the concatenation of the precoding vectors used for UE k. Also denote the DL transmit powers as $\boldsymbol{\rho} = [\rho_1 \ ... \ \rho_K]^T \in \mathbb{R}^K$ and the predocing matrix as $\mathbf{W} = [\mathbf{w}_1 \ ... \ \mathbf{w}_K] \in \mathbb{C}^{NL \times K}$. Again the selection of the precoding vector should only depend on local CSI for CFmMIMO. The most popular choice is MR precoding with

$$\mathbf{w}_{kl} = \frac{\hat{\mathbf{h}}_{kl}}{\sqrt{E\{||\hat{\mathbf{h}}_{kl}||^2\}}}. \tag{7.11}$$

DL power allocation algorithms for different local precoding schemes can be found in [66, 67, 180]. In this paper, network-wide MMSE precoding [181] and associated power allocation algorithms will be considered, requiring typically network-wide CSI. However, this paper shows that using a similar approach as for UL data transmission, this network-wide MMSE precoding and associated power allocation can still be obtained locally at each AP.

7.3 UL receive combing and power allocation

7.3.1 UL receive combining

A standard lower bound for the ergodic capacity of the UL data transmission for UE k can be obtained by rewriting (7.9) using the estimated channels as

$$\hat{s}_k = \mathbf{v}_k^H \hat{\mathbf{h}}_k s_k + \mathbf{v}_k^H \tilde{\mathbf{h}}_k s_k + \sum_{i \neq k} \mathbf{v}_k^H (\hat{\mathbf{h}}_i + \tilde{\mathbf{h}}_i) s_i + \mathbf{v}_k^H \mathbf{n}^{\mathrm{UL}} \tag{7.12}$$

and is given by the achievable UL spectral efficiency (SE) [7, 182]

$$\mathrm{SE}_k^{\mathrm{UL},1} = \frac{\tau_u}{\tau_c} E\left\{ \log_2(1 + \mathrm{SINR}_k^{\mathrm{UL,inst}}) \right\} \text{ [bits/s/Hz]} \tag{7.13}$$

with the instantaneous effective signal-to-interference-and-noise ratio $\mathrm{SINR}_k^{\mathrm{UL,inst}}$ given as

$$\frac{p_k |\mathbf{v}_k^H \hat{\mathbf{h}}_k|^2}{\sum_{i \neq k} p_i |\mathbf{v}_k^H \hat{\mathbf{h}}_i|^2 + \sum_{i=1}^{K} p_i \mathbf{v}_k^H \mathbf{C}_i \mathbf{v}_k + \mathbf{v}_k^H \mathbf{R}_{\mathbf{nn}}^{\mathrm{UL}} \mathbf{v}_k}. \tag{7.14}$$

where $\mathbf{C}_i = \mathrm{Blkdiag}\{\mathbf{C}_{i,1}, ..., \mathbf{C}_{iL}\}$. The expectation is with respect to the different channel realizations.

The UL SE is valid for any combining vector $\mathbf{v}_k$. In this paper optimal receive combining is considered and it can be seen from expression (7.13) that the optimal instantaneous combining vector can be obtained by maximizing the generalized Rayleigh quotient in the instantaneous SINR in (7.14). The optimal combining vector is unique up to a scalar multiplication, and so to make the solution unique, the solution that minimizes the mean-squared error $E\{|s_k - \hat{s}_k|^2 | \hat{\mathbf{H}}\}$ is chosen. The MMSE combining vector for UE k is then given by

$$\mathbf{v}_k^{\mathrm{MMSE}} = p_k (\hat{\mathbf{H}} \mathbf{P} \hat{\mathbf{H}}^H + \sum_{i=1}^{K} p_i \mathbf{C}_i + \mathbf{R}_{\mathbf{nn}}^{\mathrm{UL}})^{-1} \hat{\mathbf{h}}_k \tag{7.15}$$

with $\mathbf{P} = \mathrm{diag}\{p_1, ..., p_K\}$ as shown in [177].

The following theorem shows that the MMSE combining vectors for UEs $k = 1...K$, i.e., the combining matrix $\mathbf{V}^{\mathrm{MMSE}} = [\mathbf{v}_1^{\mathrm{MMSE}}, ..., \mathbf{v}_K^{\mathrm{MMSE}}]$, can be computed in a way that allows for an efficient distributed implementation.

Theorem 7.3.1. *The MMSE combining matrix* $\mathbf{V}^{\mathrm{MMSE}}$ *can be written as*

$$\mathbf{V}^{\mathrm{MMSE}} = \begin{bmatrix} \mathbf{X}_1 \\ \vdots \\ \mathbf{X}_L \end{bmatrix} \mathbf{U} = \mathbf{X}\mathbf{U} \tag{7.16}$$

with

$$\mathbf{U} = \left(\mathbf{P}^{-1} + \mathbf{X}^H \hat{\mathbf{H}}\right)^{-1} = \left(\mathbf{P}^{-1} + \sum_{l=1}^{L} \mathbf{X}_l^H \hat{\mathbf{H}}_l\right)^{-1} \tag{7.17}$$

$$\mathbf{X}_l = \left(\sum_{k=1}^{K} p_k \mathbf{C}_{kl} + \mathbf{R}^{\mathrm{UL}}_{\mathbf{n}_l \mathbf{n}_l}\right)^{-1} \hat{\mathbf{H}}_l. \tag{7.18}$$

Proof. See [177]. □

In [177], the network-wide distributed MMSE receive combining (N-DRC) algorithm is proposed based on the computation of the MMSE combining vectors in Theorem 7.3.1. The algorithm can be summarized in the following steps for each coherence block:

1. Each AP l estimates $\hat{\mathbf{H}}_l$ and computes $\mathbf{X}_l \in \mathbb{C}^{N \times K}$ as in (7.18) and $\mathbf{X}_l^H \hat{\mathbf{H}}_l$. It transmits the combined signals $\mathbf{x}_l = \mathbf{X}_l^H \mathbf{y}_l^{\mathrm{UL}} \in \mathbb{C}^K$ and the parameters $\mathbf{X}_l^H \hat{\mathbf{H}}_l \in \mathbb{C}^{K \times K}$ to the NC.
2. The available links in the network are used efficiently such that the NC obtains the in-network sums $\mathbf{x} = \sum_{l=1}^{L} \mathbf{x}_l$ and $\mathbf{X}^H \hat{\mathbf{H}} = \sum_{l=1}^{L} \mathbf{X}_l^H \hat{\mathbf{H}}_l$.
3. The NC uses $\mathbf{X}^H \hat{\mathbf{H}}$ to compute $\mathbf{U} = [\mathbf{u}_1 \ ... \ \mathbf{u}_K]$ as in (7.17) and computes the estimates $\hat{s}_k$ as $\mathbf{u}_k^H \mathbf{x}$ for all UEs.

Some important advantages of this distributed algorithm compared to a centralized algorithm, i.e., when each AP serves as a receiver that directly transmits its received signals to the NC, are repeated here:

- The NC only has to invert a $K \times K$ matrix in (7.17) instead of the $LN \times LN$ matrix in (7.15). However, this requires that each AP inverts an $N \times N$ matrix to compute $\mathbf{X}_l$, where the necessary local matrices can be precomputed and kept fixed as long as the transmit powers $\mathbf{p}$ remain unchanged.
- If the in-network sums in step 2 are computed efficiently exploiting the available network topology, this will reduce the network signaling strongly compared to the transmission of all NL signals.
- The method is also robust against link failures: if the data ($\mathbf{x}_l$ and $\mathbf{X}_l^H \hat{\mathbf{H}}_l$) from a certain AP l is not received as a term in the in-network sums, the obtained estimate will still be optimal for a network setup with AP l removed.

It is important to note that the MMSE combining vectors depend on the UL transmit powers, the noise statistics and the channel estimation $\hat{\mathbf{H}}$, which in turn depends on the pilot transmit powers, the pilot assignment strategy and the large-scale statistics. The UL SE in (7.13) is as a consequence also influenced by these parameters. In the following subsection a way to improve this achievable bound is provided, based on power allocation.

7.3.2 UL power allocation preliminaries

With UL power allocation[4] the UL transmit powers $\mathbf{p}$ are set to maximize some utility function for some UL receive combining strategy. The problem can be formulated mathematically as:

$$\begin{aligned} \max_{\mathbf{p}\in\mathcal{P}} \quad & U(\mathrm{SE}_1, ..., \mathrm{SE}_K) \\ s.t. \quad & \mathrm{SE}_k = \mathrm{SE}(\mathbf{p}, \mathbf{v}_k(\mathbf{p})) \quad \forall k \end{aligned} \tag{7.19}$$

where, for instance, (7.13) is used for SE_k and $\mathcal{P}$ is a convex region of allowed UL transmit powers $\mathbf{p}$ for the UEs, e.g., corresponding to a total power constraint or a per UE power constraint. The utility function is assumed to be (quasi-)concave and nondecreasing. In this paper, two specific utility functions are considered, but the proposed algorithm is not limited to these cases. The channel hardening makes power allocation different in CFmMIMO systems compared to single-antenna systems. While the combining vectors $\mathbf{v}_k$ will be adopted depending on small-scale variations of the channels, $\mathbf{p}$ will only be adopted to large-scale variations to effectively compute the expectations in e.g., (7.13). Since the expected value operation in the expression for the SE in (7.13) contains the logarithm, finding the optimal power allocation is difficult due to the non-trivial relation between $\mathbf{p}$ and the $\mathrm{SE}_k^{\mathrm{UL},1}(\mathbf{p}, \mathbf{v}_k)$. Therefore, a different SE formulation will be considered for the UL power allocation, which is obtained under the assumption of channel hardening[5]. For this, only the part of the desired signal received over the average channel $E\{\mathbf{v}_k^H \mathbf{h}_k\}$ is treated as

[4]The pilot transmit powers are assumed to remain fixed. The estimation of the quantities $\mathbf{C}_k$ and $\hat{\mathbf{h}}_k$ is thus not depending on the assigned UL transmit powers. Joint pilot and UL transmit power allocation methods can be found in [183, 184], but are not considered here.

[5]When the number of antennas per AP is large, the effective channels to the desired UEs are almost deterministic after combining/precoding, although the channel responses are random. This phenomenon is called channel hardening and can be expressed as $\frac{\mathbf{v}_k^H \mathbf{h}_k}{NL} \to \frac{E\{\mathbf{v}_k^H \mathbf{h}_k\}}{NL}$ if $NL \to \infty$.

the true desired signal, i.e.,

$$\begin{aligned}\hat{s}_k = E\{\mathbf{v}_k^H \mathbf{h}_k\} s_k + \left(\mathbf{v}_k^H \mathbf{h}_k - E\{\mathbf{v}_k^H \mathbf{h}_k\}\right) s_k \\ + \sum_{i \neq k} \mathbf{v}_k^H \mathbf{h}_i s_i + \mathbf{v}_k^H \mathbf{n}.\end{aligned} \tag{7.20}$$

This results in a deterministic channel under uncorrelated interference and noise for which the following SE (also referred to as the use-and-then-forget bound [7]) can be derived:

$$\mathrm{SE}_k^{\mathrm{UL},2} = \frac{\tau_u}{\tau_c} \log_2(1 + \mathrm{SINR}_k^{\mathrm{UL},2}) \text{ [bits/s/Hz]} \tag{7.21}$$

where

$$\frac{p_k |E\{\mathbf{v}_k^H \mathbf{h}_k\}|^2}{\sum_{i=1}^K p_i E\{|\mathbf{v}_k^H \mathbf{h}_i|^2\} - p_k |E\{\mathbf{v}_k^H \mathbf{h}_k\}|^2 + E\{|\mathbf{v}_k^H \mathbf{n}|^2\}} \tag{7.22}$$

defines the signal-to-interference-and-noise ratio $\mathrm{SINR}_k^{\mathrm{UL},2}$. The expectations are with respect to the different channel realizations. The expression is in theory only depending on the large-scale fading.

It is intuitively clear that the $\mathrm{SE}_k^{\mathrm{UL},2}$ is a less tight lower bound for the ergodic capacity than the achievable lower bound given by $\mathrm{SE}_k^{\mathrm{UL},1}$, since the channel estimates are not utilized in the signal estimation, i.e.,

$$\mathrm{SE}_k^{\mathrm{UL},1} \geq \mathrm{SE}_k^{\mathrm{UL},2}. \tag{7.23}$$

However, simulations in [7, Sect. 4.2] show that the bound is still tight for $LN \gg 1$, i.e., when channel hardening has its effect. The bound is also tight for a deterministic channel, i.e., when only 1 channel realization is used to compute the expectations over the channel realizations. The simulations also show that the bound is tight for any combining scheme, but that using the MMSE combining vector leads to a tighter bound than any other multiple of this MMSE combining vector, e.g., when a constraint $\mathbf{v}_k^H \hat{\mathbf{h}}_k = 1$ is used in each coherence block.

Since closed form expressions for the expectations in (7.22) are difficult to derive for the optimal MMSE combining vector (7.15)[6], the next theorem provides a way to estimate the expectations without having access to the true channels $\mathbf{H}$.

Theorem 7.3.2. *If the combining vector $\mathbf{v}_k$ is independent of the instantaneous channel estimation error $\{\tilde{\mathbf{h}}_k\}_{\forall k}$ and also independent of the instantaneous UL*

[6]There are closed form expressions available in [164, 185] when the number of antennas in the network grows to infinity, but these do not allow for an efficient distributed computation.

Table 7.1: Overview of used symbols for power allocation

Symbol	Meaning	Place of computation
γ_k	$E\{\mathbf{v}_k^H \hat{\mathbf{h}}_k\}$	NC
υ_{ki}	$E\{\lvert\mathbf{v}_k^H \hat{\mathbf{h}}_i\rvert^2\}$	NC
ξ_{ki}	$E\{\mathbf{v}_k^H \mathbf{C}_i \mathbf{v}_k\}$	NC
ν_k	$E\{\mathbf{v}_k^H \mathbf{R}_{\mathbf{nn}}^{\mathrm{UL}} \mathbf{v}_k\}$	NC
μ_k	$E\{\mathbf{v}_k^H \mathbf{v}_k\}$	NC
ξ_{ki}^l	$E\{\mathbf{v}_{kl}^H \mathbf{C}_{il} \mathbf{v}_{kl}\}$	AP
ν_k^l	$E\{\mathbf{v}_{kl}^H \mathbf{R}_{\mathbf{n}_l\mathbf{n}_l}^{\mathrm{UL}} \mathbf{v}_{kl}\}$	AP
μ_k^l	$E\{\mathbf{v}_{kl}^H \mathbf{v}_{kl}\}$	AP

noise $\mathbf{n}^{\mathrm{UL}}$*, then the expectations can be computed without knowledge of the true channel* $\mathbf{H}$*:*

$$E\{\mathbf{v}_k^H \mathbf{h}_k\} = \gamma_k \tag{7.24}$$

$$E\{\lvert\mathbf{v}_k^H \mathbf{h}_i\rvert^2\} = \upsilon_{ki} + \xi_{ki} = \upsilon_{ki} + \sum_{l=1}^{L} \xi_{ki}^l \tag{7.25}$$

$$E\{\lvert\mathbf{v}_k^H \mathbf{n}^{\mathrm{UL}}\rvert^2\} = \nu_k = \sum_{l=1}^{L} \nu_k^l. \tag{7.26}$$

The right-hand side symbols are defined in Table 7.1 and these only depend on the channel estimates and the large-scale statistics $\{\mathbf{C}_k\}_{\forall k}$ *and* $\mathbf{R}_{\mathbf{nn}}^{\mathrm{UL}}$*.*

Proof. See Appendix C.1 □

The requirements for theorem 7.3.2 are valid for the MMSE combining vector (7.15), as $\mathbf{v}_k^{\mathrm{MMSE}}$ only depends on the instantaneous channel estimates $\hat{\mathbf{H}}$ and the fixed matrices $\{\mathbf{C}\}_{\forall k}$ and $\mathbf{R}_{\mathbf{nn}}^{\mathrm{UL}}$.

The (ergodic) statistics in Table 7.1 can be estimated using (recursive) time-averaging at the NC or in a distributed way using in-network sums for ξ_{ki} and ν_k, if each AP l has access to the transformation matrix $\mathbf{U}$, since $\mathbf{v}_{kl} = \mathbf{X}_l \mathbf{u}_k$.

7.3.3 UL receive combining and power allocation

To be able to perform the power allocation problem (7.19) with $\mathrm{SE}(\mathbf{p}, \mathbf{v}_k(\mathbf{p}))$ defined as $\mathrm{SE}_k^{\mathrm{UL},2}$ in (7.21), the following alternating optimization method is proposed.

1. Set $i \leftarrow 0$ and initialize $\mathbf{p}^0$ randomly such that $\mathbf{p}^0 \in \mathcal{P}$.

2. Determine the combining matrix $\mathbf{V}^{i+1}$ for each coherence block that maximizes:

$$\begin{aligned} \max_{\mathbf{V}} \quad & U(\mathrm{SE}_1, ..., \mathrm{SE}_K) \\ s.t. \quad & \mathrm{SE}_k = \mathrm{SE}_k^{\mathrm{UL},2}(\mathbf{p}^i, \mathbf{v}_k) \quad \forall k \end{aligned} \tag{7.27}$$

   for fixed transmit powers $\mathbf{p}^i$. Since the relation between $\mathrm{SE}_k^{\mathrm{UL},2}(\mathbf{p}^i, \mathbf{v}_k)$ and $\mathbf{v}_k$ is non-trivial, (7.23) is used to obtain a tractable optimization problem:

$$\begin{aligned} \max_{\mathbf{V}} \quad & U(\mathrm{SE}_1, ..., \mathrm{SE}_K) \\ s.t. \quad & \mathrm{SE}_k = \mathrm{SE}_k^{\mathrm{UL},1}(\mathbf{p}^i, \mathbf{v}_k) \left(\geq \mathrm{SE}_k^{\mathrm{UL},2}(\mathbf{p}^i, \mathbf{v}_k) \right) \quad \forall k \end{aligned} \tag{7.28}$$

   Due to the nondecreasing function $U(\mathrm{SE}_1, ..., \mathrm{SE}_K)$, this is equivalent to maximizing $\mathrm{SINR}_k^{\mathrm{UL,inst}}$ in (7.14) for each k in each coherence block. The solution is thus given by (7.15) and (7.16).

3. Determine the optimal transmit powers $\mathbf{p}^{i+1}$ that maximize:

$$\begin{aligned} \max_{\mathbf{p} \in \mathcal{P}} \quad & U(\mathrm{SE}_1, ..., \mathrm{SE}_K) \\ s.t. \quad & \mathrm{SE}_k = \mathrm{SE}_k^{\mathrm{UL},2}(\mathbf{p}, \mathbf{v}_k^{i+1}) \quad \forall k \end{aligned} \tag{7.29}$$

4. Set $i \leftarrow i + 1$ and return to step 2.

To following theorem is relevant to determine the convergence of the proposed alternating optimization method.

Theorem 7.3.3. *Suppose that $f(\mathbf{x}_1, \mathbf{x}_2)$ is continuously differentiable over a closed convex set $\mathcal{X} = \mathcal{X}_1 \times \mathcal{X}_2$. Furthermore, suppose that for each $\mathbf{x}^i \in \mathcal{X}$, the maximizations*

$$\mathbf{x}_1^{i+1} = \arg\max_{\mathbf{z}_1 \in \mathcal{X}_1} f(\mathbf{z}_1, \mathbf{x}_2^i) \tag{7.30}$$

and

$$\mathbf{x}_2^{i+1} = \arg\max_{\mathbf{z}_2 \in \mathcal{X}_2} f(\mathbf{x}_1^{i+1}, \mathbf{z}_2) \tag{7.31}$$

are uniquely attained. Let $\{x^i\}$ be the sequence generated from a random initial point $\mathbf{x}^0 \in \mathcal{X}$ using the above equations. Then every limit point of $\{x^i\}$ is a stationary point of $\max_{\mathbf{x} \in \mathcal{X}} f(\mathbf{x})$.

Proof. The proof is a simplification of the proof in [186, Sect. 2.7] for block coordinate descent methods. Only two blocks are considered here and the maximizations in the theorem need to be replaced with a minimization of $-f(\mathbf{x})$ to obtain the same result. □

Although not fully applicable to the proposed alternating optimization method, this theorem can still be used to show that the alternating optimization method converges to a stationary point of (7.19) when the number of antennas NL goes to infinity. In that case, the bound (7.23) is tight, i.e., $\mathrm{SE}_k^{\mathrm{UL},1} \approx \mathrm{SE}_k^{\mathrm{UL},2}$ and this implies that step 3 of the alternating optimization method is optimizing (7.19) for a fixed $\mathbf{p}^i$. The maximum in optimization problems (7.27) is uniquely attained whenever U is nondecreasing, so it still needs to be checked if a unique solution to (7.29) can be found for the given utility function.

Based on this, a distributed UL receive combining and power allocation algorithm (D-UL-RCPA) is proposed in **Algorithm 8**, where the (7.16)-(7.18) is used in each coherence block and the statistics to determine $\mathrm{SE}_k^{\mathrm{UL},2}(\mathbf{p}, \mathbf{v}_k^{i+1})$ are gathered over B coherence blocks before a better power allocation is computed. If the channel statistics $\{\mathbf{R}_{kl}\}_{\forall k,l}$ remain constant and the necessary large-scale statistics are estimated without estimation error, i.e., $B \to \infty$, one can see that the proposed algorithm is basically performing the alternating optimization method with (7.27)-(7.28). It exhibits the same convergence behavior in that case. For a finite window B the large-scale statistics for the power allocation step are only obtained approximately but the algorithm will still provide a good performance compared to other methods as will be shown in the simulations sections. Simulations show also that $\mathbf{p}$ is not changing much after 3 iterations if the large-scale statistics remain constant, demonstrating the good tracking performance of the proposed algorithm.

Algorithm 8 also has the advantages listed in Subsection 7.3.1: The NC only has to deal with $K \times K$ matrices, the communications over the fronthaul network can be done efficiently using in-network sums and the algorithm is robust against link failures. The extra communication of $\mathbf{U}$ and the parameters $\{\xi_{ki}, \nu_k\}_{\forall k,i}$ are only necessary for the power allocation step, so whenever the performance of the estimation task at hand is sufficient, these steps can be removed to save network resources. Furthermore, it can be seen as an adaptive algorithm, since is adapts to slow changes in the channel statistics over time.

Algorithm 8: Distributed UL MMSE-based receive combining and power allocation (D-UL-RCPA)

Initialize $\mathbf{p} \in \mathcal{P}$.

for *each coherence block in* $\{1, ..., B\}$ **do**

1. - Each AP l estimates $\hat{\mathbf{H}}_l$ locally and computes $\mathbf{X}_l$

$$\mathbf{X}_l = \left(\sum_{k=1}^{K} p_k \mathbf{C}_{kl} + \mathbf{R}^{\mathrm{UL}}_{\mathbf{n}_l \mathbf{n}_l} \right)^{-1} \hat{\mathbf{H}}_l. \tag{7.32}$$

- Each AP l transmits the parameters $\mathbf{X}_l^H \hat{\mathbf{H}}_l \in \mathbb{C}^{K \times K}$ and the transformed signals $\mathbf{x}_l = \mathbf{X}_l^H \mathbf{y}_l^{\mathrm{UL}} \in \mathbb{C}^K$ for all received signals in the coherence block to the NC.

2. The network is used to perform in-network sums to obtain

$$\mathbf{x} = \sum_{l=1}^{L} \mathbf{x}_l, \quad \mathbf{X}^H \hat{\mathbf{H}} = \sum_{l=1}^{L} \mathbf{X}_l^H \hat{\mathbf{H}}_l. \tag{7.33}$$

3. - The NC computes $\mathbf{U}$ using (7.17) and broadcasts $\mathbf{U}$ to all APs.
   - The NC estimates the UL signals as

$$\hat{s}_k = \mathbf{u}_k^H \mathbf{x} \quad \forall k. \tag{7.34}$$

- The NC updates the large-scale statistics as

$$\gamma_k \leftarrow \gamma_k + \frac{1}{B} \mathbf{u}_k^H \mathbf{X}^H \hat{\mathbf{h}}_k \qquad \forall k \tag{7.35}$$

$$\upsilon_{ki} \leftarrow \upsilon_{ki} + \frac{1}{B} |\mathbf{u}_k^H \mathbf{X}^H \hat{\mathbf{h}}_i|^2 \qquad \forall k, i. \tag{7.36}$$

4. Each AP l updates the local large-scale statistics as

$$\xi_{ki}^l \leftarrow \xi_{ki}^l + \frac{1}{B} \mathbf{u}_k^H \mathbf{X}_l^H \mathbf{C}_{il} \mathbf{X}_l \mathbf{u}_k \qquad \forall k, i \tag{7.37}$$

$$\nu_k^l \leftarrow \nu_k^l + \frac{1}{B} \mathbf{u}_k^H \mathbf{X}_l^H \mathbf{R}^{\mathrm{UL}}_{\mathbf{n}_l \mathbf{n}_l} \mathbf{X}_l \mathbf{u}_k \qquad \forall k. \tag{7.38}$$

end

The NC gathers the large-scale statistics $\xi_{ki}, \nu_k \ \forall k, i$ (using in-network sums).

The NC solves power allocation problem (7.28) to obtain new values for $\mathbf{p}$.
Examples op optimization algorithms will be provided in Subsection 7.5.1.

The NC transmits the new values for $\mathbf{p}$ to all APs and p_k to UE k $\forall k$.

Reset $\gamma_k, \upsilon_{ki}, \xi_{ki}^l, \nu_k^l \ \forall k, i, l$ and return to step 2.

7.4 DL transmit precoding and power allocation

7.4.1 DL power allocation preliminaries

When a precoding vector $\mathbf{w}_k$ is used to encode data for UE k, the desired signal is received at UE k propagates with a gain of $\mathbf{h}_k^H \mathbf{w}_k$. The UE k does not know this gain a priori, but it can estimate its mean value $E\{\mathbf{h}_k^H \mathbf{w}_k\}$, which is a common approach in massive MIMO systems. The received DL signal can then be expressed as

$$\begin{aligned} y_k^{DL} = & E\{\mathbf{h}_k^H \mathbf{w}_k\}\sqrt{\rho_k}\zeta_k + \left(\mathbf{h}_k^H \mathbf{w}_k - E\{\mathbf{h}_k^H \mathbf{w}_k\}\right)\sqrt{\rho_k}\zeta_k \\ & + \sum_{i \neq k} \mathbf{h}_k^H \mathbf{w}_i \sqrt{\rho_i}\zeta_i + n_k^{DL}. \end{aligned} \tag{7.39}$$

Here $E\{\mathbf{h}_k^H \mathbf{w}_k\}$ represents a deterministic channel and the other terms represent uncorrelated interference and noise. The following achievable SE can then be obtained using the hardening bound [7, 66, 67]:

$$\mathrm{SE}_k^{\mathrm{DL},2} = \frac{\tau_d}{\tau_c} \log_2(1 + \mathrm{SINR}_k^{\mathrm{DL}}) \text{ [bits/s/Hz]} \tag{7.40}$$

with $\mathrm{SINR}_k^{\mathrm{DL}}$ given as

$$\frac{\rho_k |E\{\mathbf{w}_k^H \mathbf{h}_k\}|^2}{\sum_{i=1}^K \rho_i E\{|\mathbf{w}_i^H \mathbf{h}_k|^2\} - \rho_k |E\{\mathbf{w}_k^H \mathbf{h}_k\}|^2 + \sigma_k^{2,\mathrm{DL}}}. \tag{7.41}$$

Here the assumption $E\{||\mathbf{w}_k||^2\} = 1$ is not implied, while this is the case in [7, 66, 67]. The total transmit power allocated to UE k is still given by $\rho_k E\{||\mathbf{w}_k||^2\}$, which is no longer only determined by ρ_k, but is also influenced by the statistics of $E\{||\mathbf{w}_k||^2\}$.

The DL power allocation problem with a per AP total power constraint, is finally formulated as

$$\begin{aligned} \max_{\boldsymbol{\rho} \geq \mathbf{0}} \quad & U(\overline{\mathrm{SE}}_1, ..., \overline{\mathrm{SE}}_K) \\ s.t. \quad & \overline{\mathrm{SE}}_k = \mathrm{SE}_k^{\mathrm{DL},2}(\boldsymbol{\rho}, \mathbf{W}(\boldsymbol{\rho})) \quad \forall k \\ & \sum_{k=1}^K \rho_k \mu_k^l \leq P_t^l \quad \forall l \end{aligned} \tag{7.42}$$

with P_t^l the maximum transmit power of AP l and

$$\mu_k^l = E\{\mathbf{w}_{kl}^H \mathbf{w}_{kl}\}. \tag{7.43}$$

7.4.2 UL - DL duality

Instead of solving the primal problem (7.42) directly, it is proposed to solve the dual problem using a dual subgradient descent procedure. The dual problem to (7.42) can be found by introducing L dual variables $\boldsymbol{\sigma} = [\sigma_1 \ ... \ \sigma_L]^T$ for the L power constraints and an extra common dual variable λ resulting in

$$\min_{\boldsymbol{\sigma}^v \geq \mathbf{0}, \lambda \geq 0} \max_{\boldsymbol{\rho} \geq \mathbf{0}, \mathbf{W}} \mathcal{L}^{\mathrm{DL}}(\boldsymbol{\rho}, \mathbf{W}, \boldsymbol{\sigma}^v, \lambda) \tag{7.44}$$

where the Lagrangian $\mathcal{L}^{\mathrm{DL}}(\boldsymbol{\rho}, \mathbf{W}, \boldsymbol{\sigma}^v, \lambda)$ is given as

$$U(\mathrm{SE}_1^{\mathrm{DL},2}, ..., \mathrm{SE}_K^{\mathrm{DL},2}) - \lambda \sum_{l=1}^{L} \sigma_l^v \left(\sum_{k=1}^{K} \rho_k \mu_k^l - P_t^l \right). \tag{7.45}$$

For some specific cases with deterministic channels (e.g., [187,188]), it is possible to show that the duality gap between the primal and dual problem is zero, so that solving the dual problem will result in a primal optimal solution. Unfortunately this is not the case for the general CFmMIMO DL power allocation problem in (7.42), so convergence to a global optimum can not be guaranteed. However, the proposed algorithm will provide an efficient way of obtaining a set of locally optimal DL power allocation and precoding vectors.

To be able to find the optimal precoding strategy for $\mathbf{W}$, a change of variables is introduced. $\mathrm{SE}_k^{\mathrm{DL},2}$ in (7.42) is replaced with the expression for the SE of a virtual UL network $\mathrm{SE}_k^{\mathrm{UL},v} = \frac{\tau_d}{\tau_c} \log_2(1 + \mathrm{SINR}_k^{\mathrm{UL},v})$, depending on the newly introduced variables $\mathbf{p}^v$, which will replace the DL transmit powers $\boldsymbol{\rho}$. The virtual UL network $\mathrm{SINR}_k^{\mathrm{UL},v}$ depends on $\mathbf{p}^v, \mathbf{W}$ and $\boldsymbol{\sigma}$ and is defined as:

$$\frac{p_k^v |E\{\mathbf{w}_k^H \mathbf{h}_k\}|^2}{\sum_{i=1}^{K} p_i^v E\{|\mathbf{w}_k^H \mathbf{h}_i|^2\} - p_k^v |E\{\mathbf{w}_k^H \mathbf{h}_k\}|^2 + \underbrace{\sum_{l=1}^{L} \sigma_l^v \mu_k^l}_{\nu_k}}. \tag{7.46}$$

In order to show that this results in the same allowed region for $\overline{\mathrm{SE}}_k$, it can be shown that any set of DL SEs $\{\mathrm{SE}_k^{\mathrm{DL},2}\}_{\forall k}$ obtained with specific DL transmit powers $\boldsymbol{\rho} \geq \mathbf{0}$ can also be obtained as UL SEs $\{\mathrm{SE}_k^{\mathrm{UL},v}\}_{\forall k}$ with specific virtual

transmit powers $\mathbf{p}^v \geq \mathbf{0}$ and visa versa. Equating the virtual UL SE expression $\mathrm{SE}_k^{\mathrm{UL},v}$ with the DL SE expression $\mathrm{SE}_k^{\mathrm{DL},2}$ for all UEs:

$$\rho_k \cancel{|E\{\mathbf{w}_k^H \mathbf{h}_k\}|^2} \Big(\sum_{i \neq k} p_i^v E\{|\mathbf{w}_k^H \mathbf{h}_i|^2\} + \cancel{p_k^v (E\{|\mathbf{w}_k^H \mathbf{h}_k|^2\} - |E\{\mathbf{w}_k^H \mathbf{h}_k\}|^2)} + \sum_{l=1}^{L} \sigma_l^v \mu_k^l \Big) =$$

$$p_k^v \cancel{|E\{\mathbf{w}_k^H \mathbf{h}_k\}|^2} \Big(\sum_{i \neq k} \rho_i E\{|\mathbf{w}_i^H \mathbf{h}_k|^2\} + \cancel{\rho_k (E\{|\mathbf{w}_k^H \mathbf{h}_k|^2\} - |E\{\mathbf{w}_k^H \mathbf{h}_k\}|^2)} + \sigma_k^{2,\mathrm{DL}} \Big) \quad \forall k. \tag{7.47}$$

This result in the following relation between the UL and DL transmit powers:

$$\boldsymbol{\rho} = \left(\mathbf{M}(\mathbf{p}^v, \mathbf{W}, \boldsymbol{\sigma}^v)\right)^{-1} \mathrm{diag}\{\sigma_1^{2,DL}, ..., \sigma_K^{2,DL}\} \mathbf{p}^v \tag{7.48}$$

with

$$[\mathbf{M}]_{ki} = \begin{cases} \sum_{i \neq k} p_i^v E\{|\mathbf{w}_k^H \mathbf{h}_i|^2\} + \nu_k & \text{if } k = i \\ -p_k^v E\{|\mathbf{w}_i^H \mathbf{h}_k|^2\} & \text{if } k \neq i. \end{cases} \tag{7.49}$$

The matrix $\mathbf{M}$ is real-valued with positive diagonal elements and non-positive off-diagonal elements, and is column diagonally dominant. Therefore, $\mathbf{M}$ is an M-matrix [189]. As M-matrices are inverse positive, it is clear that for each $\mathbf{p}^v \geq \mathbf{0}$, solving (7.48) will yield DL transmit powers $\boldsymbol{\rho} \geq \mathbf{0}$. Similar results can be shown for the inverse relation, where $\mathbf{p}^v$ is computed from $\boldsymbol{\rho}$.

Summing all left- and right-hand sides of (7.47) for all UEs, results in the following relation between the virtual UL transmit powers and DL transmit powers:

$$\sum_{k=1}^{K} \rho_k \sum_{l=1}^{L} \sigma_l^v \mu_k^l = \sum_{k=1}^{K} p_k^v \sigma_k^{2,DL}. \tag{7.50}$$

As such the dual problem (7.44) can be written as

$$\min_{\boldsymbol{\sigma}^v \geq \mathbf{0}} \min_{\lambda \geq 0} \max_{\mathbf{p}^v \geq \mathbf{0}, \mathbf{W}} \mathcal{L}^{\mathrm{UL},v}(\mathbf{p}^v, \mathbf{W}, \boldsymbol{\sigma}^v, \lambda) \tag{7.51}$$

where the Lagrangian $\mathcal{L}^{\mathrm{UL},v}(\mathbf{p}^v, \mathbf{W}, \boldsymbol{\sigma}^v, \lambda)$ is given as

$$U(\mathrm{SE}_1^{\mathrm{UL},v}, ..., \mathrm{SE}_K^{\mathrm{UL},v}) - \lambda \left(\sum_{k=1}^{K} p_k^v \sigma_k^{2,\mathrm{DL}} - \sum_{l=1}^{L} \sigma_l^v P_t^l \right). \tag{7.52}$$

If the expressions for estimating the statistics in Theorem 7.3.2 are used in (7.46) and the expectations are replaced by immediate channel estimations, an

expression for the virtual instantaneous $\text{SINR}_k^{\text{UL},v,\text{inst}}$ is obtained as

$$\frac{p_k^v |\mathbf{w}_k^H \hat{\mathbf{h}}_k|^2}{\sum_{i \neq k} p_i^v |\mathbf{w}_k^H \hat{\mathbf{h}}_i|^2 + \sum_{i=1}^K p_i^v \mathbf{w}_k^H \mathbf{C}_i \mathbf{w}_k + \mathbf{w}_k^H \mathbf{R}_{\mathbf{nn}}^{\text{UL},v} \mathbf{w}_k} \tag{7.53}$$

with $\mathbf{R}_{\mathbf{nn}}^{\text{UL},v} = \text{Blkdiag}\{\sigma_1^v \mathbf{I}_N, ..., \sigma_L^v \mathbf{I}_N\}$. Again the optimal value for $\mathbf{w}_k$ that maximizes this Rayleigh quotient is given by a closed form formula similar to (7.15), but with $\mathbf{p}$ and $\mathbf{R}_{\mathbf{nn}}^{\text{UL}}$ replaced by $\mathbf{p}^v$ and $\mathbf{R}_{\mathbf{nn}}^{\text{UL},v}$.

This instantaneous expression for $\text{SINR}_k^{\text{UL},v,\text{inst}}$ can again be used to define a $\text{SE}_k^{\text{UL},v,1}$ as

$$\text{SE}_k^{\text{UL},v,1} = \frac{\tau_d}{\tau_c} E\left\{\log_2(1 + \text{SINR}_k^{\text{UL},v,\text{inst}})\right\} \text{ [bits/s/Hz]} \tag{7.54}$$

which provides as before a tight upper bound for the virtual $\text{SE}_k^{\text{UL},v}$, i.e.,

$$\text{SE}_k^{\text{UL},v} \leq \text{SE}_k^{\text{UL},v,1} \tag{7.55}$$

and this bound is tight for $LN \gg 1$.

Taking the equivalence defined above into account, the combined DL transmit precoding and power allocation problem can be formulated as

$$\begin{aligned} &\min_{\substack{\boldsymbol{\sigma}^v \geq \mathbf{0} \\ \lambda \geq 0}} \max_{\substack{\mathbf{p}^v \geq \mathbf{0} \\ \mathbf{W}}} U(\text{SE}_1, ..., \text{SE}_K) - \lambda \left(\sum_{k=1}^K p_k^v \sigma_k^{2,DL} - \sum_{l=1}^L \sigma_l^v P_t^l \right) \\ &s.t.\ \text{SE}_k = \text{SE}_k^{\text{UL},v}(\mathbf{p}^v, \mathbf{w}_k, \boldsymbol{\sigma}^v) \leq \text{SE}_k^{\text{UL},v,1}(\mathbf{p}^v, \mathbf{w}_k, \boldsymbol{\sigma}^v)\ \forall k \end{aligned} \tag{7.56}$$

with the optimal value for $\boldsymbol{\rho}$ defined using (7.48).

7.4.3 DL transmit precoding and power allocation

Since the dual problems (7.56) is convex in $\boldsymbol{\sigma}^v$, it can be solved via a subgradient projection algorithm, where the subgradient for $\boldsymbol{\sigma}^v$ can be found using the proposed UL-DL duality. A subgradient can be derived from (7.45) as

$$\lambda^\star(\boldsymbol{\sigma}^v) \left(P_t^l - \sum_{k=1}^K \rho_k^\star(\boldsymbol{\sigma}^v) E\{\mathbf{w}_{kl}^{\star,H}(\boldsymbol{\sigma}^v) \mathbf{w}_{kl}^\star(\boldsymbol{\sigma}^v)\} \right) \tag{7.57}$$

where $\boldsymbol{\rho}^\star(\boldsymbol{\sigma}^v), \lambda^\star(\boldsymbol{\sigma}^v)$ and $\mathbf{W}^\star(\boldsymbol{\sigma}^v)$ are the optimal solutions of $\min_{\lambda \geq 0} \max_{\boldsymbol{\rho} \geq \mathbf{0}, \mathbf{W}} \mathcal{L}^{\text{DL}}(\boldsymbol{\rho}, \mathbf{W}, \boldsymbol{\sigma}^v)$ and can also be obtained using the optimal

solutions of $\min_{\lambda\geq 0}\max_{\boldsymbol{\rho}\geq\mathbf{0},\mathbf{W}}\mathcal{L}^{\mathrm{UL},v}(\mathbf{p}^v,\mathbf{W},\boldsymbol{\sigma}^v)$ and using (7.48) to obtain $\boldsymbol{\rho}^\star(\boldsymbol{\sigma}^v)$. By inspecting $\min_{\lambda\geq 0}\max_{\mathbf{p}^v\geq\mathbf{0},\mathbf{W}}\mathcal{L}^{\mathrm{UL},v}(\mathbf{p}^v,\mathbf{W},\boldsymbol{\sigma}^v)$, it can be shown that this is the dual problem of the following virtual UL problem:

$$\begin{aligned}\max_{\mathbf{p}^v\geq\mathbf{0},\mathbf{W}}\quad & U(\mathrm{SE}_1^{\mathrm{UL},v},...,\mathrm{SE}_K^{\mathrm{UL},v})\\ s.t.\quad & \sum_{k=1}^{K}p_k^v\sigma^{2,\mathrm{DL}}\leq\sum_{l=1}^{L}\sigma_l^vP_t^l.\end{aligned}\tag{7.58}$$

The optimal solutions for $\boldsymbol{\rho}^\star(\boldsymbol{\sigma}^v)$ and $\mathbf{W}^\star(\boldsymbol{\sigma}^v)$ can alternatively be found from this virtual UL problem, which is a particular instance of problem (7.19) and can thus be solved using Algorithm 8.

However, as computing the required maximization for (7.57) in the CFmMIMO setup will require multiple iterations of Algorithm 8 over different coherence blocks, this will result in a slow tracking speed. Therefore, it is proposed to use the solutions after one iteration of the alternating optimization method to update the dual variables. Also all the subgradients (7.57) are scaled with a common factor $\lambda^\star(\boldsymbol{\sigma}^v)$, which can be compensated by the stepsize, so its computation can be avoided. The simulations in Section 7.6 will show that the convergence behavior is not affected.

The proposed algorithm to solve the DL transmit precoding and power allocation problem can thus be summarized as follows:

1. Set $i\rightarrow 0$ and initialize $\mathbf{p}^{v,0}\geq\mathbf{0},\boldsymbol{\sigma}^{v,0}\geq\mathbf{0}$ randomly
2. Determine the precoding matrix $\mathbf{W}^{i+1}$ for each coherence block that maximizes:

$$\begin{aligned}\max_{\mathbf{W}}\quad & U(\mathrm{SE}_1,...,\mathrm{SE}_K)\\ s.t.\quad & \mathrm{SE}_k=\mathrm{SE}_k^{\mathrm{UL},v,1}(\mathbf{p}^{v,i},\mathbf{w}_k,\boldsymbol{\sigma}^{v,i})\quad\forall k\end{aligned}\tag{7.59}$$

   for a fixed transmit power $\mathbf{p}^{v,i}$ and $\boldsymbol{\sigma}^{v,i}$ by using the virtual quantities in the MMSE-expression (7.15) or (7.16).
3. Determine the optimal transmit powers $\mathbf{p}^{v,i+1}$ that maximizes:

$$\begin{aligned}\max_{\mathbf{p}^v\geq\mathbf{0}}\quad & U(\mathrm{SE}_1,...,\mathrm{SE}_K)\\ s.t.\quad & \mathrm{SE}_k=\mathrm{SE}_k^{\mathrm{UL},v}(\mathbf{p}^v,\mathbf{w}_k^{i+1},\boldsymbol{\sigma}^{v,i})\quad\forall k\\ & \sum_{k=1}^{K}p_k^v\sigma_k^{2,DL}\leq\sum_{l=1}^{L}\sigma_lP_t^l\end{aligned}\tag{7.60}$$

and compute $\boldsymbol{\rho}^{i+1}$ using (7.48).

4. Update the dual variables with stepsize t_i using the current estimate for the subgradient:

$$\sigma_l^{i+1} = \max(\sigma_l^i - t_i(P_t^l - \sum_{k=1}^{K} \rho_k^{i+1} \mu_k^{l,i+1}), 0) \ \forall l. \tag{7.61}$$

5. Set $i \leftarrow i + 1$ and return to step 2.

Algorithm 9 presents the corresponding distributed DL tranmsit beamforming and power allocation algorithm (DL-D-DTTP). Algorithm 9 also has the advantages of Algorithm 8, since the communications over the fronthaul network and the local computations are similar.

It is possible for an AP to include additional constraints on its antenna powers. Examples are per-antenna power constraints or per-cluster constraints when an AP is a concatenation of different antenna arrays with local power amplifiers. The proposed algorithm can be extended by introducing an additional dual variable $\sigma_{l,m}^v$ for each additional constraint locally at AP l and redefining ν_k^l as $\sum_m \sigma_{l,m}^v \nu_k^{l,m}$ where the sum is over all the local constraints and $\nu_k^{l,m}$ is the measured power relevant for the m-th constraint. The dual variable update can be extended in a similar way. The virtual noise correlation matrix $\mathbf{R}_{\mathbf{n}_l\mathbf{n}_l}^{\mathrm{UL},v}$ in (7.62) should then include the extra dual variables on the corresponding positions. The introduction of the additional constraints at an AP increases the computational load of an AP, but not of the NC.

7.5 Further considerations

7.5.1 Examples of power allocation strategies

In this subsection, two different utility functions are introduced, which will be used for the simulations in Section 7.6. It is repeated that the requirements are that the utility function is monotonically nondecreasing in each argument SE_k and that the power allocation problem in (7.29) and (7.60) have a unique maximum that can be obtained. The details of the algorithms used to obtain the optimal solution for (7.29) and (7.60) can be found in the provide references.

[7] Note that the per-AP power constraint will only hold upon convergence of the subgradient algorithm. Therefore, it may be necessary to rescale the DL transmit powers locally at each AP l such that $\sum_{k=1}^{K} \rho_{kl} \mu_k^l \leq P_t^l$ before transmitting the DL signal. This will not influence the convergence of the algorithm.

Algorithm 9: Distributed DL MMSE-based transmit precoding and power allocation (D-DL-DTPA)

Initialize $\mathbf{p}^v, \boldsymbol{\sigma}^v$ and $\boldsymbol{\rho}$ randomly[7].

for *each coherence block in* $\{1, ..., B\}$ **do**

1. - Each AP l obtains a local estimate of $\hat{\mathbf{H}}_l$ and computes $\mathbf{X}_l$

$$\mathbf{X}_l = \left(\sum_{k=1}^{K} p_k^v \mathbf{C}_{kl} + \sigma_l^v \mathbf{I}_N \right)^{-1} \hat{\mathbf{H}}_l. \tag{7.62}$$

   - Each AP l transmits the parameters $\mathbf{X}_l^H \hat{\mathbf{H}}_l \in \mathbb{C}^{K \times K}$ to the NC.

2. The network is used to perform in-network sums to obtain

$$\mathbf{X}^H \hat{\mathbf{H}} = \sum_{l=1}^{L} \mathbf{X}_l^H \hat{\mathbf{H}}_l \tag{7.63}$$

3. - The NC computes $\mathbf{U}$ using (7.17) and broadcasts $\mathbf{U}$ to all APs.
   - The NC updates the large-scale statistics as

$$\gamma_k \leftarrow \gamma_k + \frac{1}{B} \mathbf{u}_k^H \mathbf{X}^H \hat{\mathbf{h}}_k \qquad \forall k \tag{7.64}$$

$$\upsilon_{ki} \leftarrow \upsilon_{ki} + \frac{1}{B} |\mathbf{u}_k^H \mathbf{X}^H \hat{\mathbf{h}}_i|^2 \qquad \forall k, i. \tag{7.65}$$

4. - Each AP l transmits the DL signal

$$\sum_{k=1}^{K} \mathbf{X}_l \mathbf{u}_k \sqrt{\rho_k} \zeta_k. \tag{7.66}$$

   - Each AP l updates the large-scale statistics

$$\xi_{ki}^l \leftarrow \xi_{ki}^l + \frac{1}{B} \mathbf{u}_k^H \mathbf{X}_l^H \mathbf{C}_{il} \mathbf{X}_l \mathbf{u}_k \qquad \forall k, i \tag{7.67}$$

$$\mu_k^l \leftarrow \mu_k^l + \frac{1}{B} \mathbf{u}_k^H \mathbf{X}_l^H \mathbf{X}_l \mathbf{u}_k \qquad \forall k \tag{7.68}$$

$$\nu_k^l \leftarrow \sigma_l^v \mu_k^l \qquad \forall k \tag{7.69}$$

end

The NC gathers the large-scale statistics $\xi_{ki}, \nu_k, \sum_{l=1}^{L} \sigma_l P_t^l$ for all UEs k, i (using in-network sums).

The NC solves power allocation problem (7.60) for fixed precoding vectors to obtain new values for $\mathbf{p}^v$ and find the new value for $\boldsymbol{\rho}$ using (7.48).

The NC transmits the new values for $\mathbf{p}^v, \boldsymbol{\rho}$ to all APs.

Each AP l performs a dual update as in (7.61)

Reset $\gamma_k, \upsilon_{ki}^l, \xi_{ki}^l, \nu_k^l \; \forall k, i, l$ and return to step 2.

The first utility function is the **non-weighted max-sum SE**, which represents the total number of bits per second that are transmitted without considering how these bits are assigned between the UEs. The max-sum SE problem can be expressed as

$$U(\mathrm{SE}_1, ..., \mathrm{SE}_K) = \sum_{k=1}^{K} \mathrm{SE}_k. \tag{7.70}$$

Note that the above problem is usually not convex in $\mathbf{p}$ or $\boldsymbol{\rho}$ for given combining/precoding matrices $\mathbf{V}^{i+1}, \mathbf{W}^{i+1}$ and, hence, it is hard to obtain the optimal solution [190]. There exist global optimization methods [191, 192], but their computational complexity is unsuitable for real-time applications. A pragmatic solution is to instead settle for a local optimum. Common approaches for finding a local optimum to the max-sum SE problem are the weighted MMSE method [193] or successive convex optimization [194], which result in iterative algorithms. Schemes using machine learning can potentially find better solutions [173, 174], but require some off-line training and will not provide guaranteed convergence to the optimal solution. Therefore, successive convex optimization [194] will be used for the simulations in Section 7.6.

The max-sum SE intrinsically provides a higher SE for users with good channel conditions, while leaving users with worse channel conditions at a disadvantage. Therefore, the goal of the second utility function is to provide uniform fairness for all users. The aim of the **non-weighted max-min SE fairness** is to maximize the minimum SE among all the UEs in the network:

$$U(\mathrm{SE}_1, ..., \mathrm{SE}_K) = \min_k \mathrm{SE}_k \tag{7.71}$$

Since the SE of UE k is an increasing function of the effective $\mathrm{SINR}^{\mathrm{UL},2}$ or $\mathrm{SINR}^{\mathrm{UL},v}$ respectively, maximizing the minimum SE is the same as maximizing the minimum effective SINR among all the UEs. This quasi-concave problem can be solved using the epigraph trick [149] combined with a bisection method [66, 67, 194, 195] or using fixed-point algorithms [196]. Since all these algorithms converge to a global maximum, the methods in [67] is chosen for the simulations in Section 7.6.

Other utility functions that result in convex optimization problems for fixed combining/precoding matrices $\mathbf{V}^{i+1}, \mathbf{W}^{i+1}$ [191], are for example the weighted geometric mean $\prod_k \mathrm{SE}_k^{w_k}$ and the weighted harmonic mean $(\sum_k w_k/\mathrm{SE}_k)^{-1}$ for some positive weights $\{w_k\}_{\forall k}$.

Table 7.2: Number of complex scalars communicated over each fronthaul link (either from AP to NC or from NC to AP) during B coherence blocks.

	Channel estimation	UL signal estimation	UL power allocation	DL data transmission	DL power allocation
Network-wide SEPA and DTPA	$B\tau_p NL$	$B\tau_u NL$	\	$B\tau_d NL$	\
D-UL-SEPA and D-DL-DTPA	\	$B(\tau_u K + K^2)$	$K^2 + K$	$B(\tau_d K + K^2)$	$K^2 + K$

7.5.2 Scalability

Similarly as in [177], the current D-UL-RCPA and D-DL-DTPA algorithms are scaling with the total number of UEs K in the network. They can in the same way as the scalable network-wide distributed MMSE receive combining (SN-DRC) algorithm be made scalable and this by letting the APs only serve the UEs for which they can obtain good channel estimates [74]. $\mathbf{X}_l$ will then only contain $|\mathcal{D}_l|$ non-zero columns, where $|\mathcal{D}_l|$ is the number of UEs served by AP l and is assumed to be much smaller than K. Also $\mathbf{X}_l^H \hat{\mathbf{H}}_l$ will only contain $|\mathcal{D}_l| \times |\mathcal{D}_l|$ nonzero elements. However, note that the number of parameters $\mathbf{X}^H \hat{\mathbf{H}}$ arriving at the NC in each coherence block, is still given by a full $K \times K$ matrix, but it will generally be a sparse matrix, i.e., position $\{i, k\}$ will be zero if UEs i and k have no AP in common. The provided D-UL-RCPA and D-DL-DTPA algorithms will still converge to a (suboptimal) solution, assuming that $\hat{\mathbf{h}}_{kl}$ and $\mathbf{C}_{kl}$ are zero if AP l is not serving UE k. Simulation results in 7.6 will be provided for both scalable and non-scalable networks[8].

7.5.3 Network topologies

The proposed algorithms have been described as if the network has a tree topology, where all the APs are connected and the NC is the root node. However, they are applicable to any network topology since selecting a tree topology is always possible whenever all the APs are connected [163]. The tree topology allows for an efficient way of computing the required in-network sums in D-UL-RCPA and D-DL-TPPA by starting from the leaf nodes and summing up all the required data when moving towards the root node. Therefore, many current technologies like radio-stripes [197], very large aperture mMIMO [198], distributed mMIMO [199], etc. can be used to realize the proposed algorithms.

[8]Note that all UEs will still be included in $\mathrm{SE}_k^{\mathrm{UL}}$ and $\mathrm{SE}_k^{\mathrm{DL}}$, even when they are not served by an AP since their channels will not exactly be zero. This will explain the suboptimal performance of the scalable algorithms.

Table 7.2 provides an overview of the required communications in one iteration i of the proposed algorithms compared to a network-wide setup, where each AP merely transmits its received signals to the NC. Note that quantities like $\mathbf{X}_l^H \hat{\mathbf{H}}_l$ are Hermitian symmetric, so only transmitting the upper block diagonal part suffices. The big advantage of the proposed algorithms is that the training signals do not need to be transmitted to the NC and that only K signals are broadcast over the different links instead of NL. Since τ_u, τ_d and B are typically the dominating parameters in Table 7.2, the gain in fronthaul communication can be expressed as $\mathcal{O}(\frac{NL}{K})$, which is typically equal to 4 or higher in CFmMIMO systems. Another advantage of the proposed algorithms is that the required large-scale statistics $\mathbf{R}_{kl}$ have to be available only at AP l and that the processing requirement of the NC is relaxed, i.e., it only has to invert $K \times K$ matrices instead of $NL \times NL$ matrices.

7.6 Numerical simulations

Numerical simulations are used in this section to demonstrate the performance and convergence properties of the proposed algorithms. The parameters used for the setup are presented in Table 7.3. The propagation model in [7, Sec. 4.1.3] with spatially correlated fading is used. $\tau_u = 190$ and $\tau_d = 190$ are used respectively when evaluating the SE expressions for UL and DL. A per UE transmit power constraint is used for UL power allocation and a per AP transmit power constraint for DL power allocation. The presented figures and tables are the results averaged over 50 Monte Carlo simulations. The APs and UEs are distributed uniformly at random over the area with a wrap-around technique to determine the shortest distance between a UE and the APs in each Monte Carlo simulation. The greedy pilot assignment from [74] is used to assign the pilots and to determine the UEs served by each AP for simulating a scalable network. Each APs can maximally serve 10 UEs, using this protocol. $B = 100$ channel realizations are used to estimate the expectations and to estimate the large-scale statistic of Table 7.1.

7.6.1 Numerical simulations UL

Estimation method

The first UL simulations are conducted to investigate the validity of Theorem 7.3.2 and the tightness of (7.23). This is done for a scenario where all UEs are transmitting with maximum power $p_k = 100\text{mW}\ \forall k$ and MMSE-based

Table 7.3: Key parameters of considered simulation setup, based on [74]

Parameter	Value
Network area	1 km × 1 km
Number of APs	$L = 50$
Number of antennas per AP	$N = 2, 4, 8, 16$
Number of UEs	$K = 50$
Frounthaul communication gain $\mathcal{O}(\frac{NL}{K})$	$\mathcal{O}(2), \mathcal{O}(4), \mathcal{O}(8), \mathcal{O}(16)$
Bandwidth	20 MHz
Noise model	$\mathbf{R}_{\mathbf{nn}}^{\mathrm{UL}} = \sigma^2 \mathbf{I}_M$, $\sigma_k^{2,\mathrm{DL}} = \sigma^2 \ \forall k$
Noise power	σ^2 = -94dBm
Maximum UL transmit power	100 mW
Maximum DL transmit power	P_t = 1000 mW
Samples per coherence block	$\tau_c = 200$
Channel gain at 1 km	-140.6 dB
Pathloss exponent	3.67
Height difference between AP and UE	10 m
Standard deviation of shadow fading	4
Number of coherence block	$B = 100$
Number of Monte Carlo simulations	50

combining is used. The results for different numbers of antennas per AP are shown in Figure 7.3.

$\mathrm{SE}_k^{\mathrm{UL},2}$ and the $\mathrm{SE}_k^{\mathrm{UL},2}$ (true), which is the result obtained when the true channel is used in the expectation of (7.22) instead of the method proposed in Theorem 7.3.2, are almost perfectly overlapping for all the considered setups. This shows that when a sufficiently large number of samples are used to estimate the quantities of Theorem 7.3.2, the required assumptions hold for the MMSE-based combining vector. Here $B = 100$ samples are used for the expectations, so this provides already a good estimate of the average channel statistics.

Regarding the tightness of the bound in (7.23) which can be observed by comparing $\mathrm{SE}_k^{\mathrm{UL},1}$ and the $\mathrm{SE}_k^{\mathrm{UL},2}$, it can be observed that $\mathrm{SE}_k^{\mathrm{UL},2}$ is always a lower bound for $\mathrm{SE}_k^{\mathrm{UL},1}$, but this bound becomes tighter as the number of antennas per AP increases. For the setup with $N = 16$, there is almost no difference between the different SEs, which validates the assumption of equality in the proposed algorithms.

Convergence behavior

To investigate the convergence behavior of D-UL-RCPA, the utility function over different iterations is plotted in Figure 7.4, both for max-sum and max-min power allocation. The iterations are started from a random feasible power allocation $\mathbf{p}^0 \geq \mathbf{0}$. The results are plotted for both $\mathrm{SE}_k^{\mathrm{UL},1}$ and $\mathrm{SE}_k^{\mathrm{UL},2}$ and for different numbers of antennas.

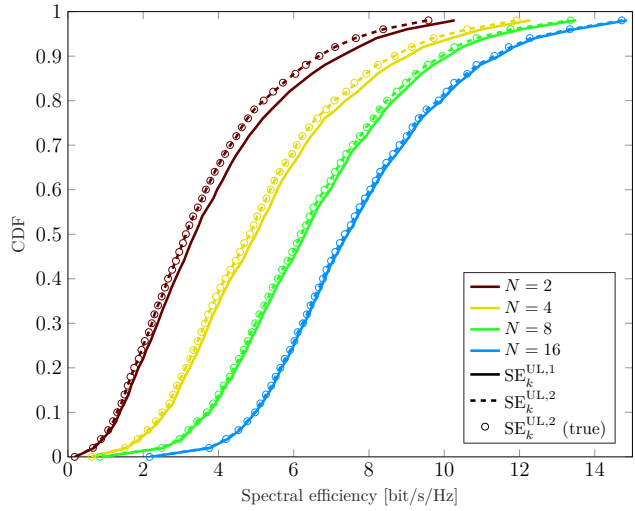

Figure 7.3: Different UL SE for MMSE combining with fixed UE transmit power.

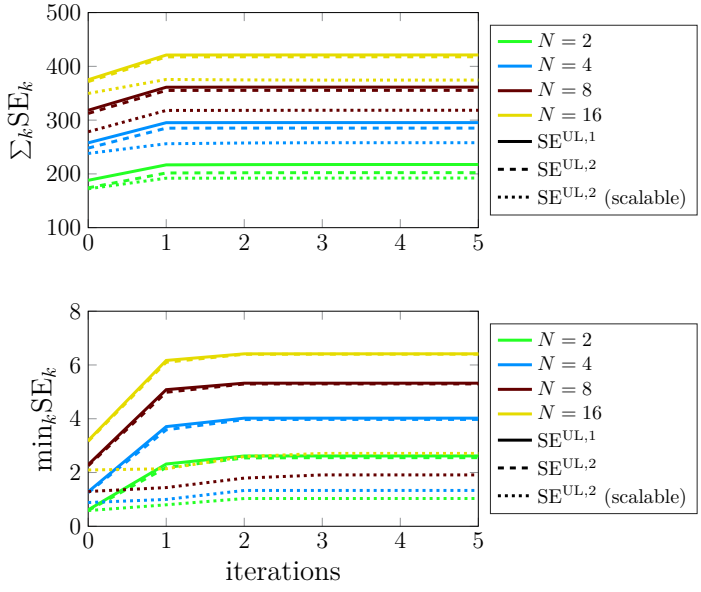

Figure 7.4: Convergence behavior of $\sum_{k=1}^{K} \mathrm{SE}_k$ and $\min_k \mathrm{SE}_k$ for D-UL-RCPA over different iterations with max-sum (upper figure) and max-min (lower figure) power allocation and a per UE transmit power constraint.

Table 7.4: $\sum_{k=1}^{K} \mathrm{SE}_k$ after convergence of D-UL-RCPA
(uniform power allocation | max-sum power allocation | max-sum power allocation scalable)

	$L = 50, N = 4, K = 50$		$L = 50, N = 16, K = 50$	
	$\mathrm{SE}^{\mathrm{UL},2}$	$\mathrm{SE}^{\mathrm{UL},1}$	$\mathrm{SE}^{\mathrm{UL},2}$	$\mathrm{SE}^{\mathrm{UL},1}$
MR	42.5|55.1|53.4	-	82.0|104.10|100.2	-
LMMSE	122.3|129.3|115.3	127.7|135.0|119.0	184.7|197.4|182.6	187.0|199.7|185.7
MMSE	248.0|285.2|258.0	257.7|295.4|262.5	371.6|417.8|374.5	375.0|421.2|376.8

Table 7.5: $\min_k \mathrm{SE}_k$ after convergence of D-UL-RCPA
(uniform power allocation | max-min power allocation | max-min power allocation scalable)

	$L = 50, N = 4, K = 50$		$L = 50, N = 16, K = 50$	
	$\mathrm{SE}^{\mathrm{UL},2}$	$\mathrm{SE}^{\mathrm{UL},1}$	$\mathrm{SE}^{\mathrm{UL},2}$	$\mathrm{SE}^{\mathrm{UL},1}$
MR	0.0|0.8|0.2	-	0.0|1.4|0.5	-
LMMSE	0.7|2.3|0.8	0.7|2.4|0.9	2.0|3.4|2.1	2.1|3.4|2.2
MMSE	1.2|4.0|1.3	1.3|4.0|1.4	3.2|6.4|2.7	3.2|6.4|2.8

As expected, both $\sum_{k=1}^{K} \mathrm{SE}_k^{\mathrm{UL},1}$ and $\sum_{k=1}^{K} \mathrm{SE}_k^{\mathrm{UL},2}$ for max-sum power allocation and $\min_k \mathrm{SE}_k^{\mathrm{UL},1}$ and $\min_k \mathrm{SE}_k^{\mathrm{UL},2}$ for max-min power allocation are monotonically increasing and reach an equilibrium point after 3 iterations for each setup. This is even the case for the max-sum power allocation, although the power allocation problem is here only solved to local optimality. The fast convergence and significant performance improvement are desirable properties of D-UL-RCPA. When considering the scalable version of the D-UL-RCPA, a small performance drop in $\sum_{k=1}^{K} \mathrm{SE}_k^{\mathrm{UL},2}$ is seen compared to the non-scalable version, while a large performance drop in $\min_k \mathrm{SE}_k^{\mathrm{UL},2}$ is observed. The latter can be explained since all UEs are still included in the computation of $\mathrm{SE}_k^{\mathrm{UL},2}$, and this has a large effect on the worst case performance.

Performance

The performance of the combining vectors and power allocation obtained after convergence of D-UL-RCPA is compared with heuristic distributed combining methods, namely MR combining and Local MMSE (LMMSE) combining. In MR combining, the local combining vector is chosen as $\mathbf{v}_{kl} = \hat{\mathbf{h}}_{kl}$ for UE k at AP l. In LMMSE, the combining vector is chosen to minimize the local MMSE criterion $E\{||s_k - \mathbf{v}_{kl}^H \mathbf{y}_l||^2 | \hat{\mathbf{H}}_l\}$ and is given as $\mathbf{v}_{kl} = p_k \left(\hat{\mathbf{H}}_l \mathbf{P} \hat{\mathbf{H}}_l^H + \sum_{i=1}^{K} p_i \mathbf{C}_{il} + \mathbf{R}_{\mathbf{n}_l \mathbf{n}_l}^{\mathrm{UL}} \right)^{-1} \hat{\mathbf{h}}_{kl}$. The optimal power allocation

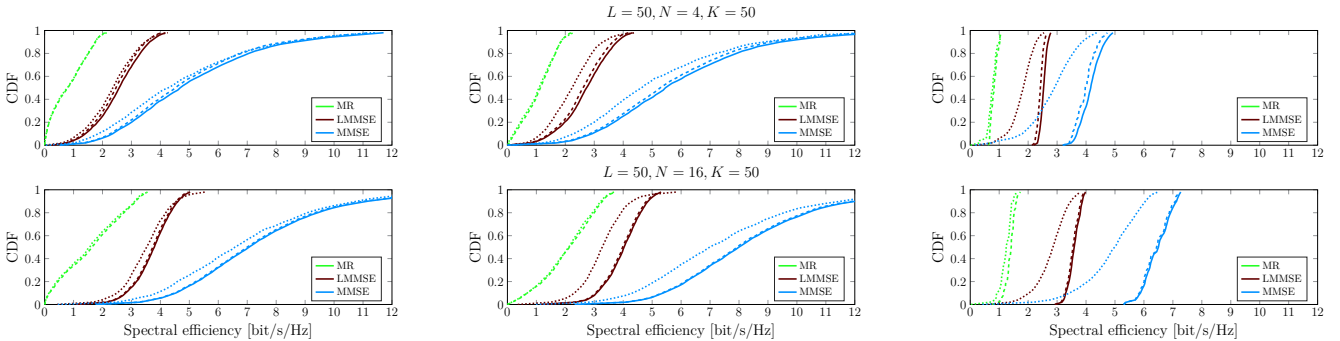

(a) Uniform power allocation. (b) Max-sum power allocation. (c) Max-min power allocation.

Figure 7.5: UL SE of $\mathrm{SE}^{\mathrm{UL},1}$ (–), $\mathrm{SE}^{\mathrm{UL},2}$ (- -) and scalable $\mathrm{SE}^{\mathrm{UL},2}$ (····) for different combining schemes.

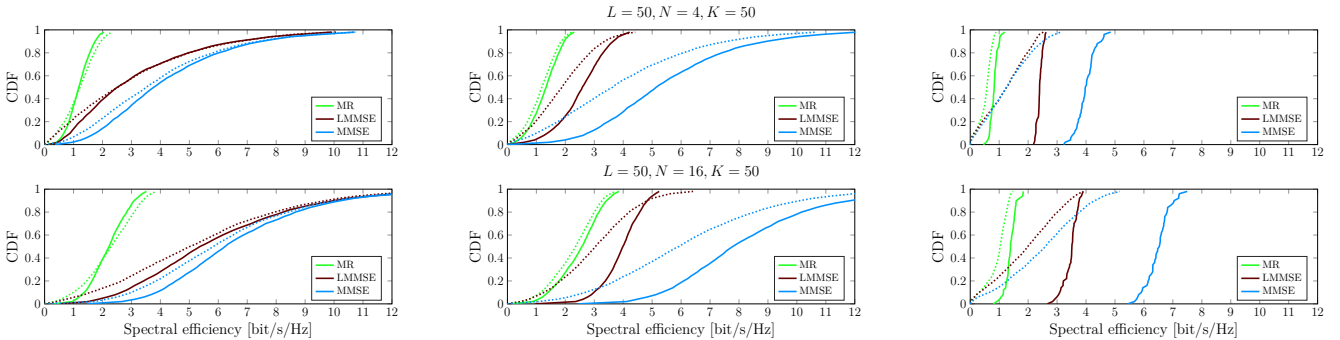

(a) Full power transmission. (b) Max-sum power allocation. (c) Max-min power allocation.

Figure 7.6: DL SE of $\mathrm{SE}^{\mathrm{UL},2}$ (–), and scalable $\mathrm{SE}^{\mathrm{UL},2}$ (····) for different combining schemes.

for both combining schemes is chosen similar as in D-UL-RCPA, but with $\mathbf{U}$ fixed to an identity matrix $\mathbf{I}_K$. The optimal power allocation for MR combining is then found in one iteration, since $\mathbf{v}_{kl}$ is independent of $\mathbf{p}$. For LMMSE combining this will result in an iterative algorithm, but convergence is here also observed after 3 iterations. The cumulative distribution function (CDF) of the UL SE per UE is provided in Figure 7.5 for 3 kinds of power allocation: uniform power allocation (where each UE transmits with maximal power), max-sum and max-min power allocations and for setups with either $N = 4$ antennas per AP or $N = 16$ antennas per AP. The values of the utility function compared to uniform power allocation are given in Table 7.4 for max-sum and Table 7.5 for max-min power allocation.

It is clear that the proposed power allocation algorithm improves the utility function for all the presented receive combining methods. MR combining requires no inversion, but its performance is always inferior to LMMSE combining. Even though LMMSE combining requires an inversion of an $N \times N$ matrix in each coherence block at each AP, while for MMSE-based combining this inversion only has to be performed after B coherence blocks at an AP l, its performance is always inferior to MMSE-based combining. Scalable version are also providing close to optimal performance, except for max-min power allocation, where to blindness towards non-included UEs imposed a large performance drop. It thus remains important to include most of the UEs as serving UEs at the AP, since not including UEs with a rather significant channel strength has a large impact on the minimal SE.

7.6.2 Numerical simulations DL

Convergence behavior

D-DL-TPPA is run for 40 iterations using a stepsize of $t_i = \min(1, 10/i)$ and initialized with virtual UL powers $p_k^{\mathrm{v},0} = 100$ mW $\forall k$ and a random feasible DL power allocation $\boldsymbol{\rho}^0 \geq \mathbf{0}$. The utility function over different iterations is plotted in Figure 7.7, both for max-sum and max-min power allocation. To verify if the constraints in all the APs are satisfied, the maximal constraint variation $\max_l \sum_{k=1}^{K} \rho_k E\{\mathbf{w}_{kl}^H \mathbf{w}_{kl}^H\}$ is shown in Figure 7.8 over the different iterations. The per AP transmit power constraints are satisfied when this is below 1000 mW.

While difficult the observe in Figure 7.7, the utility function is no longer monotonically increasing since the proposed method is based on a dual subgradient projection algorithm. However, the objective remains approximately constant after 4 iterations. Looking at the constraint violation in Figure 7.8,

Table 7.6: $\sum_{k=1}^{K} \mathrm{SE}^{\mathrm{DL},2}$ after convergence of D-DL-TPPA (full power transmission | max-sum power allocation | max-sum power allocation scalable)

	$L = 50, N = 4, K = 50$	$L = 50, N = 16, K = 50$
MR	59.8|65.7|63.8	111.3|124.2|120.1
LMMSE	128.0|162.0|125.3	197.2|297.4|194.3
MMSE	214.3|278.0|200.6	336.0|412.5|310.1

Table 7.7: $\min_k \mathrm{SE}^{\mathrm{DL},2}$ after convergence of D-DL-TPPA (full power transmission | max-min power allocation)

	$L = 50, N = 4, K = 50$	$L = 50, N = 16, K = 50$
MR	0.4|0.8|0.1	0.9|1.4|0.2
LMMSE	0.4|2.4|0.1	1.4|3.5|0.3
MMSE	0.9|4.0|0.2	2.6|6.5|0.5

it can be observed that only for $N = 4, 8, 16$ and max-sum power allocation convergence is reached after 40 iterations. For $N = 2$ is fluctuating around 1100 mW, probably because the APs have a lower degree of freedom (fewer antennas) so need more iterations with smaller stepsizes to converge. The constraint violations for max-min power allocation are converging very slowly, which is typical for dual subgradient methods. However, as will be shown in the next subsection, the performance after 40 iterations is still superior even when the DL transmit powers are normalized to satisfy the constraints.

Performance

Finally, the performance of the precoding vectors and power allocation obtained after 40 iterations of D-DL-TPPA is again compared to MR precoding and LMMSE precoding. To make sure that the per AP transmit power constraint is not violated during the evaluation, the DL transmit powers are normalized at the APs where this constraint is violated. The heuristic power allocation method proposed in [74] is used to determine the DL transmit powers for full power transmission. The cumulative distribution function (CDF) of the DL SE per UE are provided in Figure 7.6 for 3 different power allocations: full power transmission, max-sum and max-min power allocation, and for setups with either $N = 4$ antennas per AP or $N = 16$ antennas per AP. The values of the utility function compared to full power transmission are given in Table 7.6 for max-sum and Table 7.7 for max-min power allocation.

Similar observations as for the UL simulations can be made concerning the

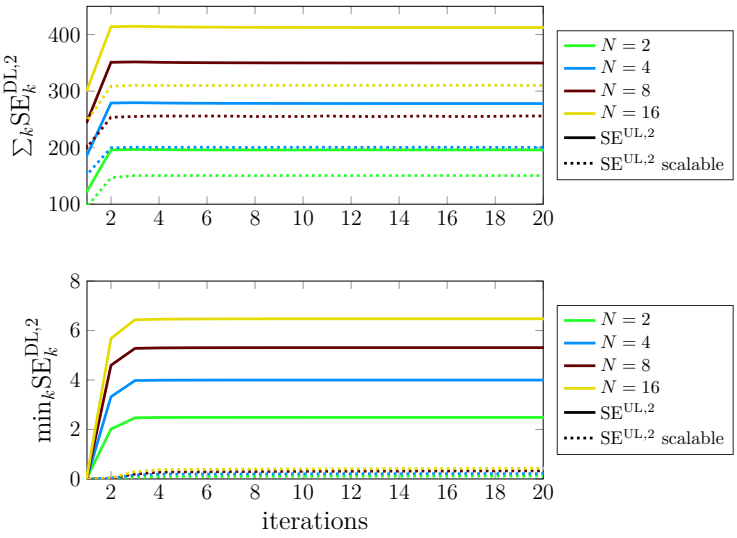

Figure 7.7: Convergence behavior of $\sum_{k=1}^{K} \mathrm{SE}_k^{\mathrm{DL},2}$ and $\min_k \mathrm{SE}_k^{\mathrm{DL},2}$ for D-DL-TPPA over different iterations with max-sum (upper figure) and max-min (lower figure) power allocation and a per AP transmit power constraint.

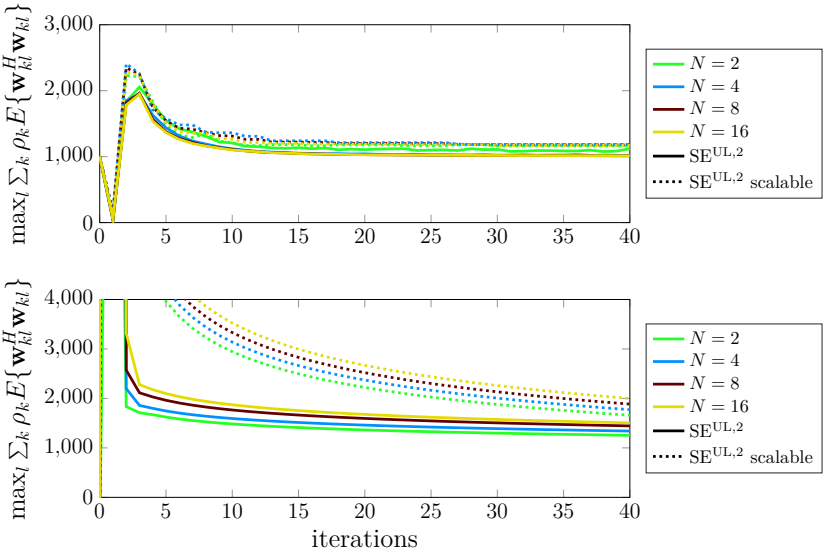

Figure 7.8: Convergence behavior of maximal constraint violation $\max_l \sum_{k=1}^{K} \rho_k E\{\mathbf{w}_{kl}^H \mathbf{w}_{kl}^H\}$ of D-DL-TPPA over different iterations with max-sum and max-min power allocation and a per AP transmit power constraint.

performance of D-DL-TPPA (both for the scalable as the non-scalable version). The proposed power allocation algorithm improves the utility function for all the presented precoding methods, MR combining requires less computational effort, but its performance is inferior and MMSE-based combining outperforms LMMSE combining.

7.7 Conclusion

This paper has presented distributed MMSE-based receive combining, transmit beamforming and power allocation strategies for both UL as well as DL data transmission in CFmMIMO systems. The necessary fronthaul communications to estimate the combining/precoding vectors and the necessary large-scale channel statistics are reduced to a minimum and rely on in-network summation that can be accomplished whenever the APs can be arranged into a tree-topology. The computations are also distributed over the different APs and the NC. It is shown that the MMSE-based algorithms reach optimal performance.

In this paper it is assumed that the data of all the UEs is transmitted to one central NC. This is not scalable when the network size and the number of UEs grow larger. Therefore, in future work, the current algorithms will be used as benchmark algorithms when designing future scalable algorithms in which not all APs serve all UEs and certain APs take some of the functionality of the NC.

Chapter 8

Distributed combined channel estimation and receive combining for user-centric CFmMIMO systems

Distributed Combined Channel Estimation and Receive Combining in Cell-Free Massive MIMO Systems.

Robbe Van Rompaey and Marc Moonen

Submitted for publication in
IEEE Transactions on Wireless Communications.

Changes include layout, representation and minor editing aspects.
The candidate's contributions as first author include all performed research and writing of the article under guidance of the co-author.

Abstract

Cell-free massive MIMO (CFmMIMO) is considered as one of the enablers to meet the demand for increasing data rates of next generation (6G) wireless communications. In user-centric CFmMIMO, each user equipment (UE) is served by a user-selected set of surrounding access points (APs), requiring efficient signal processing algorithms minimizing inter-AP communications, while still providing a good quality of service to all UEs. This paper provides algorithms for channel estimation (CE) and uplink (UL) receive combining (RC), designed for CFmMIMO channels using different assumptions on the structure of the channel covariances, i.e., the channels contain only a Line-of-Sight (LoS) component, only Non-LoS (NLoS) components (the common Rayleigh fading model), or contain both components (the general Rician fading model). The LoS component introduces correlation between the channels at different APs that can be exploited to improve the CE and the RC. The channel estimates are obtained in each AP by processing the local antenna signals of the AP, together with compressed versions of all the antenna signals of the APs serving the UE, during UL training. To make the proposed method scalable, the distributed user-centric channel estimation and receive combining (DUCERC) algorithm is presented that significantly reduces the necessary communications between the APs. The effectiveness of the proposed method and algorithm is demonstrated via numerical simulations.

Keywords Cell-free massive MIMO, CSI-free channel estimation, uplink receive combining, distributed user-centric processing, Minimum-Mean-Squared-Error (MMSE)

8.1 Introduction

A major shortcoming of currently deployed cellular massive MIMO (mMIMO) networks (5G), where each user equipment (UE) is served only by the access point (AP) of the cell it resides in, is that UEs on cell edges experience a low channel gain to their serving AP and a high interference power from nearby cells [200]. To overcome this shortcoming, the concept of cell-free mMIMO (CFmMIMO) [124, 126, 197] has been proposed as a promising next step for the next generation wireless communications (6G). Specifically, user-centric CFmMIMO [71–74] is attracting a lot of attention, by letting the UEs themselves decide by which APs they are served [72,122,201]. Cooperation between the APs using the available fronthaul communication links then allows for implementing interference-rejecting receive combining and transmit precoding algorithms effective for all UEs in the network. Hence, CFmMIMO effectively eliminates cell borders while still reusing the current network layout, which offers the potential to drastically improve the user-experience as compared to current cellular mMIMO systems.

An important prerequisite for improving the user-experience, is obtaining good channel estimates of the channels between the UE and its serving APs. Currently. minimum-mean-squared-error (MMSE)-based channel estimation (CE) [68, 74] using uplink (UL) pilots is seen as the standard, but requires perfect knowledge of the overall channel covariance, which is a rather strong assumption since the dimensions of the channel covariance grow with the number of antennas in the serving APs and furthermore the statistics are changing over time. Existing covariance estimators either require additional pilot transmission, sacrifice resources for data transmission [179], use strong assumptions on the distinguishability between channels that may not always be the case [202] or require knowledge of the pilot assignment of all the UEs in the network [166,178]. Therefore, a new data-driven channel covariance estimator for low-rank channel covariances is proposed in [123], be it in the context of cellular mMIMO. It uses a generalized eigenvalue decomposition (GEVD) of two covariances that can be estimated from the available UL data. The requirements for the system are minimal and, except for synchronization, there is no need for communication between the different cells and no prior knowledge on the background noise is required. In this paper, this method is extended to CFmMIMO systems.

CE is mostly performed independently at each AP. While this is mostly justified for Rayleigh fading channels [68, 74, 124], i.e., channels with only Non-Line-of-Sight (NLoS) components, due to the large spread in APs, this might no longer be the case for channels with an additional strong LoS component, i.e., satisfying the general Rician fading model. CFmMIMO systems with Rician fading channels are considered in [120,125,203,204], without explicitly exploiting

possible correlation between nearby APs serving a common UEs. The data-driven channel covariance estimator allows for estimating correlation between nearby APs, and is thus able to exploit this to improve the CE and in a later stage the receive combining (RC).

A low-complexity algorithm for local CE is presented in [205], requiring less resources to estimate the necessary CSI. A time-of-arrival (TOA)-based scheme that first estimates the TOA of the multipath channel and then filters out interfering signals is presented in [206]. The TOA-based CE depends only on the currently received signal without the need for channel state information (CSI). Both methods are compared to least-squares (LS) CE, but the estimation performance does not come close to MMSE-based CE. Methods based on machine learning [207–209] are arising and giving good estimation performance, especially for mmWave channels, since these channels can only approximately be described by Rayleigh and Rician fading models. While these methods reduce the online computational complexity, they require offline training and are tailored to particular setups.

UL RC [170] uses the acquired CSI to obtain a good estimate of the transmitted UL data. Popular UL RC choices in CFmMIMO are maximum-ratio (MR) combing [66, 71, 126, 171], local MMSE combining [68] and regularized zero-forcing [210,211]. In this paper, user-centric MMSE combining will be considered, requiring typically CSI of all antenna signals available in the user-centric network. It will be shown that optimal MMSE-based RC can efficiently be derived from the proposed CE by computing a few parameters.

The newly presented CE and RC methods will first be derived in a centralized setting, i.e., as if all antenna signals serving a certain UE are gathered in one point of the network. As this requires a large communication bandwidth and furthermore introduces a single point of failure, a distributed algorithm will be presented, based on existing algorithms in wireless sensor networks [83, 100, 101, 212]. The channel estimates can then be obtained by processing the local antenna signals in each AP, together with compressed versions of all the antenna signals of the APs serving the UE and computing a few extra parameters using in-networks sums.

8.1.1 Novelty and paper outline

The novelty of this paper can be summarized as follows:

- Section 8.2 proposes a randomized pilot assignment protocol for CFmMIMO systems, allowing to estimate the channel covariance based

on the observed UL data. Derivations of the corresponding optimal MMSE-based CE and RC are given for general channel covariances.

- Section 8.3 proposes different data-based covariance estimation methods, based on different assumptions on the structure of the channel covariances, i.e., the channels contain only NLoS components (Rayleigh fading), only a LoS component, or contain both components (Rician fading). It uses a GEVD-based procedure and presents closed-form expressions for GEVD-based CE and RC.
- In Section 8.4, a distributed algorithm is proposed to obtain the GEVD-based CE and RC in a scalable way, denoted with the GEVD-based distributed user-centric CE and RC (DUCERC) algorithm. The communication cost and convergence properties are also discussed. Furthermore, Section 8.5 explains how all channels estimates, available at each AP, can be used to improve the RC and can be included in the DUCERC algorithm.
- Section 8.6 provides numerical simulations in a simulated CFmMIMO system to evaluate the performance of the proposed centralized and distributed methods.

8.1.2 Notations

Bold lower case letters $\mathbf{a}$ are used to denote complex vectors, bold upper case letters $\mathbf{A}$ are used to denote complex matrices and the font $\mathbb{A}$ is used to denote submatrices, e.g., if $\mathbf{A} \in \mathbb{C}^{M \times N}$ then $\mathbb{A} \in \mathbb{C}^{P \times Q}$ with $P \leq M$ and $Q \leq N$. $\mathbf{I}_R$ is an $R \times R$ identity matrix and $\mathbf{0}_{M \times N}$ is an all zero matrix of dimension $M \times N$. $|\cdot|, ||\cdot||_F, \cdot^H$ and $tr\{\cdot\}$ denote the absolute value, Frobenius norm, conjugate Hermitian operation and trace operation respectively. $E\{.\}$ is the expected value operator, where the expectation is defined with respect to the different channel realizations. $\lfloor \cdot \rfloor_0$ denotes $max(0, \cdot)$ and blkdiag$\{\mathbf{A}_1, ..., \mathbf{A}_K\}$ denotes a block diagonal matrix with $\mathbf{A}_1, ..., \mathbf{A}_K$ on its block diagonal. Finally $\mathcal{U}[a, b)$ denotes the uniform distribution in the interval $[a, b)$ and $\mathcal{NC}(\mathbf{a}, \mathbf{A})$ is the complex Gaussian distribution with mean $\mathbf{a}$ and covariance $\mathbf{A}$.

8.2 Channel and signal model

Consider a CFmMIMO network with K single antenna UEs and L APs, each having N antennas[1] and local processing capabilities. Only a subset of the APs can observe the signal transmitted by UE k with a high enough SINR. This subset will be denoted as:

$$\mathcal{M}_k = \{l|\text{AP } l \text{ observes UE } k\} = \{1, ..., L_k\} \tag{8.1}$$

where $\{1, ..., L_k\}$ defines a specific ordering of the APs for UE k.

The local antenna signal $\mathbf{y}_l$ of AP l can be written as[2]

$$\mathbf{y}_l^t = \sum_{k \in \mathcal{D}_l} \mathbf{h}_{kl}^t s_k + \mathbf{n}_l^t \in \mathbb{C}^N \tag{8.2}$$

where $\mathbf{h}_{kl}^t$ is the channel between UE k and AP l which can be assumed fixed in one coherence block t of τ samples [72], $\mathbf{n}_l^t$ is an additive noise component with covariance $\overline{\mathbf{R}}_{\mathbf{n}_l\mathbf{n}_l}$ and s_k is the signal transmitted by UE k, assumed to have unit transmit power. When UE k is using a transmit power p_k different from unity, the channel can be redefined as the virtual channel $\mathbf{h}_k\sqrt{p_k}$, such that again the transmit power becomes one. This simplification is used throughout the paper to avoid complicated formulas. Finally, the set

$$\mathcal{D}_l = \{k|l \in \mathcal{M}_k\} \tag{8.3}$$

is the set of UEs that AP l observes.

To make the setup scalable, only the antenna signals of the APs in $\mathcal{M}_k$ will be used to estimate s_k. Therefore, a user-centric (sub-)network $\mathcal{M}_k$ will be formed to serve UE k as depicted in Figure 8.1 and their antenna signals are gathered in the (combined) user-centric antenna signals $\mathbf{y}^{\mathcal{M}_k t}k$ as

$$\mathbf{y}^{\mathcal{M}_k t} = \mathbf{h}_k^{\mathcal{M}_k t} s_k + \sum_{\bar{k} \in \overline{\mathcal{P}}_k} \mathbf{h}_{\bar{k}}^{\mathcal{M}_k t} s_{\bar{k}} + \mathbf{n}^{\mathcal{M}_k t} \in \mathbb{C}^{NL_k} \tag{8.4}$$

where $\mathbf{y}^{\mathcal{M}_k t} = [\mathbf{y}_1^{t^H} \ ... \ \mathbf{y}_{L_k}^{t^H}]^H$, $\mathbf{h}_k^{\mathcal{M}_k t} = [\mathbf{h}_{k1}^{t^H} \ ... \ \mathbf{h}_{kL_k}^{t^H}]^H$ and $\mathbf{n}^{\mathcal{M}_k t} = [\mathbf{n}_1^{t^H} \ ... \ \mathbf{n}_{L_k}^{t^H}]^H$. Note that $\mathbf{h}_k^{\mathcal{M}_k t} \triangleq \mathbf{h}_k^t$ and both notations will be used. Also $\mathbf{h}_{\bar{k}}^{\mathcal{M}_k t}$ contains the channels from UE $\bar{k}$ to the APs in $\mathcal{M}_k$. This can be

[1] The methods and algorithms proposed in this paper can easily be extended to scenarios where different APs have a different number of antennas (for ease of notation the same number of antennas are assumed throughout the paper).

[2] Note that abstraction is made of the practical Orthogonal Frequency Division Multiplexing (OFDM) based multi-carrier modulation. [6, Sec. 2] explains how this simplification can be derived.

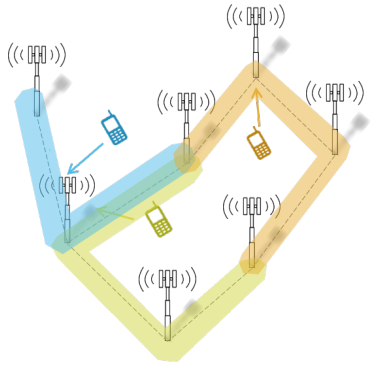

Figure 8.1: Network with user-centric (sub)-networks

written as $\mathbf{E}_{\bar{k}}^{\mathcal{M}_k}\mathbf{h}_{\bar{k}}^t$ where $\mathbf{E}_{\bar{k}}^{\mathcal{M}_k} \in \mathbb{C}^{NL_k \times NL_{\bar{k}}}$ is a selection matrix that selects the channels $\mathbf{h}_{\bar{k}l}^t$ in $\mathbf{h}_{\bar{k}}^t$ if AP $l \in \mathcal{M}_k$ and inserts zero channels elsewhere. It is further assumed that the noise is uncorrelated between the APs, so $\overline{\mathbf{R}}_{\mathbf{nn}}^{\mathcal{M}_k} = \text{blkdiag}\{\overline{\mathbf{R}}_{\mathbf{n}_1\mathbf{n}_1}, ..., \overline{\mathbf{R}}_{\mathbf{n}_{L_k}\mathbf{n}_{L_k}}\}$. Finally the set

$$\mathcal{P}_k = \{\bar{k} | \mathcal{M}_{\bar{k}} \cap \mathcal{M}_k \neq \emptyset\} = \{1, ..., K_k\} \tag{8.5}$$

denotes the UEs that cause interference in the antenna signals $\mathbf{y}^{\mathcal{M}_k t}$ where $\{1, ..., K_k\}$ denotes a specific ordering of the UEs for UE k and $\overline{\mathcal{P}}_k \triangleq \mathcal{P}_k \setminus \{k\}$.

8.2.1 Channel model

The channel $\mathbf{h}_k^t$ is assumed to remain constant during one coherence block and is typically modeled as being drawn from an independent correlated Rician fading distribution [125]:

$$\mathbf{h}_k^t = \overline{\mathbf{h}}_k e^{j\varphi_k^t} + \mathbf{g}_k^t \tag{8.6}$$

with $\varphi_k^t \sim \mathcal{U}[0, 2\pi)$ and $\mathbf{g}_k^t \sim \mathcal{NC}(\mathbf{0}, \overline{\mathbf{G}}_k)$ in each coherence block. Here, $\overline{\mathbf{h}}_k$ is the LoS component, $e^{j\varphi_k^t}$ is a random phase shift and $\overline{\mathbf{G}}_k \in \mathbb{C}^{NL_k \times NL_k}$ is the positive (semi-)definite spatial channel covariance describing the large-scale fading, including geometric pathloss, shadowing, antenna gains and spatial channel correlation [7]. The Gaussian distribution models the small-scale fading of the NLoS component. The LoS component and large-scale fading are assumed to remain constant over several thousands of coherence blocks. Further note that

$$E\{\mathbf{h}_k^t\} = \mathbf{0}_{NL_k} \text{ and } E\{\mathbf{h}_k^t \mathbf{h}_k^{t^H}\} = \overline{\mathbf{h}}_k \overline{\mathbf{h}}_k^H + \overline{\mathbf{G}}_k \triangleq \overline{\mathbf{R}}_k. \tag{8.7}$$

It is common in the CFmMIMO literature to assume that the channels of different APs are independently distributed, i.e., $E\{\mathbf{h}_{kl}^t \mathbf{h}_{k\bar{l}}^{t^H}\} = \mathbf{0}_{N\times N}$ for $l \neq \bar{l}$, so that $\overline{\mathbf{R}}_k$ in (8.7) is block diagonal and that CE can be performed independently at each AP, based on $\overline{\mathbf{R}}_{kl}$[3]. This is often a valid assumption due to the large spatial distribution of the APs in the network. While this is valid for the NLoS component, this assumption is no longer valid for the LoS component $\overline{\mathbf{h}}_k$, since user-centric processing is considered here and only APs in the neighborhood of UE k are serving UE k, Therefore, it is allowed to have correlation between the APs, represented by non-zero non-diagonal elements in $\overline{\mathbf{R}}_k$. This will have a significant impact on the execution of the CE.

It is further assumed that channels from different UEs are uncorrelated $E\{\mathbf{h}_k^t \mathbf{h}_{\bar{k}}^{t^H}\} = \mathbf{0}_{NL_k \times NL_{\bar{k}}}$.

8.2.2 Channel estimation

The samples in one coherence block will be divided into τ_p samples for CE and τ_u samples for UL data transmission. The CE procedure from [123] will be adopted here, which is summarized as follows. Since there are τ_p orthogonal pilot sequences, each UE can randomly pick one of these pilot sequences in each coherence block. It is also assumed that the serving APs are aware of the chosen pilot sequences, which can for example be accomplished using pseudo-random generators with the same seed. The received antenna signals at the APs can then be despreaded using the τ_p different pilot sequences, denoted by $\mathbf{y}_{all_k}^t[p]$ where $p = 1, ..., \tau_p$ is the index of the pilot sequence. The signal obtained after despreading with the correct pilot sequence is denoted by $\mathbf{y}_{\tau_k}^t$. As shown in [123], these signals can be written as:

$$\mathbf{y}_{\tau_k}^t = \sqrt{\tau_p}\mathbf{h}_k^t + \sqrt{\tau_p} \sum_{\bar{k}\in\overline{\mathcal{P}}_k} \mathbf{h}_{\bar{k}}^{\mathcal{M}_k t}\delta_{\bar{k}} + \mathbf{n}^{\mathcal{M}_k t} \tag{8.8}$$

$$\mathbf{y}_{all_k}^t[p] = \sqrt{\tau_p}\mathbf{h}_k^t\delta_k + \sqrt{\tau_p} \sum_{\bar{k}\in\overline{\mathcal{P}}_k} \mathbf{h}_{\bar{k}}^{\mathcal{M}_k t}\delta_{\bar{k}} + \mathbf{n}^{\mathcal{M}_k t} \tag{8.9}$$

where $\delta_{\bar{k}}$ is a random variable with $E\{\delta_{\bar{k}}\} = \frac{1}{\tau_p}$ and $E\{\delta_{\bar{k}}^2\} = \frac{1}{\tau_p}$. It models the probability that UEs have chosen the same pilot sequence in one coherence block. The additive noise $\mathbf{n}^{\mathcal{M}_k t}$ has still the same covariance $\overline{\mathbf{R}}_{\mathbf{nn}}^{\mathcal{M}_k}$ as the noise in (8.4). The factor $\sqrt{\tau_p}$ is an extra gain factor emerging from the despreading procedure.

[3]Note that the index l as in $\overline{\mathbf{R}}_{kl}$ will be used to denote the lth diagonal block of $\overline{\mathbf{R}}_k$.

Expressions for the covariances of the signals in (8.8) and (8.9) are also derived in [123] as:

$$\overline{\mathbf{R}}_{\tau_k} = E\{\mathbf{y}^t_{\tau_k}\mathbf{y}^{t^H}_{\tau_k}\} = \tau_p\overline{\mathbf{R}}_k + \sum_{\bar{k}\in\overline{\mathcal{P}}_k}\overline{\mathbf{R}}^{\mathcal{M}_k}_{\bar{k}} + \overline{\mathbf{R}}^{\mathcal{M}_k}_{\mathbf{nn}} \tag{8.10}$$

$$\overline{\mathbf{R}}_{all_k} = E\{\frac{1}{\tau_p}\sum_{p=1}^{\tau_p}\mathbf{y}^t_{all_k}[p]\mathbf{y}^{t^H}_{all_k}[p]\} = \overline{\mathbf{R}}_k + \sum_{\bar{k}\in\overline{\mathcal{P}}_k}\overline{\mathbf{R}}^{\mathcal{M}_k}_{\bar{k}} + \overline{\mathbf{R}}^{\mathcal{M}_k}_{\mathbf{nn}}$$

where $\overline{\mathbf{R}}^{\mathcal{M}_k}_{\bar{k}}$ is defined as $\mathbf{E}^{\mathcal{M}_k}_{\bar{k}}\overline{\mathbf{R}}_{\bar{k}}\mathbf{E}^{\mathcal{M}_k{}^H}_{\bar{k}}$.

The reason for performing CE using a random pilot allocation scheme, is that these covariances allow for obtaining an expression for the (unknown) channel covariance:

$$\Rightarrow \overline{\mathbf{R}}_k = \frac{1}{\tau_p - 1}\left(\overline{\mathbf{R}}_{\tau_k} - \overline{\mathbf{R}}_{all_k}\right) \tag{8.11}$$

which will be necessary to compute a CE filter.

In practice $\overline{\mathbf{R}}_{\tau_k}$ and $\overline{\mathbf{R}}_{all_k}$ will be estimated[4] from the data using a moving average filter:

$$\mathbf{R}_{\tau_k}(t) = \frac{1}{T}\sum_{\bar{t}=t-T+1}^{t}\mathbf{y}^{\bar{t}}_{\tau_k}\mathbf{y}^{\bar{t}^H}_{\tau_k} \tag{8.12}$$

or a recursive averaging filter:

$$\mathbf{R}_{\tau_k}(t) = (1-\lambda)\mathbf{R}_{\tau_k}(t-1) + \lambda\mathbf{y}^t_{\tau_k}\mathbf{y}^{t^H}_{\tau_k}. \tag{8.13}$$

However, directly estimating $\mathbf{R}_k$ using (8.11) and the estimated covariances $\mathbf{R}_{\tau_k}$ and $\mathbf{R}_{all_k}$, will not result in a good estimate for $\mathbf{R}_k$ [123]: it may result in an estimate that is not positive (semi-)definite and/or antenna signals with a poor signal-to-noise ratio may influence the estimation. Therefore, based on different assumptions on the structure of $\overline{\mathbf{R}}_k$, different estimation methods will be provided in Section 8.3 to overcome this issue.

The optimal MMSE-based CE filter is then obtained by minimizing the MMSE criterion [125]:

$$\overline{\mathbf{W}}_k = \arg\min_{\boldsymbol{W}_k} E\{||\mathbf{h}^t_k - \boldsymbol{W}^H_k\mathbf{y}^t_{\tau_k}||^2\} = \sqrt{\tau_p}(\overline{\mathbf{R}}_{\tau_k})^{-1}\overline{\mathbf{R}}_k \tag{8.14}$$

[4]The notation $\bar{\cdot}$ will be used to denote true ('oracle') quantities. Quantities without overline will denote estimated quantities based on the available data.

since $E\{\mathbf{y}_{\tau_k}^t \mathbf{h}_k^{tH}\} = \sqrt{\tau_p}\overline{\mathbf{R}}_k$. This results in an unbiased estimate $\mathbf{h}_k^t \sim \mathcal{NC}(\hat{\overline{\mathbf{h}}}_k^t, \overline{\mathbf{C}}_k)$ with

$$\hat{\overline{\mathbf{h}}}_k^t = \overline{\mathbf{W}}_k^H \mathbf{y}_{\tau_k}^t \tag{8.15}$$

$$\overline{\mathbf{C}}_k = E\{(\hat{\overline{\mathbf{h}}}_k^t - \mathbf{h}_k^t)(\hat{\overline{\mathbf{h}}}_k^t - \mathbf{h}_k^t)^H\} = \overline{\mathbf{R}}_k - \sqrt{\tau_p}\overline{\mathbf{R}}_k \overline{\mathbf{W}}_k.$$

Note that when $\overline{\mathbf{R}}_{\tau_k}$ and $\overline{\mathbf{R}}_k$ are not block diagonal, $\overline{\mathbf{W}}_k$ will generally not be a block diagonal matrix either. Therefore, all signals in $\mathbf{y}_{\tau_k}^t$ will be needed to compute a channel estimate $\hat{\overline{\mathbf{h}}}_{kl}^t$ of the channel between UE k and a certain AP l and not only the local signals $\mathbf{y}_{\tau_k l}^t$ available at AP l. Efficient distributed algorithms will be provided in Section 8.3 to prevent that all these signals have to be gathered at some point in the network, while still obtaining the correct local channel estimate.

8.2.3 Receive combining

The next τ_u samples will be used by UE k to transmit τ_u data signals. The data signal s_k will be estimated in the network by linearly combining the antenna signals in (8.4) with a receive combiner $\mathbf{v}_k^t \in \mathbb{C}^{NL_k}$ estimated using the acquired channel estimates. This linear combining can be performed in the user-centric network if each AP in $\mathcal{M}_k$ selects the local receive combiner $\mathbf{v}_{kl}^t \in \mathbb{C}^N$ in $\mathbf{v}_k^t = [\mathbf{v}_{k1}^{tH} \ \ldots \ \mathbf{v}_{kL_k}^{tH}]^H$ and computes the local estimate as $\hat{s}_{kl} = \mathbf{v}_{kl}^{tH} \mathbf{y}_l^t$. If the APs in $\mathcal{M}_k$ are organized in a certain topology (as will be discussed in Section 8.4), they can compute an in-network sum to obtain the final estimate as $\hat{s}_k = \sum_{l \in \mathcal{M}_k} \hat{s}_{kl} = \mathbf{v}_k^{tH} \mathbf{y}_k^t$.

MMSE-based RC will be considered here and the MMSE-based receive combiner $\overline{\mathbf{v}}_k^t$, which only uses the acquired channel estimates of UE k, is given as follows:

$$\begin{aligned}
\overline{\mathbf{v}}_k^t &= \arg\min_{\boldsymbol{v}_k} E\{|s_k - \boldsymbol{v}_k^H \mathbf{y}^{\mathcal{M}_k t}|^2 | \mathbf{h}_k^t \sim \mathcal{NC}(\hat{\overline{\mathbf{h}}}_k^t, \overline{\mathbf{C}}_k)\} \qquad (8.16)\\
&= \Big(\sum_{\bar{k} \in \overline{\mathcal{P}}_k} \overline{\mathbf{R}}_{\bar{k}}^{\mathcal{M}_k} + \overline{\mathbf{R}}_{\mathbf{nn}}^{\mathcal{M}_k} + \overline{\mathbf{C}}_k + \hat{\overline{\mathbf{h}}}_k^t \hat{\overline{\mathbf{h}}}_k^{tH} \Big)^{-1} \hat{\overline{\mathbf{h}}}_k^t \\
&= \Big(\overline{\mathbf{R}}_{\tau_k} - \tau_p \overline{\mathbf{R}}_k + \overline{\mathbf{C}}_k + \hat{\overline{\mathbf{h}}}_k^t \hat{\overline{\mathbf{h}}}_k^{tH} \Big)^{-1} \hat{\overline{\mathbf{h}}}_k^t
\end{aligned}$$

where the fact that

$$E\{\mathbf{y}^{\mathcal{M}_k t}\mathbf{y}^{\mathcal{M}_k t^H}|\mathbf{h}_k^t \sim \mathcal{NC}(\hat{\overline{\mathbf{h}}}_k^t, \overline{\mathbf{C}}_k)\} = \tag{8.17}$$
$$\sum_{\bar{k}\in\overline{\mathcal{P}}_k} E\{\mathbf{h}_{\bar{k}}^{\mathcal{M}_k t}\mathbf{h}_{\bar{k}}^{\mathcal{M}_k t^H}\} + E\{\mathbf{n}^{\mathcal{M}_k t}\mathbf{n}^{\mathcal{M}_k t}\} + E\{\mathbf{h}_k^t\mathbf{h}_k^{t^H}|\mathbf{h}_k^t\}$$

is used in the second step of (8.16). This receive combiner only requires knowledge of the channel estimate of UE k whereas the interference/noise will be canceled based on their presence in $\overline{\mathbf{R}}_{\tau_k}$.

A different MMSE-based receive combiner can be constructed when channel estimates of all the other UEs in $\mathcal{P}_k$ are available, which will be referred to as multi-user RC and will be considered in Section 8.5. The expression for this receive combiner $\overline{\mathbf{w}}_k^t$ is given by

$$\begin{aligned}\overline{\mathbf{w}}_k^t &= \arg\min_{\boldsymbol{w}_k} E\{|s_k - \boldsymbol{w}_k^H\mathbf{y}^{\mathcal{M}_k t}|^2|\{\mathbf{h}_{\bar{k}}^{\mathcal{M}_k t} \sim \mathcal{NC}(\hat{\overline{\mathbf{h}}}_{\bar{k}}^{\mathcal{M}_k t}, \overline{\mathbf{C}}_{\bar{k}}^{\mathcal{M}_k})\}_{\forall\bar{k}\in\mathcal{P}_k}\} \\ &= \left(\overline{\mathbf{R}}_{\mathbf{nn}}^{\mathcal{M}_k} + \sum_{\bar{k}\in\mathcal{P}_k}(\overline{\mathbf{C}}_{\bar{k}}^{\mathcal{M}_k} + \hat{\overline{\mathbf{h}}}_{\bar{k}}^{\mathcal{M}_k t}\hat{\overline{\mathbf{h}}}_{\bar{k}}^{\mathcal{M}_k t^H})\right)^{-1}\hat{\overline{\mathbf{h}}}_k^t \\ &= \left(\overline{\mathbf{R}}_{all_k} + \sum_{\bar{k}\in\mathcal{P}_k}(\overline{\mathbf{C}}_{\bar{k}}^{\mathcal{M}_k} - \overline{\mathbf{R}}_{\bar{k}}^{\mathcal{M}_k} + \hat{\overline{\mathbf{h}}}_{\bar{k}}^{\mathcal{M}_k t}\hat{\overline{\mathbf{h}}}_{\bar{k}}^{\mathcal{M}_k t^H})\right)^{-1}\hat{\overline{\mathbf{h}}}_k^t\end{aligned} \tag{8.18}$$

where $\overline{\mathbf{C}}_{\bar{k}}^{\mathcal{M}_k}$ is defined as $\mathbf{E}_{\bar{k}}^{\mathcal{M}_k}\overline{\mathbf{C}}_{\bar{k}}\mathbf{E}_{\bar{k}}^{\mathcal{M}_k H}$.

The expressions for the receive combiner filters $\mathbf{v}_k^t$ and $\mathbf{w}_k^t$ show that user-centric CSI is required to compute them, so this can again only be accomplished when all the user-centric antenna signals in $\mathbf{y}^{\mathcal{M}_k t}$ are available. In the next section, expressions for the channel estimates and receive combiners will be derived depending on the channel model of $\overline{\mathbf{R}}_k$ and assuming that all user-centric antenna signals are centralized at some point in the user-centric network. It will become clear that the expressions allow for efficient distributed processing, which will be further elaborated upon in Section 8.4.

8.3 Centralized GEVD-based CE and RC

Performing the subtraction as in (8.11) using estimated covariances $\mathbf{R}_{\tau_k}$ and $\mathbf{R}_{all_k}$ and without taking into account possible knowledge on the structure of $\overline{\mathbf{R}}_k$, has some significant drawbacks [123]. Therefore, it is proposed to estimate

$\mathbf{R}_k$ by minimizing the following objective

$$\mathbf{R}_k = \arg\min_{\boldsymbol{R}_k} \|\mathbf{R}_{\tau_k}^{-1/2}\big(\mathbf{R}_{\tau_k} - \mathbf{R}_{all_k} - (\tau_p - 1)\boldsymbol{R}_k\big)\mathbf{R}_{\tau_k}^{-H/2}\|_F^2 \tag{8.19}$$

with some constraints on the structure of $\boldsymbol{R}_k$ (a default constraint is that $\mathbf{R}_k$ should be positive semi-definite). In this section, three different channel models are imposed and closed-form expressions for the channel estimates and receive combiner $\mathbf{v}_k^t$ are derived. The channel models are: (i) block diagonal $\overline{\mathbf{R}}_k$ with a local rank constraint, (ii) $\overline{\mathbf{R}}_k$ with a user-centric low rank and (iii) a combination of (i) and (ii).

8.3.1 Block diagonal $\overline{\mathbf{R}}_k$ with a local rank R^B

In this subsection, a block diagonal $\overline{\mathbf{R}}_k$ will be considered, where only the diagonal blocks $\overline{\mathbf{R}}_{kl}$ for $l \in \mathcal{M}_k$ (see footnote 3) are non-zero. This is the most commonly assumed model in CFmMIMO literature [71], since the LoS-component in (8.6) is often neglected in rich scattering scenarios. When the channel is seen as a superposition of multipath components, coming from an area localized around the UE, this often results in a low rank channel covariance $\overline{\mathbf{R}}_{kl}$ [7, 166]. Simulations in [123] show that a rank R^B equal to $N/2$ gives a good performance for these channel models.

For these reasons, the following structure is imposed on $\overline{\mathbf{R}}_k$:

$$\overline{\mathbf{R}}_k = \overline{\mathbf{Q}}_k^B \overline{\mathbf{\Sigma}}_k^B \overline{\mathbf{Q}}_k^{B^H} \tag{8.20}$$

with submatrices $\overline{\mathbf{Q}}_k^B$ and $\overline{\mathbf{\Sigma}}_k^B$ defined as

$$\begin{aligned} \overline{\mathbf{Q}}_k^B &= \text{blkdiag}\{\overline{\mathbb{Q}}_{k1}^B, ..., \overline{\mathbb{Q}}_{kL_k}^B\} \\ \overline{\mathbf{\Sigma}}_k^B &= \text{blkdiag}\{\overline{\mathbb{\Sigma}}_{k1}^B, ..., \overline{\mathbb{\Sigma}}_{kL_k}^B\} \end{aligned} \tag{8.21}$$

and where $\overline{\mathbb{Q}}_{kl}^B \in \mathbb{C}^{N \times R^B}$ and $\overline{\mathbb{\Sigma}}_{kl}^B \in \mathbb{C}^{R^B \times R^B}$ are also submatrices.

Since $\overline{\mathbf{R}}_{\tau_k}, \overline{\mathbf{R}}_{\tau_k}^{-1}$ and $\overline{\mathbf{R}}_{all_k}$ are then also block diagonal, (8.19) decomposes in L_k subproblems that can be solved optimally using L_k GEVDs [110]:

$$\begin{aligned} \mathbf{R}_{\tau_k l} &= \mathbf{Q}_{kl}^B \mathbf{Q}_{kl}^{B^H} \\ \mathbf{R}_{all_k l} &= \mathbf{Q}_{kl}^B \mathbf{\Sigma}_{all_k l}^B \mathbf{Q}_{kl}^{B^H}. \end{aligned} \tag{8.22}$$

Here $\mathbf{Q}_{kl}^B$ is an invertible matrix and its Hermitian inverse contains the generalized eigenvectors as columns. Also $\mathbf{\Sigma}_{all_k l}^B$ is a diagonal matrix containing

the inverse of the generalized eigenvalues and the diagonal elements are sorted from small to large. Let $\mathbb{\Sigma}^B_{all_k,l}$ denote the $R^B \times R^B$ diagonal matrix with the first R^B columns and rows of $\mathbf{\Sigma}^B_{all_k l}$. The optimal solution for $\mathbf{R}_{kl}$ is then given by [110]

$$\mathbf{R}_{kl} = \mathbb{Q}^B_{kl} \mathbb{\Sigma}^B_{kl} \mathbb{Q}^{B^H}_{kl} \tag{8.23}$$

where

$$\begin{aligned} \mathbb{\Sigma}^B_{kl} &= \frac{1}{\tau_p - 1} \lfloor \mathbf{I}_{R^B} - \mathbb{\Sigma}^B_{all_k l} \rfloor_0 \\ \mathbb{Q}^B_{kl} &= \mathbf{Q}^B_{kl} [\mathbf{I}_{R^B} \ \mathbf{0}_{R^B \times (N - R^B)}]^H. \end{aligned} \tag{8.24}$$

Also define

$$\mathbb{X}^B_{kl} = \left(\mathbf{Q}^B_{kl}\right)^{-H} [\mathbf{I}_{R^B} \ \mathbf{0}_{R^B \times (N - R^B)}]^H = \mathbf{R}^{-1}_{\tau_k l} \mathbb{Q}^B_{kl} \tag{8.25}$$

such that $\mathbb{X}^{B^H}_{kl} \mathbb{Q}^B_{kl} = \mathbf{I}_{R^B}$. The optimal channel covariance $\mathbf{R}_k$ is then obtained by substituting (8.24) into (8.21).

The MMSE-based CE filter $\mathbf{W}_k$ with the estimated quantities and the estimated $\mathbf{R}_k$ is then also block diagonal with lth block diagonal

$$\mathbf{W}_{kl} = \sqrt{\tau_p} \mathbf{R}^{-1}_{\tau_k l} \mathbf{R}_{kl} = \sqrt{\tau_p} \mathbb{X}^B_{kl} \mathbb{\Sigma}^B_{kl} \mathbb{Q}^{B^H}_{kl}. \tag{8.26}$$

The corresponding channel estimates are given by

$$\begin{aligned} \hat{\mathbf{h}}^t_{kl} &= \mathbf{W}^H_{kl} \mathbf{y}^t_{\tau_k} = \mathbb{Q}^B_{kl} \underbrace{\sqrt{\tau_p} \mathbb{\Sigma}^B_{kl} \mathbb{X}^{B^H}_{kl} \mathbf{y}^t_{\tau_k l}}_{\mathbf{z}^{t,B}_{kl}} \\ \mathbf{C}_{kl} &= \mathbf{R}_{kl} - \sqrt{\tau_p} \mathbf{W}^H_{kl} \mathbf{R}_{kl} = \mathbb{Q}^B_{kl} \underbrace{\left(\mathbb{\Sigma}^B_{kl} - \tau_p \left(\mathbb{\Sigma}^B_{kl} \right)^2 \right)}_{\mathbb{\Psi}^B_{kl}} \mathbb{Q}^{B^H}_{kl} \end{aligned} \tag{8.27}$$

and the final channel estimates are given as $\hat{\mathbf{h}}^t_k = [\hat{\mathbf{h}}^{t^H}_{k1} \ ... \ \hat{\mathbf{h}}^{t^H}_{kL_k}]^H$ and $\mathbf{C}_k = \text{blkdiag}\{\mathbf{C}_{k1}, ..., \mathbf{C}_{kL_k}\}$.

The expression for the receive combiner $\mathbf{v}^t_k$ based on the estimated quantities becomes

$$\begin{aligned} \mathbf{v}^t_k &= \left(\mathbf{R}_{\tau_k} - \tau_p \mathbf{R}_k + \mathbf{C}_k + \hat{\mathbf{h}}^t_k \hat{\mathbf{h}}^{t^H}_k \right)^{-1} \hat{\mathbf{h}}^t_k \\ &= \begin{bmatrix} \mathbb{X}^B_{k1} \left(\mathbf{I}_{R^B} - \tau_p \mathbb{\Sigma}^B_{k1} + \mathbb{\Psi}^B_{k1} \right)^{-1} \mathbf{z}^{t,B}_{k1} \\ \vdots \\ \mathbb{X}^B_{kL_k} \left(\mathbf{I}_{R^B} - \tau_p \mathbb{\Sigma}^B_{kL_k} + \mathbb{\Psi}^B_{kL_k} \right)^{-1} \mathbf{z}^{t,B}_{kL_k} \end{bmatrix} (1 + \alpha^t_k)^{-1} \end{aligned} \tag{8.28}$$

with

$$\alpha_k^t = \sum_{l \in \mathcal{M}_k} \mathbf{z}_{kl}^{t,B^H} \left(\mathbf{I}_{R^B} - \tau_p \mathbb{\Sigma}_{kl}^B + \mathbb{\Psi}_{kl}^B \right)^{-1} \mathbf{z}_{kl}^{t,B}. \tag{8.29}$$

Hence, both CE as well as RC can be performed locally, except for the scalar multiplication with $(1+\alpha_k^t)^{-1}$ in $\mathbf{v}_{kl}^t = \mathbb{X}_{kl}^B \left(\mathbf{I}_{R^B} - \tau_p \mathbb{\Sigma}_{kl}^B + \mathbb{\Psi}_{kl}^B \right)^{-1} \mathbf{z}_{kl}^{t,B} (1+\alpha_k^t)^{-1}$. Therefore, α_k^t needs to be computed using an in-network sum, which is then the only required communication between the APs[5].

8.3.2 Low rank $\overline{\mathbf{R}}_k$ with rank R^L

In this subsection, a channel model will be assumed where the LoS component dominates the NLoS components and arrives at the serving APs in a coherent way, such that it enforces strong correlation between the channels in the APs. Hence, a low rank R^L on $\overline{\mathbf{R}}_k$ will be assumed where $R^L = 1$ is able to cover this LoS component (possibly including some early reflections).

The following structure is thus imposed on $\overline{\mathbf{R}}_k$:

$$\overline{\mathbf{R}}_k = \overline{\mathbb{Q}}_k^L \overline{\mathbb{\Sigma}}_k^L \overline{\mathbb{Q}}_k^{L^H} \tag{8.30}$$

with

$$\overline{\mathbb{Q}}_k^L = [\overline{\mathbb{Q}}_{k1}^{L^H} \ \ldots \ \overline{\mathbb{Q}}_{kL_k}^{L^H}]^H \in \mathbb{C}^{NL_k \times R^L}, \ \overline{\mathbb{\Sigma}}_k^L \in \mathbb{C}^{R^L \times R^L}. \tag{8.31}$$

Since $\overline{\mathbf{R}}_{\tau_k}$ and $\overline{\mathbf{R}}_{all_k}$ are no longer block diagonal, (8.19) has to be solved by means of a GEVD involving all the antenna signals in the user-centric network:

$$\begin{aligned} \mathbf{R}_{\tau_k} &= \mathbf{Q}_k^L \mathbf{Q}_k^{L^H} \\ \mathbf{R}_{all_k} &= \mathbf{Q}_k^L \mathbf{\Sigma}_{all_k}^L \mathbf{Q}_k^{L^H}. \end{aligned} \tag{8.32}$$

Here $\mathbf{Q}_k^L$ is again an invertible matrix and its Hermitian inverse contains the generalized eigenvectors as columns. Also $\mathbf{\Sigma}_{all_k}^L$ is a diagonal matrix containing the inverse of the generalized eigenvalues and the diagonal elements are sorted from small to large. Let $\mathbb{\Sigma}_{all_k}^L$ denote the $R^L \times R^L$ diagonal matrix with the first R^L columns and rows of $\mathbf{\Sigma}_{all_k}^L$. The optimal solution is then given by:

$$\mathbf{R}_k = \mathbb{Q}_k^L \mathbb{\Sigma}_k^L \mathbb{Q}_k^{L^H} \tag{8.33}$$

[5] In most applications, e.g., when the spectral efficiency (SE) needs to be maximized, one is already satisfied with a receive combiner up to a multiple of $\mathbf{v}_k^t$. This communication can thus be dropped or embedded in a final single channel equalizer.

where

$$\begin{aligned}\mathbb{\Sigma}_k^L &= \frac{1}{\tau_p - 1}\lfloor \mathbf{I}_{R^L} - \mathbb{\Sigma}_{all_k}^L \rfloor_0 \\ \mathbb{Q}_k^L &= \mathbf{Q}_k^L [\mathbf{I}_{R^L}\ \mathbf{0}_{R^L \times (NL_k - R^L)}]^H.\end{aligned} \tag{8.34}$$

Also define

$$\mathbb{X}_k^L = \left(\mathbf{Q}_k^L\right)^{-H} [\mathbf{I}_{R^L}\ \mathbf{0}_{R^L \times (NL_k - R^L)}]^H = \mathbf{R}_{\tau_k}^{-1}\mathbb{Q}_k^L \tag{8.35}$$

such that $\mathbb{X}_{kl}^{L^H}\mathbb{Q}_{kl}^L = \mathbf{I}_{R^L}$.

The MMSE-based CE filter $\mathbf{W}_k$ with the estimated quantities is then given as

$$\mathbf{W}_k = \sqrt{\tau_p}\mathbf{R}_{\tau_k}^{-1}\mathbf{R}_k = \sqrt{\tau_p}\mathbb{X}_k^L\mathbb{\Sigma}_k^L\mathbb{Q}_k^{L^H} \tag{8.36}$$

and the corresponding channel estimates are given by

$$\begin{aligned}\hat{\mathbf{h}}_k^t &= \mathbf{W}_k^H\mathbf{y}_{\tau_k}^t = \mathbb{Q}_k^L \underbrace{\sqrt{\tau_p}\mathbb{\Sigma}_k^L\mathbb{X}_k^{L^H}\mathbf{y}_{\tau_k}^t}_{\mathbf{z}_k^{t,L}} \\ \mathbf{C}_k &= \mathbf{R}_k - \sqrt{\tau_p}\mathbf{W}_k^H\mathbf{R}_k = \mathbb{Q}_k^L \underbrace{\left(\mathbb{\Sigma}_k^L - \tau_p\left(\mathbb{\Sigma}_k^L\right)^2\right)}_{\mathbb{\Psi}_k^L}\mathbb{Q}_k^{L^H}.\end{aligned} \tag{8.37}$$

The receive combiner $\mathbf{v}_k^t$ can be written as

$$\begin{aligned}\mathbf{v}_k^t &= \left(\mathbf{R}_{\tau_k} - \tau_p\mathbf{R}_k + \mathbf{C}_k + \hat{\mathbf{h}}_k^t\hat{\mathbf{h}}_k^{t,H}\right)^{-1}\hat{\mathbf{h}}_k^t \\ &= \mathbb{X}_k^L\left(\mathbf{I}_{R^L} - \tau_p\mathbb{\Sigma}_k^L + \mathbb{\Psi}_k^L + \mathbf{z}_k^{t,L}\mathbf{z}_k^{t,L^H}\right)^{-1}\mathbf{z}_k^{t,L}.\end{aligned} \tag{8.38}$$

The CE and RC can no longer be performed locally, since the antenna signals $\mathbf{y}^{\mathcal{M}_k t}$ needs to be centralized to be able to compute the GEVD of $\mathbf{R}_{\tau_k}$ and $\mathbf{R}_{all_k}$. However, the expressions show that when $\mathbb{X}_k^{L^H}\mathbf{y}_{\tau_k}^t$ (which contains only R^L channels) and $\mathbb{Q}_{kl}^L, \mathbb{X}_{kl}^L, \mathbb{\Sigma}_k^L$ are available, local version can still be obtained.

8.3.3 Superposition of R^B-block diagonal and R^L-low rank $\overline{\mathbf{R}}_k$

In this subsection, a channel model will be assumed that is a superposition of the channel models assumed in Subsections 8.3.1 and 8.3.2. It thus allows for both

NLoS components enforcing a local low rank R^B as well as LoS components enforcing a user-centric low rank R^L. It encompasses the previous models as special cases, obtained by either setting R^B or R^L equal to 0.

The following structure is imposed on $\overline{\mathbf{R}}_k$:

$$\overline{\mathbf{R}}_k = \underbrace{\overline{\mathbf{Q}}_k^B \overline{\mathbf{\Sigma}}_k^B \overline{\mathbf{Q}}_k^{B^H}}_{\overline{\mathbf{R}}_k^B} + \underbrace{\overline{\mathbb{Q}}_k^L \overline{\mathbb{\Sigma}}_k^L \overline{\mathbb{Q}}_k^{L^H}}_{\overline{\mathbf{R}}_k^L} \tag{8.39}$$

where $\overline{\mathbf{Q}}_k^B$, $\overline{\mathbf{\Sigma}}_k^B$ and $\overline{\mathbb{Q}}_k^L$ are defined as in (8.21) and (8.31).

An algorithm to estimate these terms is provided in Algorithm 10. It is an alternating optimization algorithm that solves (8.40). Convergence of Algorithm 10 can be proven by arguing that every step of the algorithm decreases the objective function and the objective function is bounded from below by 0. Hence, after convergence, a limit point of (8.40) must be reached.

Algorithm 10: Rank $\{R^B, R^L\}$ GEVD-based channel covariance estimation

The objective that will be minimized to determine a solution for $\boldsymbol{R}_k^B$ and $\boldsymbol{R}_k^L$ is

$$\|\mathbf{R}_{\tau_k}^{-1/2}\big(\mathbf{R}_{\tau_k} - \mathbf{R}_{all_k} - (\tau_p - 1)(\boldsymbol{R}_k^B + \boldsymbol{R}_k^L)\big)\mathbf{R}_{\tau_k}^{-H/2}\|_F^2 \tag{8.40}$$

where the structure of $\boldsymbol{R}_k^B$ and $\boldsymbol{R}_k^L$ is given by (8.39).

1 Initialize $\mathbf{R}_k^{B,0}$ as $\mathbf{0}_{NL_k \times NL_k}$ and $n \leftarrow 0$.

2 Solve (8.40) for $\mathbf{R}_k^L$ with $\mathbf{R}_k^B = \mathbf{R}_k^{B,n}$ fixed. The solution is given by performing the GEVD [110]:

$$\begin{aligned} \mathbf{R}_{\tau_k} &= \mathbf{Q}_k^{L,n} \mathbf{Q}_k^{L,n^H} \\ \mathbf{R}_{all_k} + (\tau_p - 1)\mathbf{R}_k^{B,n} &= \mathbf{Q}_k^{L,n} \mathbf{\Sigma}_{all_k}^{L,n} \mathbf{Q}_k^{L,n^H} \end{aligned} \tag{8.41}$$

where $\mathbb{\Sigma}_{all_k}^{L,n}$ is defined as before. The optimal solution is then given as:

$$\mathbb{\Sigma}_k^{L,n+1} = \frac{1}{\tau_p - 1} \lfloor \mathbf{I}_{R^L} - \mathbb{\Sigma}_{all_k}^{L,n} \rfloor_0 \tag{8.42}$$

$$\mathbb{Q}_k^{L,n+1} = \mathbf{Q}_k^{L,n} [\mathbf{I}_{R^L} \ \mathbf{0}_{R^L \times NL_k - R^L}]^H \tag{8.43}$$

$$\mathbb{X}_k^{L,n+1} = \mathbf{R}_{\tau_k}^{-1} \mathbb{Q}_k^{L,n+1} \tag{8.44}$$

$$\mathbf{R}_k^{L,n+1} = \mathbb{Q}_k^{L,n+1} \mathbb{\Sigma}_k^{L,n+1} \mathbb{Q}_k^{L,n+1^H}. \tag{8.45}$$

3 Set $\mathbf{R}_k^{B,n+1} = \mathbf{R}_k^{B,n}$ and for $l \in \{1, ..., L_k\}$:

- Solve (8.40) for $\mathbf{R}_{kl}^B$ with $\mathbf{R}_{k\bar{l}}^B = \mathbf{R}_{k\bar{l}}^{B,n+1}\ \forall \bar{l} \neq l$ and $\mathbf{R}_k^L = \mathbf{R}_k^{L,n+1}$ fixed. This can be accomplished by setting $\mathbf{R}_k^B = \mathbf{H}_{kl}\mathbf{R}_{kl}^B\mathbf{H}_{kl}^H + \mathbf{R}_{k,-l}^{B,n+1}$ where $\mathbf{R}_{k,-l}^{B,n+1}$ is equal to $\mathbf{R}_k^{B,n+1}$ except for a zero-block on the position of $\mathbf{R}_{kl}^B$. The problem is then optimally solved using a prior knowledge GEVD (PK-GEVD) [212]:

$$\mathbf{H}_{kl} = \begin{bmatrix}\mathbf{0}_{N\times N(l-1)} & \mathbf{I}_N & \mathbf{0}_{N\times N(L_k-l-1)}\end{bmatrix}^H \tag{8.46}$$

$$\mathbf{B}_{kl} = \begin{bmatrix}\mathbf{I}_{N(l-1)} & \mathbf{0}_{N(l-1)\times N} & \mathbf{0} \\ \mathbf{0} & \mathbf{0}_{N(L_k-1)\times N} & \mathbf{I}_{N(L_k-l-1)}\end{bmatrix}^H \tag{8.47}$$

$$\mathbf{F}_{kl} = \mathbf{H}_{kl} - \mathbf{B}_{kl}\left(\mathbf{B}_{kl}^H\mathbf{R}_{\tau_k}\mathbf{B}_{kl}\right)^{-1}\mathbf{B}_{kl}^H\mathbf{R}_{\tau_k}\mathbf{H}_{kl} \tag{8.48}$$

$$\begin{aligned}\mathbf{F}_{kl}^H\mathbf{R}_{\tau_k}\mathbf{F}_{kl} &= \mathbf{Q}_{kl}^{B,n}\mathbf{Q}_{kl}^{B,n^H} \\ \mathbf{F}_{kl}^H\left(\mathbf{R}_{all_k} + (\tau_p - 1)\left(\mathbf{R}_k^{L,n+1} + \mathbf{R}_{k,-l}^{B,n+1}\right)\right)\mathbf{F}_{kl} &= \mathbf{Q}_{kl}^{B,n}\mathbf{\Sigma}_{all_k,l}^{B,n}\mathbf{Q}_{kl}^{B,n^H}\end{aligned} \tag{8.49}$$

where $\mathbb{\Sigma}_{all_kl}^{B,n}$ is defined as before. The optimal solution is then given as:

$$\mathbb{\Sigma}_{kl}^{B,n+1} = \frac{1}{\tau_p - 1}\lfloor \mathbf{I}_{R^B} - \mathbb{\Sigma}_{all_kl}^{B,n}\rfloor_0 \tag{8.50}$$

$$\mathbb{Q}_{kl}^{B,n+1} = \mathbf{Q}_{kl}^{B,n}[\mathbf{I}_{R^B}\ \mathbf{0}_{R^B\times N-R^B}]^H \tag{8.51}$$

$$\mathbb{X}_{kl}^{B,n+1} = \left(\mathbf{R}_{\tau_k l} - \tau_p\mathbb{Q}_{kl}^{L,n+1}\mathbb{\Sigma}_k^{L,n+1}\mathbb{Q}_{kl}^{L,n+1^H}\right)^{-1}\mathbb{Q}_{kl}^{B,n+1} \tag{8.52}$$

$$\mathbf{R}_{kl}^{B,n+1} = \mathbb{Q}_{kl}^{B,n+1}\mathbb{\Sigma}_{kl}^{B,n+1}\mathbb{Q}_{kl}^{B,n+1^H}. \tag{8.53}$$

4 $n \leftarrow n + 1$ and return to step 2.

Algorithm 10 also defines the following quantities:

$$\begin{aligned}\mathbb{X}_{kl}^B &= \left(\mathbf{R}_{\tau_k l} - \tau_p\mathbb{Q}_{kl}^L\mathbb{\Sigma}_k^L\mathbb{Q}_{kl}^{L^H}\right)^{-1}\mathbb{Q}_{kl}^B,\ l = 1, ..., L_k \\ \mathbb{X}_k^L &= [\mathbb{X}_{k1}^{L^H}\ ...\ \mathbb{X}_{kL_k}^{L^H}]^H = \mathbf{R}_{\tau_k}^{-1}\mathbb{Q}_k^L.\end{aligned} \tag{8.54}$$

It is assumed that, upon convergence of Algorithm 10, $\mathbf{R}_{\tau_k} - \tau_p\mathbb{Q}_k^L\mathbb{\Sigma}_k^L\mathbb{Q}_k^{L^H}$ can be approximated as a block diagonal matrix[6]. Consequently, the following

[6]This is only the case if $\overline{\mathbf{R}}_{\mathbf{nn}}^{\mathcal{M}_k}$ and $\overline{\mathbf{R}}_{\bar{k}}^{\mathcal{M}_k}$ for all $\bar{k} \neq k$ are block diagonal. If this is note the case, then this matrix will no longer be block diagonal and the provided formulas only

identity is assumed to be valid:

$$\left(\mathbf{R}_{\tau_k} - \tau_p \mathbb{Q}_k^L \mathbb{\Sigma}_k^L \mathbb{Q}_k^{L^H}\right)^{-1} \mathbf{Q}_k^B \approx \mathbf{X}_k^B. \tag{8.55}$$

with $\mathbf{X}_k^B = \text{blkdiag}\{\mathbb{X}_{k1}^B, ..., \mathbb{X}_{kL_k}^B\}$.

Based on the approximation in (8.55), the CE filter can be written as

$$\begin{aligned}\mathbf{W}_k &= \sqrt{\tau_p}\mathbf{R}_{\tau_k}^{-1}\mathbf{R}_k = \sqrt{\tau_p}\mathbf{R}_{\tau_k}^{-1}\left(\mathbf{Q}_k^B \mathbf{\Sigma}_k^B \mathbf{Q}_k^{B^H} + \mathbb{Q}_k^L \mathbb{\Sigma}_k^L \mathbb{Q}_k^{L^H}\right) \\ &\approx \sqrt{\tau_p}\mathbf{X}_k^B \mathbf{\Sigma}_k^B \mathbf{Q}_k^{B^H} + \sqrt{\tau_p}\mathbb{X}_k^L \mathbb{\Sigma}_k^L \dot{\mathbb{Q}}_k^H \end{aligned} \tag{8.56}$$

with

$$\begin{aligned}\dot{\mathbb{Q}}_k &\triangleq \mathbb{Q}_k^L - \tau_p \mathbf{Q}_k^B \mathbf{\Sigma}_k^B \mathbf{Q}_k^{B^H} \mathbb{X}_k^L \left(\mathbf{I}_{R^L} - \tau_p \mathbb{\Sigma}_k^L\right)^{-1} \\ &= \mathbb{Q}_k^L - \tau_p \mathbf{Q}_k^B \mathbf{\Sigma}_k^B \mathbf{X}_k^{B^H} \mathbb{Q}_k^L. \end{aligned} \tag{8.57}$$

A proof for (8.56) can be found in Appendix D.1. The equality in (8.57) can be derived by multiplying (D.2) with $\mathbf{Q}_k^{B^H}$.

The channel estimates are then given by

$$\hat{\mathbf{h}}_k^t \approx \mathbf{Q}_k^B \underbrace{\sqrt{\tau_p}\mathbf{\Sigma}_k^B \mathbf{X}_k^{B^H} \mathbf{y}_{\tau_k}^t}_{\mathbf{z}_k^{t,B}} + \dot{\mathbb{Q}}_k \underbrace{\sqrt{\tau_p}\mathbb{\Sigma}_k^L \mathbb{X}_k^{L^H} \mathbf{y}_{\tau_k}^t}_{\mathbf{z}_k^{t,L}} \tag{8.58}$$

$$\mathbf{C}_k \approx \mathbf{Q}_k^B \underbrace{\left(\mathbf{\Sigma}_k^B - \tau_p \left(\mathbf{\Sigma}_k^B\right)^2\right)}_{\mathbf{\Psi}_k^B} \mathbf{Q}_k^{B^H} + \dot{\mathbb{Q}}_k \underbrace{\left(\mathbb{\Sigma}_k^L - \tau_p \left(\mathbb{\Sigma}_k^L\right)^2\right)}_{\mathbb{\Psi}_k^L} \dot{\mathbb{Q}}_k^H.$$

This last result can be obtained by combining $\mathbf{C}_k = \mathbf{R}_k - \sqrt{\tau_p}\mathbf{W}_k^H \mathbf{R}_k$ with (8.21), (8.56) and (8.57).

Note that $\dot{\mathbb{Q}}_k = [\dot{\mathbb{Q}}_{k1}^H \ ... \ \dot{\mathbb{Q}}_{kL_k}^H]^H$ with

$$\dot{\mathbb{Q}}_{kl} = \mathbb{Q}_{kl}^L - \tau_p \mathbb{Q}_{kl}^B \mathbb{\Sigma}_{kl}^B \mathbb{X}_{kl}^{B^H} \mathbb{Q}_{kl}^L \tag{8.59}$$

hold as approximations. However, as the simulations will show, the resulting CE and RC are still performing well.

and thus

$$\begin{aligned}\hat{\mathbf{h}}_{kl}^{t} &\approx \mathbb{Q}_{kl}^{B} \underbrace{\sqrt{\tau_p}\mathbb{\Sigma}_{kl}^{B}\mathbb{X}_{kl}^{B^H}\mathbf{y}_{\tau_k l}^{t}}_{\mathbf{z}_{kl}^{t,B}} + \dot{\mathbb{Q}}_{kl}\mathbf{z}_{k}^{t,L} \\ \mathbf{C}_{kl} &\approx \mathbb{Q}_{kl}^{B} \underbrace{\left(\mathbb{\Sigma}_{kl}^{B} - \tau_p\left(\mathbb{\Sigma}_{kl}^{B}\right)^2\right)}_{\mathbb{\Psi}_{k}^{B}} \mathbb{Q}_{k}^{B^H} + \dot{\mathbb{Q}}_{kl}\mathbb{\Psi}_{k}^{L}\dot{\mathbb{Q}}_{kl}^{H}.\end{aligned} \tag{8.60}$$

This shows that only a subset of the estimation quantities and $\mathbb{X}_{k}^{L^H}\mathbf{y}_{\tau_k}^{t}$ is necessary to compute local channel estimates.

The expression for the receive combiner $\mathbf{v}_{k}^{t}$ is given in (8.61), where again the matrix inversion lemma is used to rewrite the equation:

$$\begin{aligned}\mathbf{v}_{k}^{t} =& \Bigg(\underbrace{\mathbf{R}_{\tau_k} - \tau_p\mathbb{Q}_{k}^{L}\mathbb{\Sigma}_{k}^{L}\mathbb{Q}_{k}^{L^H} + \mathbb{Q}_{k}^{B}\left(-\tau_p\mathbb{\Sigma}_{k}^{B} + \mathbb{\Psi}_{k}^{B}\right)\mathbb{Q}_{k}^{B^H}}_{\mathbf{B}_k} + \dot{\mathbb{Q}}_{k}\mathbb{\Psi}_{k}^{L}\dot{\mathbb{Q}}_{k}^{H} + \\ & [\mathbb{Q}_{k}^{B}\mathbf{z}_{k}^{t,B}\ \dot{\mathbb{Q}}_{k}]\begin{bmatrix}1\\ \mathbf{z}_{k}^{t,L}\end{bmatrix}\begin{bmatrix}1\\ \mathbf{z}_{k}^{t,L}\end{bmatrix}^{H}[\mathbb{Q}_{k}^{B}\mathbf{z}_{k}^{t,B}\ \dot{\mathbb{Q}}_{k}]^{H}\Bigg)^{-1}[\mathbb{Q}_{k}^{B}\mathbf{z}_{k}^{t,B}\ \dot{\mathbb{Q}}_{k}]\begin{bmatrix}1\\ \mathbf{z}_{k}^{t,L}\end{bmatrix} \\ =& \mathbf{B}_{k}^{-1}[\mathbb{Q}_{k}^{B}\mathbf{z}_{k}^{t,B}\ \dot{\mathbb{Q}}_{k}]\left(\mathbf{I}_{1+R^L} + \begin{bmatrix}1 & \mathbf{z}_{k}^{t,L^H}\\ \mathbf{z}_{k}^{t,L} & \mathbf{z}_{k}^{t,L}\mathbf{z}_{k}^{t,L^H} + \mathbb{\Psi}_{k}^{L}\end{bmatrix}\begin{bmatrix}\alpha_{k}^{t} & \boldsymbol{\beta}_{k}^{t^H}\\ \boldsymbol{\beta}_{k}^{t} & \mathbf{\Gamma}_{k}\end{bmatrix}\right)^{-1}\begin{bmatrix}1\\ \mathbf{z}_{k}^{t,L}\end{bmatrix}.\end{aligned} \tag{8.61}$$

The following identities, avoiding the inversion of $\mathbf{B}_k$, are also approximately valid (assuming that $\mathbf{B}_k$ is block diagonal):

$$\begin{aligned}\mathbf{B}_{k}^{-1}\mathbb{Q}_{k}^{B}\mathbf{z}_{k}^{t,B} \approx& \mathbb{X}_{k}^{B}\Big(\mathbf{I}_{L_k R^B} + \mathbb{\Sigma}_{k}^{B} - \tau_p\mathbb{\Sigma}_{k}^{B} - \tau_p\left(\mathbb{\Sigma}_{k}^{B}\right)^2\Big)^{-1}\mathbf{z}_{k}^{t,B} \\ \mathbf{B}_{k}^{-1}\dot{\mathbb{Q}}_{k} \approx& \mathbb{X}_{k}^{L}\left(\mathbf{I}_{R^L} - \tau_p\mathbb{\Sigma}_{k}^{L}\right)^{-1} - \mathbb{X}_{k}^{B}\left(\mathbf{I}_{L_k R^B} + \left(\mathbb{\Sigma}_{k}^{B}\right)^{-1}\right)^{-1}\mathbb{X}_{k}^{B^H}\mathbb{Q}_{k}^{L}\end{aligned} \tag{8.62}$$

and the lth block row can consequently be written as

$$\begin{aligned}[\mathbf{B}_{k}^{-1}\mathbb{Q}_{k}^{B}\mathbf{z}_{k}^{t,B}]_l \approx& \mathbb{X}_{kl}^{B}\Big(\mathbf{I}_{R^B} + \mathbb{\Sigma}_{kl}^{B} - \tau_p\mathbb{\Sigma}_{kl}^{B} - \tau_p\left(\mathbb{\Sigma}_{kl}^{B}\right)^2\Big)^{-1}\mathbf{z}_{kl}^{t,B} \\ [\mathbf{B}_{k}^{-1}\dot{\mathbb{Q}}_{k}]_l \approx& \mathbb{X}_{kl}^{L}\left(\mathbf{I}_{R^L} - \tau_p\mathbb{\Sigma}_{k}^{L}\right)^{-1} - \mathbb{X}_{kl}^{B}\left(\mathbf{I}_{R^B} + \left(\mathbb{\Sigma}_{kl}^{B}\right)^{-1}\right)^{-1}\mathbb{X}_{kl}^{B^H}\mathbb{Q}_{kl}^{L}.\end{aligned} \tag{8.63}$$

The following quantities are also used in (8.61) and they can be simplified as:

$$\alpha_k^t = \mathbf{z}_k^{t,B^H} \mathbb{Q}_k^{B^H} \mathbf{B}_k^{-1} \mathbb{Q}_k^B \mathbf{z}_k^{t,B} \tag{8.64}$$

$$= \sum_{l \in \mathcal{M}_k} \mathbf{z}_{kl}^{t,B^H} \left(\mathbf{I}_{R^B} + \mathbb{\Sigma}_{kl}^B - \tau_p \mathbb{\Sigma}_{kl}^B - \tau_p \left(\mathbb{\Sigma}_{kl}^B \right)^2 \right)^{-1} \mathbf{z}_{kl}^{t,B}$$

$$\boldsymbol{\beta}_k^t = \dot{\mathbb{Q}}_k^H \mathbf{B}_k^{-1} \mathbb{Q}_k^B \mathbf{z}_k^{t,B} \tag{8.65}$$

$$= \sum_{l \in \mathcal{M}_k} \mathbb{Q}_{kl}^{L^H} \mathbb{X}_{kl}^B \left(\mathbf{I}_{R^B} + \mathbb{\Sigma}_{kl}^B \right)^{-1} \mathbf{z}_{kl}^{t,B}$$

$$\boldsymbol{\Gamma}_k = \dot{\mathbb{Q}}_k^H \mathbf{B}_k^{-1} \dot{\mathbb{Q}}_k^H \tag{8.66}$$

$$= \left(\mathbf{I}_{R^L} - \tau_p \mathbb{\Sigma}_k^L \right)^{-1} - (1 + \tau_p) \sum_{l \in \mathcal{M}_k} \mathbb{Q}_{kl}^{L^H} \mathbb{X}_{kl}^B \left(\mathbf{I}_{R^B} + \left(\mathbb{\Sigma}_{kl}^B \right)^{-1} \right)^{-1} \mathbb{X}_{kl}^{B^H} \mathbb{Q}_{kl}^L.$$

The local version of the receive combiner $\mathbf{v}_{kl}^t$ is then given as:

$$\mathbf{v}_{kl}^t = \mathbf{B}_{kl}^{-1} [\mathbf{Q}_{kl}^B \mathbf{z}_{kl}^{t,B} \ \dot{\mathbb{Q}}_{kl}] \left(\mathbf{I}_{1+R^L} + \begin{bmatrix} 1 & \mathbf{z}_k^{t,L^H} \\ \mathbf{z}_k^{t,L} & \mathbf{z}_k^{t,L} \mathbf{z}_k^{t,L^H} + \mathbb{\Psi}_k^L \end{bmatrix} \begin{bmatrix} \alpha_k^t & \boldsymbol{\beta}_k^{t^H} \\ \boldsymbol{\beta}_k^t & \boldsymbol{\Gamma}_k \end{bmatrix} \right)^{-1} \begin{bmatrix} 1 \\ \mathbf{z}_k^{t,L} \end{bmatrix}. \tag{8.67}$$

Similar as in Subsection 8.3.2, the CE and RC can no longer be performed locally since $\mathbf{R}_{\tau_k}$ and $\mathbf{R}_{all_k}$ are required for Algorithm 10. However, the expressions show that when $\mathbb{X}_k^{L^H} \mathbf{y}_{\tau_k}^t$ (which only contains R^L signals) and other local quantities are available together with $\alpha_k^t, \boldsymbol{\beta}_k^t, \boldsymbol{\Gamma}_k$ as in (8.64) - (8.66) (which can be computed using in-network sums), the local channel estimates and receive combiner can still be obtained. This will lay the foundation for the distributed algorithm presented in the next section.

8.4 Distributed GEVD-based CE and RC

To prevent having to transmit all NL_k antenna signals in $\mathbf{y}^{\mathcal{M}_k t}$ to a central processing unit in the user-centric network, a distributed algorithm is presented in this section that converges (under certain conditions) to the same solution as the centralized GEVD-based CE and RC, discussed in Section 8.3. Since the models in Subsections 8.3.1 and 8.3.2 are special cases of the model in Subsection 8.3.3, the distributed algorithm will only be presented for the latter model.

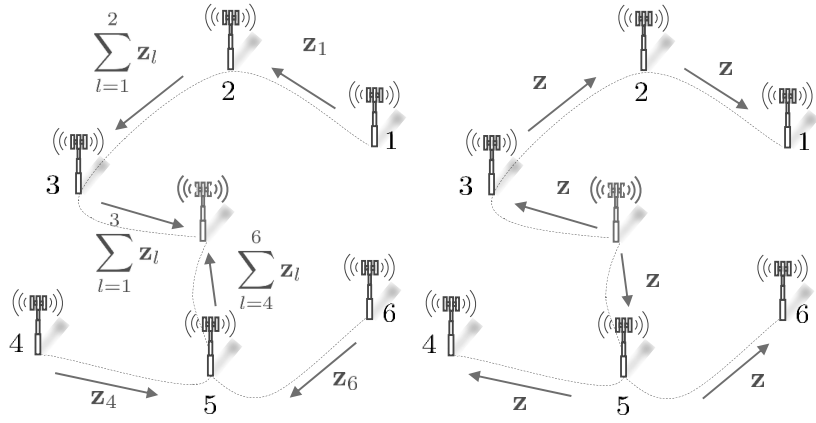

Figure 8.2: Tree based in-network sums for user-centric CFmMIMO using 2 phases: (i) in-network summation towards root-AP and (ii) broadcast of sum by root-AP to all APs $l \in \mathcal{M}_k$.

To organize the inter-AP communication in an efficient way, the user-centric network should be able to perform in-network sums for each UE k, i.e., it should be able to compute $\sum_{l \in \mathcal{M}_k} \mathbf{z}_l$ where $\mathbf{z}_l$ is a certain quantity or parameter. Methods to obtain in-network sums with minimal communication requirements are available in literature, e.g., relying on consensus or gossip methods [49, 155]. However, these methods typically need many iterations to converge, as well as multiple broadcasts of intermediate summed quantities. Therefore, based on [100], a method is proposed to calculate the in-network sums which relies on a tree topology that is formed using the set of available links in the user-centric network with minimal communication requirements (only two transmissions for each link). Figure 8.2 explains the organization of the communication.

For the CE, the proposed algorithm requires computing the in-network sum of $R^L \tau_p$ signals received during the pilot phase of each coherence block and $R^L \times R^L$ parameters per iteration. The RC only requires computing the in-network sum of $(1 + R^L) \times (1 + R^L)$ parameters for each coherence block. Each AP also has to perform computations on a smaller number of input signals, i.e., only the local antenna signals and a compressed R^L dimensional-version of the antenna signals of the other APs. The distributed algorithm is referred to as the rank $\{R^B, R^L\}$ GEVD-based distributed user-centric CE and RC (DUCERC) algorithm and can be related to the distributed algorithms referred to as DANSE, TI-DANSE and GEVD-DANSE of [83, 100, 101] designed for

wireless sensor networks. Different iterations in the proposed algorithm are estimating the parameters on consecutive data segments, and, since the channel covariances are changing, this will allow for an efficient tracking of these changes if the changes are not too abrupt. A drawback of the DUCERC algorithm is the slower adaptation and tracking speed compared to the centralized GEVD-based CE and RC, since the DUCERC algorithm needs multiple iterations on the same data to converge to a stationary solution.

8.4.1 Algorithm description

The rank $\{R^B, R^L\}$ GEVD-based DUCERC algorithm is presented in Algorithm 11. This is a block-iterative round-robin algorithm[7], where the updating AP (denoted by index q) performs similar operations as in Algorithm 10 using data of T coherence blocks. A token is then passed to the next AP, becoming the new updating AP, and this is continued in a cyclic manner.

In one iteration n, each AP compresses the received signals $\mathbf{y}_l^t$ during the pilot phase with $\mathbf{F}_{kl}^n \in \mathbb{C}^{N \times R^L}$ to obtain χ_{kl}^t as in (8.69). Using in-network sums and after subtracting its own compressed channel as in (8.69), it receives a new R^L-dimensional channel $\chi_{k,-l}^t$ which it appends to its local antenna signal to obtain the local extended antenna signal $\tilde{\mathbf{y}}_l^t = [\mathbf{y}_l^{t^H} \;\; \chi_{k,-l}^{t^H}]^H$. This extended antenna signal is then used to perform one iteration of Algorithm 10 (one GEVD and one PK-GEVD). To this end, the updating AP needs an estimate of the block diagonal component present in $\chi_{k,-l}^t$, which is given by $\xi_{k,-l}^n = \sum_{l \in \mathcal{M}_k \setminus \{q\}} \mathbf{F}_{kl}^{n^H} \mathbf{R}_{kl}^{B,n} \mathbf{F}_{kl}^n$ and is easily computed using in-network sums. The compression matrix of the updating AP q is then updated as in (8.72), allowing the algorithm to make progress in convergence.

The local GEVD results in the extended solutions $\tilde{\mathbb{Q}}_{kq}^{L,n+1}, \tilde{\mathbb{X}}_{kq}^{L,n+1}$. The first N rows then correspond to local estimates of $\mathbb{Q}_{kq}^{L,n+1}, \mathbb{X}_{kq}^{L,n+1}$, which are required for the CE and RC as noted in Section 8.3. The local PK-GEVD directly results in $\mathbb{Q}_{kq}^{B,n+1}, \mathbb{\Sigma}_{kq}^{B,n+1}, \mathbb{X}_{kq}^{B,n+1}$ and $\mathbf{R}_{kq}^{B,n+1}$, which are also required for the CE and RC. CE and RC can then be performed as presented in step 5. RC requires knowledge of $\alpha_k^t, \boldsymbol{\beta}_k^t, \boldsymbol{\Gamma}_k$ for each coherence block, which can be computed using in-network sums as in (8.64) - (8.66) by replacing the centralized solutions with the solutions in the current iteration.

[7] Instead of round-robin updates, asynchronous updating as discussed in [85] can also be performed, but this is not discussed here for ease of exposition.

Algorithm 11: Rank $\{R^B, R^L\}$ GEVD-based distributed user-centric CE and RC (DUCERC)

1 Set $n \leftarrow 0, q \leftarrow 1$ and initialize $\mathbf{F}_{kl}^0, \forall l \in \mathcal{M}_k$ randomly.

2 - Each AP $l \in \mathcal{M}_k$ compresses $T\tau_p$ pilot signals of T coherence blocks to $\chi_{kl}^n \in \mathbb{C}^{R^L}$:

$$\chi_{kl}^t = \mathbf{F}_{kl}^{n\,H}\, \mathbf{y}_l^t. \tag{8.68}$$

- The network is used to construct $T\tau_p$ in-network sum $\sum_{l\in\mathcal{M}_k} \chi_{kl}^t$ and each AP $l \in \mathcal{M}_k$ subtracts their compressed version from this to obtain

$$\chi_{k,-l}^t = \sum_{l\in\mathcal{M}_k} \chi_{kl}^t - \chi_{kl}^t \tag{8.69}$$

and appends this to its antenna signal $\tilde{\mathbf{y}}_l^t = [\mathbf{y}_l^{t\,H}\ \chi_{k,-l}^{t\,H}]^H$.

- The network is also used to construct the in-network sum

$$\xi_k^n = \sum_{l\in\mathcal{M}_k} \mathbf{F}_{kl}^{n\,H}\, \mathbf{R}_{kl}^{B,n} \mathbf{F}_{kl}^n \in \mathbb{C}^{R^L\times R^L}. \tag{8.70}$$

3 At update AP q:

- Set $\tilde{\mathbf{R}}_{kq}^{B,n} = \text{blkdiag}\{\mathbf{R}_{kq}^{B,n}, \xi_{k,-q}^n\}$ with $\xi_{k,-q}^n = \xi_k^n - \mathbf{F}_{kq}^{n\,H} \mathbf{R}_{kq}^{B,n} \mathbf{F}_{kq}^n$ and compute $\tilde{\mathbf{R}}_{\tau_k q}$, $\tilde{\mathbf{R}}_{all_k q}$ from $\tilde{\mathbf{y}}_q^t$.
- Compute $\tilde{\mathbb{Q}}_{kq}^{L,n+1}, \tilde{\mathbb{\Sigma}}_{kq}^{L,n+1}, \tilde{\mathbb{X}}_{kq}^{L,n+1}$ and $\tilde{\mathbf{R}}_{kq}^{L,n+1}$ form the GEVD of $\{\tilde{\mathbf{R}}_{\tau_k q}, \tilde{\mathbf{R}}_{all_k q} + (\tau_p - 1)\tilde{\mathbf{R}}_{kq}^{B,n}\}$ similar as in (8.42) - (8.45).
- Compute $\mathbb{Q}_{kq}^{B,n+1}, \mathbb{\Sigma}_{kq}^{B,n+1}, \mathbb{X}_{kq}^{B,n+1}$ and $\mathbf{R}_{kq}^{B,n+1}$ from the PK-GEVD of $\{\tilde{\mathbf{R}}_{\tau_k q}, \tilde{\mathbf{R}}_{all_k q} + (\tau_p - 1)(\tilde{\mathbf{R}}_{kq}^{L,n+1} + \tilde{\mathbf{R}}_{k,-q}^{B,n})\}$ similar as in (8.50) - (8.53) with

$$\tilde{\mathbf{H}}_{kq} = [\mathbf{I}_N\ \mathbf{0}_{N\times R^L}]^H,\ \tilde{\mathbf{B}}_{kq} = [\mathbf{0}_{R^L\times N}\ \mathbf{I}_{R^L}]^H \tag{8.71}$$

and $\dot{\mathbb{Q}}_{kq}^{n+1} = \mathbb{Q}_{kq}^{L,n+1} - \tau_p \mathbb{Q}_{kq}^{B,n+1} \mathbb{\Sigma}_{kq}^{B,n+1} \mathbb{X}_{kq}^{B,n+1} \mathbb{Q}_{kq}^{L,n+1}$.

- Update the compression matrix as

$$\mathbf{F}_{kq}^{n+1} = \mathbb{X}_{kq}^{L,n+1} \left(\mathbb{X}_{k,-q}^{L,n+1}\right)^{-1} \tag{8.72}$$

with $\mathbb{X}_{k,-q}^{L,n+1} = [\mathbf{0}_{R^L\times N}\ \mathbf{I}_{R^L}]\tilde{\mathbb{X}}_{kq}^{L,n+1}$.

4 Other APs $l \in \mathcal{M}_k \setminus \{q\}$ copy their previous quantities, i.e., $\tilde{\mathbb{Q}}_{kl}^{L,n+1} = \tilde{\mathbb{Q}}_{kl}^{L,n}$ etc.

8.4.2 Convergence analysis

The proposed algorithm is a combination of the DACGEE algorithm proposed in [128] and PK-GEVD-DANSE in [212]. DACGEE assumes a fully-connected network, whereas the current algorithm uses in-network sums as a communication protocol, which reduces the communication overhead and

5 - Each AP $l \in \mathcal{M}_k$ computes channels estimates for $t = 1...T$

$$\begin{aligned} \mathbf{z}_{kl}^{t,B} &= \sqrt{\tau_p}\mathbb{Z}_{kl}^{B,n+1}\mathbb{X}_{kl}^{B,n+1^H}\mathbf{y}_{\tau_k l}^{t} \\ \mathbf{z}_{kl}^{t,L} &= \sqrt{\tau_p}\tilde{\mathbb{Z}}_{kl}^{L,n+1}\tilde{\mathbb{X}}_{kl}^{L,n+1^H}\tilde{\mathbf{y}}_{\tau_k}^{t} \\ \mathbf{h}_{kl}^{t} &= \mathbb{Q}_{kl}^{B,n+1}\mathbf{z}_{kl}^{t,B} + \dot{\mathbb{Q}}_{kl}^{n+1}\mathbf{z}_{kl}^{t,L}. \end{aligned} \tag{8.73}$$

- The network is used to construct $\alpha_k^t, \boldsymbol{\beta}_k^t, \boldsymbol{\Gamma}_k$ as in (8.64) - (8.66) for $t = 1...T$.
- Each AP $l \in \mathcal{M}_k$ compute the receive combiner $\mathbf{v}_{kl}^t$ as in (8.67) for $t = 1...T$.
- The receive combiners are then used to obtain estimates of the data transmitted by UE k during the UL data transmission phase as the in-network sum $\hat{s}_k = \sum_{l \in \mathcal{M}_k} \mathbf{v}_{kl}^{t^H} \mathbf{y}_l$.

6 $n \leftarrow n+1$, $q \leftarrow (q \mod L_k) + 1$ and return to step 2.

makes the algorithm topology-independent since any connected network can be transformed to a tree [163]. The following theorem can then be stated.

Theorem 8.4.1. *Assume that*

- *at a certain iteration $\bar{n}$ $\mathbf{R}_k^{B,\bar{n}}$ is kept fixed, i.e., the third bullet in step 3 of Algorithm 11 is not executed or results in the same solution,*
- $\mathbf{R}_{\tau_k}$, $\mathbf{R}_{all_k}$ *are invertible,*
- $\tilde{\mathbf{R}}_{\tau_k q}$, $\tilde{\mathbf{R}}_{all_k q}$ *are perfectly estimated using an infinite observation window in each iteration,*

the DUCERC algorithm converges for any initialization of its parameters to the solution provided in Subsection 8.3.3, i.e., when $n \to \infty$ and $\forall l \in \mathcal{M}_k$, $\mathbb{X}_{kl}^{L,n} = \mathbb{X}_{kl}^{L}$, $\mathbb{Q}_{kl}^{L,n} = \mathbb{Q}_{kl}^{L}$, $\mathbb{Z}_{kq}^{L,n} = \mathbb{Z}_{q}^{L}$ with $\mathbf{R}_k^B = \mathbf{R}_k^{B,\bar{n}}$. The corresponding CE and RC then also converge since DUCERC uses distributed versions of the expressions in Subsection 8.3.3.

Proof. See Appendix D.2. □

To prove convergence of DUCERC to the same solution as Algorithm 10, it should also be proven that for a fixed $\mathbf{R}_k^{L,\bar{n}}$, the DUCERC algorithm converges. However, as shown in [212], this will require compression of the local antenna signals to $2R^B$ channels and this for each $l \in \mathcal{M}_k$. Since R^B is typically $N/2$, this will not result in a communication cost reduction. Therefore, this is replaced

by the heuristic solution in the third bullet of step 3, which does not require any extra communication. Hence, convergence cannot be shown for this algorithm, but simulations will show that the algorithm still provides similar performance as the centralized solution.

8.4.3 Communication cost

The communicational cost of the DUCERC algorithm is determined by the following in-network sums:

- $R^L \tau_p$ signals received during the pilot phase of each coherence block,
- $R^L \times R^L$ parameters[8] per iteration to compute ξ_k^n for the user-centric GEVD,
- $(1 + R^L) \times (1 + R^L)$ parameters $(\alpha_k^t, \boldsymbol{\beta}_k^t, \boldsymbol{\Gamma}_k)$ for the RC in each coherence block.

Moreover, there is also a need for in-network sums of τ_u signals received during the UL data transmission phase of each coherence block. This should be compared to having to transmit all $NL_k\tau_p$ signals received during the pilot phase of each coherence block to a central processing unit in the network. This central central processing unit then computes all quantities as in Subsection 8.3.3, and transmits $\mathbf{v}_{kl}^t$ back to each AP for the RC phase. It is clear that when R^L is small (e.g., one or two), this results in a large communication cost reduction. Also the computations are done in the network using smaller input signals, so there is no need for a strong centralized processing unit.

Note that the communication cost is even more reduced for the channel models presented in Subsection 8.3.1 and 8.3.2. In the first case, $R^L = 0$, so the only necessary communication will be α_k^t during each coherence block. In the second case, χ_k^n, α_k^t, $\boldsymbol{\beta}_k^t$ will be zero, and $\boldsymbol{\Gamma}_k$ consists of quantities that are locally available, so only the $R^L \tau_p$ signals received during the pilot phase of each coherence block must be communicated.

[8]Note that these matrices are Hermitian symmetric, so it suffices to only compute the upper (or) lower triangular block via in-network sums, which will decrease the communication even further.

8.5 Distributed multi-user RC

The proposed DUCERC algorithm as discussed in Section 8.4, is operating separately for each UE k. Since an AP l is typically involved in multiple user-centric networks, i.e., one for each UE $\bar{k} \in \mathcal{D}_l$, it then obtains channels estimates for all $\bar{k} \in \mathcal{D}_l$. These channel estimates give an immediate estimation of the interference, as present in the expression of the receive combiner $\mathbf{w}_k^t$ in (8.18), while $\overline{\mathbf{R}}_{\bar{k}}^{\mathcal{M}_k}$ gives information on the interference averaged over all coherence blocks. The expression for (8.18) can be written using the quantities defined in Section 8.3. To this end, the following quantity is defined:

$$\mathbf{R}_{\bar{k}}^{\mathcal{M}_k} = \mathbf{E}_{\bar{k}}^{\mathcal{M}_k} \mathbf{R}_{\bar{k}} \mathbf{E}_{\bar{k}}^{\mathcal{M}_k{}^H} \tag{8.74}$$

which possibly contains zero-columns and rows if some APs that serve UE k are not observing UE $\bar{k}$. So the proposed procedure to estimate $\mathbf{R}_{\bar{k}}$ automatically results in an estimate for $\mathbf{R}_{\bar{k}}^{\mathcal{M}_k}$. The following quantities can be similarly defined:

$$\mathbf{Q}_{\bar{k}}^{\mathcal{M}_k,B} = \mathbf{E}_{\bar{k}}^{\mathcal{M}_k} \mathbf{Q}_{\bar{k}}^{B}, \mathbf{X}_{\bar{k}}^{\mathcal{M}_k,B} = \mathbf{E}_{\bar{k}}^{\mathcal{M}_k} \mathbf{X}_{\bar{k}}^{B}, \mathbb{Q}_{\bar{k}}^{\mathcal{M}_k,L} = \mathbf{E}_{\bar{k}}^{\mathcal{M}_k} \mathbb{Q}_{\bar{k}}^{L}, \dot{\mathbb{Q}}_{\bar{k}}^{\mathcal{M}_k} = \mathbf{E}_{\bar{k}}^{\mathcal{M}_k} \dot{\mathbb{Q}}_{\bar{k}}. \tag{8.75}$$

The user-centric receive combiner $\mathbf{w}_k^t$ can then be written as

$$\mathbf{w}_k^t \approx \underbrace{\left(\mathbf{R}_{all_k} - \sum_{\bar{k} \in \mathcal{P}_k} \left(\mathbb{Q}_{\bar{k}}^{\mathcal{M}_k,L} \mathbb{\Sigma}_{\bar{k}}^{L} \mathbb{Q}_{\bar{k}}^{\mathcal{M}_k,L^H} + \mathbf{Q}_{\bar{k}}^{\mathcal{M}_k,B} \mathbf{\Sigma}_{\bar{k}}^{B} \mathbf{Q}_{\bar{k}}^{\mathcal{M}_k,B^H} \right) \right)}_{\mathbf{M}_k} + \tag{8.76}$$

$$\sum_{\bar{k} \in \mathcal{P}_k} [\mathbf{Q}_{\bar{k}}^{\mathcal{M}_k,B} \mathbf{z}_{\bar{k}}^{t,B} \ \dot{\mathbb{Q}}_{\bar{k}}^{\mathcal{M}_k}] \begin{bmatrix} 1 & \mathbf{z}_{\bar{k}}^{t,L^H} \\ \mathbf{z}_{\bar{k}}^{t,L} & \mathbf{z}_{\bar{k}}^{t,L} \mathbf{z}_{\bar{k}}^{t,L^H} + \mathbb{\Psi}_{\bar{k}}^{L} \end{bmatrix} \begin{bmatrix} \mathbf{z}_{\bar{k}}^{t,B^H} \mathbf{Q}_{\bar{k}}^{\mathcal{M}_k,B^H} \\ \dot{\mathbb{Q}}_{\bar{k}}^{\mathcal{M}_k{}^H} \end{bmatrix} \Bigg)^{-1} [\mathbf{Q}_k^B \mathbf{z}_k^{t,B} \ \dot{\mathbb{Q}}_k] \begin{bmatrix} 1 \\ \mathbf{z}_k^{t,L} \end{bmatrix}$$

$$= \mathbf{M}_k^{-1} \mathbf{N}_k \left(\mathbf{I}_{K_k(1+R^L)} + \mathbf{S}_k \right)^{-1} \begin{bmatrix} \mathbf{0}_{(k-1)(1+R^L)} \\ 1 \\ \mathbf{z}_k^{t,L} \\ \mathbf{0}_{(K_k-k)(1+R^L)} \end{bmatrix}$$

with

$$\mathbf{S}_k = \underbrace{\begin{bmatrix} \mathbf{I}_{K_k} & \text{blkdiag}\{\mathbf{z}_1^{t,L}, ..., \mathbf{z}_{K_k}^{t,L}\}^H \\ \text{blkdiag}\{\mathbf{z}_1^{t,L}, ..., \mathbf{z}_{K_k}^{t,L}\} & \text{blkdiag}\{\mathbf{z}_1^{t,L} \mathbf{z}_1^{t,L^H} + \mathbb{\Psi}_1^{L}, ..., \mathbf{z}_{K_k}^{t,L} \mathbf{z}_{K_k}^{t,L^H} + \mathbb{\Psi}_{K_k}^{L}\} \end{bmatrix}}_{\mathbf{\Psi}_k} \mathbf{N}_k \mathbf{M}_k^{-1} \mathbf{N}_k. \tag{8.77}$$

Here it is again assumed that $\mathbf{M}_k$ is block diagonal with diagonal elements

$$\mathbf{M}_{kl} = \mathbf{R}_{all_k l} - \sum_{\bar{k} \in \mathcal{D}_l} \left(\mathbb{Q}_{\bar{k}l}^{\mathcal{M}_k, L} \mathbb{\Sigma}_{\bar{k}}^{L} \mathbb{Q}_{\bar{k}l}^{\mathcal{M}_k, L^H} + \mathbb{Q}_{\bar{k}l}^{\mathcal{M}_k, B} \mathbb{\Sigma}_{\bar{k}l}^{B} \mathbb{Q}_{\bar{k}l}^{\mathcal{M}_k, B^H} \right) \tag{8.78}$$

that can be computed locally at each AP, since it has access to all these quantities. The following quantity and its lth block row is also defined in (8.76):

$$\mathbf{N}_k = [\mathbb{Q}_1^{\mathcal{M}_k, B} \mathbf{z}_1^{t,B} \ ... \ \mathbb{Q}_{K_k}^{\mathcal{M}_k, B} \mathbf{z}_{K_k}^{t,B} \ \dot{\mathbb{Q}}_1^{\mathcal{M}_k} \ ... \ \dot{\mathbb{Q}}_{K_k}^{\mathcal{M}_k}] \tag{8.79}$$

$$[\mathbf{N}_k]_l = [\mathbb{Q}_{1l}^{B} \mathbf{z}_{1l}^{t,B} \ ... \ \mathbb{Q}_{K_k l}^{B} \mathbf{z}_{K_k l}^{t,B} \ \dot{\mathbb{Q}}_{1l} \ ... \ \dot{\mathbb{Q}}_{K_k l}] \tag{8.80}$$

where superscript ^{k} can be removed in $[\mathbf{N}_k]_l$ by setting $\dot{\mathbb{Q}}_{\bar{k}l}, \mathbb{Q}_{\bar{k}l}^{B} \mathbf{z}_{\bar{k}l}^{t,B}$ to zero if $\bar{k} \notin \mathcal{D}_l$.

Note that $\mathbf{S}_k \in \mathbb{C}^{K_k(1+R^L) \times K_k(1+R^L)}$ can then be computed using in-network sums as

$$\mathbf{S}_k = \sum_{l \in \mathcal{M}_k} \mathbf{\Psi}_k [\mathbf{N}_k]_l^H \mathbf{M}_{kl}^{-1} [\mathbf{N}_k]_l. \tag{8.81}$$

If an AP l has access to $\mathbf{S}_k$, it can compute the local version of the receive combiner $\mathbf{w}_{kl}^t$ as

$$\mathbf{w}_{kl}^t \approx \mathbf{M}_{kl}^{-1} [\mathbf{N}_k]_l \left(\mathbf{I}_{K_k(1+R^L)} + \mathbf{S}_k \right)^{-1} \begin{bmatrix} \mathbf{0}_{(k-1)(1+R^L)} \\ 1 \\ \mathbf{z}_k^{t,L} \\ \mathbf{0}_{(K_k-k)(1+R^L)} \end{bmatrix}. \tag{8.82}$$

This receive combiner can be easily included in Algorithm 11 by replacing the second bullet in step 5 with the computation of the in-network sum of $\mathbf{S}_k$ and the third bullet with computing $\mathbf{w}_{kl}^t$ using (8.82). This increases the communication cost by a factor K_k during RC. Intermediate receive combiners, where only a subset of the strongest interfering UE are included in $\mathcal{P}_k$ can similarly be derived and will decrease the communication cost. As a limit, i.e., when $\mathcal{P}_k = \{k\}$, the filter $\mathbf{v}_k^t$ will again be obtained.

8.6 Simulations

In this section, simulations for the centralized and distributed GEVD-based CE and RC are conducted to compare the effect of using different rank constraints and to investigate convergence properties. To this end, a scenario is simulated

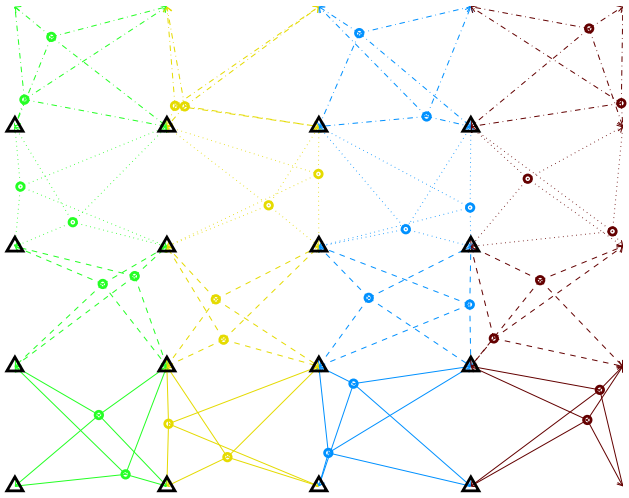

Figure 8.3: CFmMIMO setup with $L = 16$ and $K = 32$ and using the wrap-around technique

with $L = 16$ APs arranged in a square grid of 300m. The wrap-around technique is used to simulate an infinite network. Two UEs are randomly positioned in each square, such that $K = 32$. $\mathcal{M}_k$ is given by the four surrounding APs as indicated in Figure 8.3 ($L_k = 4$). The transmit power is set to 100mW and τ_p is set to 4. All provided results are averaged over 20 Monte Carlo realizations. The large-scale fading coefficient $\bar{\mathbf{G}}_k$ as defined in Subsection 8.2.1, is simulated as a block diagonal matrix with $\bar{\mathbf{G}}_{kl}$ modeled as given in [7, Section 2.6]. The LoS component $\bar{\mathbf{h}}_k$ is modeled as in [7, Section 1.3], normalized such that $||\bar{\mathbf{h}}_{kl}||^2 = \text{tr}\{\bar{\mathbf{G}}_{kl}\}$. The channels are then generated as

$$\mathbf{h}_k^t = \sqrt{1-\beta}\bar{\mathbf{h}}_k e^{j\varphi_k^t} + \sqrt{\beta}\mathbf{g}_k^t \tag{8.83}$$

where β is a control parameter and is chosen such that $\text{tr}\{\bar{\mathbf{R}}_k\}$ is independent of β. Here $\beta = 0$ models only a LoS component, $\beta = 1$ models only a NLoS component, and $0 < \beta < 1$ models a combination of both components.

The performance measure used is a standard capacity lower bound [7] referred to as the achievable spectral efficiency (SE) and is given by

$$\mathrm{SE}_k = \frac{\tau_u}{\tau_p + \tau_u} E\{\log_2\left(1 + \mathrm{SINR}_k^t\right)\} \text{ with} \tag{8.84}$$

$$\mathrm{SINR}_k^t = \frac{|\mathbf{v}_k^{t\,H} \widehat{\overline{\mathbf{h}}}_k^t|^2}{\sum_{\bar{k} \in \overline{\mathcal{P}}_k} |\mathbf{v}_k^{t\,H} \widehat{\overline{\mathbf{h}}}_{\bar{k}}^{\mathcal{M}_k t}|^2 + \mathbf{v}_k^{t\,H}\Big(\sum_{\bar{k} \in \mathcal{P}_k} \overline{\mathbf{C}}_{\bar{k}}^{\mathcal{M}_k} + \overline{\mathbf{R}}_{\mathbf{nn}}^{\mathcal{M}_k}\Big)\mathbf{v}_k^t}$$

where the channel estimates are given by the optimal MMSE-based channel estimates. Note that the MMSE-based receive combiner $\bar{\mathbf{w}}_k^t$ maximizes SINR_k^t.

Finally the LS method is shown as reference, which uses the channel estimate $\frac{1}{\sqrt{\tau_p}}\mathbf{y}_{\tau_k}^t$ and uses MR combining for the RC.

8.6.1 Results for centralized GEVD-based CE and RC

The CE performance depends on the estimation of $\mathbf{R}_{\tau_k}$ and $\mathbf{R}_{all_k}$ using the signals obtained during the pilot phase. MMSE-based CE assumes perfect knowledge of these matrices, including perfect knowledge of $\mathbf{R}_k$. The matrices are better estimated whenever the number of coherence blocks T increases and the RC will also improve with better channel estimates. Therefore, the sum-SE for 2 cases, i.e., $T = 10000$ and $T = 500$, is provided in Figure 8.4 for different values of β and for different combinations of $\{R^B, R^L\}$.

For $T = 1000$, it is observed that estimating $\mathbf{w}_k$ by using a rank $\{N, 1\}$ GEVD achieves the best performance and that its performance is close to the performance of the MMSE-based receive combiner $\overline{\mathbf{w}}_k$. Similarly, estimating $\mathbf{v}_k$ by using a rank $\{N, 1\}$ GEVD also achieves a performance very close to the performance of the MMSE-based receive combiner $\bar{\mathbf{v}}_k$. This shows that approximating $\mathbf{R}_{\tau_k} - \tau_p \mathbb{Q}_k^L \mathbb{\Sigma}_k^L \mathbb{Q}_k^{L\,H}$, $\mathbf{B}_k$ and $\mathbf{M}_k$ as block diagonal matrices is valid with the used channel estimates. Rank approximations with $R^B = 0$ work best for small β and increasing R^L gives better performance since $\mathbf{R}_k$ can be better approximated. Rank approximation with $R^L = 0$ is also performing well, but including R^L has clearly some benefits for channels with a LoS component. Using $R^B = N/2$ instead of N only reduces the performance slightly. This is because most of the generalized eigenvalues in $\mathbb{\Sigma}_k^B$ are close to zero (or negative and thereby set to zero using $[\cdot]_0$), so setting R^B to $N/2$ gives good results and saves some complexity in the computation of the GEVD.

For $T = 500$, similar observations can be made. The only exception is that the performance of estimating $\mathbf{w}_k$ by using a rank $\{N/2, 1\}$ GEVD has dropped drastically. This can be explained by the fact that some channels with low

SINR are poorly estimated, but their channel estimates are still included in $\mathbf{w}_k$. Therefore, when working with smaller values for T, it is advised to use the receive combiner $\mathbf{v}_k$, which has also a lower communication cost in DUCERC.

8.6.2 Results for rank $\{R^B, R^L\}$ GEVD-based DUCERC

In this section, the convergence of rank $\{R^B, R^L\}$ GEVD-based DUCERC is investigated and compared to the centralized performance. The results for different iterations of DUCERC are provided in Figure 8.5 and this for both the sum-SE as well as for the MSE-difference between the centralized and the distributed solution. T and β are set to 10000 and 0.5 respectively.

Looking at the achieved performance, it is observed that the DUCERC algorithm converges to a value similar to that of the centralized algorithm, and this already after 20 iterations. However, from the convergence figure, it is clear that there is only convergence to the machine precision when $R^B = 0$. When $R^B \neq 0$ this is no longer the case (as pointed out in Subsection 8.4.2), but the distributed filters are still achieving similar performance.

8.7 Conclusion

In this paper, a novel channel covariance estimator has been presented for user-centric CFmMIMO channels satisfying a general Rician fading model, i.e., with both LoS and NLoS components. The LoS component introduces correlation between the channels at different APs that can be exploited to improve the CE and in a later stage the RC. The proposed methods perform CE using GEVDs of two covariances that are estimated from the available UL data. The transmitted signals can then be obtained by processing the local antenna signals, together with R^L compressed versions of all the antenna signals of all the APs serving the UE. To make the proposed method scalable, the DUCERC algorithm has been presented, which reduces the required communications between the APs to a minimum and relies on in-network sums that can be accomplished whenever the APs can be arranged into a tree-topology. All the computations are then distributed over the different APs. Simulations have shown that the performance of the proposed GEVD-based centralized and distributed CE and RC is close to the performance of optimal MMSE-based CE and RC with perfect CSI.

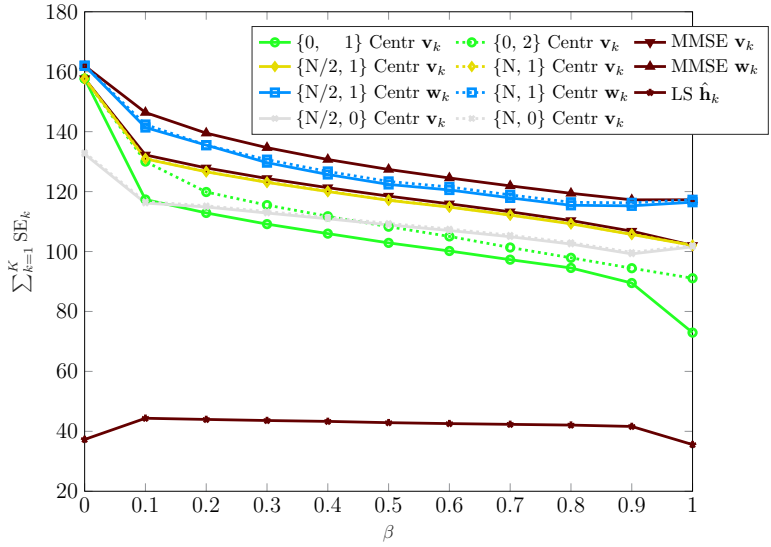

(a) $T = 10000$

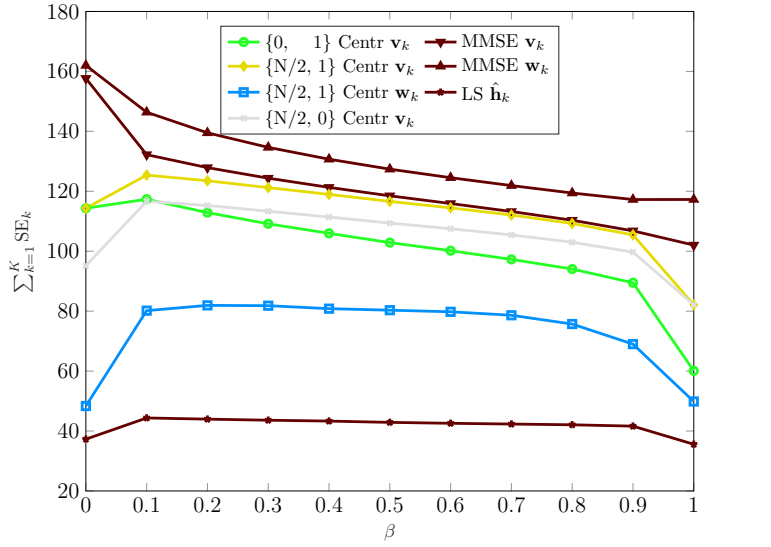

(b) $T = 500$

Figure 8.4: Performance of proposed centralized rank $\{R^B, R^L\}$ GEVD-based RC and CE.

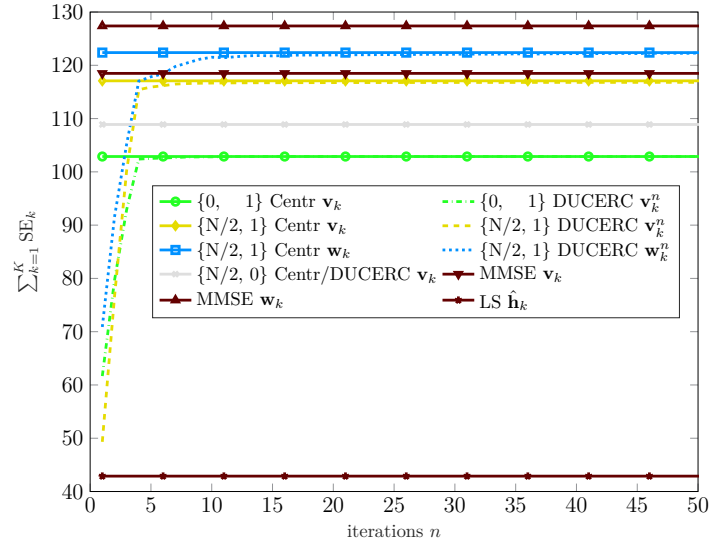

(a) Performance

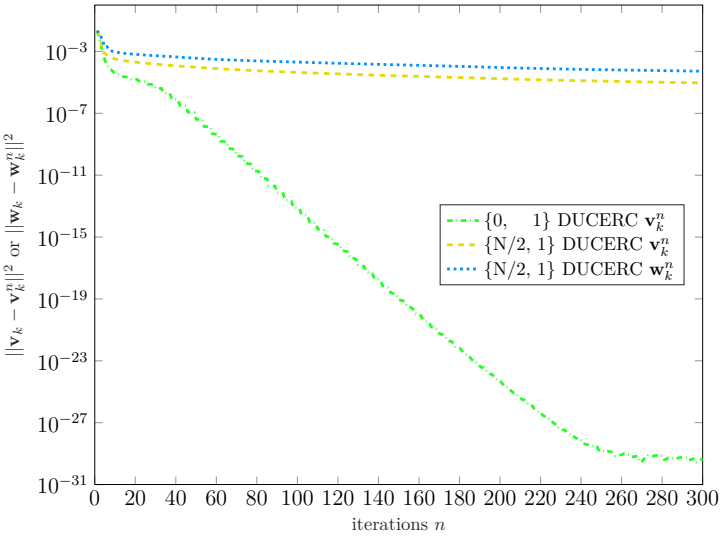

(b) Convergence

Figure 8.5: Performance and convergence of rank $\{R^B, R^L\}$ DUCERC for $T = 10000$ and $\beta = 0.5$.

Chapter 9

Conclusion

9.1 Summary and conclusions

This thesis has presented novel distributed algorithms for wired and wireless sensor and actuator networks (SANs), by exploiting the multi-applicability of the multi-channel Wiener filter (MWF) to different digital signal processing (DSP) tasks as elaborated in Chapter 2 (speech enhancement, sound zoning, channel estimation and receive combining). In the developed algorithms, nodes apply local linear compressions to their signals and/or parameters, resulting in two important benefits. Firstly, this strongly reduces the communication cost and the reduction is larger whenever a node consist of more local sensors. Secondly, due to these compressions, nodes have only access to reduced-dimensional input signals/parameters, reducing the local complexity requirements. Nonetheless, the distributed algorithms are designed to obtain similar estimation performance as when all the input signals/parameters are available at a fusion center (FC) or at each node. Furthermore, the presented algorithms are designed to work for topology-independent (tree-based) SANs, making them applicable to every connected SAN. The exception is the PK-GEVD-DANSE algorithm, which is explained in Chapter 3 using a fully-connected topology, although Subsection 3.4.4 showed how the algorithm can be adapted to work in a tree-like topology.

In the remainder of this chapter, the main contributions of this thesis will be highlighted. Most of the contributions are related to the novel distributed algorithms, although some distributed algorithms started from novel centralized DSP methods, which are also discussed.

Improved signal enhancement by including partial prior knowledge on the desired source subspace

The GEVD-MWF is currently seen as one of the best blind, data-dependent MWF for signal enhancement. It is able to estimate the desired source subspace using a GEVD of estimated correlation matrices. However, often not enough samples are available to estimate the necessary correlation matrices or VAD errors cause biased estimates, resulting in poor performance. Chapter 3 has therefore presented a novel centralized PK-GEVD-MWF, where partial prior knowledge of the desired sources steering matrix has been included in the signal subspace estimation. The prior knowledge can, for instance, be available in an acoustic scenario if nodes have prior knowledge on the location of the desired sources and on their local microphone array geometry, or when they have access to clean noise references. The combination of multiple nodes with local partial prior knowledge has never been investigated before. Chapter 3 has shown that including prior knowledge to the GEVD-MWF results in the centralized PK-GEVD-MWF, consisting of a cascade of three different blocks. The first block corresponds to a centralized LCMV-beamformer, that used local noise references (available as a result of the prior knowledge) to cancel the noise in the desired source direction. The second block corresponds to a GEVD-MWF working on reduced dimensional inputs. The final block is a selection and scaling block, to produce the node-specific desired signals. Simulations demonstrated the benefits of including prior knowledge, even in situations with estimation errors in the correlation matrices.

Distributed signal and parameter estimation for WASANs

Part I of the thesis, consisting of Chapters 3-5, has developed distributed algorithms for WASANs, where the per-node processing steps are defined, together with the compression rules for the signals/parameters that needed to be broadcast. In particular, Part I of this thesis offered the following distributed algorithms for WASANs.

Chapter 3 dealt with a WSN in which nodes are required to estimate a node-specific desired signal, defined w.l.o.g. as the desired source component in some reference sensors, from noisy sensor signals observations in a distributed way. It was explained in a WSN setup, but part of the simulations were done in a WASN. The centralized solution used a PK-GEVD-MWF, including the prior knowledge available at all the nodes. The resulting PK-GEVD-DANSE algorithm showed that the same filter can still be obtained by allowing the nodes to broadcast twice the number of compressed signals compared to the

original GEVD-DANSE algorithm, where the number of broadcast signals is equal to the dimension of the implied low-rank structure during the GEVD. This was because, together with a compression using the local PK-GEVD-MWF filter, also a compression of the local noise references was necessary to provide a converging algorithm. It has been shown via simulations that the PK-GEVD-DANSE algorithm converges to the centralized PK-GEVD-MWF as if each node would have access to all the sensor signals and prior knowledge in the network. Convergence was faster than convergence of GEVD-DANSE with the same rank, since more degrees of freedom are available with PK-GEVD-DANSE (twice the number as GEVD-DANSE). Batch- and block-mode simulations have demonstrated the improved performance of PK-GEVD-DANSE compared to GEVD-DANSE in terms of oSNR and oSER for a simulated WASN.

Chapter 4 considered estimating the node-specific sound zoning filter for ACC-based sound zoning in a WASAN in a distributed way. It was presented in a setup where each node consists of one loudspeaker and multiple local error microphones and each node was able to decide which of their error microphones belonged to the bright zone (high desired signal power) and the dark zone (low desired signal power). To obtain this, a network-wide objective involving the acoustic coupling between all the loudspeakers and microphones in the WASAN was proposed where the optimal solution was based on a centralized GEVD. However, this required that each node transmitted two high-dimensional matrices to an FC (or all the other nodes). The DAG-ACC algorithm was then proposed to allow for a fully distributed implementation. In-network summations of high-dimensional vectors (no longer matrices) were still required, but the local processing capabilities of each node were strongly simplified, i.e., they were no longer required to compute a GEVD. Also local storage requirements were strongly reduced, if two extra in-network summations were computed. The proposed DAG-ACC algorithm outperformed the non-cooperative distributed solution after only a few iterations and converged to the centralized solution, as was illustrated by computer simulations.

The distributed algorithm, presented in Chapter 5, estimated PM-based sound zoning filters for multiple desired input signals. It was presented in a setup where the nodes consist of only loudspeaker (arrays) with local power constraints and where the nodes have access to the error microphones gathered over the area using wireless links. While the centralized sound zoning solution required gathering all impulse responses in the WASAN at each node/in a FC and solving a large QCQP with many constraints, this was no longer the case for the presented DA-PM algorithm. The DA-PM algorithm required no exchange of (compressed) signals/parameters between different nodes, and it is the only distributed algorithms with this convenient property in this thesis. Cooperation was still possible, by letting the nodes solve a modified local version of the

QCQP including information that could be estimated based on the received error microphone signals. The modified local QCQP differed from the stand-alone QCQP problem, where only the local impulse responses were taken into account. It was shown both theoretically and via simulations that the DA-PM algorithm converged to the centralized solution, and that it outperformed the stand-alone solution after two iterations.

Novel channel covariance estimation technique based on a randomized pilot assignment for (CF)mMIMO systems

A novel channel covariance estimation procedure for mMIMO systems has been presented, explained for cellular mMIMO systems in Appendix E and for CFmMIMO systems in Chapter 8. Compared to state-of-the-art methods where useful data samples are sacrificed to obtain clean channel estimates, the novel procedure was able to estimate the channel covariance without sacrificing data samples. This was done by letting each UE pick a random pilot in each coherence block, instead of letting the UEs use the same pilot in each coherence block. This allowed the APs to distinguish between two correlation matrices: one before and one after despreading. The difference ideally gave a scaled estimate of the channel covariance matrix. Performing the subtraction based on a low-rank GEVD-based matrix approximation problem provided better estimation performance as shown in Appendix E. It revealed that the best approximation was obtained if only 30% of the generalized eigenvalues were considered. In Chapter 8, this procedure was generalized to channel covariance matrices for Rician fading channels, resulting in an alternating optimization procedure, switching between GEVD-based and PK-GEVD-based approximations.

Distributed channel and signal estimation for CFmMIMO systems

Part II of the thesis, consisting of Chapters 6-8, developed distributed algorithm for channel estimation and signal estimation (a.k.a. receive combining) for CFmMIMO systems. The presented per-AP processing tasks and fusion rules depended on the considered channel fading model. Also different setups with either a central NC or fully in-network processing with master APs were investigated. In particular, Part II of this thesis offered the following distributed algorithms for CFmMIMO systems.

Chapters 6 and 7 considered channel estimation and uplink receive combining for CFmMIMO systems with a NC for final decoding decisions and considered

the commonly used Rayleigh fading channel model. The channels between different APs were then assumed to be independent, such that MMSE-based channel estimation could be performed locally at each AP, without requiring inter-AP communications. The channel covariance matrix was assumed to be known a priori, but the method proposed in Appendix E could also be used here. Distributed receive combining, on the other hand, required cooperation between the APs, defined by the N-DRC algorithm. Instead of broadcasting all the channel estimates in each coherence block, the N-DRC algorithm proposed to compress the local antenna signals to a signal with K channels, were K denoted the number of considered UEs, and compute some compressed channel related parameters. These compressions could then be transmitted to the NC using efficient in-network summations to strongly lower the communication cost, compared to having to transmit all antenna signals to the NC and process them. Using the matrix-inversion-lemma, it was then shown that the NC could obtain optimal MMSE-based signal estimates for all the considered UEs by using the received compressed antenna signals and parameters.

Chapter 8 dealt with channel estimation and uplink receive combining for user-centric CFmMIMO systems with master APs and considered the general Rician fading channel model. Rayleigh fading can be considered as a special case of Rician fading without a LoS component, so this was also covered in this chapter. The LoS component introduced correlation between the channels at different AP and it was shown that at least R^L compressed versions of the received antenna signals during the pilot phase are necessary to obtain (approximately) optimal channel estimates (R^L denotes the assumed rank of the LoS component of a UE in the channel covariance matrix). The DUCERC algorithm was then presented to reduce the necessary communications between the APs during the channel estimation phase to a minimum, again relying on R^L efficient in-network summations that are performed in local UE-specific networks. Distributed receive combiners, necessary to compress the uplink data efficiently, were also defined in the DUCERC and required exchanging some compressed parameters, again using efficient in-network summations. The receive combiners could then be computed locally at each AP. Numerical simulations in a user-centric CFmMIMO system showed that the performance of the proposed DUCERC algorithm is close to the estimation performance provided by optimal MMSE-based processing.

Framework for distributed power allocation and downlink transmit precoding

Optimal MMSE-based power allocation and transmit precoding in its original form could only be performed at the NC if all antenna signals and channel

estimation parameters are transmitted to it, which implied a large fronthaul communication overhead. Otherwise, heuristic transmit precoding schemes had to be used at the APs, strongly reducing the fronthaul communication overhead, but optimal performance could no longer be guaranteed. Therefore, Chapter 7 presented the MMSE-based D-UL-RCPA and D-DL-TPPA algorithms that did not require the large communication cost and yet attained this optimal performance. They proposed a distributed alternating optimization framework where local combining/precoding vectors were computed only at the APs and compressed parameters related to the necessary large-scale channel statistics of the system were transmitted to the NC. The NC was then responsible for determining the optimal power allocations parameters (for UL or DL) based on a general utility, e.g., non-weighted max-sum and max-min SE. Simulations showed that the proposed algorithms outperform heuristic power allocation methods, both in UL and DL.

Performance analysis of scalable user-centric CFmMIMO systems

Scalability of the proposed distributed algorithm was an important challenge, especially for CFmMIMO systems, where the number of UEs grows with the network size. Therefore, scalable versions of the distributed algorithms were also proposed and analyzed in the second part of the thesis.

In Chapter 6, it was shown that the SN-DRC and the SP-DRC algorithms were valid alternatives for the none scalable N-DRC. The drop in performance was minimal for SN-DRC, while the number of serving UEs at an AP was strongly reduced. The computations in the SP-DRC algorithm were even independent of the total number of UEs in the network, albeit at the cost of a significant performance loss compared to N-DRC and SN-DRC. Chapter 7 performed simulations with both non-scalable and scalable versions of the D-UL-RCPA and D-DL-TPPA algorithms. Both versions of the algorithms performed well when max-sum SE was used as utility. However, for non-weighted max-min SE, it was shown that it remains important to estimate the channel of many UEs at each AP, since not including UEs with a rather significant channel strength has a large impact on the minimal SE. Chapter 8 started from user-centric processing with data-aggregation in a user-specific master AP, so scalability was directly included in the presented problem statement.

Distributed tracking of environmental changes or changes in signal characteristics

All the presented algorithms were updating local filter coefficients and local compression rules iteratively over time, each time based on newly estimated correlation matrices or impulse responses. Although this is not directly incorporated in the distributed algorithms in Chapter 6 and 7, this can still be included in the channel estimation step, supposing that the channel covariance matrix is also re-estimated in each iteration when the UEs are mobile. This makes all the presented distributed algorithms adaptive over time, allowing them to track small environmental changes like movements of desired sources, temperature changes, ... It should be stressed that centralized processing can track the changes over time faster, since the distributed algorithms required multiple iterations to converge to the optimal centralized solution, and will hence experience a slower tracking speed.

9.2 Suggestions for future research

In addition to the difficult issues that have already been tackled in this thesis, additional research is suggested to examine the following design issues.

Firstly some suggestions for further research were already given throughout the main text. In Chapter 3 it is suggested to find efficient centralized and distributed algorithms for scenarios where the prior knowledge is not accurate but can be introduced as a soft constraint. Authors in [13] proposed a framework where the final filter is a convex combination between a solely data-based GEVD-MWF and a prior knowledge based PK-GEVD-MWF where the weights are determined based on the reliability of the prior knowledge. The same principle can be applied to obtain the filter in a distributed way by using a convex combination of the filters obtained with GEVD-DANSE and PK-GEVD-DANSE. However, this will require broadcast signals for both GEVD-DANSE and PK-GEVD-DANSE, which might become too large, so further research is required. In Chapters 4 and 5, the tracking performance of the distributed sound zoning filter should be empirically investigated when the impulse responses are changing quickly, possibly requiring novel impulse response estimation techniques, related to the channel covariance estimation techniques using random training sequences of Appendix E and Chapter 8. Finally Appendix E suggested a more thorough investigation of the required low-rank in the GEVD step, based on measured channels.

Chapter 8 investigated uplink channel estimation and receive combining for user-centric CFmMIMO systems with master APs and for Rician fading channels. However, the obtained channel estimates could also serve to perform (optimal) downlink transmit precoding, combined with determining (optimal) power allocation strategies. When all the APs that are causing a non-negligible interference at the antenna of a UE are included in the local user-centric network of that UE, uplink-downlink duality [191] can again be invoked and the virtual uplink network will be the same as the considered uplink system with a different noise correlation matrix. The power allocation problem can then be solved in an efficient distributed way using only communications between neighboring master-APs, by relying on well known diffusion [79–82], distributed alternating direction method of multipliers (ADMM) [213–215] or primal-dual method of multipliers (PDMM) [216] based strategies. The correlation between the channels at different APs might require a similar communication strategy as used in the local uplink networks for channel estimation and receive combining, albeit that the noise correlation matrix is determined by the power allocation algorithm, so different compressed training signals might need to be exchanged. Furthermore, the use of local user-centric networks fits in the concept of 'different interest' DSP, where the desired sources between the local networks are different. However, the construction of these local networks in an efficient way is still an open problem, since it depends on the observed SNR, available bandwidth, computational power at the node and the available links. There should be a trade-off between these constraints and some kind of utility measure quantifying the performance gain when a node is added to the local network.

Sampling rate offsets (SROs) due to variations in temperature, crystal imperfections, etc. are causing differences in the actual frequencies of the oscillators driving the analog-digital converters of the distributed nodes despite their equal nominal frequencies. However, the algorithms developed in this thesis assumed that the sampling rates between the nodes are synchronized to perform coherent signal processing, so SROs will lead to significant performance degradations in the developed algorithms. In wired SANs, the network might have an absolute time (phase) reference, but the fronthaul network cannot provide a sufficiently accurate common time and frequency reference. Therefore, AP synchronization and TDD reciprocity calibration are two critical problems to enable CFmMIMO. There exist methods that deal with these synchronization issues, e.g., based on Over-the-Air signaling [217], AirSync [218] or high-precision Global Position System (GPS) [219], but perfect timing synchronization remains almost impossible over large networks, even with almost perfectly synchronized clocks. In wired SANs, the problem is also persistent due to the large variety in different hardware devices, requiring efficient methods that can detect and compensate such SROs in a blind framework (as in [220–225]). It is therefore important to investigate and theoretically analyze similar methods and find

efficient ways to integrate them in existing distributed algorithms.

Apart from the considered signal and parameter estimation problems, a SAN can also be used to implement machine learning algorithms for other applications [226,227]. The federated learning idea can allow distributed devices to work together to learn complex models while maintaining control over privacy and local training data. The data transmitted by the nodes through the wireless/wired network include suggestions for local model updates (i.e., the model's weights), which are either aggregated or distributed to all the nodes, to perform a network-wide model update.

To end, there are still a lot of open challenges to wired and wireless SANs that are not tackled in this thesis. Data privacy is an import one, in case the nodes do not wish to share their (compressed) signals/parameters. Encryption-based methods can be applied to the exchange signals [228, 229]. However, these methods strongly increase the per-node computational complexity and might make the solution suboptimal. Therefore, this issue should already be taken into account when designing the compression rules. Also ways to make the distributed algorithm robust to communication channel effects (noise and quantization errors) [130, 230], should be investigated, since this might again require different compression rules. Another challenge is that the topology of a SAN might change in between iterations, e.g., because of mobility of the nodes, communication link failures, or malfunction of nodes. The uplink N-DRC (and variant) of Chapter 6 is already robust to failures of certain APs/links, since it computes the optimal solution even if the data of an AP is not included in the networks summations. However, this is only possible since the channels between the APs are assumed to be uncorrelated. Distributed algorithms that allows the nodes to reconverge quickly to the new centralized solution are more desirable and should be investigated in future research.

Part III

Appendices

Appendix A

GEVD-based speech and noise correlation matrix estimation for MWF-based noise reduction

GEVD Based Speech and Noise Correlation Matrix Estimation for Multichannel Wiener Filter Based Noise Reduction.

Robbe Van Rompaey and Marc Moonen

Published in
Proceedings of the *2018 26th European Signal Processing Conference (EUSIPCO)*, Rome, Italy, 2018, pp. 2544-2548.

©2018 IEEE Reprint, with permission from:
R. Van Rompaey and M. Moonen, "GEVD Based Speech and Noise Correlation Matrix Estimation for Multichannel Wiener Filter Based Noise Reduction" in *2018 26th European Signal Processing Conference (EUSIPCO)*, Rome, Italy, pp. 2544-2548, 2018.
Changes include layout, mathematical notation, representation and minor editing aspects.
The candidate's contributions as first author include all performed research and writing of the article under guidance of the co-author.

Abstract

In a single speech source noise reduction scenario, the frequency domain correlation matrix of the speech signal is often assumed to be a rank-1 matrix. In multichannel Wiener filter (MWF) based noise reduction, this assumption may be used to define an optimization criterion to estimate the positive definite speech correlation matrix together with the noise correlation matrix, from sample 'speech+noise' and 'noise-only' correlation matrices. The estimated correlation matrices then define the MWF. In generalized eigenvalue decomposition (GEVD) based MWF, this optimization criterion involves a prewhitening with the sample 'noise-only' correlation matrix, which in particular leads to a compact expression for the MWF. However, a more accurate form would include a prewhitening with the estimated noise correlation matrix instead of with the sample 'noise-only' correlation matrix. Unfortunately this leads to a more difficult optimization problem, where the prewhitening indeed involves one of the optimization variables. In this paper, it is demonstrated that the modified optimization criterion, remarkably, leads to only minor modifications in the estimated correlation matrices and eventually the same MWF, which justifies the use of the original optimization criterion as a simpler substitute.

Keywords Noise reduction, speech enhancement, Wiener filter, multichannel Wiener filter (MWF), generalized eigenvalue decomposition (GEVD).

A.1 Introduction

Multichannel noise reduction is an important speech processing task in cell phones, hearing instruments and speech recognition systems. To suppress the environmental noise while minimizing speech distortion, a crucial operation is the estimation of a valid frequency domain speech correlation matrix and noise correlation matrix. The estimated correlation matrices then define the multichannel Wiener filter (MWF).

The speech and noise correlation matrices are assumed to agree with the considered scenario, i.e., in a scenario with S speech sources, the speech correlation matrix is assumed to be a positive definite rank S matrix. In this paper, we consider a single speech source scenario ($S = 1$). In multichannel Wiener filter (MWF) based noise reduction, this assumption may then be used to define an optimization criterion to estimate the rank-1 speech correlation matrix together with the noise correlation matrix, from sample 'speech+noise' and 'noise-only' correlation matrices [110]. In generalized eigenvalue decomposition (GEVD) based MWF, this optimization criterion involves a prewhitening with the sample 'noise-only' correlation matrix, which in particular leads to a compact expression for the MWF. However, a more accurate form would include a prewhitening with the estimated noise correlation matrix instead of with the sample 'noise-only' correlation matrix. Unfortunately this leads to a more difficult optimization problem, where the prewhitening indeed involves one of the optimization variables.

In this paper, it is demonstrated that the modified optimization criterion leads to only minor modifications in the estimated correlation matrices and eventually the same MWF, which justifies the use of the original optimization criterion as a simpler substitute. The conclusions from the experiments in [110] are by consequence also valid when the modified optimization criterion is adopted.

The remainder of this paper is organized as follows. In Section A.2 the MWF is reviewed and the need for a proper estimation of the rank-1 speech and noise correlation matrix is discussed. Also some common optimization criteria to estimate the speech correlation matrix together with the noise correlation matrices, from sample 'speech+noise' and 'noise-only' correlation matrices, are presented. In Section A.3 the modified optimization criterion is presented together with a derivation of its optimal solution.

A.2 Problem statement

A.2.1 MWF based noise reduction

Let N denote the number of observed microphone signals. Frequency domain processing is considered where the N complex microphone signals of a frequency bin (bin index omitted for brevity) are stacked in a vector $\mathbf{x}$, and consist of a single speech source component $\mathbf{x}_s$ and additive noise component $\mathbf{x}_n$:

$$\mathbf{x} = \mathbf{x}_s + \mathbf{x}_n. \tag{A.1}$$

If the speech and noise signals are assumed to be uncorrelated then the correlation matrices

$$\mathbf{R}_{\mathbf{x}_{r_1}} = E\{\mathbf{x}\mathbf{x}^H\} \quad \mathbf{R}_{\mathbf{s}_{r_1}} = E\{\mathbf{x}_s\mathbf{x}_s^H\} \quad \mathbf{R}_{\mathbf{n}_{r_1}} = E\{\mathbf{x}_n\mathbf{x}_n^H\} \tag{A.2}$$

can be related by

$$\mathbf{R}_{\mathbf{x}_{r_1}} = \mathbf{R}_{\mathbf{s}_{r_1}} + \mathbf{R}_{\mathbf{n}_{r_1}} \tag{A.3}$$

where $E\{.\}$ is the expected value operator. Here $\mathbf{R}_{\mathbf{s}_{r_1}}$ is a rank-1 matrix for a single speech source scenario.

The MWF is a linear filter estimating a specific desired signal based on the observed signals $\mathbf{x}$. The desired signal can be arbitrarily chosen to be the (unknown) speech component of the first microphone signal $\mathbf{e}_1^H\mathbf{x}_\mathbf{s}$, where $\mathbf{e}_1$ denotes the first unity vector. The MWF minimizes the Mean Squared Error (MSE) criterion:

$$J_{MWF}(\mathbf{w}) = E\{|\mathbf{w}^H\mathbf{x} - \mathbf{e}_1^H\mathbf{x}_\mathbf{s}|^2\}. \tag{A.4}$$

where ^{H} denotes the Hermitian transpose.

The optimal solution is given by

$$\mathbf{w}_{MWF} = (\mathbf{R}_{\mathbf{s}_{r_1}} + \mathbf{R}_{\mathbf{n}_{r_1}})^{-1}\mathbf{R}_{\mathbf{s}_{r_1}}\mathbf{e}_1. \tag{A.5}$$

The correlation matrices $\mathbf{R}_{\mathbf{x}_{r_1}}$ and $\mathbf{R}_{\mathbf{n}_{r_1}}$ are first estimated by (recursive) time-averaging during 'noise+speech' periods and 'noise only' periods respectively, where the distinction is based on a speech activity detection, assuming that the noise and speech are (spatially) stationary. This results in the sample 'speech+noise' matrix $\mathbf{R}_\mathbf{x}$ and the sample 'noise-only' correlation matrix $\mathbf{R}_\mathbf{n}$. $\mathbf{R}_{\mathbf{s}_{r_1}}$ may then be estimated (based on (A.3)) as the difference between the sample 'speech+noise' correlation matrix $\mathbf{R}_\mathbf{x}$ and the sample 'noise-only' correlation matrix $\mathbf{R}_\mathbf{n}$, i.e.,

$$\mathbf{R}_\mathbf{s} = \mathbf{R}_\mathbf{x} - \mathbf{R}_\mathbf{n}. \tag{A.6}$$

However, $\mathbf{R_s}$ has mostly a rank larger than one, especially in low SNR scenarios, such that better correlation matrix estimation methods are necessary. In [110], the estimation of a positive definite rank-1 speech correlation matrix $\mathbf{R}_{\mathbf{s}_{r_1}}$ and a corresponding noise correlation matrix $\mathbf{R}_{\mathbf{n}_{r_1}}$ is presented based on two different optimization criteria depending on the sample 'speech+noise' correlation matrix $\mathbf{R_x}$ and the sample 'noise-only' correlation matrices $\mathbf{R_n}$. These are explained in the next sections.

A.2.2 EVD based speech and noise correlation matrix estimation

A first optimization criterion defined in [110] is used to estimate the correlation matrices as

$$\min_{\mathbf{R}_{\mathbf{n}_{r_1}},\text{rank}(\mathbf{R}_{\mathbf{s}_{r_1}})=1} \alpha \parallel \mathbf{R_x} - (\mathbf{R}_{\mathbf{n}_{r_1}} + \mathbf{R}_{\mathbf{s}_{r_1}}) \parallel_F^2 + (1-\alpha) \parallel \mathbf{R_n} - \mathbf{R}_{\mathbf{n}_{r_1}} \parallel_F^2 \tag{A.7}$$

where α is a constant ($0 \leq \alpha \leq 1$) assigning a weight to the different approximations and $\| \cdot \|_F$ denotes the Frobenius norm. The solution to this problem is based on the symmetric eigenvalue decomposition [111] of $\mathbf{R_x} - \mathbf{R_n} = \mathbf{K}\mathbf{D}\mathbf{K}^H$ with the eigenvalues sorted from high to low in $\mathbf{D}$ and is given by

$$\mathbf{R}_{\mathbf{s}_{r_1}} = \mathbf{K}\text{diag}\{D_1, 0, ..., 0\}\mathbf{K}^H \tag{A.8}$$

$$\mathbf{R}_{\mathbf{n}_{r_1}} = \alpha(\mathbf{R_x} - \mathbf{R}_{\mathbf{s}_{r_1}}) + (1-\alpha)\mathbf{R_n}. \tag{A.9}$$

A.2.3 GEVD-based speech and noise correlation matrix estimation

In the optimization criterion in (A.7), an unweighted Frobenius norm with absolute (squared) approximation errors is used. As suggested in [110], it can be more appropriate to consider relative approximation errors depending on the noise. To this end a noise prewhitening operation is included depending on the GEVD of the matrix pencil $\{\mathbf{R_x}, \mathbf{R_n}\}$ [104, 148]:

$$\begin{aligned} \mathbf{R_n} &= \mathbf{Q}\mathbf{\Sigma}_n\mathbf{Q}^H \\ \mathbf{R_x} &= \mathbf{Q}\mathbf{\Sigma}_x\mathbf{Q}^H \\ \Rightarrow \mathbf{R_x}\mathbf{R_n}^{-1} &= \mathbf{Q}\mathbf{\Sigma}_x\mathbf{\Sigma}_n^{-1}\mathbf{Q}^{-1} = \mathbf{Q}\mathbf{\Sigma}\mathbf{Q}^{-1} \end{aligned} \tag{A.10}$$

where $\mathbf{Q}$ is an invertible matrix, the columns of which are unique up to a scalar and define the generalized eigenvectors. $\mathbf{\Sigma}_x, \mathbf{\Sigma}_n$ and $\mathbf{\Sigma}$ are real-valued diagonal matrices where $\mathbf{\Sigma}_x = \text{diag}\{\sigma_{x_1}, .., \sigma_{x_N}\}, \mathbf{\Sigma}_n = \text{diag}\{\sigma_{n_1}, .., \sigma_{n_N}\}$, and $\mathbf{\Sigma} = \text{diag}\{\frac{\sigma_{x_1}}{\sigma_{n_1}}, .., \frac{\sigma_{x_N}}{\sigma_{n_N}}\}$ define the generalized eigenvalues sorted from high to low.

From the GEVD of the matrix pencil $\{\mathbf{R_x}, \mathbf{R_n}\}$, the prewhitening matrix is defined as $\mathbf{V}_n = \mathbf{\Sigma}_n^{-1/2}\mathbf{Q}^{-1}$ such that $\mathbf{R_n} = (\mathbf{V}_n^H\mathbf{V}_n)^{-1}$ and $\mathbf{V}_n\mathbf{R_n}\mathbf{V}_n^H = \mathbf{I}_N$ and (A.7) is reformulated as:

$$\min_{\mathbf{R}_{\mathbf{n}_{r_1}}, \text{rank}(\mathbf{R}_{\mathbf{s}_{r_1}})=1} \alpha \parallel \mathbf{V}_n \left(\mathbf{R_x} - (\mathbf{R}_{\mathbf{n}_{r_1}} + \mathbf{R}_{\mathbf{s}_{r_1}})\right) \mathbf{V}_n^H \parallel_F^2 + (1-\alpha) \parallel \mathbf{V}_n \left(\mathbf{R_n} - \mathbf{R}_{\mathbf{n}_{r_1}}\right) \mathbf{V}_n^H \parallel_F^2 . \quad \text{(A.11)}$$

The solution to this problem is based on the GEVD and is given by

$$\mathbf{R}_{\mathbf{s}_{r_1}} = \mathbf{Q}\text{diag}\{\sigma_{x_1} - \sigma_{n_1}, 0, ..., 0\}\mathbf{Q}^H \quad \text{(A.12)}$$

$$\mathbf{R}_{\mathbf{n}_{r_1}} = \mathbf{Q}\text{diag}\{\sigma_{n_1}, \alpha\sigma_{x_2} + (1-\alpha)\sigma_{n_2}, ..., \alpha\sigma_{x_N} + (1-\alpha)\sigma_{n_N}\}\mathbf{Q}^H. \quad \text{(A.13)}$$

As it was stated in [110], the GEVD effectively selects the mode with the highest SNR and it allows a more reliable estimation of the rank-1 speech correlation matrix. In the considered MWF context, the GEVD-based estimation outperforms (in terms of SNR improvement achieved by the MWF) other correlation matrix estimation methods, like the first column decomposition or EVD based estimation, at the cost of a more sophisticated matrix decomposition. Also note that unlike the EVD-based MWF, the GEVD-based MWF is completely immune to scaling and linear combining of the input signals [231], i.e., the output signal and output SNR is independent of such scaling and combining, which is a desirable property.

A.3 Modified GEVD-based speech and noise correlation matrix estimation

In stead of using the sample 'noise-only' correlation matrix $\mathbf{R_n}$ for the prewhitening as in (A.11), it may be more accurate to use the estimated noise correlation matrix, i.e., reformulate (A.11) as

$$\min \alpha \parallel \mathbf{V} \left(\mathbf{R_x} - (\mathbf{R}_{\mathbf{n}_{r_1}} + \mathbf{R}_{\mathbf{s}_{r_1}})\right) \mathbf{V}^H \parallel_F^2 + (1-\alpha) \parallel \mathbf{V} \left(\mathbf{R_n} - \mathbf{R}_{\mathbf{n}_{r_1}}\right) \mathbf{V}^H \parallel_F^2$$

where the matrix $\mathbf{V}$ defines the prewhitening but is now part of the optimization problem and connected with the noise correlation matrix $\mathbf{R}_{\mathbf{n}_{r_1}}$ by the constraint

$$\mathbf{R}_{\mathbf{n}_{r_1}} = \mathbf{R}_{\mathbf{n}_{r_1}}^{1/2}\mathbf{R}_{\mathbf{n}_{r_1}}^{H/2} = \mathbf{V}^{-1}\mathbf{V}^{-H} = (\mathbf{V}^H\mathbf{V})^{-1}. \tag{A.14}$$

Unfortunately the technique used to solve (A.11) in [110] can not be used to solve (**??**). However, as the next theorem states, the GEVD again forms the solution to this modified criterion.

Theorem A.3.1. *The matrix* $\mathbf{R}_{\mathbf{n}_{r_1}}$ *and positive definite rank-1 matrix* $\mathbf{R}_{\mathbf{s}_{r_1}}$ *that form the only stationary point of the modified optimization problem* (**??**) *are given by*

$$\mathbf{R}_{\mathbf{s}_{r_1}} = \mathbf{Q}\text{diag}\{\sigma_{x_1} - \sigma_{n_1}, 0, ..., 0\}\mathbf{Q}^H \tag{A.15}$$

$$\mathbf{R}_{\mathbf{n}_{r_1}} = \mathbf{Q}\text{diag}\{\sigma_{n_1}, \frac{\alpha\sigma_{x_2}^2 + (1-\alpha)\sigma_{n_2}^2}{\alpha\sigma_{x_2} + (1-\alpha)\sigma_{n_2}}, ..., \frac{\alpha\sigma_{x_N}^2 + (1-\alpha)\sigma_{n_N}^2}{\alpha\sigma_{x_N} + (1-\alpha)\sigma_{n_N}}\}\mathbf{Q}^H \tag{A.16}$$

if $\sigma_{x_1} - \sigma_{n_1} \geq 0$*, else given by*

$$\mathbf{R}_{\mathbf{s}_{r_1}} = \mathbf{0} \tag{A.17}$$

$$\mathbf{R}_{\mathbf{n}_{r_1}} = \mathbf{Q}(\alpha\mathbf{\Sigma}_x + (1-\alpha)\mathbf{\Sigma}_n)^{-1}(\alpha\mathbf{\Sigma}_x^2 + (1-\alpha)\mathbf{\Sigma}_n^2)Q^H \tag{A.18}$$

where $\mathbf{Q}, \mathbf{\Sigma}_n, \mathbf{\Sigma}_x$ *are defined in* (A.10).

Proof. The modified optimization criterion in (**??**) can be simplified using (A.14) leading to

$$J(\mathbf{V}, \mathbf{R}_{\mathbf{s}_{r_1}}) = \alpha \parallel \mathbf{V}\mathbf{R}_{\mathbf{x}}\mathbf{V}^H - \mathbf{I}_N - \mathbf{V}\mathbf{R}_{\mathbf{s}_{r_1}}\mathbf{V}^H \parallel_F^2 + (1-\alpha) \parallel \mathbf{V}\mathbf{R}_{\mathbf{n}}\mathbf{V}^H - \mathbf{I} \parallel_F^2 . \tag{A.19}$$

Replacing the (unknown) Hermitian matrix $\mathbf{V}\mathbf{R}_{\mathbf{x}}\mathbf{V}^H$ by its EVD defining a unitary matrix $\mathbf{P}$ and real diagonal matrix $\mathbf{\Lambda}$ gives

$$\mathbf{V}\mathbf{R}_{\mathbf{x}}\mathbf{V}^H = \mathbf{P}\mathbf{\Lambda}\mathbf{P}^H \tag{A.20}$$

and

$$\mathbf{V}\mathbf{R}_{\mathbf{x}}\mathbf{V}^H - \mathbf{I}_N = \mathbf{P}(\mathbf{\Lambda} - \mathbf{I}_N)\mathbf{P}^H. \tag{A.21}$$

Then it is known from low rank matrix approximation theory that the optimal positive definite rank-1 matrix $\mathbf{R}_{\mathbf{s}_{r_1}}$ is given by

$$\mathbf{V}\mathbf{R}_{\mathbf{s}_{r_1}}\mathbf{V}^H = \lambda_{max}\mathbf{u}_{max}\mathbf{u}_{max}^H \tag{A.22}$$

with $\lambda_{max} = \max(\{\lambda_i - 1\}_{i=1..N}, 0)$, to make $\mathbf{R}_{\mathbf{s}_{r_1}}$ positive definite. Also $\mathbf{u}_{max}$ is a column of $\mathbf{P}$ and unitary ($\mathbf{u}_{max}^H \mathbf{u}_{max} = 1$). Here it is assumed that the largest eigenvalue λ_{max} is unique[1], so that $\mathbf{u}_{max}$ is uniquely determined (up to a sign ambiguity). Hence the first part in the r.h.s of (A.19) can be rewritten as

$$\| \mathbf{V}\mathbf{R}_{\mathbf{x}}\mathbf{V}^H - \mathbf{I}_N - \mathbf{V}\mathbf{R}_{\mathbf{s}_{r_1}}\mathbf{V}^H \|_F^2 = \| \mathbf{V}\mathbf{R}_{\mathbf{x}}\mathbf{V}^H - \mathbf{I}_N \|_F^2 - \lambda_{max}^2. \tag{A.23}$$

Assume from now on that $\lambda_{max} > 0$ and denote the corresponding largest eigenvalue of $\mathbf{V}\mathbf{R}_{\mathbf{x}}\mathbf{V}^H$ with Λ_{max}. The case where $\lambda_{max} = 0$ will be discussed at the end of the proof.

The optimization criterion (A.19) is currently given by

$$J(\mathbf{V}) = \alpha \| \mathbf{V}\mathbf{R}_{\mathbf{x}}\mathbf{V}^H - \mathbf{I}_N \|_F^2 - \alpha\lambda_{max}(\mathbf{V})^2 + (1-\alpha) \| \mathbf{V}\mathbf{R}_{\mathbf{n}}\mathbf{V}^H - \mathbf{I}_N \|_F^2 \tag{A.24}$$

$$\begin{aligned} &= \alpha tr(\mathbf{V}\mathbf{R}_{\mathbf{x}}\mathbf{V}^H\mathbf{V}\mathbf{R}_{\mathbf{x}}\mathbf{V}^H - 2\mathbf{V}\mathbf{R}_{\mathbf{x}}\mathbf{V}^H + \mathbf{I}_N) \\ &\quad + (1-\alpha) tr(\mathbf{V}\mathbf{R}_{\mathbf{n}}\mathbf{V}^H\mathbf{V}\mathbf{R}_{\mathbf{n}}\mathbf{V}^H - 2\mathbf{V}\mathbf{R}_{\mathbf{n}}\mathbf{V}^H + \mathbf{I}_N) - \alpha\lambda_{max}(\mathbf{V})^2 \end{aligned} \tag{A.25}$$

where $tr(\cdot)$ denotes the trace operation. To find possible stationary points of this non-constrained optimization problem (only constraint is that $\mathbf{V}$ is invertible), the following differential are defined:

$$\begin{aligned} df_1(\mathbf{V}) &= dtr\left(\mathbf{V}\mathbf{R}\mathbf{V}^H\right) \\ &= tr\left(\mathbf{R}\mathbf{V}^H d\mathbf{V} + d\mathbf{V}^H\mathbf{V}\mathbf{R}\right) \end{aligned} \tag{A.26}$$

$$\begin{aligned} df_2(\mathbf{V}) &= dtr\left(\mathbf{V}\mathbf{R}\mathbf{V}^H\mathbf{V}\mathbf{R}^H\mathbf{V}^H\right) \\ &= tr\left((\mathbf{R}\mathbf{V}^H\mathbf{V}\mathbf{R}^H\mathbf{V}^H + \mathbf{R}^H\mathbf{V}^H\mathbf{V}\mathbf{R}\mathbf{V}^H)d\mathbf{V}\right. \\ &\quad \left. + d\mathbf{V}^H(\mathbf{V}\mathbf{R}^H\mathbf{V}^H\mathbf{V}\mathbf{R} + \mathbf{V}\mathbf{R}\mathbf{V}^H\mathbf{V}\mathbf{R}^H)\right) \end{aligned} \tag{A.27}$$

$$\begin{aligned} df_3(\mathbf{V}) &= d\lambda_{max}^2(\mathbf{V}) \\ &= 2\lambda_{max} d\lambda_{max}(\mathbf{V}) \\ &= 2\lambda_{max}\mathbf{u}_{max}^H d(\mathbf{V}\mathbf{R}_{\mathbf{x}}\mathbf{V}^H - \mathbf{I}_N)\mathbf{u}_{max} \\ &= 2\lambda_{max} tr\left(\mathbf{R}_{\mathbf{x}}\mathbf{V}^H\mathbf{u}_{max}\mathbf{u}_{max}^H d\mathbf{V} + d\mathbf{V}^H\mathbf{u}_{max}\mathbf{u}_{max}^H\mathbf{V}\mathbf{R}_{\mathbf{x}}\right) \end{aligned} \tag{A.28}$$

[1]The case where λ_{max} has a multiplicity larger than one is not considered here for the sake of a compact exposition.

where the linear and cyclic properties of the trace operation are used in (A.26) - (A.28) and the derivative of an eigenvalue with multiplicity of one as discussed in [232] is used in (A.28).

Now using a result from [233] that if the differential $df(\mathbf{V})$ can be written as

$$df(\mathbf{V}) = tr(\mathbf{A}_0^T d\mathbf{V} + d\mathbf{V}^H \mathbf{A}_1) \tag{A.29}$$

where $\mathbf{A}_0$ and $\mathbf{A}_1$ may depend on $\mathbf{V}$ and ^{T} denotes the transpose operation, then the partial derivatives of $f(\mathbf{V})$ with respect to the complex-valued matrix $\mathbf{V}$ and to the complex conjugate of $\mathbf{V}$ (denoted with $\mathbf{V}^*$) is given by

$$\frac{\partial f(\mathbf{V})}{\partial \mathbf{V}} = \mathbf{A}_0, \quad \frac{\partial f(\mathbf{V})}{\partial \mathbf{V}^*} = \mathbf{A}_1. \tag{A.30}$$

Combining (A.26), (A.27) and (A.28) with (A.30), an equation for stationary points of $J(\mathbf{V})$ is obtained as

$$\begin{aligned}\frac{\partial}{\partial \mathbf{V}^*} J = {} & 2\alpha \mathbf{V}\mathbf{R}_\mathbf{x}\mathbf{V}^H\mathbf{V}\mathbf{R}_\mathbf{x} - 2\alpha \mathbf{V}\mathbf{R}_\mathbf{x} - 2(1-\alpha)\mathbf{V}\mathbf{R}_\mathbf{n} \\ & + 2(1-\alpha)\mathbf{V}\mathbf{R}_\mathbf{n}\mathbf{V}^H\mathbf{V}\mathbf{R}_\mathbf{n} - 2\alpha\lambda_{max}\mathbf{u}_{max}\mathbf{u}_{max}^H\mathbf{V}\mathbf{R}_\mathbf{x} = \mathbf{0}.\end{aligned}$$

Dividing both sides by 2 and multiplying with $\mathbf{V}^H\mathbf{u}_{max}$ gives

$$\begin{aligned}\mathbf{0} = {} & \alpha\mathbf{V}\mathbf{R}_\mathbf{x}\mathbf{V}^H\mathbf{V}\mathbf{R}_\mathbf{x}\mathbf{V}^H\mathbf{u}_{max} - \alpha\mathbf{V}\mathbf{R}_\mathbf{x}\mathbf{V}^H\mathbf{u}_{max} - (1-\alpha)\mathbf{V}\mathbf{R}_\mathbf{n}\mathbf{V}^H\mathbf{u}_{max} \\ & + (1-\alpha)\mathbf{V}\mathbf{R}_\mathbf{n}\mathbf{V}^H\mathbf{V}\mathbf{R}_\mathbf{n}\mathbf{V}^H\mathbf{u}_{max} - \alpha\lambda_{max}\mathbf{u}_{max}\mathbf{u}_{max}^H\mathbf{V}\mathbf{R}_\mathbf{x}\mathbf{V}^H\mathbf{u}_{max} \\ = {} & \alpha\Lambda_{max}^2\mathbf{u}_{max} - \alpha\Lambda_{max}\mathbf{u}_{max} + (1-\alpha)(\mathbf{V}\mathbf{R}_\mathbf{n}\mathbf{V}^H\mathbf{V}\mathbf{R}_\mathbf{n}\mathbf{V}^H - \mathbf{V}\mathbf{R}_\mathbf{n}\mathbf{V}^H)\mathbf{u}_{max} \\ & - \alpha(\Lambda_{max}-1)\Lambda_{max}\mathbf{u}_{max}.\end{aligned} \tag{A.31}$$

This simplifies to

$$(\mathbf{V}\mathbf{R}_\mathbf{n}\mathbf{V}^H\mathbf{V}\mathbf{R}_\mathbf{n}\mathbf{V}^H - \mathbf{V}\mathbf{R}_\mathbf{n}\mathbf{V}^H)\mathbf{u}_{max} = \mathbf{0}. \tag{A.32}$$

Hence $\mathbf{u}_{max}$ is an eigenvector of $\mathbf{V}\mathbf{R}_\mathbf{n}\mathbf{V}^H\mathbf{V}\mathbf{R}_\mathbf{n}\mathbf{V}^H - \mathbf{V}\mathbf{R}_\mathbf{n}\mathbf{V}^H = \mathbf{V}\mathbf{R}_\mathbf{n}\mathbf{V}^H(\mathbf{V}\mathbf{R}_\mathbf{n}\mathbf{V}^H - \mathbf{I}_N) = (\mathbf{V}\mathbf{R}_\mathbf{n}\mathbf{V}^H - \mathbf{I}_N)\mathbf{V}\mathbf{R}_\mathbf{n}\mathbf{V}^H$ with eigenvalue zero, so also an eigenvector of $\mathbf{V}\mathbf{R}_\mathbf{n}\mathbf{V}^H$ with eigenvalue one or zero. Since $\mathbf{R}_\mathbf{n}$ and $\mathbf{V}$ are assumed to be invertible, $\mathbf{V}\mathbf{R}_\mathbf{n}\mathbf{V}^H$ must be nonsingular and hence $\mathbf{u}_{max}$ must be an eigenvector of $\mathbf{V}\mathbf{R}_\mathbf{n}\mathbf{V}^H$ with eigenvalue one. If $\mathbf{u}_{max}$ is an eigenvector of $\mathbf{V}\mathbf{R}_\mathbf{x}\mathbf{V}^H$ and of $\mathbf{V}\mathbf{R}_\mathbf{n}\mathbf{V}^H$, it is also an eigenvector with eigenvalue Λ_{max} of

$$(\mathbf{V}\mathbf{R}_\mathbf{x}\mathbf{V}^H)(\mathbf{V}\mathbf{R}_\mathbf{n}\mathbf{V}^H)^{-1} = \mathbf{V}\mathbf{R}_\mathbf{x}\mathbf{R}_\mathbf{n}^{-1}\mathbf{V}^{-1}. \tag{A.33}$$

By substituting the GEVD (A.10) of $\{\mathbf{R_x}, \mathbf{R_n}\}$ in (A.33), the eigenvalue decomposition of (A.33) is obtained as

$$\mathbf{V}\mathbf{R_x}\mathbf{R_n}^{-1}\mathbf{V}^{-1} = \tilde{\mathbf{V}}(\mathbf{\Sigma}_x\mathbf{\Sigma}_n^{-1})\tilde{\mathbf{V}}^{-1} \tag{A.34}$$

with $\tilde{\mathbf{V}} = \mathbf{V}\mathbf{Q}$.

Hence $\mathbf{u}_{max}$ is the normalized version the column of $\tilde{\mathbf{V}}$ corresponding to the eigenvalue Λ_{max}. Assume that $\frac{\sigma_{x_1}}{\sigma_{n_1}} = \Lambda_{max}$. Then $\mathbf{u}_{max}$ can be written as

$$\mathbf{u}_{max} = \frac{\tilde{\mathbf{V}}\mathbf{e}_1}{\|\tilde{\mathbf{V}}e_1\|} = \frac{1}{\sigma_{v_1}^{1/2}}\tilde{\mathbf{V}}\mathbf{e}_1. \tag{A.35}$$

Plugging (A.35) and (A.10) into the stationary point equation (A.31), results in

$$\begin{aligned} 0 = {} & \alpha\tilde{\mathbf{V}}\mathbf{\Sigma}_x\tilde{\mathbf{V}}^H\tilde{\mathbf{V}}\mathbf{\Sigma}_x\mathbf{Q}^H - \alpha\tilde{\mathbf{V}}\mathbf{\Sigma}_x\mathbf{Q}^H + (1-\alpha)\tilde{\mathbf{V}}\mathbf{\Sigma}_n\tilde{\mathbf{V}}^H\tilde{\mathbf{V}}\mathbf{\Sigma}_n\mathbf{Q}^H \\ & - (1-\alpha)\tilde{\mathbf{V}}\mathbf{\Sigma}_n\mathbf{Q}^H - \alpha\frac{\lambda_{max}}{\sigma_{v_1}}\tilde{\mathbf{V}}\mathbf{e}_1\mathbf{e}_1^H\tilde{\mathbf{V}}^H\tilde{\mathbf{V}}\mathbf{\Sigma}_x\mathbf{Q}^H \end{aligned} \tag{A.36}$$

Since $\mathbf{Q}^H$ and $\tilde{\mathbf{V}}$ are invertible, right-multiplying with $\tilde{\mathbf{V}}^{-1}$ and left-multiplying with $\mathbf{Q}^{-H}$ gives

$$0 = \alpha\mathbf{\Sigma}_x\mathbf{\Sigma}_\mathbf{V}\mathbf{\Sigma}_x + (1-\alpha)\mathbf{\Sigma}_n\mathbf{\Sigma}_\mathbf{V}\mathbf{\Sigma}_n - \alpha\frac{\lambda_{max}}{\sigma_{v_1}^2}\mathbf{e}_1\mathbf{e}_1^H\mathbf{\Sigma}_\mathbf{V}\mathbf{\Sigma}_x - \alpha\mathbf{\Sigma}_x - (1-\alpha)\mathbf{\Sigma}_n \tag{A.37}$$

where $\mathbf{\Sigma}_\mathbf{V} = \tilde{\mathbf{V}}^H\tilde{\mathbf{V}}$ and $\sigma_{v_1} = (\mathbf{\Sigma}_\mathbf{V})_{1,1}$.

It can be verified that in general $\mathbf{\Sigma}_\mathbf{V}$ has to be diagonal ($\mathbf{\Sigma}_\mathbf{V} = \text{diag}\{\sigma_{v_1}, .., \sigma_{v_N}\}$) to solve (A.37). Using the fact that $\lambda_{max} = \Lambda_{max} - 1 = \frac{\sigma_{x_1}}{\sigma_{n_1}} - 1$, finally $\mathbf{\Sigma}_\mathbf{V}$ is obtained as:

$$\begin{aligned} \mathbf{\Sigma}_\mathbf{V} = {} & \text{diag}\{\alpha\sigma_{x_1}^2 + (1-\alpha)\sigma_{n_1}^2, ..., \alpha\sigma_{x_N}^2 + (1-\alpha)\sigma_{n_N}^2\}^{-1} \\ & \left(\begin{bmatrix} \alpha\sigma_{x_1} + (1-\alpha)\sigma_{n_1} & \cdots & 0 \\ \vdots & \ddots & \vdots \\ 0 & \cdots & \alpha\sigma_{x_N} + (1-\alpha)\sigma_{n_N} \end{bmatrix} \right. \\ & \left. - \begin{bmatrix} \alpha\lambda_{max}\sigma_{x_1} & 0 & \cdots & 0 \\ 0 & 0 & \cdots & 0 \\ \vdots & \vdots & \ddots & \vdots \\ 0 & 0 & \cdots & 0 \end{bmatrix} \right) = \text{diag}\{\sigma_{n_1}^{-1}, ..., \frac{\alpha\sigma_{x_N} + (1-\alpha)\sigma_{n_N}}{\alpha\sigma_{x_N}^2 + (1-\alpha)\sigma_{n_N}^2}\}. \end{aligned} \tag{A.38}$$

The optimal solution is thus shown to be

$$\mathbf{V} = \mathbf{\Sigma}_{\mathbf{V}}^{1/2}\mathbf{Q}^{-1} \tag{A.39}$$

$$\mathbf{R}_{\mathbf{n}_{r_1}} = (\mathbf{V}^H\mathbf{V})^{-1} = \mathbf{Q}\mathbf{\Sigma}_{\mathbf{V}}^{-1}\mathbf{Q}^H \tag{A.40}$$

$$\mathbf{R}_{\mathbf{s}_{r_1}} = \mathbf{V}^{-1}\mathbf{u}_{max}\lambda_{max}\mathbf{u}_{max}^H\mathbf{V}^{-H} = \frac{1}{\sigma_{v_1}}\mathbf{Q}\mathbf{\Sigma}_{\mathbf{V}}^{-1/2}\mathbf{\Sigma}_{\mathbf{V}}^{1/2}\mathbf{e}_1(\frac{\sigma_{x_1}}{\sigma_{n_1}} - 1)\mathbf{e}_1^H\mathbf{\Sigma}_{\mathbf{V}}^{1/2}\mathbf{\Sigma}_{\mathbf{V}}^{-1/2}\mathbf{Q}^H$$

$$= \mathbf{Q}\mathrm{diag}\{\sigma_{x_1} - \sigma_{n_1}, 0, ..., 0\}\mathbf{Q}^H \tag{A.41}$$

It remains to show that Λ_{max} is equal to the largest generalized eigenvalue ratio $\frac{\sigma_{x_1}}{\sigma_{n_1}}$. This can be seen from the fact that Λ_{max} is the largest positive eigenvalue of $\mathbf{V}\mathbf{R}_{\mathbf{x}}\mathbf{V}^H = \mathbf{P}\mathbf{\Lambda}\mathbf{P}^H$. Indeed the eigenvalues of $\mathbf{V}\mathbf{R}_{\mathbf{x}}\mathbf{V}^H$ can be determined using (A.10) and (A.39):

$$\mathbf{\Lambda} = \mathrm{diag}\{\frac{\sigma_{x_1}}{\sigma_{n_1}}, \{\frac{\alpha\frac{\sigma_{x_i}^2}{\sigma_{n_i}^2} + (1-\alpha)\frac{\sigma_{x_i}}{\sigma_{n_i}}}{\alpha\frac{\sigma_{x_i}^2}{\sigma_{n_i}^2} + (1-\alpha)}\}_{i=2..N}\}. \tag{A.42}$$

It suffices that $\frac{\sigma_{x_1}}{\sigma_{n_1}} (\geq 1) \geq \max(\{\frac{\sigma_{x_i}}{\sigma_{n_i}}\}_{i=2..N})$ since then

$$\alpha(\frac{\sigma_{x_1}}{\sigma_{n_1}} - 1)\frac{\sigma_{x_i}^2}{\sigma_{n_i}^2} + (1-\alpha)(\frac{\sigma_{x_1}}{\sigma_{n_1}} - \frac{\sigma_{x_i}}{\sigma_{n_i}}) \geq 0 \quad \forall i \tag{A.43}$$

or equivalently

$$\frac{\sigma_{x_1}}{\sigma_{n_1}} \geq \frac{\alpha\frac{\sigma_{x_i}^2}{\sigma_{n_i}^2} + (1-\alpha)\frac{\sigma_{x_i}}{\sigma_{n_i}}}{\alpha\frac{\sigma_{x_i}^2}{\sigma_{n_i}^2} + (1-\alpha)} \quad \forall i. \tag{A.44}$$

From this it is seen that $\frac{\sigma_{x_1}}{\sigma_{n_1}}$ is the largest eigenvalue of $\mathbf{V}\mathbf{R}_{\mathbf{x}}\mathbf{V}^H$.

The previous derivation up to (A.38) is also valid for the trivial case where $\lambda_{max} = 0$. For this case the solution is obtained as

$$\mathbf{R}_{\mathbf{s}_{r_1}} = \mathbf{0} \tag{A.45}$$

$$\mathbf{R}_{\mathbf{n}_{r_1}} = \mathbf{Q}\mathrm{diag}\{\frac{\alpha\sigma_{x_1}^2 + (1-\alpha)\sigma_{n_1}^2}{\alpha\sigma_{x_1} + (1-\alpha)\sigma_{n_1}}, \frac{\alpha\sigma_{x_2}^2 + (1-\alpha)\sigma_{n_2}^2}{\alpha\sigma_{x_2} + (1-\alpha)\sigma_{n_2}}, ...$$

$$..., \frac{\alpha\sigma_{x_N}^2 + (1-\alpha)\sigma_{n_N}^2}{\alpha\sigma_{x_N} + (1-\alpha)\sigma_{n_N}}\}\mathbf{Q}^H$$

$$= \mathbf{Q}(\alpha\mathbf{\Sigma}_x + (1-\alpha)\mathbf{\Sigma}_n)^{-1}(\alpha\mathbf{\Sigma}_x^2 + (1-\alpha)\mathbf{\Sigma}_n^2)\mathbf{Q}^H. \tag{A.46}$$

where the optimal $\mathbf{R}_{\mathbf{n}_{r_1}}$ is simply a non-linear interpolation depending on α between $\mathbf{R}_{\mathbf{x}}$ and $\mathbf{R}_{\mathbf{n}}$. □

Remark I: An extension of the proof to a scenario with S speech sources is possible in a similar way where the optimal rank-S speech correlation matrix $\mathbf{R}_{\mathbf{s}_{r_S}}$ is then given by:

$$\mathbf{R}_{\mathbf{s}_{r_S}} = \mathbf{Q}\text{diag}\{\sigma_{x_1} - \sigma_{n_1}, ..., \sigma_{x_S} - \sigma_{n_S}, 0, ..., 0\}\mathbf{Q}^H \tag{A.47}$$

where $\sigma_{x_1} - \sigma_{n_1}, ..., \sigma_{x_S} - \sigma_{n_S}$ are the S largest generalized eigenvalue differences.

While the optimal $\mathbf{R}_{\mathbf{s}_{r_1}}$ in (A.15) is the same as in (A.12), the $\mathbf{R}_{\mathbf{n}_{r_1}}$ in (A.16) is different from (A.13). The resulting α-dependent interpolation between the generalized eigenvalues is more involved in (A.16) than the simpler linear interpolation in (A.13). However, the resulting MWF (A.5) is straightforwardly shown to be the same in both cases and is given by

$$\mathbf{w}_{MWF} = \mathbf{Q}^{-H}\text{diag}\{\frac{\sigma_{x_1} - \sigma_{n_1}}{\sigma_{x_1}}, 0, ..., 0\}\mathbf{Q}^H\boldsymbol{e}_1. \tag{A.48}$$

This justifies the use of the original optimization criterion (A.11) as a simpler substitute. Formula (A.48) demonstrates also that the GEVD-based $\mathbf{w}_{MWF}$ is independent of the value of α in the optimization criterion, which is a desirable property.

Remark II: The solution for $\lambda_{max} = 0$ has the same optimal solution, i.e., $\mathbf{V} = \mathbf{R}_{\mathbf{n}_{r_1}}^{-1/2}$, as the solution minimizing:

$$\min_{\mathbf{V}} \alpha \parallel \mathbf{V}\mathbf{R}_{\mathbf{x}}\mathbf{V}^H - \mathbf{I}_N \parallel_F^2 + (1-\alpha) \parallel \mathbf{V}\mathbf{R}_{\mathbf{n}}\mathbf{V}^H - \mathbf{I}_N \parallel_F^2 . \tag{A.49}$$

This can be seen as a single matrix approximation $(\mathbf{V}^H\mathbf{V})^{-1}$ to two matrices $\mathbf{R}_{\mathbf{x}}$ and $\mathbf{R}_{\mathbf{n}}$. However, extending this to more than two matrices is not trivial and depends on a joint diagonalization of the concerning matrices. This is generally not possible in an exact way, since the diagonalization problem becomes overdetermined and is only possible for matrices possessing a common structure [234, 235].

Appendix B

Appendix to Chapter 3

B.1 Useful identities

For the derivations in Appendix B.2 and B.3, the following theorem is needed:

Theorem B.1.1. *Given an $M \times L$-dimensional matrix $\mathbf{A}$ with $M \geq L$ and linearly independent columns. Let $\mathbf{A}_\perp$ denote the $M \times M - L$-dimensional matrix whose columns span the nullspace of $\mathbf{A}^H$ such that $\mathbf{A}^H\mathbf{A}_\perp = \mathbf{0}$ and $[\mathbf{A}\mathbf{A}_\perp]$ is full rank. The identity matrix $\mathbf{I}_M$ can then uniquely be decomposed as follows:*

$$\mathbf{I}_M = \mathbf{A}\left(\mathbf{A}^H\mathbf{A}\right)^{-1}\mathbf{A}^H + \mathbf{A}_\perp\left(\mathbf{A}_\perp^H\mathbf{A}_\perp\right)^{-1}\mathbf{A}_\perp^H \tag{B.1}$$

Proof. This can be seen from

$$\begin{aligned}\mathbf{I}_M &= [\mathbf{A}\ \mathbf{A}_\perp][\mathbf{A}\ \mathbf{A}_\perp]^{-1}[\mathbf{A}\ \mathbf{A}_\perp]^{-H}[\mathbf{A}\ \mathbf{A}_\perp]^H \\ &= [\mathbf{A}\ \mathbf{A}_\perp]\left([\mathbf{A}\ \mathbf{A}_\perp]^H[\mathbf{A}\ \mathbf{A}_\perp]\right)^{-1}[\mathbf{A}\ \mathbf{A}_\perp]^H \\ &= [\mathbf{A}\ \mathbf{A}_\perp]\begin{bmatrix}\mathbf{A}^H\mathbf{A} & \mathbf{0} \\ \mathbf{0} & \mathbf{A}_\perp^H\mathbf{A}_\perp\end{bmatrix}^{-1}[\mathbf{A}\ \mathbf{A}_\perp]^H\end{aligned} \tag{B.2}$$

□

Applying Theorem B.1.1 using the matrices $\mathbf{A} = \mathbf{R}_{\mathbf{nn}}^{-1/2}\mathbf{H}$ and $\mathbf{A}_\perp = \mathbf{R}_{\mathbf{nn}}^{H/2}\mathbf{B}$ results in

$$\mathbf{I}_M = \mathbf{R}_{\mathbf{nn}}^{-1/2}\mathbf{H}\left(\mathbf{H}^H\mathbf{R}_{\mathbf{nn}}^{-1}\mathbf{H}\right)^{-1}\mathbf{H}^H\mathbf{R}_{\mathbf{nn}}^{-H/2} + \mathbf{R}_{\mathbf{nn}}^{H/2}\mathbf{B}\left(\mathbf{B}^H\mathbf{R}_{\mathbf{nn}}\mathbf{B}\right)^{-1}\mathbf{B}^H\mathbf{R}_{\mathbf{nn}}^{1/2} \tag{B.3}$$

or equivalent

$$\mathbf{R_{nn}} = \mathbf{H}\left(\mathbf{H}^H\mathbf{R_{nn}}^{-1}\mathbf{H}\right)^{-1}\mathbf{H}^H + \mathbf{R_{nn}}\mathbf{B}\left(\mathbf{B}^H\mathbf{R_{nn}}\mathbf{B}\right)^{-1}\mathbf{B}^H\mathbf{R_{nn}}. \tag{B.4}$$

B.2 Equivalence between (3.9) and (3.10)

To remove the constraint $\mathbf{B}^H\mathbf{R_{ss}}\mathbf{B} = \mathbf{0}$, $\mathbf{R_{ss}}$ is parameterized as

$$\mathbf{R_{ss}} = \mathbf{H}\boldsymbol{R}_{\hat{\mathbf{s}}\hat{\mathbf{s}}}\mathbf{H}^H \tag{B.5}$$

and the constraint on the rank of $\mathbf{R_{ss}}$ can be directly transfered to the same constraint on the $L \times L$-dimensional matrix $\mathbf{R}_{\hat{\mathbf{s}}\hat{\mathbf{s}}}$. The optimization problem is then reduced to

$$\underset{\text{rank}(\boldsymbol{R}_{\hat{\mathbf{s}}\hat{\mathbf{s}}})=R}{\arg\min} \parallel \mathbf{R_{nn}}^{-1/2}\left(\mathbf{R_{yy}} - \mathbf{R_{nn}} - \mathbf{H}\boldsymbol{R}_{\hat{\mathbf{s}}\hat{\mathbf{s}}}\mathbf{H}^H\right)\mathbf{R_{nn}}^{-H/2} \parallel_F^2 . \tag{B.6}$$

Define the $M \times L$-dimensional matrix $\mathbf{C}$ and $M \times (M-L)$-dimensional matrix $\mathbf{C}^c$ as follows (assuming $\begin{bmatrix}\mathbf{H} & \mathbf{R_{nn}}\mathbf{B}\end{bmatrix}$ is full rank):

$$\begin{bmatrix}\mathbf{C}^H \\ \mathbf{C}^{c,H}\end{bmatrix}\begin{bmatrix}\mathbf{H} & \mathbf{R_{nn}}\mathbf{B}\end{bmatrix} = \begin{bmatrix}\mathbf{I}_L & \mathbf{0} \\ \mathbf{0} & \mathbf{I}_{M-L}\end{bmatrix} \tag{B.7}$$

Inserting an identity matrix on certain positions in (B.6) does not change the optimal value for $\mathbf{R}_{\hat{\mathbf{s}}\hat{\mathbf{s}}}$, so (B.6) is equivalent to:

$$\begin{aligned}\underset{\text{rank}(\boldsymbol{R}_{\hat{\mathbf{s}}\hat{\mathbf{s}}})=R}{\arg\min} \parallel \begin{bmatrix}\mathbf{R_{nn}}^{-1/2}\mathbf{H} & \mathbf{R_{nn}}^{1/2}\mathbf{B}\end{bmatrix}\begin{bmatrix}\mathbf{C}^H \\ \mathbf{C}^{c,H}\end{bmatrix}(\mathbf{R_{yy}} - \mathbf{R_{nn}} \\ -\mathbf{H}\boldsymbol{R}_{\hat{\mathbf{s}}\hat{\mathbf{s}}}\mathbf{H}^H)\begin{bmatrix}\mathbf{C} & \mathbf{C}^c\end{bmatrix}\begin{bmatrix}\mathbf{H}^H\mathbf{R_{nn}}^{-H/2} \\ \mathbf{B}^H\mathbf{R_{nn}}^{H/2}\end{bmatrix} \parallel_F^2 .\end{aligned} \tag{B.8}$$

(B.8) can then be further expanded as

$$\begin{aligned}\underset{\text{rank}(\boldsymbol{R}_{\hat{\mathbf{s}}\hat{\mathbf{s}}})=R}{\arg\min} \parallel \begin{bmatrix}\mathbf{R_{nn}}^{-1/2}\mathbf{H} & \mathbf{0} \\ \mathbf{0} & \mathbf{R_{nn}}^{H/2}\mathbf{B}\end{bmatrix}\Bigg(\begin{bmatrix}\mathbf{C}^H\mathbf{R_{yy}} - \mathbf{R_{nn}}\mathbf{C} & \mathbf{C}^H\mathbf{R_{yy}} - \mathbf{R_{nn}}\mathbf{C}_\perp \\ \mathbf{C}_\perp^H\mathbf{R_{yy}} - \mathbf{R_{nn}}\mathbf{C} & \mathbf{C}_\perp^H\mathbf{R_{yy}} - \mathbf{R_{nn}}\mathbf{C}_\perp\end{bmatrix} \\ - \begin{bmatrix}\boldsymbol{R}_{\hat{\mathbf{s}}\hat{\mathbf{s}}} & \mathbf{0} \\ \mathbf{0} & \mathbf{0}\end{bmatrix}\Bigg)\begin{bmatrix}\mathbf{H}^H\mathbf{R_{nn}}^{-H/2} & \mathbf{0} \\ \mathbf{0} & \mathbf{B}^H\mathbf{R_{nn}}^{1/2}\end{bmatrix} \parallel_F^2 .\end{aligned} \tag{B.9}$$

One can notice that only the left upper block part of the resulting matrix inside the Frobenius norm of (B.9) is influenced by $\mathbf{R}_{\hat{\mathbf{s}}\hat{\mathbf{s}}}$, so the optimization problem (B.9) can be simplified to:

$$\underset{\text{rank}(\boldsymbol{R}_{\hat{\mathbf{s}}\hat{\mathbf{s}}})=R}{\arg\min} \parallel \mathbf{R_{nn}}^{-1/2}\mathbf{H}(\mathbf{C}^H\mathbf{R_{yy}}\mathbf{C} - \mathbf{C}^H\mathbf{R_{nn}}\mathbf{C} - \boldsymbol{R}_{\hat{\mathbf{s}}\hat{\mathbf{s}}})\mathbf{H}^H\mathbf{R_{nn}}^{-H/2} \parallel_F^2 \tag{B.10}$$

One can also show that $\mathbf{C}^H\mathbf{R_{nn}}\mathbf{C} = \left(\mathbf{H}^H\mathbf{R_{nn}^{-1}}\mathbf{H}\right)^{-1}$ by combining (B.4) and (B.7). So now by plugging in the definitions of (3.16) in (B.10), the reduced equivalent optimization problem to (3.9) is finally given by

$$\underset{\text{rank}(\boldsymbol{R}_{\hat{\mathbf{s}}\hat{\mathbf{s}}})=R}{\arg\min} \parallel \mathbf{R}_{\hat{\mathbf{n}}\hat{\mathbf{n}}}^{-1/2}\left(\mathbf{R}_{\hat{\mathbf{y}}\hat{\mathbf{y}}} - \mathbf{R}_{\hat{\mathbf{n}}\hat{\mathbf{n}}} - \boldsymbol{R}_{\hat{\mathbf{s}}\hat{\mathbf{s}}}\right)\mathbf{R}_{\hat{\mathbf{n}}\hat{\mathbf{n}}}^{-H/2} \parallel_F^2 . \tag{B.11}$$

B.3 Derivation of rank R PK-GEVD-MWF

(3.5) Substituting estimate $\mathbf{R_{ss}}$ of (3.17) and $\mathbf{R_{nn}}$ as $\bar{\mathbf{R}}_{\mathbf{ss}}$ and $\bar{\mathbf{R}}_{\mathbf{nn}}$ respectively in (3.5) reveals to the following identities:

$$\begin{aligned}
\mathbf{W}_k &= \left(\mathbf{R_{nn}} + \mathbf{R_{ss}}\right)^{-1}\mathbf{R_{ss}}\mathbf{E}_{\mathbf{d}_k} \\
&= \left(\mathbf{R_{nn}} + \mathbf{H}\hat{\mathbb{Q}}\Sigma_{\hat{\mathbf{s}}\hat{\mathbf{s}}}\hat{\mathbb{Q}}^H\mathbf{H}^H\right)^{-1}\mathbf{H}\hat{\mathbb{Q}}\Sigma_{\hat{\mathbf{s}}\hat{\mathbf{s}}}\hat{\mathbb{Q}}^H\mathbf{H}^H\mathbf{E}_{\mathbf{d}_k} \\
&= \left(\mathbf{I}_M - \left(\mathbf{R_{nn}} + \mathbf{H}\hat{\mathbb{Q}}\Sigma_{\hat{\mathbf{s}}\hat{\mathbf{s}}}\hat{\mathbb{Q}}^H\mathbf{H}^H\right)^{-1}\mathbf{R_{nn}}\right)\mathbf{E}_{\mathbf{d}_k} \\
&= \left(\mathbf{I}_M - \left(\mathbf{R_{nn}^{-1}} - \mathbf{R_{nn}^{-1}}\mathbf{H}\hat{\mathbb{Q}}\left(\Sigma_{\hat{\mathbf{s}}\hat{\mathbf{s}}}^{-1} + \hat{\mathbb{Q}}^H\mathbf{H}^H\mathbf{R_{nn}^{-1}}\mathbf{H}\hat{\mathbb{Q}}\right)^{-1}\hat{\mathbb{Q}}^H\mathbf{H}^H\mathbf{R_{nn}^{-1}}\right)\mathbf{R_{nn}}\right)\mathbf{E}_{\mathbf{d}_k} \\
&= \mathbf{R_{nn}^{-1}}\mathbf{H}\hat{\mathbb{Q}}\left(\Sigma_{\hat{\mathbf{s}}\hat{\mathbf{s}}}^{-1} + \hat{\mathbb{Q}}^H\mathbf{H}^H\mathbf{R_{nn}^{-1}}\mathbf{H}\hat{\mathbb{Q}}\right)^{-1}\hat{\mathbb{Q}}^H\mathbf{H}^H\mathbf{E}_{\mathbf{d}_k} \\
&= \mathbf{C}\mathbf{R}_{\hat{\mathbf{n}}\hat{\mathbf{n}}}^{-1}\hat{\mathbb{Q}}\left(\Sigma_{\hat{\mathbf{s}}\hat{\mathbf{s}}}^{-1} + \hat{\mathbb{Q}}^H\mathbf{R}_{\hat{\mathbf{n}}\hat{\mathbf{n}}}^{-1}\hat{\mathbb{Q}}\right)^{-1}\hat{\mathbb{Q}}^H\mathbf{H}^H\mathbf{E}_{\mathbf{d}_k} \\
&= \mathbf{C}(\mathbf{R}_{\hat{\mathbf{n}}\hat{\mathbf{n}}} + \hat{\mathbb{Q}}\Sigma_{\hat{\mathbf{s}}\hat{\mathbf{s}}}\hat{\mathbb{Q}}^H)^{-1}\hat{\mathbb{Q}}\Sigma_{\hat{\mathbf{s}}\hat{\mathbf{s}}}\hat{\mathbb{Q}}^H\mathbf{H}^H\mathbf{E}_{\mathbf{d}_k} \\
&= \mathbf{C}\hat{\mathbf{W}}\mathbf{H}^H\mathbf{E}_{\mathbf{d}_k}.
\end{aligned} \tag{B.12}$$

The matrix inversion lemma is used in the fourth step. In the sixth step, the identity $\mathbf{C}^H\mathbf{R_{nn}}\mathbf{C} = \mathbf{R}_{\hat{\mathbf{n}}\hat{\mathbf{n}}} = \left(\mathbf{H}^H\mathbf{R_{nn}^{-1}}\mathbf{H}\right)^{-1}$ derived from (B.4) and (B.7) is used, which implies also that $\mathbf{R_{nn}^{-1}}\mathbf{H} = \mathbf{C}\mathbf{R}_{\hat{\mathbf{n}}\hat{\mathbf{n}}}^{-1}$. In the last step, the GEVD-MWF expression for the reduce matrix pencil $\{\mathbf{R}_{\hat{\mathbf{n}}\hat{\mathbf{n}}}, \mathbf{R}_{\hat{\mathbf{y}}\hat{\mathbf{y}}}\}$ is identified:

$$\hat{\mathbf{W}} = (\mathbf{R}_{\hat{\mathbf{n}}\hat{\mathbf{n}}} + \hat{\mathbb{Q}}\Sigma_{\hat{\mathbf{s}}\hat{\mathbf{s}}}\hat{\mathbb{Q}}^H)^{-1}\hat{\mathbb{Q}}\Sigma_{\hat{\mathbf{s}}\hat{\mathbf{s}}}\hat{\mathbb{Q}}^H \tag{B.13}$$

which is equivalent to the expression in (3.19).

B.4 Proof of Theorem 3.4.2

To prove the sufficient statistic property of the compression $\mathbf{W}_{kk}, \mathbf{\Lambda}_{kk}$, for each node k, an extra lemma is needed. For this theorem, the node-specific compression matrices $\mathbb{X}_B^k$, $\mathbb{\Lambda}_B^k$ and $\mathbf{J}_B^k$ are defined as

$$\mathbb{X}_B^k = \begin{bmatrix} \mathbf{0} & \mathbb{X}_{<k} & \mathbf{0} \\ \mathbf{I}_{M_k} & \mathbf{0} & \mathbf{0} \\ \mathbf{0} & \mathbf{0} & \mathbb{X}_{>k} \end{bmatrix}, \; \mathbb{\Lambda}_B^k = \begin{bmatrix} \mathbf{0} & \mathbb{\Lambda}_{<k} & \mathbf{0} \\ \mathbf{I}_{L_k} & \mathbf{0} & \mathbf{0} \\ \mathbf{0} & \mathbf{0} & \mathbb{\Lambda}_{>k} \end{bmatrix} \tag{B.14}$$

$$\mathbf{J}_B^k = \begin{bmatrix} \mathbf{0} & \mathbb{X}_{<k} & \mathbf{0} & \mathbf{B}_{<k}\mathbb{\Lambda}_{<k} & \mathbf{0} \\ \mathbf{I}_{M_k} & \mathbf{0} & \mathbf{0} & \mathbf{0} & \mathbf{0} \\ \mathbf{0} & \mathbf{0} & \mathbb{X}_{>k} & \mathbf{0} & \mathbf{B}_{>k}\mathbb{\Lambda}_{>k} \end{bmatrix} \tag{B.15}$$

where[1] $\{.\}_{<k} = \text{Blkdiag}\{\{.\}_1, ..., \{.\}_{k-1}\}$ and $\{.\}_{>k} = \text{Blkdiag}\{\{.\}_{k+1}, ..., \{.\}_K\}$.

Lemma B.4.1. *Consider the (compressed) maximization problem (related to* (3.22)*)*

$$\begin{aligned} \underset{\tilde{\mathbb{X}}_k \in \mathbb{C}^{M_k+2R(K-1)\times R}}{\arg\max} \quad & tr\{\tilde{\mathbb{X}}_k \mathbf{J}_B^{k,H} \mathbf{R}_{\mathbf{yy}} \mathbf{J}_B^k \tilde{\mathbb{X}}_k\} \\ s.t. \quad & \tilde{\mathbb{X}}_k^H \mathbf{J}_B^{k,H} \mathbf{R}_{\mathbf{nn}} \mathbf{J}_B^k \tilde{\mathbb{X}}_k = \mathbf{I}_R \\ & \mathbb{\Lambda}_B^{k,H} \mathbf{B}^H \mathbf{R}_{\mathbf{nn}} \mathbf{J}_B^k \tilde{\mathbb{X}}_k = \mathbf{0}. \end{aligned} \tag{B.16}$$

The solution

$$\tilde{\mathbb{X}}_k = \begin{bmatrix} \mathbb{X}_{kk} \\ \mathbf{I}_{-k} \\ \mathbf{0}_{-k} \end{bmatrix} \tag{B.17}$$

fulfills the KKT-condition of (B.16) *with the same objective* $tr\{\tilde{\mathbb{X}}_k \mathbf{J}_B^{k,H} \mathbf{R}_{\mathbf{yy}} \mathbf{J}_B^k \tilde{\mathbb{X}}_k\}$ *as the objective of the (non-compressed) maximization problem in* (3.22) *corresponding to its optimal solution* $\mathbb{X}$*. Furthermore the Lagrange parameter corresponding to the last constraint of* (B.16) *and solution* (B.17) *is given by*

$$\tilde{\mathbb{\Lambda}}_k = \begin{bmatrix} \mathbb{\Lambda}_{kk} \\ \mathbf{I}_{-k} \end{bmatrix}. \tag{B.18}$$

Proof. See Appendix B.5. □

Lemma B.4.1 states that problem (3.22) can be solved equivalently by solving (B.16) instead and this is the case for every node k. The proof of Theorem 3.4.2 can now be stated.

[1] It is noted that the diagonal blocks are not square here, i.e., in this case Blkdiag(.) is not a block diagonal matrix in the strict sense.

Proof. The proof starts by noticing that the obtained local sensor signals $\tilde{\mathbf{y}}_k^{i^\star}$ at node k can be related to the sensor signal $\mathbf{y}$ using the node-specific compression matrix $\mathbf{V}_B^{i^\star,k}$:

$$\mathbf{V}_B^{i^\star,k} = \mathbf{J}_B^k \mathbf{M}_B^{i^\star,k} \tag{B.19}$$

via $\tilde{\mathbf{y}}_k^{i^\star} = \mathbf{V}_B^{i^\star,k,H}\mathbf{y}$ where

$$\mathbf{M}_B^{i^\star k} = \text{Blkdiag}\{\mathbf{I}_{M_k}, \mathbf{G}_1^{i^\star,1}, ..., \mathbf{G}_{k-1}^{i^\star,1}, \mathbf{G}_{k+1}^{i^\star,1}, ..., \mathbf{G}_K^{i^\star,1}, \mathbf{G}_1^{i^\star,2}, ..., \mathbf{G}_{k-1}^{i^\star,2}, \mathbf{G}_{k+1}^{i^\star,2}, ..., \mathbf{G}_K^{i^\star,2}\} \tag{B.20}$$

is a fixed block diagonal matrix, which is actually unknown at node k (except for the first $M_k \times M_k$ identity matrix in $\mathbf{M}_B^{i^\star,k}$). As shown in Section 3.3, $\tilde{\mathbf{W}}_k^{i^\star+1}$ of node k can be computed via a transformation of the optimal solution $\tilde{\mathbb{Y}}_k$ of the following optimization problem:

$$\begin{aligned} \underset{\tilde{\mathbb{Y}}_k \in \mathbb{C}^{M_k+2R(K-1)\times R}}{\arg\max} \quad & \text{tr}\{\tilde{\mathbb{Y}}_k \mathbf{M}_B^{i^\star,k,H} \mathbf{J}_B^{k,H} \mathbf{R}_{\mathbf{yy}} \mathbf{J}_B^k \mathbf{M}_B^{i^\star,k} \tilde{\mathbb{Y}}_k\} \\ s.t. \quad & \tilde{\mathbb{Y}}_k^H \mathbf{M}_B^{i^\star,k,H} \mathbf{J}_B^{k,H} \mathbf{R}_{\mathbf{nn}} \mathbf{J}_B^k \mathbf{M}_B^{i^\star,k} \tilde{\mathbb{Y}}_k = \mathbf{I}_R \\ & \tilde{\mathbf{B}}_k^H \mathbf{M}_B^{i^\star,k,H} \mathbf{R}_{\mathbf{nn}} \mathbf{J}_B^k \mathbf{M}_B^{i^\star,k} \tilde{\mathbb{Y}}_k = \mathbf{0}. \end{aligned} \tag{B.21}$$

The last constraint can be written as

$$\text{Blkdiag}\{\mathbf{I}_{M_k}, \mathbf{G}_1^{i^\star,2}, ..., \mathbf{G}_{k-1}^{i^\star,2}, \mathbf{G}_{k+1}^{i^\star,2}, ..., \mathbf{G}_K^{i^\star,2}\} \mathbb{\Lambda}_B^{k,H} \mathbf{B}^H \mathbf{R}_{\mathbf{nn}} \mathbf{J}_B^k \mathbf{M}_B^{i^\star,k} \tilde{\mathbb{Y}}_k = \mathbf{0} \tag{B.22}$$

or equivalently (since $\mathbf{G}_k^{i^\star,2}$ are invertible matrices) as

$$\mathbb{\Lambda}_B^{k,H} \mathbf{B}^H \mathbf{R}_{\mathbf{nn}} \mathbf{J}_B^k \mathbf{M}_B^{i^\star,k} \tilde{\mathbb{Y}}_k = \mathbf{0}. \tag{B.23}$$

Since $\mathbf{M}_B^{i^\star,k}$ is non-singular, problem (B.21) is equivalent to problem (B.16) and as such Lemma B.4.1 gives the optimal solution of (B.21) via the relation

$$\mathbf{M}_B^{i^\star,k} \tilde{\mathbb{Y}}_k = \tilde{\mathbb{X}}_k = \begin{bmatrix} \mathbb{X}_{kk} \\ \mathbf{I}_{-k} \\ \mathbf{0}_{-k} \end{bmatrix}. \tag{B.24}$$

Since $\tilde{\mathbf{W}}_k^{i^\star+1}$ is given by a transformation of $\tilde{\mathbb{Y}}_k$, this implies

$$\tilde{\mathbf{W}}_k^{i^\star+1} = (\mathbf{M}_B^{i^\star,k})^{-1} \tilde{\mathbb{X}}_k \mathbf{G}_k^{i^\star+1} \tag{B.25}$$

with $\mathbf{G}_k^{i^\star+1}$ a transformation matrix. The first M_k rows of $\tilde{\mathbf{W}}_k^{i+1}$ can then be expressed as $\tilde{\mathbb{X}}_{kk}\mathbf{G}_k^{i^\star+1}$. Comparing this to (3.29), shows that $\mathbf{G}_k^{i^\star+1}$ can be

chosen equal to $\mathbf{G}_k$ such that the optimal solution (3.18) is obtained. Equation (B.25) is then equivalent to (3.42).

As similar procedure can be used to show the same result for $\tilde{\mathbf{\Lambda}}_k^{i^\star}$, which concludes the proof. □

B.5 Proof of Lemma B.4.1

Proof. As before, the Langrangian function $L(\tilde{\mathbb{X}}_k, \boldsymbol{M}, \tilde{\mathbb{\Lambda}}_k)$ [149] corresponding to the problem given in (B.16) can be written as:

$$\begin{aligned}\mathrm{tr}\{\tilde{\mathbb{X}}_k \mathbf{J}_B^{k,H} \mathbf{R}_{\mathbf{yy}} \mathbf{J}_B^k \tilde{\mathbb{X}}_k\} - \mathrm{tr}\{\tilde{\mathbb{\Lambda}}_k^H \mathbb{\Lambda}_B^{k,H} \mathbf{B}^H \mathbf{R}_{\mathbf{nn}} \mathbf{J}_B^k \tilde{\mathbb{X}}_k + \tilde{\mathbb{X}}_k^H \mathbf{J}_B^{k,H} \mathbf{R}_{\mathbf{nn}} \mathbf{B} \mathbb{\Lambda}_B^k \tilde{\mathbb{\Lambda}}_k\} \\ + \mathrm{tr}\{\boldsymbol{M}^H (\tilde{\mathbb{X}}_k^H \mathbf{J}_B^{k,H} \mathbf{R}_{\mathbf{nn}} \mathbf{J}_B^k \tilde{\mathbb{X}}_k - \mathbf{I}_R) + (\tilde{\mathbb{X}}_k^H \mathbf{J}_B^{k,H} \mathbf{R}_{\mathbf{nn}} \mathbf{J}_B^k \tilde{\mathbb{X}}_k - \mathbf{I}_R) \boldsymbol{M}\}.\end{aligned} \tag{B.26}$$

The KKT condition can then be defined as the following set of equations

$$\begin{aligned}\nabla_{\tilde{\mathbb{X}}_k^*} L =& \mathbf{J}_B^{k,H} \mathbf{R}_{\mathbf{yy}} \mathbf{J}_B^k \tilde{\mathbb{X}}_k - \mathbf{J}_B^{k,H} \mathbf{R}_{\mathbf{nn}} \mathbf{B} \mathbb{\Lambda}_B^k \tilde{\mathbb{\Lambda}}_k + \mathbf{J}_B^{k,H} \mathbf{R}_{\mathbf{nn}} \mathbf{J}_B^k \tilde{\mathbb{X}}_k (\boldsymbol{M} + \boldsymbol{M}^H) = \mathbf{0} \\ \nabla_{\boldsymbol{M}} L =& \tilde{\mathbb{X}}_k^H \mathbf{J}_B^{k,H} \mathbf{R}_{\mathbf{nn}} \mathbf{J}_B^k \tilde{\mathbb{X}}_k - \mathbf{I}_R = \mathbf{0} \\ \nabla_{\tilde{\mathbb{\Lambda}}_k^*} L =& \mathbb{\Lambda}_B^{k,H} \mathbf{B}^H \mathbf{R}_{\mathbf{nn}} \mathbf{J}_B^k \tilde{\mathbb{X}}_k = \mathbf{0}.\end{aligned} \tag{B.27}$$

Using (B.17) for $\tilde{\mathbb{X}}_k$ and (B.18) for $\tilde{\mathbb{\Lambda}}_k$, the equations can be transformed to

$$\begin{aligned}&\mathbf{J}_B^{k,H} \left(\mathbf{R}_{\mathbf{yy}} \mathbb{X} + \mathbf{R}_{\mathbf{nn}} \mathbb{X} (\boldsymbol{M} + \boldsymbol{M}^H) - \mathbf{R}_{\mathbf{nn}} \mathbf{B} \mathbb{\Lambda} \right) = \mathbf{0} \\ &\mathbb{X}^H \mathbf{R}_{\mathbf{nn}} \mathbb{X} - \mathbf{I}_R = \mathbf{0} \\ &\mathbb{\Lambda}_B^{k,H} \mathbf{B}^H \mathbf{R}_{\mathbf{nn}} \mathbb{X} = \mathbf{0}.\end{aligned} \tag{B.28}$$

The correctness of these equations can easily be verified since (3.24) holds for $\mathbb{X}$ and $\mathbb{\Lambda}$. Consequently, the same value for the (real) diagonal matrix $\boldsymbol{M}$ can be picked. Since for both problems (3.22) and (B.16), the objective is given by $\mathrm{tr}\{\boldsymbol{M}\}$, this shows that these problems are equivalent. □

Appendix C

Appendix to Chapter 7

C.1 Proof of Theorem 7.3.2

Proof. By using $\mathbf{h}_k = \hat{\mathbf{h}}_k + \tilde{\mathbf{h}}_k$ with $\hat{\mathbf{h}}_k$ and $\tilde{\mathbf{h}}_k$ independent random variables, the required expectations for Theorem 7.3.2 can be written as:

$$\begin{aligned} E\{\mathbf{v}_k^H \mathbf{h}_k\} &= E\{\mathbf{v}_k^H \hat{\mathbf{h}}_k\} + E\{\mathbf{v}_k^H \tilde{\mathbf{h}}_k\} \\ &= E\{\mathbf{v}_k^H \hat{\mathbf{h}}_k\} \end{aligned} \tag{C.1}$$

$$\begin{aligned} E\{|\mathbf{v}_k^H \mathbf{h}_i|^2\} &= E\{\mathbf{v}_k^H (\hat{\mathbf{h}}_i + \tilde{\mathbf{h}}_i)(\hat{\mathbf{h}}_i + \tilde{\mathbf{h}}_i)^H \mathbf{v}_k\} \\ &= E\{|\mathbf{v}_k^H \hat{\mathbf{h}}_i|^2\} + E\{\mathbf{v}_k^H \tilde{\mathbf{h}}_i \tilde{\mathbf{h}}_i^H \mathbf{v}_k\} \\ &= E\{|\mathbf{v}_k^H \hat{\mathbf{h}}_i|^2\} + E\{\mathbf{v}_k^H E\{\tilde{\mathbf{h}}_i \tilde{\mathbf{h}}_i^H\} \mathbf{v}_k\} \\ &= E\{|\mathbf{v}_k^H \hat{\mathbf{h}}_i|^2\} + E\{\mathbf{v}_k^H \mathbf{C}_i \mathbf{v}_k\} \\ &= E\{|\mathbf{v}_k^H \hat{\mathbf{h}}_i|^2\} + E\{\sum_{l=1}^{L} \mathbf{v}_{kl}^H \mathbf{C}_{il} \mathbf{v}_{kl}\} \\ &= E\{|\mathbf{v}_k^H \hat{\mathbf{h}}_i|^2\} + \sum_{l=1}^{L} E\{\mathbf{v}_{kl}^H \mathbf{C}_{il} \mathbf{v}_{kl}\} \end{aligned} \tag{C.2}$$

where in (C.1) and (C.2) independence between $\mathbf{v}_k$ and the zero-mean channel estimate $\tilde{\mathbf{h}}_k$ is used. Similarly, it is possible to rewrite the last expectation as

$$\begin{aligned} E\{|\mathbf{v}_k^H \mathbf{n}^{\mathrm{UL}}|^2\} &= E\{|\mathbf{v}_k^H \mathbf{n}^{\mathrm{UL}} \mathbf{n}^{\mathrm{UL},H} \mathbf{v}_k|^2\} \\ &= E\{\mathbf{v}_k^H E\{\mathbf{n}^{\mathrm{UL}} \mathbf{n}^{\mathrm{UL},H}\} \mathbf{v}_k\} \\ &= E\{\mathbf{v}_k^H \mathbf{R}_{\mathbf{nn}}^{\mathrm{UL}} \mathbf{v}_k\} \\ &= E\{\sum_{l=1}^{L} \mathbf{v}_{kl}^H \mathbf{R}_{\mathbf{n}_l \mathbf{n}_l}^{\mathrm{UL}} \mathbf{v}_{kl}\} \\ &= \sum_{l=1}^{L} E\{\mathbf{v}_{kl}^H \mathbf{R}_{\mathbf{n}_l \mathbf{n}_l}^{\mathrm{UL}} \mathbf{v}_{kl}\} \end{aligned} \tag{C.3}$$

where this time independence between $\mathbf{v}_k$ and the additive uplink noise vector $\mathbf{n}^{\mathrm{UL}}$ is used. □

Appendix D

Appendix to Chapter 8

D.1 Proof of (8.56)

Proof. Start by writing $\mathbf{R}_{\tau_k}^{-1}$ using the matrix inversion lemma:

$$\mathbf{R}_{\tau_k}^{-1} = \Big(\underbrace{\left(\mathbf{R}_{\tau_k} - \tau_p \mathbb{Q}_k^L \mathbb{\Sigma}_k^L \mathbb{Q}_k^L\right)}_{\mathbf{A}} + \tau_p \mathbb{Q}_k^L \mathbb{\Sigma}_k^L \mathbb{Q}_k^L \Big)^{-1} \tag{D.1}$$

$$= \mathbf{A}^{-1} - \mathbf{A}^{-1}\mathbb{Q}_k^L \left(\left(\tau_p \mathbb{\Sigma}_k^L\right)^{-1} + \mathbb{Q}_k^{L^H} \mathbf{A}^{-1} \mathbb{Q}_k^L \right)^{-1} \mathbb{Q}_k^{L^H} \mathbf{A}^{-1}.$$

Also note that

$$\mathbf{A}^{-1}\mathbb{Q}_k^L = \mathbf{R}_{\tau_k}^{-1}\mathbb{Q}_k^L \left(\mathbf{I}_{R^L} - \tau_p \mathbb{\Sigma}_k^L \mathbb{Q}_k^{L^H} \mathbf{R}_{\tau_k}^{-1} \mathbb{Q}_k^L \right)^{-1} \tag{D.2}$$

$$= \mathbf{R}_{\tau_k}^{-1}\mathbb{Q}_k^L \left(\mathbf{I}_{R^L} - \tau_p \mathbb{\Sigma}_k^L \right)^{-1}$$

and

$$\mathbb{Q}_k^{L^H} \mathbf{A}^{-1} \mathbb{Q}_k^L = \left(\mathbf{I}_{R^L} - \tau_p \mathbb{\Sigma}_k^L \right)^{-1} \tag{D.3}$$

which uses the fact that the columns in $\mathbb{Q}_k^L$ are normalized such that $\mathbb{Q}_k^{L^H} \mathbf{R}_{\tau_k}^{-1} \mathbb{Q}_k^L = \mathbb{Q}_k^{L^H} \mathbb{X}_k^L = \mathbf{I}_{R^L}$.

By substituting (D.2) and (D.3) in (D.1) and after some straightforward manipulations, the following identity is obtained:

$$\mathbf{R}_{\tau_k}^{-1} = \mathbf{A}^{-1} - \mathbf{R}_{\tau_k}^{-1}\mathbb{Q}_k^L \tau_p \mathbb{\Sigma}_k^L \left(\mathbf{I}_{R^L} - \tau_p \mathbb{\Sigma}_k^L \right)^{-1} \mathbb{Q}_k^{L^H} \mathbf{R}_{\tau_k}^{-1}. \tag{D.4}$$

Finally, by using

$$\begin{aligned} \mathbf{A}^{-1}\mathbf{Q}_k^B &\approx \mathbf{X}_k^B \\ \mathbf{R}_{\tau_k}^{-1}\mathbb{Q}_k^L &= \mathbb{X}_k^L \end{aligned} \tag{D.5}$$

and

$$\mathbf{R}_{\tau_k}^{-1}\mathbf{Q}_k^B \approx \mathbf{X}_k^B - \mathbb{X}_k^L \tau_p \mathbb{\Sigma}_k^L \left(\mathbf{I}_{R^L} - \tau_p \mathbb{\Sigma}_k^L\right)^{-1} \mathbb{X}_k^{L^H} \mathbf{Q}_k^B \tag{D.6}$$

in (8.56) and after rearranging, the desired result is obtained. □

D.2 Proof of Theorem 8.4.1

In this section, the convergence proof for the simplified (virtual) algorithm (VA) provided in Algorithm 12 is given. This is a simplified version of steps 1-4 and 6 of Algorithm 11 whenever the block diagonal quantities are kept constant during the algorithm and when the covariance matrices $\tilde{\mathbf{R}}_{\tau_k q}$ and $\tilde{\mathbf{R}}_{all_k q}$ are perfectly estimated. Theorem 8.4.1 will be proven for this algorithm, by linking Algorithm 12 to another VA for which convergence can be proven.

Before introducing the VA, it has to be marked that instead of performing a joint diagonalization as in (8.32) and computing $\mathbb{X}_k^L$ as $\mathbf{R}_{\tau_k}^{-1}\mathbb{Q}_k^L$, it is also possible to compute $\mathbb{X}_k^L$ directly from:

$$\mathbb{X}_k^L = \arg\min_{\mathbb{X}_k} \mathbb{X}_k^H (\mathbf{R}_{all_k} + (\tau_p - 1)\mathbf{R}_k^{B,\bar{n}})\mathbb{X}_k \tag{D.11}$$

$$s.t.\ \mathbb{X}_k^H \mathbf{R}_{\tau_k} \mathbb{X}_k = \mathbf{I}_{R^L}$$

where $\mathbb{\Sigma}_{all_k}^L = \mathbb{X}_k^{L^H} \mathbf{R}_{all_k} \mathbb{X}_k^L$. Note that $\mathbb{X}_k^L$ (without iteration index n) will be used to denote optimal solutions. $\mathbb{Q}_k^L$ can then be found as $\mathbf{R}_{\tau_k}\mathbb{X}_k^L$.

A VA that searches for the R^L generalized eigenvectors of $\{(\mathbf{R}_{all_k} + (\tau_p - 1)\mathbf{R}_k^{B,\bar{n}}), \mathbf{R}_{\tau_k}\}$ corresponding to the smallest generalized eigenvalues is provided in Algorithm 13. It is an alternating optimization algorithm with the following convergence property:

Theorem D.2.1. *For any initialization of Algorithm 13,* $\lim_{n\to\infty} \underline{\mathbb{X}}_k^{L,n+1}$ *exists, i.e., Algorithm 13 converges. Furthermore* $\mathbb{X}_k^{L,n+1}$ *converges to the same solution as* (D.11)*, i.e.,* $\lim_{n\to\infty} \underline{\mathbb{X}}_k^{L,n+1} = \mathbb{X}_k^L$*. Moreover* $\lim_{n\to\infty} \underline{\mathbb{\Sigma}}_{all_k}^{L,n} = \mathbb{\Sigma}_{all_k}^L$*.*

Proof. The proof can be constructed similarly to the proof of Theorem II in [101], albeit that there are a few key differences to be pointed out for

Algorithm 12: Simplified version of Algorithm 11

1 Set $n \leftarrow 0$, $q \leftarrow 1$ and initialize $\mathbf{F}_{kl}^{0}\ \forall l \in \mathcal{M}_k$ randomly.

2 Construct the AP-specific compression matrix $\check{\mathbf{J}}_{kq}^{n}$

$$\tilde{\mathbf{J}}_{kq}^{n} = \begin{bmatrix} \mathbf{0}_{(q-1)N \times N} & \mathbf{F}_{k,<q}^{n} \\ \mathbf{I}_N & \mathbf{0}_{N \times R^L} \\ \mathbf{0}_{(L_k-q)N \times N} & \mathbf{F}_{k,>q}^{n} \end{bmatrix} \tag{D.7}$$

with $\mathbf{F}_{k,<q}^{n} = [\mathbf{F}_{k1}^{n\,H} ... \mathbf{F}_{k,q-1}^{n\,H}]^H$, $\mathbf{F}_{k,>q}^{n} = [\mathbf{F}_{k,q+1}^{n\,H} ... \mathbf{F}_{kL_k}^{n\,H}]^H$.

3 AP q estimates $\tilde{\mathbf{R}}_{all_k q}, \tilde{\mathbf{R}}_{all_k q}^{B,n}$ and $\tilde{\mathbf{R}}_{\tau_k q}$ perfectly as

$$\begin{aligned} \tilde{\mathbf{R}}_{all_k q} &= \tilde{\mathbf{J}}_{kq}^{n\,H} \mathbf{R}_{all_k} \tilde{\mathbf{J}}_{kq}^{n} \\ \tilde{\mathbf{R}}_{kq}^{B,\bar{n}} &= \tilde{\mathbf{J}}_{kq}^{n\,H} \mathbf{R}_{k}^{B,\bar{n}} \tilde{\mathbf{J}}_{kq}^{n} \\ \tilde{\mathbf{R}}_{\tau_k q} &= \tilde{\mathbf{J}}_{kq}^{n\,H} \mathbf{R}_{\tau_k} \tilde{\mathbf{J}}_{kq}^{n}. \end{aligned} \tag{D.8}$$

4 Compute $\tilde{\mathbb{Q}}_{kq}^{L,n+1}, \tilde{\mathbb{\Sigma}}_{kq}^{L,n+1}, \tilde{\mathbb{\Sigma}}_{all_k q}^{L,n+1}, \tilde{\mathbb{X}}_{kq}^{L,n+1}$ and $\tilde{\mathbf{R}}_{kq}^{L,n+1}$ from the GEVD of $\{\tilde{\mathbf{R}}_{\tau_k q}, \tilde{\mathbf{R}}_{all_k q} + (\tau_p - 1)\tilde{\mathbf{R}}_{kq}^{B,n}\}$ similar as in (8.42) - (8.45).

5 Update the compression matrix as

$$\mathbf{F}_{kq}^{n+1} = \mathbb{X}_{kq}^{L,n+1} \left(\mathbb{X}_{k,-q}^{L,n+1}\right)^{-1} \tag{D.9}$$

which is equivalent to

$$\mathbf{F}_{k}^{n+1} = \tilde{\mathbf{J}}_{k}^{n} \tilde{\mathbb{X}}_{kq}^{L,n+1} \left(\mathbb{X}_{k,-q}^{L,n+1}\right)^{-1}. \tag{D.10}$$

6 $n \leftarrow n+1$ and $q \leftarrow (q \mod L_k) + 1$ and return to step 2.

completeness. Firstly, everywhere in the algorithm, $\mathbf{R_{yy}}$ and $\mathbf{R_{nn}}$ have to be replaced with $(\mathbf{R}_{all_k} + (\tau_p - 1)\mathbf{R}_{k}^{B,\bar{n}})$ and $\mathbf{R}_{\tau_k}$respectively. Secondly, instead of searching for the R^L generalized eigenvectors corresponding the the smallest generalized eigenvalues, a maximization in (D.15) is used to obtain the R^L generalized eigenvectors corresponding the the largest generalized eigenvalues. However, the proof is still valid if the words 'max', 'increase' and '$\geq$' (e.g., in $f(\underline{\mathbb{X}}^{i+1}) \geq f(\underline{\mathbb{X}}^{i})$) are merely replaced with 'min', 'decrease' and '$\leq$'. Finally, the algorithm in [101] defines the AP-specific compression matrix $\mathbf{J}_{kq}^{n}$ as

$$\mathbf{J}_{kq}^{n} = \begin{bmatrix} \mathbf{0} & \text{blkdiag}\{\underline{\mathbb{X}}_{k1}^{n} ... \underline{\mathbb{X}}_{k,q-1}^{n}\} & \mathbf{0}_{(q-1)N \times (L_k-q)N} \\ \mathbf{I}_N & \mathbf{0}_{N \times (q-1)N} & \mathbf{0}_{N \times (L_k-q)N} \\ \mathbf{0} & \mathbf{0}_{(L_k-q)N \times (q-1)N} & \text{blkdiag}\{\underline{\mathbb{X}}_{k,q+1}^{n} ... \underline{\mathbb{X}}_{kL_k}^{n}\} \end{bmatrix} \tag{D.12}$$

whereas here the compression matrix is defined as in (D.13). This has no further

impact on the provided arguments in the proof, so the proof is also valid for the compression matrix in (D.13). □

Algorithm 13: VA to estimate the R^L generalized eigenvectors

1 Set $n \leftarrow 0$, $q \leftarrow 1$ and initialize $\underline{\mathbb{X}}_{kl}^{L,0}$ $\forall l \in \mathcal{M}_k$ randomly.

2 Construct the AP-specific compression matrix $\breve{\mathbf{J}}_{kq}^{n}$

$$\breve{\mathbf{J}}_{kq}^{n} = \begin{bmatrix} \mathbf{0}_{(q-1)N \times N} & \underline{\mathbb{X}}_{k,<q}^{n} \\ \mathbf{I}_N & \mathbf{0}_{N \times R^L} \\ \mathbf{0}_{(L_k - q)N \times N} & \underline{\mathbb{X}}_{k,>q}^{n} \end{bmatrix}. \tag{D.13}$$

3 AP q estimates $\breve{\mathbf{R}}_{all_k q}, \breve{\mathbf{R}}_{all_k q}^{B,n}$ and $\breve{\mathbf{R}}_{\tau_k q}$ perfectly as

$$\begin{aligned} \breve{\mathbf{R}}_{all_k q} &= \breve{\mathbf{J}}_{kq}^{n\,H} \mathbf{R}_{all_k} \breve{\mathbf{J}}_{kq}^{n} \\ \breve{\mathbf{R}}_{kq}^{B,\bar{n}} &= \breve{\mathbf{J}}_{kq}^{n\,H} \mathbf{R}_{k}^{B,\bar{n}} \breve{\mathbf{J}}_{kq}^{n} \\ \breve{\mathbf{R}}_{\tau_k q} &= \breve{\mathbf{J}}_{kq}^{n\,H} \mathbf{R}_{\tau_k} \breve{\mathbf{J}}_{kq}^{n}. \end{aligned} \tag{D.14}$$

4 Compute $\breve{\underline{\mathbb{X}}}_{kq}^{L,n+1}$ as

$$\begin{aligned} \breve{\underline{\mathbb{X}}}_{kq}^{L,n+1} = \underset{\breve{\underline{\mathbb{X}}}_{kq}}{\arg\min}\ & \breve{\underline{\mathbb{X}}}_{kq}^{H} \left(\breve{\mathbf{R}}_{all_k} + (\tau_p - 1) \breve{\mathbf{R}}_{kq}^{B,\bar{n}} \right) \breve{\underline{\mathbb{X}}}_{kq} \\ s.t.\ & \breve{\underline{\mathbb{X}}}_{kq}^{H} \breve{\mathbf{R}}_{\tau_k} \breve{\underline{\mathbb{X}}}_{kq}. \end{aligned} \tag{D.15}$$

5 $\underline{\mathbb{X}}_{k}^{L,n+1} = \breve{\mathbf{J}}_{kq}^{n} \breve{\underline{\mathbb{X}}}_{kq}^{L,n+1}$ and $\underline{\mathbb{\Sigma}}_{all_k}^{L,n+1} = \breve{\underline{\mathbb{X}}}_{kq}^{L,n+1\,H} \left(\breve{\mathbf{R}}_{all_k} + (\tau_p - 1) \breve{\mathbf{R}}_{kq}^{B,\bar{n}} \right) \breve{\underline{\mathbb{X}}}_{kq}^{L,n+1}$.

6 $n \leftarrow n+1$ and $q \leftarrow (q \mod L_k) + 1$ and return to step 2.

The next lemma links Algorithm 12 to Algorithm 13.

Lemma D.2.2. *If Algorithm 12 and Algorithm 13 are initialized with the same matrix, i.e., $\underline{\mathbb{X}}_{kl}^{L,0} = \mathbf{F}_{kl}^{L,0}$ $\forall l$, then Algorithm 12 will produce the sequence*

$$\mathbf{F}_{k}^{n} = \underline{\mathbb{X}}_{k}^{L,n} \left(\mathbb{X}_{k,-q}^{L,n} \right)^{-1} \quad \forall n \in \mathbb{N}_0 \tag{D.16}$$

$$\tilde{\underline{\mathbb{\Sigma}}}_{all_k q}^{L,n} = \underline{\mathbb{\Sigma}}_{all_k}^{L,n} \qquad \forall n \in \mathbb{N}_0. \tag{D.17}$$

Using (D.10) *and Theorem D.2.2, this also implies that*

$$\lim_{n \to \infty} \tilde{\mathbf{J}}_{kq}^{n} \tilde{\mathbb{X}}_{kq}^{L,n} = \lim_{n \to \infty} \mathbf{F}_{k}^{n} \mathbb{X}_{k,-q}^{L,n} = \lim_{n \to \infty} \underline{\mathbb{X}}_{k}^{L,n} = \mathbb{X}_{k}^{L}. \tag{D.18}$$

Proof. By defining $\mathbb{X}_{k,-q}^{L,0} = \mathbf{I}_{R^L}$, the lemma holds for $n = 0$. The lemma will be proven using an inductive argument. To this end, it is assumed that the lemma holds up to iteration n with updating AP $\bar{q}$, i.e., $\mathbf{F}_k^n = \underline{\mathbb{X}}_k^n \left(\mathbb{X}_{k,-\bar{q}}^{L,n}\right)^{-1}$, from which it will be shown that $\mathbf{F}_k^{n+1} = \underline{\mathbb{X}}_k^{n+1} \left(\mathbb{X}_{k,-q}^{L,n+1}\right)^{-1}$ with q the next updating node. The following relation follows directly from (D.7) and (D.13):

$$\tilde{\mathbf{J}}_{kq}^n = \breve{\mathbf{J}}_{kq}^n \begin{bmatrix} \mathbf{I}_N & \mathbf{0}_{N\times R^L} \\ \mathbf{0}_{R^L\times N} & \left(\mathbb{X}_{k,-\bar{q}}^{L,n}\right)^{-1} \end{bmatrix}. \tag{D.19}$$

Since $\tilde{\mathbb{X}}_{kq}^{n+1}$ in step 2 of Algorithm 12 is the optimal solution of

$$\tilde{\mathbb{X}}_{kq}^{L,n+1} = \arg\min_{\tilde{\mathbb{X}}_{kq}} \tilde{\mathbb{X}}_{kq}^H \tilde{\mathbf{J}}_{kq}^{n\,H} \left(\mathbf{R}_{all_k} + (\tau_p - 1)\mathbf{R}_{kq}^{B,\bar{n}}\right) \tilde{\mathbf{J}}_{kq}^n \tilde{\mathbb{X}}_{kq}$$

$$s.t.\ \tilde{\mathbb{X}}_{kq}^H \tilde{\mathbf{J}}_{kq}^{n\,H} \mathbf{R}_{\tau_k} \tilde{\mathbf{J}}_{kq}^n \tilde{\mathbb{X}}_{kq} \tag{D.20}$$

and $\breve{\mathbb{X}}_{kq}^{L,n+1}$ is given by (D.15), the optimal solutions can be found using (D.19). The optimal solutions are then equal up to a certain matrix multiplication

$$\tilde{\mathbb{X}}_{kq}^{n+1} = \begin{bmatrix} \mathbf{I}_N & \mathbf{0}_{N\times R^L} \\ \mathbf{0}_{R^L\times N} & \mathbb{X}_{k,-\bar{q}}^{L,n} \end{bmatrix} \breve{\mathbb{X}}_{kq}^{n+1} \tag{D.21}$$

where the invertibility of $\mathbb{X}_{k,-q}^{L,n}$ is used.

As a consequence, $\mathbf{F}_k^{n+1}$ can be written as

$$\begin{aligned} \mathbf{F}_k^{n+1} &= \tilde{\mathbf{J}}_k^n \tilde{\mathbb{X}}_{kq}^{L,n+1} \left(\mathbb{X}_{k,-q}^{L,n+1}\right)^{-1} \\ &= \breve{\mathbf{J}}_k^n \breve{\mathbb{X}}_{kq}^{L,n+1} \left(\mathbb{X}_{k,-q}^{L,n+1}\right)^{-1} \\ &= \underline{\mathbb{X}}_k^{L,n+1} \left(\mathbb{X}_{k,-q}^{L,n+1}\right)^{-1} \end{aligned} \tag{D.22}$$

which proves the lemma by an induction argument.

The fact that $\tilde{\underline{\Sigma}}^{L,n}_{all_k q} = \underline{\Sigma}^{L,n}_{all_k}$ can easily be shown using

$$\begin{aligned}
\tilde{\underline{\Sigma}}^{L,n+1}_{all_k q} &= \tilde{\mathbb{X}}^{L,n+1^H}_{kq} \left(\tilde{\mathbf{R}}_{all_k} + (\tau_p - 1)\tilde{\mathbf{R}}^{B,\bar{n}}_{kq} \right) \tilde{\mathbb{X}}^{L,n+1}_{kq} \qquad \text{(D.23)} \\
&= \tilde{\mathbb{X}}^{L,n+1^H}_{kq} \tilde{\mathbf{J}}^{n^H}_{k} \left(\mathbf{R}_{all_k} + (\tau_p - 1)\mathbf{R}^{B,\bar{n}}_{kq} \right) \tilde{\mathbf{J}}^{n}_{k} \tilde{\mathbb{X}}^{L,n+1}_{kq} \\
&= \breve{\mathbb{X}}^{L,n+1^H}_{kq} \breve{\mathbf{J}}^{n^H}_{k} \left(\mathbf{R}_{all_k} + (\tau_p - 1)\mathbf{R}^{B,\bar{n}}_{kq} \right) \breve{\mathbf{J}}^{n}_{k} \breve{\mathbb{X}}^{L,n+1}_{kq} \\
&= \breve{\mathbb{X}}^{L,n+1^H}_{kq} \left(\breve{\mathbf{R}}_{all_k} + (\tau_p - 1)\breve{\mathbf{R}}^{B,\bar{n}}_{kq} \right) \breve{\mathbb{X}}^{L,n+1}_{kq} \\
&= \underline{\Sigma}^{L,n+1}_{all_k}.
\end{aligned}$$

□

Lemma D.2.2 partly proves Theorem 8.4.1. It only remains to show that $\lim_{n\to\infty} \mathbb{Q}^{L,n+1}_k = \hat{\mathbb{Q}}^L_k$ which can be proven as follows [236]:

$$\begin{aligned}
\lim_{n\to\infty} \tilde{\mathbb{Q}}^{L,n+1}_{kq} &= \lim_{n\to\infty} \tilde{\mathbf{R}}_{\tau_k q} \tilde{\mathbb{X}}^{L,n}_{kq} \\
&= \lim_{n\to\infty} \tilde{\mathbf{J}}^{n}_{kq} \mathbf{R}_{\tau_k} \tilde{\mathbf{J}}^{n}_{kq} \tilde{\mathbb{X}}^{L,n}_{kq}. \qquad \text{(D.24)}
\end{aligned}$$

Theorem D.2.2 then shows that, upon convergence, $\mathbb{X}^L_k = \tilde{\mathbf{J}}^{n}_{kq} \tilde{\mathbb{X}}^{L,n}_{kq}$. (D.24) can thus be written as

$$\begin{aligned}
\lim_{n\to\infty} \tilde{\mathbb{Q}}^{L,n+1}_{kq} &= \lim_{n\to\infty} \tilde{\mathbf{J}}^{n}_{kq} \mathbf{R}_{\tau_k} \mathbb{X}^L_k \\
&= \lim_{n\to\infty} \tilde{\mathbf{J}}^{n}_{kq} \mathbb{Q}^L_k. \qquad \text{(D.25)}
\end{aligned}$$

Selecting the first N rows of (D.25) $\forall q$ then gives the desired result.

Appendix E

GEVD-based low-rank MMSE channel estimation for uplink cellular mMIMO systems

GEVD-based Low-Rank Channel Covariance Matrix Estimation and MMSE Channel Estimation for Uplink Cellular Massive MIMO Systems.

Robbe Van Rompaey and Marc Moonen

Published in
Proceedings of the *2022 30th European Signal Processing Conference (EUSIPCO)*, Belgrado, Serbia, 2022, pp. 1-5.

©2022 IEEE Reprint, with permission from:
R. Van Rompaey and M. Moonen, "GEVD-based Low-Rank Channel Covariance Matrix Estimation and MMSE Channel Estimation for Uplink Cellular Massive MIMO Systems" in *2022 30th European Signal Processing Conference (EUSIPCO)*, Belgrado, Serbia, pp. 1-5, 2022.
Changes include layout, representation and minor editing aspects.
The candidate's contributions as first author include all performed research and writing of the article under guidance of the co-author.

Abstract

Uplink channel estimation is a crucial component for the performance of cellular massive MIMO systems. However, when the number of user equipments (UEs) grows, the sharing of the available resources causes interference between UEs in neighboring cells. Minimum mean squared error (MMSE) channel estimators have been proposed to mitigate this interference, but these require estimates of the channel covariance matrices. Therefore, a new channel covariance matrix estimator for low-rank channel covariance matrices is presented in this paper, using a generalized eigenvalue decomposition (GEVD) of two covariance matrices that can be estimated from the available uplink data. The requirements for the systems are minimal and, except for synchronization, there is no need for communication between the different cells and no prior knowledge on the background noise is required. Approximate MMSE estimators are also derived based on the newly proposed channel covariance matrix estimator. The effectiveness of the proposed methods is demonstrated in numerical simulations.

Keywords Covariance matrix estimation, random pilot allocation, low-rank channel model, generalized eigenvalue decomposition (GEVD), massive MIMO

E.1 Introduction

Massive MIMO (multiple input multiple output) is a key technology for current generation cellular networks [19, 176, 185]. Base stations (BSs) are deploying hundreds of antennas, enabling spatial multiplexing of several user equipments (UEs) per cell, both in uplink and downlink, with simple linear signal processing methods [237]. The increasing number of UEs, and as a consequence the sharing of the available pilots whenever the coherence blocks are limited in size, causes interference between UEs in neighboring cells. To make it possible for a BS to separate the UEs that it serves from the interference, second-order statistical information present in the channel covariance matrices has to be exploited during the channel estimation.

The channel covariance matrices are commonly assumed to be perfectly known in massive MIMO literature, which is a strong assumption since the matrix dimension grows with the number of antennas and furthermore the statistics are changing over time. Existing covariance matrix estimators either use additional pilot overhead, sacrifice samples for data transmission [179], use strong separability conditions that might not always hold [202] or require knowledge of the used pilots of all the UEs in the network [166, 178]. Therefore, a new channel covariance matrix estimator for low-rank channel covariance matrices is presented in this paper, using a generalized eigenvalue decomposition (GEVD) of two covariance matrices that can be estimated from the available uplink data. The requirements for the system are minimal and, except for synchronization, there is no need for communication between the different cells and no prior knowledge on the background noise is required. Approximate MMSE estimators are also derived based on the newly proposed channel covariance matrix estimator. The effectiveness of the proposed methods is demonstrated in numerical simulations.

E.2 Channel and signal model

E.2.1 Channel model

A cellular massive MIMO system with L cells is considered where each cell contains a BS with N antennas and K single-antenna UEs. The channel from UE k in cell l to the BS in cell j is denoted by $\mathbf{h}_{jlk} \in \mathbb{C}^N$ and is assumed to remain constant during a coherence block of τ_c samples. Superscript $.^t$ will be used to denote the quantities in coherence block t, e.g., $\mathbf{h}_{jkl}^t$. A common channel model for $\mathbf{h}_{jkl}^t$ is that it is drawn from a correlated Rayleigh fading

realization $\mathcal{NC}(\mathbf{0}, \overline{\mathbf{R}}_{jlk})$, where $\overline{\mathbf{R}}_{jlk} \in \mathbb{C}^{N \times N}$ is the positive semi-definite channel covariance matrix describing the large-scale fading, including geometric pathloss, shadowing, antenna gains, and spatial channel correlation [7]. The complex Gaussian distribution around $\overline{\mathbf{R}}_{jlk}$ models the small-scale fading. Due to the different positions of the UEs, it is assumed that the channels for different UEs are uncorrelated, i.e., $E\{\mathbf{h}_{jlk}^{t}\mathbf{h}_{jmi}^{t,H}\} = \mathbf{0}$ if $\{l,k\} \neq \{m,i\}$, where $E\{.\}$ denotes the expected value operator, with respect to different channel realizations and $.^H$ is the Hermitian transpose operator. Measurements in [238] show that the matrices $\{\overline{\mathbf{R}}_{jlk}\}$ remain constant over several thousands of coherence blocks, where this large number is denoted by T.

The scattering is mostly localized around the UE, since the BSs are elevated and hence have limited scattering in their near-field [166]. The multipath components defining the total channel $\mathbf{h}_{jlk}$ are therefor arriving from a specific localized region in the network, so that the matrices $\{\overline{\mathbf{R}}_{jlk}\}$ can be approximated by low-rank matrices, where the rank is denoted by R. $\overline{\mathbf{R}}_{jlk}$ can thus be approximated as a sum of R rank-1 terms:

$$\overline{\mathbf{R}}_{jlk} = \sum_{r=1}^{R} \overline{\mathbf{q}}_{jlk,r}\overline{\mathbf{q}}_{jlk,r}^{H} \tag{E.1}$$

where $\overline{\mathbf{q}}_{jlk,r}$ will be defined later. This implies that the channel $\mathbf{h}_{jlk}^{t}$ in coherence block t can be modeled as

$$\mathbf{h}_{jlk}^{t} = \sum_{r=1}^{R} \overline{\mathbf{q}}_{jlk,r}\overline{z}_{jlk,r}^{t} = \overline{\mathbb{Q}}_{jlk}\overline{\mathbf{z}}_{jlk}^{t} \tag{E.2}$$

where the normal complex variables $\overline{\mathbf{z}}_{jlk}^{t} = [\overline{z}_{jlk,1}^{t} \ ... \ \overline{z}_{jlk,R}^{t}]^T$ with $.^T$ the transpose operator, are independently drawn from $\mathcal{NC}(0,1)$ and $\overline{\mathbb{Q}}_{jlk} = [\overline{\mathbf{q}}_{jlk,1} \cdots \overline{\mathbf{q}}_{jlk,R}]$.

E.2.2 Signal model

The samples in one coherence block of τ_c samples are divided in τ_p samples for uplink channel estimation and τ_u samples for uplink data transmission with $\tau_c = \tau_p + \tau_u$. With τ_p samples available, the network can predefine τ_p different orthogonal and unitary pilot sequences $\{\mathbf{s}_b\}$ where

$$\mathbf{s}_b = [s_b(1) \ ... \ s_b(\tau_p)]^T, \ b = 1...\tau_p \tag{E.3}$$

with $\mathbf{s}_b^H\mathbf{s}_b = \tau_p$ and $\mathbf{s}_b^H\mathbf{s}_c = 0$ if $b \neq c$. In the uplink channel estimation phase, each UE k in each cell l selects randomly one of the τ_p pilot sequences in each

		Coherence block															
		1				2				3				...	T			
		$\mathbf{s}_1$	$\mathbf{s}_2$	$\mathbf{s}_3$	$\mathbf{s}_4$	$\mathbf{s}_1$	$\mathbf{s}_2$	$\mathbf{s}_3$	$\mathbf{s}_4$	$\mathbf{s}_1$	$\mathbf{s}_2$	$\mathbf{s}_3$	$\mathbf{s}_4$	...	$\mathbf{s}_1$	$\mathbf{s}_2$	$\mathbf{s}_3$	$\mathbf{s}_4$
UE	1													...				
	2													...				
	3													...				
	4													...				
	...		...				...				...			...		...		
	K													...				

Table E.1: Example of random allocation of 4 pilot sequences over K UEs in a certain cell.

coherence block t , the index of this pilot sequence is denoted by b_{lk}^t. An example is provided in Table E.1. The UEs transmits the chosen pilot sequence with powers $\{p_{lk}\}$. The signal received at BS j is then given as

$$\mathbf{y}_j^t(p) = \sum_{l=1}^{L} \sum_{k=1}^{K} \sqrt{p_{lk}} \mathbf{h}_{jlk}^t s_{b_{lk}^t}(p) + \mathbf{n}_j^t(p), \ p = 1...\tau_p \tag{E.4}$$

where p is the sample index and $\mathbf{n}_j^t(p)$ is the background noise at BS j.

In the uplink data transmission phase, each UE k in each cell l transmits the unitary signal $s_{lk}(u)$ with zero mean and power p_{lk}. The received signal at BS j is then given as

$$\mathbf{y}_j^t(u) = \sum_{l=1}^{L} \sum_{k=1}^{K} \sqrt{p_{lk}} \mathbf{h}_{jlk}^t s_{lk}(u) + \mathbf{n}_j^t(u), \ u = 1...\tau_u. \tag{E.5}$$

Note that the indices p and u are used to distinguish between the different phases. BS j has to detect the uplink data from the UEs in its cell, i.e., $s_{jk}(u)$ for $k = 1...K$. To perform receive combining strategies like maximum-ratio (MR), (regularized) zero-forcing (RZF) or minimum mean squared error (MMSE) combining [7, 125], good estimates of the channels of the K UEs in cell j are required. The background noise $\mathbf{n}_j^t$ is assumed to be zero-mean complex Gaussian, but with an unknown spatial covariance matrix $\overline{\mathbf{R}}_{\mathbf{n}_j\mathbf{n}_j} = E\{\mathbf{n}_j^t \mathbf{n}_j^{t,H}\}$. It is often assumed to be white noise with a diagonal covariance matrix, but here a more general noise model is used, where the noise can be correlated between the antennas of a BS. This happens for example when there are located jamming signals nearby the BS.

E.3 Optimal MMSE channel estimation

The signal obtained from (E.4) after despreading with pilot sequence b_{jk}^t can be represented as

$$\mathbf{y}_j^{t,\text{pilot}}[b_{jk}^t] = \sum_{u=1}^{\tau_p} \mathbf{y}_j^t(p) s_{b_{jk}^t}^*(p) \tag{E.6}$$

$$= \sum_{l=1}^{L}\sum_{i=1}^{K} \delta_{jk,li}^t \sqrt{p_{li}}\tau_p \mathbf{h}_{jli}^t + \underbrace{\sum_{u=1}^{\tau_p} \mathbf{n}_j^t(p) s_{b_{jk}^t}^*(p)}_{\mathbf{n}_j^{t,\text{pilot}}[b_{jk}^t]}$$

where the random variable $\delta_{jk,li}^t$ is 1 with probability $1/\tau_p$ and 0 otherwise since all other UEs randomly pick 1 of the τ_p pilot sequences and $\delta_{jk,jk}^t$ is deterministic and equal to 1.

Based on the despread signal in (E.6) a linear MMSE channel estimation criterion, similar to [72, Sect. 4.2], can be defined to obtain an estimate $\overline{\mathbf{h}}_{jjk}^t = \overline{\mathbf{W}}_{jk}^H \mathbf{y}_j^{t,\text{pilot}}[b_{jk}^t]$ of $\mathbf{h}_{jjk}^t$ in the current coherence block t:

$$\overline{\mathbf{W}}_{jk} = \arg\min_{\boldsymbol{W}_{jk}} E\{||\mathbf{h}_{jjk}^t - \boldsymbol{W}_{jk}^H \mathbf{y}_j^{t,\text{pilot}}[b_{jk}^t]||^2\}. \tag{E.7}$$

The optimal solution of (E.7) is given as

$$\overline{\mathbf{W}}_{jk} = \sqrt{p_{jk}} \left(\overline{\mathbf{R}}_{jjk}^{\text{pilot}}\right)^{-1} \overline{\mathbf{R}}_{jjk} \tag{E.8}$$

where

$$\overline{\mathbf{R}}_{jjk}^{\text{pilot}} = \frac{1}{\tau_p} E\{\mathbf{y}_j^{t,\text{pilot}}[b_{jk}^t] \mathbf{y}_j^{t,\text{pilot},H}[b_{jk}^t]\} \tag{E.9}$$

$$= p_{jk}\tau_p \overline{\mathbf{R}}_{jjk} + \sum_{i\neq k} p_{ji} \overline{\mathbf{R}}_{jji} + \sum_{l\neq j}\sum_{i=1}^{K} p_{li} \overline{\mathbf{R}}_{jli} + \overline{\mathbf{R}}_{\mathbf{n}_j\mathbf{n}_j}$$

since the channels between different UEs are uncorrelated and are also uncorrelated with the background noise. The fact that $E\{\delta_{jk,li}^{t^2}\} = \frac{1}{\tau_p}$ is also used. For the background noise term, the following derivation is used:

$$E\{\mathbf{n}_j^{t,\text{pilot}}[b_{jk}^t] \mathbf{n}_j^{t,\text{pilot},H}[b_{jk}^t]\} = E\left\{ \left(\sum_{u=1}^{\tau_p} \mathbf{n}_j^t(p) s_{b_{jk}^t}^*(p)\right) \left(\sum_{u=1}^{\tau_p} \mathbf{n}_j^{t,H}(p) s_{b_{jk}^t}(p)\right)^H \right\}$$

$$= \sum_{u=1}^{\tau_p} E\{|s_{b_{jk}^t}(p)|^2\} E\{\mathbf{n}_j^t \mathbf{n}_j^{t,H}\} = \tau_p \overline{\mathbf{R}}_{\mathbf{n}_j\mathbf{n}_j}$$

where the cross terms in the second step are zero since the noise is uncorrelated between different samples.

An important difference with the MMSE channel estimation method proposed in [72, Sect. 4.1,] is that now all UEs appear as interfering UEs in (E.9), while in [72] it is assumed that the pilot sequences for all the UEs are predetermined and fixed, so that only UEs sharing the same pilot sequence appear as interfering UEs. However, this assumption requires prior knowledge of the channel statistics of all the UEs and the background noise, while the proposed method allows for a more efficient estimation method which will be discussed next.

E.4 Low-rank channel estimation

E.4.1 Low-rank covariance matrix estimator

In practice the covariance matrices $\overline{\mathbf{R}}_{jjk}^{\text{pilot}}$ and $\overline{\mathbf{R}}_{jjk}$ have to be estimated from the available data. $\overline{\mathbf{R}}_{jjk}^{\text{pilot}}$ can be estimated using time averaging over the last T coherence blocks, possibly using a diagonal regularizer as in [179, 239], since perfect synchronization and knowledge of b_{jk}^t at the BS j is assumed. The fact that a BS needs to know the pilot sequences of a user can simply be implemented by defining infinitely many (pseudo)-random sequences (that can for example be constructed using a pseudo-random number generator with a seed) and letting the user pick one during a start-up phase. No other communication is then needed afterwards. The estimation will be denoted as $\mathbf{R}_{jjk}^{\text{pilot}}$ (without the overline). $\overline{\mathbf{R}}_{jjk}$ as in (E.1) can not immediately be estimated, since the channel is unknown. However, the combined covariance matrix $\mathbf{R}_j^{\text{all}}$ can be estimated from all available antenna signals during both the channel estimation phase and uplink data transmission phase, which is an estimate of

$$\begin{aligned}\overline{\mathbf{R}}_j^{\text{all}} &= E\left\{\frac{1}{\tau_p}\sum_{p=1}^{\tau_p}\mathbf{y}_j^t(p)\mathbf{y}_j^{t,H}(p)+\frac{1}{\tau_u}\sum_{u=1}^{\tau_u}\mathbf{y}_j^t(u)\mathbf{y}_j^{t,H}(u)\right\}\\ &= \sum_{l=1}^{L}\sum_{i=1}^{K}p_{li}\overline{\mathbf{R}}_{jli}+\overline{\mathbf{R}}_{\mathbf{n}_j\mathbf{n}_j}. \end{aligned} \tag{E.10}$$

When comparing (E.9) and (E.10), it can be stated that $\overline{\mathbf{R}}_{jjk}^{\text{pilot}}$ is the covariance matrix estimated after despreading and $\overline{\mathbf{R}}_j^{\text{all}}$ is the covariance matrix estimated before despreading. They differ only in a contribution depending on $\overline{\mathbf{R}}_{jjk}$. The

following relation can thus be derived:

$$p_{jk}\overline{\mathbf{R}}_{jjk} = \frac{1}{\tau_p - 1}\left(\overline{\mathbf{R}}_{jjk}^{\text{pilot}} - \overline{\mathbf{R}}_{j}^{\text{all}}\right). \tag{E.11}$$

However, simply replacing $\overline{\mathbf{R}}_{jjk}^{\text{pilot}}$ and $\overline{\mathbf{R}}_{j}^{\text{all}}$ with the estimated quantities $\mathbf{R}_{jjk}^{\text{pilot}}$ and $\mathbf{R}_{j}^{\text{all}}$ in (E.11) will not result in a good estimate $\mathbf{R}_{jjk}$ of $\overline{\mathbf{R}}_{jjk}$ since it will generally not satisfy the assumed rank assumption in (E.1) and might even result in an indefinite estimate $\mathbf{R}_{jjk}$. One known remedy consists in using a rank-approximation based on the GEVD [110, 148] of the matrix pencil $\{\mathbf{R}_{jjk}^{\text{pilot}}, \mathbf{R}_{j}^{\text{all}}\}$ given as

$$\mathbf{R}_{jjk}^{\text{pilot}} = \mathbf{Q}_{jjk}\mathbf{\Sigma}_{jjk}\mathbf{Q}_{jjk}^{H} = \sum_{r=1}^{N}\sigma_{jjk,r}\mathbf{q}_{jjk,r}\mathbf{q}_{jjk,r}^{H} \tag{E.12}$$

$$\mathbf{R}_{j}^{\text{all}} = \mathbf{Q}_{jjk}\mathbf{Q}_{jjk}^{H} = \sum_{r=1}^{N}\mathbf{q}_{jjk,r}\mathbf{q}_{jjk,r}^{H} \tag{E.13}$$

where $\mathbf{\Sigma}_{jjk} = \text{diag}\{\sigma_{jjk,1}, ..., \sigma_{jjk,N}\}$ is a diagonal matrix with the generalized eigenvalues sorted from large to small and the columns of $\mathbf{X}_{jjk} = \mathbf{Q}_{jjk}^{-H}$ contain the generalized eigenvectors. The eigenvectors are normalized such that $\mathbf{X}_{jjk}^{H}\mathbf{R}_{j}^{\text{all}}\mathbf{X}_{jjk} = \mathbf{I}$. The optimal rank R estimate $\mathbf{R}_{jjk}$ is given by keeping only the rank-1 terms belonging to the R largest eigenvalues greater than one in (E.11)

$$p_{jk}\mathbf{R}_{jjk} = \sum_{r=1}^{R}\frac{\sigma_{jjk,r} - 1}{\tau_p - 1}\mathbf{q}_{jjk,r}\mathbf{q}_{jjk,r}^{H} = \mathbb{Q}_{jjk}\mathbb{\Lambda}_{jjk}\mathbb{Q}_{jjk}^{H} \tag{E.14}$$

where $\mathbb{\Lambda}_{jjk} = \text{diag}\{\frac{\sigma_{jjk,1}-1}{\tau_p-1}, ..., \frac{\sigma_{jjk,R}-1}{\tau_p-1}\}$.

As stated in [110], the GEVD-based approximation effectively selects the modes with the highest SINR, since approximation errors are weighted relative to the interference and noise aggregated in $\mathbf{R}_{j}^{\text{all}}$. Also note that unlike other rank-approximations of (E.11), the GEVD-based approximation is immune to scaling and linear combining of the signals, i.e., the output signal and output SINR is independent of such scaling and combining, which is a desirable property.

The proposed covariance matrix estimator is data-driven and requires only synchronization and knowledge of the chosen pilot sequence b_{jk}^{t} of the UEs in cell j in each coherence block. There is no need for prior knowledge of $\overline{\mathbf{R}}_{jjk}$ (except for the rank R of $\overline{\mathbf{R}}_{jjk}$), $\overline{\mathbf{R}}_{\mathbf{n}_j\mathbf{n}_j}$, or any prior knowledge on the statistics or pilot sequences of the UEs in other cells $l \neq j$.

E.4.2 Low-rank approximate MMSE estimator

When the estimated quantities are used to calculate the filter in (E.7), the following filter is obtained:

$$\begin{aligned}\mathbf{W}_{jk} &= \sqrt{p_{jk}} \left(\mathbf{Q}_{jjk} \mathbf{\Sigma}_{jjk} \mathbf{Q}_{jjk}^H \right)^{-1} \frac{1}{p_{jk}} \mathbb{Q}_{jjk} \mathbb{\Lambda}_{jjk} \mathbb{Q}_{jjk}^H \\ &= \frac{1}{\sqrt{p_{jk}}} \mathbb{X}_{jjk} \mathbb{\Upsilon}_{jjk} \mathbb{Q}_{jjk}^H \end{aligned} \tag{E.15}$$

where $\mathbb{\Upsilon}_{jjk} = \frac{1}{\tau_p - 1} \text{diag}\{ \frac{\sigma_{jjk,1} - 1}{\sigma_{jjk,1}}, ..., \frac{\sigma_{jjk,R} - 1}{\sigma_{jjk,R}} \} = \text{diag}\{ \upsilon_{jjk,1}, ..., \upsilon_{jjk,R} \}$ and $\mathbb{X}_{jjk} = [\mathbf{x}_{jjk,1} \ ... \ \mathbf{x}_{jjk,R}]$ contains the first R columns of $\mathbf{X}_{jjk}$. The final low-rank approximate MMSE estimate for the channel of UE k in coherence block t is then given as

$$\begin{aligned}\hat{\mathbf{h}}_{jjk}^t &= \mathbf{W}_{jk}^H \mathbf{y}_j^{t,\text{pilot}}[b_{jk}^t] = \frac{1}{\sqrt{p_{jk}}} \mathbb{Q}_{jjk} \mathbb{\Upsilon}_{jjk} \mathbb{X}_{jjk}^H \mathbf{y}_j^{t,\text{pilot}}[b_{jk}^t] \\ &= \frac{1}{\sqrt{p_{jk}}} \sum_{r=1}^{R} \mathbf{q}_{jjk,r} \underbrace{\upsilon_{jjk,r} \left(\mathbf{x}_{jjk,r}^H \mathbf{y}_j^{t,\text{pilot}}[b_{jk}^t] \right)}_{z_{jjk,r}^t}. \end{aligned} \tag{E.16}$$

Comparing this expression for $\hat{\mathbf{h}}_{jjk}^t$ with the model used for $\mathbf{h}_{jjk}^t$ in (E.2), it can be observed that the estimation method produces an estimate that exactly fits in this model. The random variable $\bar{\mathbf{z}}_{jjk}^t$ of (E.2) is estimated from the despread signal $\mathbf{y}_j^{t,\text{pilot}}[b_{jk}^t]$ using a simple inner-product with the corresponding eigenvector $\mathbf{x}_{jjk,r}$ and some scalars depending on the generalized eigenvalues.

E.4.3 Improved low-rank approximate MMSE estimator

An improved low-rank approximate MMSE estimator can be derived based on (E.6). When computing the expectation in (E.7), the activity of all the UEs is represented by the random variable $\delta_{jk,li}^t$. Since BS j is aware of the used pilot sequences of the UEs in its cell, this information can be used to improve the MMSE estimator:

$$\mathbf{y}_j^{t,\text{pilot,impr}}[b_{jk}^t] = \sum_{i=1}^{K} \bar{\delta}_{jk,ji}^t \sqrt{p_{ji}} \tau_p \mathbf{h}_{jji}^t + \sum_{l \neq j} \sum_{i=1}^{K} \delta_{jk,li}^t \sqrt{p_{li}} \tau_p \mathbf{h}_{jli}^t + \mathbf{n}_j^{t,\text{pilot}}[b_{jk}^t] \tag{E.17}$$

where $\bar{\delta}^t_{jk,ji}$ is now deterministic and either equal to 0 or 1 and $\bar{\delta}^t_{jk,jk} = 1$. The corresponding cell-specific covariance matrix that now depends on the coherence block index t is given as (alternative to (E.9))

$$\begin{aligned}\overline{\mathbf{R}}^{\text{pilot,impr,t}}_{jjk} &= \frac{1}{\tau_p} E\{\mathbf{y}^{t,\text{pilot,impr}}_j[b^t_{jk}]\mathbf{y}^{t,\text{pilot,impr},H}_j[b^t_{jk}]\} \\ &= \sum_{i=1}^{K} \bar{\delta}^{t^2}_{jk,ji} p_{ji}\tau_p \overline{\mathbf{R}}_{jji} + \sum_{l\neq j}\sum_{i=1}^{K} p_{li}\overline{\mathbf{R}}_{jli} + \overline{\mathbf{R}}_{\mathbf{n}_j\mathbf{n}_j} \\ &= \overline{\mathbf{R}}^{\text{pilot}}_{jjk} + \sum_{i\neq k}(\bar{\delta}^{t^2}_{jk,ji}\tau_p - 1)p_{ji}\overline{\mathbf{R}}_{jji}\end{aligned} \tag{E.18}$$

where $\overline{\mathbf{R}}^{\text{pilot}}_{jjk}$ is defined as in (E.9). By replacing the covariance matrices $\overline{\mathbf{R}}^{\text{pilot}}_{jjk}$ and $\overline{\mathbf{R}}_{jji}$ with their estimated quantities as explained in Subsection E.4.1, an improved low-rank approximate MMSE estimate $\hat{\mathbf{h}}^{t,\text{impr}}_{jjk} = \mathbf{W}^{\text{impr},t,H}_{jk}\mathbf{y}^{t,\text{pilot,impr}}_j[b^t_{jk}]$ can be obtained where

$$\mathbf{W}^{\text{impr},t}_{jk} = \left(\mathbf{R}^{\text{pilot}}_{jjk} + \sum_{i\neq k}(\bar{\delta}^{t^2}_{jk,ji}\tau_p - 1)p_{ji}\mathbf{R}_{jji}\right)^{-1}\mathbf{R}_{jjk}. \tag{E.19}$$

Although this estimator uses more of the information available at BS j, it is important to note that the provided improved low-rank approximate MMSE estimator requires an extra matrix inversion for each UE in its cell, while this is not required for the low-rank approximate MMSE estimator of Subsection E.4.2.

E.5 Numerical simulations

The same multicell setup with $L = 7$ hexagonal cells as in [178,179] is considered. There are $K = 10$ UEs per cell in a ring around the BS (there are 70 UEs in total) and each BS has a uniform linear array with $N = 100$ antennas. The multipath components from a UE arrive uniformly distributed in an angular interval (10°) centered around the geographical angle to the UE [240]. This results in channel covariance matrices with approximately 25 dominant eigenvalues.

The normalized MSE (NMSE) (averaged over 20 Monte-Carlo runs), $E\{||\mathbf{h}_{jjk} - \hat{\mathbf{h}}_{jjk}||^2\}/\text{tr}\{\overline{\mathbf{R}}_{jjk}\}$, for an average UE in the center cell is used as a performance metric. The proposed low-rank approximate MMSE estimator is calculated for different ranks: $R = 30$ and $R = 60$, denoted with *GEVD 30* and *GEVD*

60 respectively, and also when the subtraction in (E.11) is used instead of the GEVD to estimate the channel covariance matrices, denoted with *SUBT*. The performance of the MMSE estimator with perfect channel covariance matrix knowledge (*MMSE random*) in (E.8) is also shown. Similar results are shown for the proposed improved approximate MMSE estimator, denoted with the word *impr*. As baseline, the simple least-square estimation (*LS fixed*) that does not require covariance matrix information is shown in a scenario where each UE is allocated with a fixed pilot sequence for all coherence blocks [179]. Also the MMSE estimate with perfect channel covariance matrix knowledge (*MMSE fixed*) for the fixed pilot allocation regime is provided as absolute lower bound.

Figure E.1 shows that a relative small number of coherence blocks (300) suffices to obtain an accurate channel estimate for the proposed methods. The estimators with a rank constraint on the channel covariance matrix outperform the estimators without the rank constraint (SUBT) and $R = 30$ works better for the current setup than $R = 60$, since it can already capture the dominant eigenspace. The proposed GEVD-based procedure focuses on the modes with the highest power in the estimated covariance matrices and neglect the other modes, that typically contain more estimation error noise than useful signal power. The improved approximate MMSE estimator is also outperforming the approximate MMSE estimator when there are enough coherence blocks available for the estimation procedure. Since all the estimates of the channel covariance matrices are used to calculate the filter in (E.19), this will only perform well when they are estimated using enough samples. Although not shown in Figure E.1, it should be noted that the *SUBT*-curve will converge to the *MMSE fixed*-curve when $T \to \infty$ while the *GEVD*-curves perform worse, since the rank assumption on the channel covariance matrices is only approximately valid for this setup.

In Figure E.2, the performance with respect to the number of available pilot sequences τ_p is shown for $T = 1500$ coherence blocks. The seemingly arbitrary shapes of the curves with a fixed pilot allocation emerge from the fact that the pilots are allocated in a cyclic way, starting from the leftmost UE in a cell and the cycle is not restarted in the neighboring cell. It is again observed that the proposed low-rank estimators outperform the estimates obtained with subtraction of the covariance matrices and the baseline LS-method. *GEVD 30* provides the best performance, independently of the number of available pilot sequences. Increasing τ_p, increases the dominance of $\overline{\mathbf{R}}_{jjk}$ in (E.9), and has thus a positive impact on the channel estimation performance.

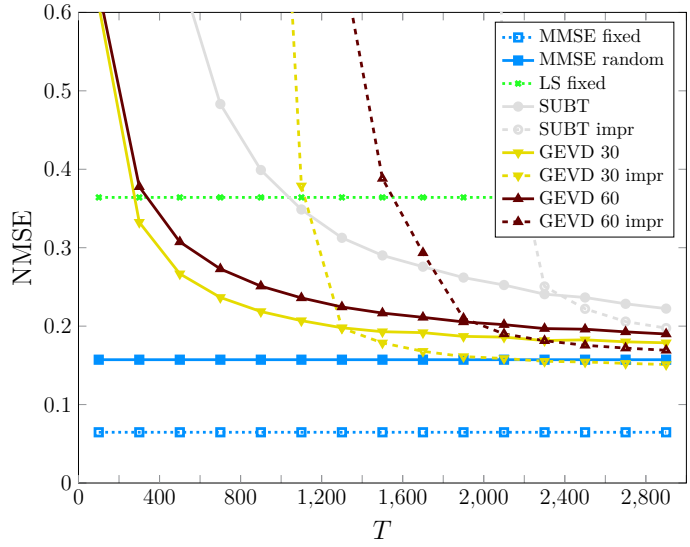

Figure E.1: NMSE for an average intra-cell UE for different estimators with $\tau_p = 10$ when the number of coherence block is varied.

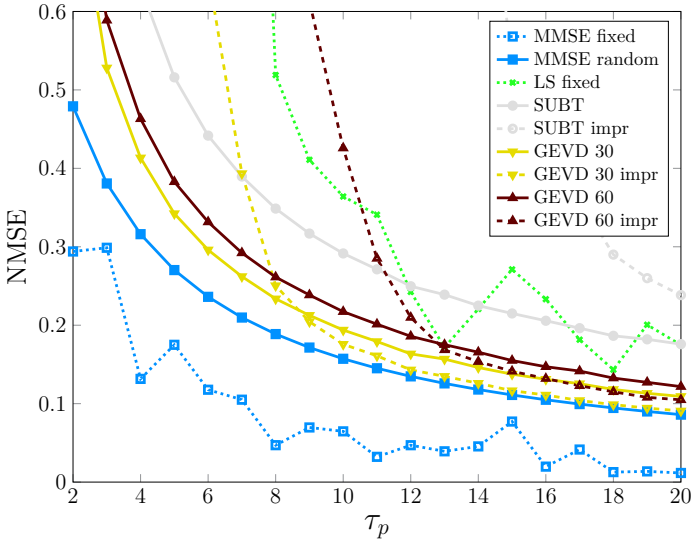

Figure E.2: NMSE for an average intra-cell UE for different estimators with $T = 1500$ when the number of pilot sequences is varied.

E.6 Conclusion

In this paper, a new uplink channel covariance matrix estimator has been presented for low-rank channel covariance matrices, using a GEVD of two covariance matrices that are estimated from the available uplink data. The requirements for the systems are minimal, i.e., UEs in a cell can randomly choose a pilot sequence in each coherence block and only the BS in its cell should be aware of its choice. Except for synchronization, there is no need for communication between the different BSs and no prior knowledge on the background noise is required. The derived approximate MMSE and improved approximate MMSE estimators have been shown to provide a good estimate of the true channel, even when only a small number of coherence blocks is available, while a simple subtraction of the two covariance matrices provides inferior performance due to estimation errors.

Determining the optimal rank of the GEVD will be part of future research, since it depends strongly on the dimension of the dominant eigenspace of the channel covariance matrix and the estimation errors unavoidably present in the data-based estimations of the required covariance matrices. Further statistical analysis is required at this point.

Bibliography

[1] R. Verdone, D. Dardari, G. Mazzini, and A. Conti, *Wireless Sensor and Actuator Networks: Technologies, Analysis and Design*. Academic Press, 2010.

[2] Benesty Jacob, Chen Jingdong, and Huang Yiteng, *Microphone Array Signal Processing*. Springer Science & Business Media, 2008.

[3] Brandstein Michael and Ward Darren, *Microphone Arrays: Signal Processing Techniques and Applications*. Springer Science & Business Media, 2001.

[4] Benesty Jacob, I. Cohen, and Chen Jingdong, *Fundamentals of Signal Enhancement and Array Signal Processing*. John Wiley & Sons, 2008.

[5] M. F. Simon Galvez, S. J. Elliott, and J. Cheer, "Time Domain Optimization of Filters Used in a Loudspeaker Array for Personal Audio," *IEEE/ACM Transactions on Audio, Speech and Language Processing*, vol. 23, no. 11, pp. 1869–1878, nov 2015.

[6] T. L. Marzetta and H. Q. Ngo, *Fundamentals of massive MIMO*. Cambridge University Press, 2016.

[7] E. Björnson, J. Hoydis, and L. Sanguinetti, "Massive MIMO Networks: Spectral, Energy, and Hardware Efficiency," *Foundations and Trends® in Signal Processing*, vol. 11, no. 3-4, pp. 154–655, 2017.

[8] B. K. Prasad, "Binaural hearing: Physiological and Clinical View," *Archives of Otolaryngology and Rhinology*, vol. 6, no. 2, may 2020.

[9] R. H. Gifford and L. J. Revit, "Speech Perception for Adult Cochlear Implant Recipients in a Realistic Background Noise: Effectiveness of Preprocessing Strategies and External Options for Improving Speech Recognition in Noise," *Journal of the American Academy of Audiology*, vol. 21, pp. 441–451, 2010.

[10] R. H. Gifford, M. F. Dorman, S. W. Sheffield, K. Teece, and A. P. Olund, "Availability of binaural cues for bilateral implant recipients and bimodal listeners with and without preserved hearing in the implanted ear," *Audiology & neuro-otology*, vol. 19, no. 1, pp. 57–71, 2014.

[11] J. Szurley, A. Bertrand, B. Van Dijk, and M. Moonen, "Binaural noise cue preservation in a binaural noise reduction system with a remote microphone signal," *IEEE/ACM Transactions on Audio, Speech and Language Processing*, vol. 24, no. 5, pp. 952–966, may 2016.

[12] R. Ali, G. Bernardi, T. Van Waterschoot, and M. Moonen, "Methods of Extending a Generalized Sidelobe Canceller with External Microphones," *IEEE/ACM Transactions on Audio, Speech and Language Processing*, vol. 27, no. 9, pp. 1349–1364, 2019.

[13] R. Ali, T. Van Waterschoot, and M. Moonen, "An integrated MVDR beamformer for speech enhancement using a local microphone array and external microphones," *EURASIP Journal on Audio, Speech, and Music Processing*, no. 10, pp. 1–20, 2021.

[14] S. Shamai and B. M. Zaidel, "Enhancing the cellular downlink capacity via co-processing at the transmitting end," *IEEE 53rd Vehicular Technology Conference (VTC)*, pp. 1745–1749, 2001.

[15] S. Zhou, M. Zhao, X. Xu, J. Wang, and Y. Yao, "Distributed wireless communication system: A new architecture for future public wireless access," *IEEE Communications Magazine*, vol. 41, no. 3, pp. 108–113, 2003.

[16] M. Boldi, A. Tölli, M. Olsson, E. Hardouin, T. Svensson, F. Boccardi, L. Thiele, and V. Jungnickel, "Coordinated Multipoint (comp) Systems," in *Mobile and Wireless Communications for IMT-Advanced and Beyond*. Wiley Telecom, aug 2011, pp. 121–155.

[17] E. Björnson, R. Zakhour, D. Gesbert, and B. Ottersten, "Cooperative multicell precoding: Rate region characterization and distributed strategies with instantaneous and statistical CSI," *IEEE Transactions on Signal Processing*, vol. 58, no. 8, pp. 4298–4310, 2010.

[18] ITU, "M2410 - Minimum requirements related to technical performance for IMT-2020 radio interface(s)," Tech. Rep., 2017.

[19] E. Björnson, L. Sanguinetti, H. Wymeersch, J. Hoydis, and T. L. Marzetta, "Massive MIMO is a reality—What is next?: Five promising research directions for antenna arrays," *Digital Signal Processing*, vol. 94, pp. 3–20, nov 2019.

[20] A. Flammini, P. Ferrari, D. Marioli, E. Sisinni, and A. Taroni, "Wired and wireless sensor networks for industrial applications," *Microelectronics Journal*, vol. 40, no. 9, pp. 1322–1336, sep 2009.

[21] R. E. Mohamed, A. I. Saleh, M. Abdelrazzak, and A. S. Samra, "Survey on Wireless Sensor Network Applications and Energy Efficient Routing Protocols," *Wireless Personal Communications*, vol. 101, no. 2, pp. 1019–1055, jul 2018.

[22] M. F. Othman and K. Shazali, "Wireless Sensor Network Applications: A Study in Environment Monitoring System," *Procedia Engineering*, vol. 41, pp. 1204–1210, jan 2012.

[23] L. M. Borges, F. J. Velez, and A. S. Lebres, "Survey on the characterization and classification of wireless sensor network applications," *IEEE Communications Surveys and Tutorials*, vol. 16, no. 4, pp. 1860–1890, 2014.

[24] D. Estrin, L. Girod, G. J. Pottie, and M. Srivastava, "Instrumenting the world with wireless sensor networks," in *2001 IEEE International Conference on Acoustics, Speech, and Signal Processing (ICASSP)*, 2001, pp. 2033–2036.

[25] S. Haykin and K. J. R. Liu, *Handbook on Array Processing and Sensor Networks*. John Wiley & Sons, 2010.

[26] C. Buratti, A. Conti, D. Dardari, and R. Verdone, "An overview on wireless sensor networks technology and evolution," *Sensors*, vol. 9, no. 9, pp. 6869–6896, aug 2009.

[27] M. Kocakulak and I. Butun, "An overview of Wireless Sensor Networks towards internet of things," in *2017 IEEE 7th Annual Computing and Communication Workshop and Conference (CCWC)*, 2017, pp. 1–6.

[28] M. A. Alsheikh, S. Lin, D. Niyato, and H. P. Tan, "Machine learning in wireless sensor networks: Algorithms, strategies, and applications," *IEEE Communications Surveys and Tutorials*, vol. 16, no. 4, pp. 1996–2018, apr 2014.

[29] D. Praveen Kumar, T. Amgoth, and C. S. R. Annavarapu, "Machine learning algorithms for wireless sensor networks: A survey," *Information Fusion*, vol. 49, pp. 1–25, sep 2019.

[30] M. Dener, Y. Özkök, and C. Bostancıoğlu, "Fire Detection Systems in Wireless Sensor Networks," *Procedia - Social and Behavioral Sciences*, vol. 195, pp. 1846–1850, jul 2015.

[31] G. Wittenburg, N. Dziengel, C. Wartenburger, and J. Schiller, "A System for Distributed Event Detection in Wireless Sensor Networks," in *2010 9th ACM/IEEE International Conference on Information Processing in Sensor Networks (IPSN)*, 2010, pp. 94–104.

[32] A. Coluccia, G. Parisi, and A. Fascista, "Detection and Classification of Multirotor Drones in Radar Sensor Networks: A Review," *Sensors*, vol. 20, no. 4172, jul 2020.

[33] A. Hassani, A. Bertrand, and M. Moonen, "Tracking of a rotating object in a wireless sensor network using fuzzy based adaptive IMM filter," in *2012 19th IEEE Symposium on Communications and Vehicular Technology in the Benelux (SCVT)*, 2012, pp. 1–6.

[34] J. Heidemann, M. Stojanovic, and M. Zorzi, "Underwater sensor networks: applications, advances and challenges," *Philosophical Transactions of the Royal Society A*, vol. 370, pp. 158–175, 2012.

[35] A. Bertrand, "Distributed Signal Processing for Wireless EEG Sensor Networks," *IEEE Transactions on Neural Systems and Rehabilitation Engineering*, vol. 23, no. 6, pp. 923–935, nov 2015.

[36] R. Negra, I. Jemili, and A. Belghith, "Wireless Body Area Networks: Applications and Technologies," *Procedia Computer Science*, vol. 83, pp. 1274–1281, jan 2016.

[37] H. Shen and G. Bai, "Routing in wireless multimedia sensor networks: A survey and challenges ahead," *Journal of Network and Computer Applications*, vol. 71, pp. 30–49, aug 2016.

[38] I. F. Akyildiz, T. Melodia, and K. R. Chowdury, "Wireless multimedia sensor networks: A survey," *IEEE Wireless Communications*, vol. 14, no. 6, pp. 32–39, dec 2007.

[39] B. Al Hayani and H. Ilhan, "Image Transmission Over Decode and Forward Based Cooperative Wireless Multimedia Sensor Networks for Rayleigh Fading Channels in Medical Internet of Things (MIoT) for Remote Health-Care and Health Communication Monitoring," *Journal of Medical Imaging and Health Informatics*, vol. 10, no. 1, pp. 160–168, sep 2019.

[40] A. Bertrand and M. Moonen, "Robust distributed noise reduction in hearing aids with external acoustic sensor nodes," *Eurasip Journal on Advances in Signal Processing*, vol. 2009, pp. 1–14, 2009.

[41] M. Cobos, F. Antonacci, A. Alexandridis, A. Mouchtaris, and B. Lee, "A survey of sound source localization methods in wireless acoustic sensor networks," *Wireless Communications and Mobile Computing*, vol. 2017, pp. 1–24, 2017.

[42] A. Bertrand, "Applications and trends in wireless acoustic sensor networks: A signal processing perspective," in *2011 18th IEEE Symposium on Communications and Vehicular Technology in the Benelux (SCVT)*, 2011, pp. 1–6.

[43] S. Ruiz, T. van Waterschoot, and M. Moonen, "Distributed Combined Acoustic Echo Cancellation and Noise Reduction in Wireless Acoustic Sensor and Actuator Networks," *IEEE/ACM Transactions on Audio, Speech and Language Processing*, vol. 30, pp. 534–547, 2022.

[44] R. Van Rompaey and M. Moonen, "Distributed adaptive acoustic contrast control for node-specific sound zoning in a wireless acoustic sensor and actuator network," in *2020 28th European Signal Processing Conference (EUSIPCO)*, 2021, pp. 481–485.

[45] ——, "Sound Zoning in an Ad-hoc Wireless Acoustic Sensor and Actuator Network," in *2021 29th European Signal Processing Conference (EUSIPCO)*, 2021, pp. 101–105.

[46] A. Bertrand, J. Callebaut, and M. Moonen, "Adaptive distributed noise reduction for speech enhancement in wireless acoustic sensor networks," in *2010 International Workshop on Acoustic Signal Enhancement (IWAENC)*, 2010, pp. 1–4.

[47] S. Markovich Golan, S. Gannot, and I. Cohen, "A reduced bandwidth binaural MVDR beamformer," in *2010 International Workshop on Acoustic Signal Enhancement (IWAENC)*, 2010, pp. 1–4.

[48] S. Doclo, M. Moonen, T. Van Den Bogaert, and J. Wouters, "Reduced-bandwidth and distributed MWF-based noise reduction algorithms for binaural hearing aids," *IEEE Transactions on Audio, Speech and Language Processing*, vol. 17, no. 1, pp. 38–51, jan 2009.

[49] Y. Zeng and R. C. Hendriks, "Distributed delay and sum beamformer for speech enhancement via randomized gossip," *IEEE Transactions on Audio, Speech and Language Processing*, vol. 22, no. 1, pp. 260–273, 2014.

[50] R. Heusdens, G. Zhang, R. C. Hendriks, Y. Zeng, and W. B. Kleijn, "Distributed MVDR Beamforming for (Wireless) Microphone Networks Using Message Passing," in *2012 International Workshop on Acoustic Signal Enhancement (IWAENC)*, 2012, pp. 1–4.

[51] Y. Zeng, R. C. Hendriks, and R. Heusdens, "Clique-based distributed beamforming for speech enhancement in wireless sensor networks," in *2013 21st European Signal Processing Conference (EUSIPCO)*, 2013, pp. 1–5.

[52] E. Hansler and G. Schmidt, *Acoustic echo and noise control : a practical approach*. Wiley-Interscience, 2004.

[53] E. A. P. Habets, "Towards multi-microphone speech dereverberation using spectral enhancement and statistical reverberation models," in *2008 Asilomar Conference on Signals, Systems and Computers*, 2008, pp. 806–810.

[54] P. A. Naylor and N. D. Gaubitch, *Speech Dereverberation*. Springer-Verlag London, 2010.

[55] T. van Waterschoot and M. Moonen, "Distributed estimation and equalization of room acoustics in a wireless acoustic sensor network," in *2012 20th European Signal Processing Conference (EUSIPCO)*, 2010, pp. 2709–2713.

[56] J. C. Chen, K. Yao, and R. E. Hudson, "Source localization and beamforming," *IEEE Signal Processing Magazine*, vol. 19, no. 2, pp. 30–39, 2002.

[57] A. Canclini, P. Bestagini, F. Antonacci, M. Compagnoni, A. Sarti, and S. Tubaro, "A robust and low-complexity source localization algorithm for asynchronous distributed microphone networks," *IEEE Transactions on Audio, Speech and Language Processing*, vol. 23, no. 10, pp. 1563–1575, oct 2015.

[58] D. Ayllon, R. Gil-Pita, M. Rosa-Zurera, and H. Krim, "Real-time multiple DOA estimation of speech sources in wireless acoustic sensor networks," in *2015 IEEE International Conference on Acoustics, Speech and Signal Processing (ICASSP)*, 2015, pp. 2709–2713.

[59] L. Wang, J. D. Reiss, and A. Cavallaro, "Over-Determined Source Separation and Localization Using Distributed Microphones," *IEEE/ACM Transactions on Audio, Speech and Language Processing*, vol. 24, no. 9, pp. 1573–1588, sep 2016.

[60] M. Ferrer, M. De Diego, G. Piñero, and A. González, "Active noise control over adaptive distributed networks," *Signal Processing*, vol. 107, pp. 82–95, feb 2015.

[61] J. Plata-Chaves, A. Bertrand, and M. Moonen, "Incremental multiple error filtered-X LMS for node-specific active noise control over wireless acoustic sensor networks," in *2016 IEEE Sensor Array and Multichannel Signal Processing Workshop (SAM)*, 2016, pp. 1–5.

[62] J. Lorente, C. Antoñanzas, M. Ferrer, and A. González, "Block-based distributed adaptive filter for active noise control in a collaborative network," in *2015 23rd European Signal Processing Conference (EUSIPCO)*, 2015, pp. 310–314.

[63] T. Betlehem, W. Zhang, M. A. Poletti, and T. D. Abhayapala, "Personal sound zones: Delivering interface-free audio to multiple listeners," *IEEE Signal Processing Magazine*, vol. 32, no. 2, pp. 81–91, 2015.

[64] D. Gesbert, S. Hanly, H. Huang, S. Shamai Shitz, O. Simeone, and W. Yu, "Multi-cell MIMO cooperative networks: A new look at interference," *IEEE Journal on Selected Areas in Communications*, vol. 28, no. 9, pp. 1380–1408, 2010.

[65] E. Björnson, L. Van Der Perre, S. Buzzi, and E. G. Larsson, "Massive MIMO in sub-6 GHz and mmWave: Physical, practical, and use-case differences," *IEEE Wireless Communications*, vol. 26, no. 2, pp. 100–108, apr 2019.

[66] H. Q. Ngo, A. Ashikhmin, H. Yang, E. G. Larsson, and T. L. Marzetta, "Cell-Free Massive MIMO Versus Small Cells," *IEEE Transactions on Wireless Communications*, vol. 16, no. 3, pp. 1834–1850, 2017.

[67] E. Nayebi, A. Ashikhmin, T. L. Marzetta, H. Yang, and B. D. Rao, "Precoding and Power Optimization in Cell-Free Massive MIMO Systems," *IEEE Transactions on Wireless Communications*, vol. 16, no. 7, pp. 4445–4459, 2017.

[68] E. Björnson and L. Sanguinetti, "Making Cell-Free Massive MIMO Competitive with MMSE Processing and Centralized Implementation," *IEEE Transactions on Wireless Communications*, vol. 19, no. 1, pp. 77–90, 2020.

[69] S. Payami and F. Tufvesson, "Channel measurements and analysis for very large array systems at 2.6 GHz," in *2012 6th European Conference on Antennas and Propagation (EuCAP)*, 2012, pp. 433–437.

[70] J. Huang, R. A. N. Duan, C. Cui, and J. X. Jiang, "Recent Progress on C-RAN Centralization and Cloudification," *IEEE Access*, vol. 2, pp. 1030–1039, 2014.

[71] S. Buzzi and C. D'Andrea, "Cell-Free Massive MIMO : User-Centric Approach," *IEEE wireless communications letters*, vol. 6, no. 6, pp. 706–709, 2017.

[72] Ö. T. Demir, E. Björnson, and L. Sanguinetti, "Foundations of User-Centric Cell-Free Massive MIMO," *Foundations and Trends® in Signal Processing*, vol. 14, no. 3-4, pp. 162–472, 2021.

[73] S. Chen, J. Zhang, J. Zhang, E. Björnson, and B. Ai, "A survey on user-centric cell-free massive MIMO systems," *Digital Communications and Networks*, 2021.

[74] E. Björnson and L. Sanguinetti, "Scalable Cell-Free Massive MIMO Systems," *IEEE Transactions on Communications*, vol. 68, no. 7, pp. 4247–4261, 2020.

[75] A. Bertrand and M. Moonen, "Distributed signal estimation in sensor networks where nodes have different interests," *Signal Processing*, vol. 92, no. 7, pp. 1679–1690, 2012.

[76] S. V. Macua, P. Belanovic, and S. Zazo, "Consensus-based distributed principal component analysis in wireless sensor networks," in *2010 IEEE Workshop on Signal Processing Advances in Wireless Communications, (SPAWC)*, 2010, pp. 1–5.

[77] K. Avrachenkov, M. E. Chamie, and G. Neglia, "A local average consensus algorithm for wireless sensor networks," in *2011 International Conference on Distributed Computing in Sensor Systems and Workshops (DCOSS)*, 2011, pp. 1–6.

[78] C. G. Lopes and A. H. Sayed, "Incremental adaptive strategies over distributed networks," *IEEE Transactions on Signal Processing*, vol. 55, no. 8, pp. 4064–4077, 2007.

[79] J. Chen and A. H. Sayed, "Distributed Pareto Optimization via Diffusion Strategies," *IEEE Journal of Selected Topcis in Signal Processing*, vol. 7, no. 2, pp. 205–220, 2013.

[80] A. H. Sayed, "Diffusion Adaptation Over Networks," *Academic Press Library in Signal Processing*, vol. 3, pp. 323–453, 2014.

[81] C. G. Lopes and A. H. Sayed, "Diffusion least-mean squares over adaptive networks: Formulation and performance analysis," *IEEE Transactions on Signal Processing*, vol. 56, no. 7 II, pp. 3122–3136, jul 2008.

[82] F. S. Cattivelli, C. G. Lopes, and A. H. Sayed, "Diffusion recursive least-squares for distributed estimation over adaptive networks," *IEEE Transactions on Signal Processing*, vol. 56, no. 5, pp. 1865–1877, 2008.

[83] A. Bertrand and M. Moonen, "Distributed Adaptive Node-Specific Signal Estimation in Fully Connected Sensor Networks—Part I: Sequential Node Updating," *IEEE Transactions on Signal Processing*, vol. 58, no. 10, pp. 5277–5291, 2010.

[84] A. Hassani, "Distributed Signal Processing Algorithms for Multi- Task Wireless Acoustic Sensor Networks," Ph.D. dissertation, KU Leuven, 2017.

[85] A. Bertrand and M. Moonen, "Distributed Adaptive Node-Specific Signal Estimation in Fully Connected Sensor Networks—Part II: Simultaneous and Asynchronous Node Updating," *IEEE Transactions on Signal Processing*, vol. 58, no. 10, pp. 5292–5306, 2010.

[86] F. de la Hucha Arce, F. Rosas, M. Moonen, M. Verhelst, and A. Bertrand, "Energy-vs-performance trade-offs in speech enhancement in wireless acoustic sensor networks," in *2015 23rd European Signal Processing Conference (EUSIPCO)*, 2015, pp. 1561–1565.

[87] J. A. Khan, H. K. Qureshi, A. Iqbal, and C. Lacatus, "Energy management in Wireless Sensor Networks: A survey," *Computers & Electrical Engineering*, vol. 41, pp. 159–176, jan 2015.

[88] F. de la Hucha Arce, M. Moonen, M. Verhelst, and A. Bertrand, "Distributed adaptive node-specific signal estimation in a wireless sensor network with noisy links," *Signal Processing*, vol. 166, no. 107220, jan 2020.

[89] N. X. Tien, S. Kim, and J. M. Rhee, "A Novel Variant of the Minimizing Re-Transmissions Technique for Wired Networks," *Asia-pacific Proceedings of Applied Science and Engineering for Better Human Life*, vol. 4, pp. 102–106, 2016.

[90] M. Abu Alsheikh, S. Lin, D. Niyato, and H. P. Tan, "Rate-distortion balanced data compression for wireless sensor networks," *IEEE Sensors Journal*, vol. 16, no. 12, pp. 5072–5083, jun 2016.

[91] T. Srisooksai, K. Keamarungsi, P. Lamsrichan, and K. Araki, "Practical data compression in wireless sensor networks: A survey," *Journal of Network and Computer Applications*, vol. 35, no. 1, pp. 37–59, jan 2012.

[92] J. Uthayakumar, T. Vengattaraman, and P. Dhavachelvan, "A new lossless neighborhood indexing sequence (NIS) algorithm for data compression in wireless sensor networks," *Ad Hoc Networks*, vol. 83, pp. 149–157, feb 2019.

[93] K. Zhang, X. R. Li, P. Zhang, and H. Li, "Optimal linear estimation fusion - Part VI: Sensor data compression," in *2003 6th International Conference on Information Fusion (FUSION)*, 2003, pp. 221–228.

[94] M. Gastpar, P. L. Dragotti, and M. Vetterli, "The distributed Karhunen-Loève transform," *IEEE Transactions on Information Theory*, vol. 52, no. 12, pp. 5177–5196, dec 2006.

[95] I. D. Schizas, G. B. Giannakis, and Z.-Q. Luo, "Distributed estimation using reduced dimensionality sensor observations," *IEEE Transactions on Signal Processing*, vol. 55, no. 8, pp. 4284–4299, 2007.

[96] Z.-Q. Luo, G. B. Giannakis, and S. Zhang, "Optimal linear decentralized estimation in a bandwidth constrained sensor network," in *2005 IEEE International Symposium on Information Theory (ISIT)*, 2005, pp. 1441–1445.

[97] J. Szurley, A. Bertrand, and M. Moonen, "Distributed adaptive node-specific signal estimation in heterogeneous and mixed-topology wireless sensor networks," *Signal Processing*, vol. 117, pp. 44–60, dec 2015.

[98] A. Bertrand and M. Moonen, "Efficient sensor subset selection and link failure response for linear MMSE signal estimation in wireless sensor networks," in *2010 18nd European Signal Processing Conference (EUSIPCO)*, 2010, pp. 1092–1096.

[99] ——, "Distributed adaptive estimation of node-specific signals in wireless sensor networks with a tree topology," *IEEE Transactions on Signal Processing*, vol. 59, no. 5, pp. 2196–2210, may 2011.

[100] J. Szurley, A. Bertrand, and M. Moonen, "Topology-Independent Distributed Adaptive Node-Specific Signal Estimation in Wireless Sensor Networks," *IEEE Transactions on Signal and Information Processing over Networks*, vol. 3, no. 1, pp. 130–144, 2017.

[101] A. Hassani, A. Bertrand, and M. Moonen, "GEVD-Based Low-Rank Approximation for Distributed Adaptive Node-Specific Signal Estimation in Wireless Sensor Networks," *IEEE Transactions on Signal Processing*, vol. 64, no. 10, pp. 2557–2572, 2016.

[102] J. Plata-Chaves, A. Bertrand, and M. Moonen, "Distributed signal estimation in a wireless sensor network with partially-overlapping node-specific interests or source observability," in *2015 IEEE International Conference on Acoustics, Speech and Signal Processing (ICASSP)*, vol. 2015-Augus, 2015, pp. 5808–5812.

[103] D. Tse and P. Viswanath, *Fundamentals of Wireless Communication*. Cambridge University Press, 2005.

[104] S. Doclo and M. Moonen, "GSVD-based optimal filtering for single and multimicrophone speech enhancement," *IEEE Transactions on Signal Processing*, vol. 50, no. 9, pp. 2230–2244, sep 2002.

[105] S. Doclo, "Multi-microphone noise reduction and dereverberation techniques for speech applications," Ph.D. dissertation, KU Leuven, 2003.

[106] S. M. R. Nahar and A. Kai, "Robust Voice Activity Detector by combining sequentially trained Deep Neural Networks," in *2016 International Conference On Advanced Informatics: Concepts, Theory And Application (ICAICTA)*, 2016, pp. 1–5.

[107] L. K. Hamaidi, M. Muma, and A. M. Zoubir, "Robust distributed multi-speaker voice activity detection using stability selection for sparse non-negative feature extraction," in *2017 25th European Signal Processing Conference (EUSIPCO)*, 2017, pp. 161–165.

[108] X. L. Zhang and J. Wu, "Deep belief networks based voice activity detection," *IEEE Transactions on Audio, Speech and Language Processing*, vol. 21, no. 4, pp. 697–710, 2013.

[109] C. Dai, L. Luo, H. Peng, and Q. Sun, "A Method Based on Support Vector Machine for Voice Activity Detection on Isolated Words," in *2018 13th International Conference on Computer Science & Education (ICCSE)*, 2018, pp. 1–4.

[110] R. Serizel, M. Moonen, B. Van Dijk, and J. Wouters, "Low-rank Approximation Based Multichannel Wiener Filter Algorithms for Noise Reduction with Application in Cochlear Implants," *IEEE/ACM Transactions on Audio, Speech and Language Processing*, vol. 22, no. 4, pp. 785–799, apr 2014.

[111] ——, "Rank-1 approximation based multichannel wiener filtering algorithms for noise reduction in cochlear implants," in *2013 IEEE International Conference on Acoustics, Speech and Signal Processing (ICASSP)*, 2013, pp. 8634–8638.

[112] J. K. Nielsen, T. Lee, J. R. Jensen, and M. G. Christensen, "Sound Zones as an Optimal Filtering Problem," in *2018 52nd Asilomar Conference on Signals, Systems, and Computers*, 2018, pp. 1075–1079.

[113] S. J. Elliott, I. M. Stothers, and P. A. Nelson, "A multiple error LMS algorithm and its application to the active control of sound and vibration," *IEEE Transactions on Acoustics, Speech and Signal Processing*, vol. 35, no. 10, pp. 1423–1434, 1987.

[114] D. H. Schellekens, M. B. Moller, and M. Olsen, "Time domain acoustic contrast control implementation of sound zones for low-frequency input signals," in *2016 IEEE International Conference on Acoustics, Speech and Signal Processing (ICASSP)*, 2016, pp. 365–369.

[115] D. Wallace and J. Cheer, "The Design of Personal Audio Systems for Speech Transmission Using Analytical and Measured Responses," in *2019 IEEE International Conference on Acoustics, Speech and Signal Processing (ICASSP)*, 2019, pp. 8003–8007.

[116] P. Coleman, P. J. B. Jackson, M. Olik, M. B. Møller, M. Olsen, and J. Abildgaard Pedersen, "Acoustic contrast, planarity and robustness of sound zone methods using a circular loudspeaker array," *The Journal of the Acoustical Society of America*, vol. 135, no. 4, pp. 1929–1940, 2014.

[117] M. Shin, S. Q. Lee, F. M. Fazi, P. A. Nelson, D. Kim, S. Wang, K. H. Park, and J. Seo, "Maximization of acoustic energy difference between two spaces," *The Journal of the Acoustical Society of America*, vol. 128, no. 1, pp. 121–131, 2010.

[118] S. Kim, J. W. Choi, and B. Shim, "Downlink Pilot Precoding and Compressed Channel Feedback for FDD-Based Cell-Free Systems," *IEEE Transactions on Wireless Communications*, vol. 19, no. 6, pp. 3658–3672, jun 2020.

[119] A. Abdallah and M. M. Mansour, "Efficient Angle-Domain Processing for FDD-Based Cell-Free Massive MIMO Systems," *IEEE Transactions on Communications*, vol. 68, no. 4, pp. 2188–2203, apr 2020.

[120] J. Zhang, J. Fan, B. Ai, and D. W. K. Ng, "NOMA-Based Cell-Free Massive MIMO over Spatially Correlated Rician Fading Channels," in *2020 IEEE International Conference on Communications (ICC)*, 2020, pp. 1–6.

[121] Y. Zhao, I. G. Niemegeers, and S. H. De Groot, "Power Allocation in Cell-Free Massive MIMO: A Deep Learning Method," *IEEE Access*, vol. 8, no. 1, pp. 87 185–87 200, 2020.

[122] S. Chen, J. J. Zhang, E. Björnson, J. J. Zhang, and B. Ai, "Structured Massive Access for Scalable Cell-Free Massive MIMO Systems," *IEEE Journal on Selected Areas in Communications*, vol. 39, no. 4, pp. 1086–1100, apr 2021.

[123] R. Van Rompaey and M. Moonen, "GEVD-based Low-Rank Channel Covariance Matrix Estimation and MMSE Channel Estimation for Uplink Cellular Massive MIMO Systems," in *2022 30th European Signal Processing Conference (EUSIPCO)*, 2022, pp. 1641–1645.

[124] H. Q. Ngo, A. Ashikhmin, H. Yang, E. G. Larsson, and T. L. Marzetta, "Cell-Free Massive MIMO: Uniformly great service for everyone," in *2015 IEEE Workshop on Signal Processing Advances in Wireless Communications (SPAWC)*, 2015, pp. 201–205.

[125] Ö. Özdogan, E. Björnson, and E. G. Larsson, "Massive MIMO with Spatially Correlated Rician Fading Channels," *IEEE Transactions on Communications*, vol. 67, no. 5, pp. 3234–3250, 2019.

[126] J. Zhang, S. Chen, Y. Lin, J. Zheng, B. Ai, and L. Hanzo, "Cell-Free Massive MIMO: A New Next-Generation Paradigm," *IEEE Access*, vol. 7, pp. 99 878–99 888, 2019.

[127] J. Szurley, A. Bertrand, and M. Moonen, "Improved tracking performance for distributed node-specific signal enhancement inwireless acoustic sensor networks," in *2013 IEEE International Conference on Acoustics, Speech and Signal Processing (ICASSP)*, 2013, pp. 336–340.

[128] A. Bertrand and M. Moonen, "Distributed adaptive generalized eigenvector estimation of a sensor signal covariance matrix pair in a fully connected sensor network," *Signal Processing*, vol. 106, pp. 209–214, jan 2015.

[129] T. He, S. Krishnamurthy, L. Luo, T. Yan, L. Gu, R. Stoleru, G. Zhou, Q. Cao, P. Vicaire, J. A. Stankovic, T. F. Abdelzaher, J. Hui, and B. Krogh, "VigilNet: An Integrated Sensor Network System for Energy-Efficient Surveillance," *ACM Transactions on Sensor Networks*, vol. 2, no. 1, pp. 1–38, feb 2006.

[130] A. Shirazinia, S. Dey, D. Ciuonzo, and P. S. Rossi, "Massive MIMO for Decentralized Estimation of a Correlated Source," *IEEE Transactions on Signal Processing*, vol. 64, no. 10, pp. 2499–2512, 2016.

[131] D. Ciuonzo, P. S. Rossi, and P. K. Varshney, "Distributed Detection in Wireless Sensor Networks under Multiplicative Fading via Generalized Score-tests," *IEEE Internet of Things Journal*, pp. 1–13, 2021.

[132] L. Hu, X. Wang, and S. Wang, "Decentralized Underwater Target Detection and Localization," *IEEE Sensors Journal*, vol. 21, no. 2, pp. 2385–2399, 2021.

[133] J. Kuriakose, S. Joshi, R. Vikram Raju, and A. Kilaru, "A Review on Localization in Wireless Sensor Networks," *Advances in Signal Processing and Intelligent Recognition Systems*, vol. 264, pp. 599–610, 2014.

[134] S. Markovich-Golan, S. Gannot, and I. Cohen, "Distributed multiple constraints generalized sidelobe canceler for fully connected wireless acoustic sensor networks," *IEEE Transactions on Audio, Speech and Language Processing*, vol. 21, no. 2, pp. 343–356, 2013.

[135] H. Teutsch, "Modal array signal processing: Principles and applications of acoustic wavefield decomposition," *Lecture Notes in Control and Information Sciences*, vol. 348, pp. 1–258, 2007.

[136] A. Geusens, A. Bertrand, B. Cornelis, and M. Moonen, "Multi-channel noise reduction in hearing aids with wireless access to an external reference signal," in *2012 International Workshop on Acoustic Signal Enhancement (IWAENC)*, 2012, pp. 1–4.

[137] R. Van Rompaey and M. Moonen, "Distributed Adaptive Node-Specific Signal Estimation in a Wireless Sensor Network with Partial Prior Knowledge of the Desired Source Steering Vector," in *2019 27th European Signal Processing Conference (EUSIPCO)*, 2019, pp. 1–5.

[138] R. Nassif, S. Vlaski, and A. H. Sayed, "Adaptation and Learning Over Networks Under Subspace Constraints—Part I: Stability Analysis," *IEEE Transactions on Signal Processing*, vol. 68, pp. 1346–1360, 2020.

[139] S. Kitić, L. Albera, N. Bertin, and R. Gribonval, "Physics-Driven Inverse Problems Made Tractable With Cosparse Regularization," *IEEE Transactions on Signal Processing*, vol. 64, no. 2, pp. 335–348, 2016.

[140] J. Murray-bruce and P. L. Dragotti, "A Sampling Framework for Solving Physics-Driven Inverse Source Problems," *IEEE Transactions on Signal Processing*, vol. 65, no. 24, pp. 6365–6380, 2017.

[141] M. Bellalouna and A. Ghabri, "A priori methods for fault tolerance in wireless sensor networks," in *2013 World Congress on Computer and Information Technology (WCCIT)*. IEEE, 2013, pp. 1–6.

[142] S. Gannot, E. Vincent, S. Markovich-Golan, and A. Ozerov, "A Consolidated Perspective on Multimicrophone Speech Enhancement and Source Separation," *IEEE/ACM Transactions on Audio, Speech and Language Processing*, vol. 25, no. 4, pp. 692–730, 2017.

[143] A. Bertrand and M. Moonen, "Distributed node-specific LCMV beamforming in wireless sensor networks," *IEEE Transactions on Signal Processing*, vol. 60, no. 1, pp. 233–246, 2012.

[144] ——, "Distributed LCMV beamforming in a wireless sensor network with single-channel per-node signal transmission," *IEEE Transactions on Signal Processing*, vol. 61, no. 13, pp. 3447–3459, 2013.

[145] Z. Li, K. Fai, C. Yiu, Y.-h. Dai, and S. Nordholm, "Distributed LCMV beamformer design by randomly permuted ADMM," *Digital Signal Processing*, vol. 106, no. 102820, pp. 1–9, 2020.

[146] R. Van Rompaey and M. Moonen, "GEVD based speech and noise correlation matrix estimation for multichannel Wiener filter based noise reduction," in *2018 26th European Signal Processing Conference (EUSIPCO)*, 2018, pp. 2544–2548.

[147] B. R. Breed and J. Strauss, "A short proof of the equivalence of LCMV and GSC beamforming," *IEEE Signal Processing Letters*, vol. 9, no. 6, pp. 168–169, jun 2002.

[148] M. Dendrinos, S. Bakamidis, and G. Carayannis, "Speech enhancement from noise: A regenerative approach," *Speech Communication*, vol. 10, no. 1, pp. 45–57, feb 1991.

[149] S. Boyd and L. Vandenberghe, *Convex Optimization*. Cambridge University Press, 2004.

[150] J. B. Allen and D. A. Berkley, "Image method for efficiently simulating small-room acoustics," *The Journal of the Acoustical Society of America*, vol. 65, no. 4, pp. 943–950, 1979.

[151] M. Nilsson, S. D. Soli, and J. A. Sullivan, "Development of the Hearing In Noise Test for the measurement of speech reception thresholds in quiet and in noise," *The Journal of the Acoustical Society of America*, vol. 95, no. 2, pp. 1085–1099, 1994.

[152] C. Antoñanzas, M. Ferrer, A. González, M. De Diego, and G. Piñero, "Diffusion algorithm for active noise control in distributed networks," in *2015 22nd International Congress on Sound and Vibration*, 2015.

[153] G. Piñero, C. Botella, M. De Diego, M. Ferrer, and A. González, "On the feasibility of personal audio systems over a network of distributed loudspeakers," in *2017 25th European Signal Processing Conference (EUSIPCO)*, 2017, pp. 2729–2733.

[154] J.-H. Chang and F. Jacobsen, "Sound field control with a circular double-layer array of loudspeakers," *The Journal of the Acoustical Society of America*, vol. 131, no. 6, pp. 4518–4525, 2012.

[155] A. Dimakis, S. Kar, J. Moura, M. G. Rabbat, and A. Scaglione, "Gossip algorithms for distributed signal processing," *Proceedings of the IEEE*, vol. 98, no. 11, pp. 1847–1864, 2010.

[156] J. Plata-Chaves, M. H. Bahari, M. Moonen, and A. Bertrand, "Unsupervised diffusion-based LMS for node-specific parameter estimation over wireless sensor networks," in *2016 IEEE International Conference on Acoustics, Speech and Signal Processing (ICASSP)*, 2016, pp. 4159–4163.

[157] R. Nassif, C. Richard, A. Ferrari, and A. H. Sayed, "Multitask Diffusion Adaptation over Asynchronous Networks," *IEEE Transactions on Signal Processing*, vol. 64, no. 11, pp. 2835–2850, 2016.

[158] S. J. Elliott and C. C. Boucher, "Interaction Between Multiple Feedforward active control systems," *IEEE Transactions on Speech and Audio Processing*, vol. 2, no. 4, pp. 521–530, 1994.

[159] P. Yuxue and S. Pengfei, "Online secondary path modeling method with auxiliary noise power scheduling strategy for multi-channel adaptive active noise control system," *Journal of Low Frequency Noise Vibration and Active Control*, vol. 38, no. 2, pp. 740–752, 2019.

[160] G. H. Golub and C. F. Van Loan, *Matrix Computations*. JHU Press, 2012.

[161] M. R. Hestenes and W. Karush, "A method of gradients for the calculation of the characteristic roots and vectors of a real symmetric matrix," *Journal of Research of the National Bureau of Standards*, vol. 47, no. 1, pp. 45–61, 1951.

[162] Y. T. Feng and D. R. Owen, "Conjugate gradient methods for solving the smallest eigenpair of large symmetric eigenvalue problems," *International Journal for Numerical Methods in Engineering*, vol. 39, no. 13, pp. 2209–2229, 1996.

[163] H. Chen, A. Campbell, B. Thomas, and A. Tamir, "Minimax flow tree problems," *Networks*, vol. 54, pp. 117–129, 2009.

[164] E. Nayebi, A. Ashikhmin, T. L. Marzetta, and B. D. Rao, "Performance of cell-free massive MIMO systems with MMSE and LSFD receivers," in *2016 50th Asilomar Conference on Signals, Systems and Computers*, 2017, pp. 203–207.

[165] E. Nayebi, A. Ashikhmin, T. L. Marzetta, and H. Yang, "Cell-Free Massive MIMO systems," in *2016 50th Asilomar Conference on Signals, Systems and Computers*, 2016, pp. 695–699.

[166] H. Xie, F. Gao, and S. Jin, "An Overview of Low-Rank Channel Estimation for Massive MIMO Systems," *IEEE Access*, vol. 4, pp. 7313–7321, 2016.

[167] C. K. Wen, S. Jin, K.-K. Wong, J.-C. Chen, and P. Ting, "Channel Estimation for Massive MIMO Using Gaussian-Mixture Bayesian Learning," *IEEE Transactions on Wireless Communications*, vol. 14, no. 3, pp. 1356–1368, 2015.

[168] T. L. Marzetta, "Noncooperative Cellular Wireless with Unlimited Numbers of Base Station Antennas," *IEEE Transactions on Wireless Communications*, vol. 9, no. 11, pp. 3590–3600, 2010.

[169] G. Interdonato, P. Frenger, and E. G. Larsson, "Scalability Aspects of Cell-Free Massive MIMO," in *2019 IEEE International Conference on Communications (ICC)*, 2019, pp. 1–6.

[170] M. Bashar, K. Cumanan, A. G. Burr, M. Debbah, and H. Q. Ngo, "On the Uplink Max – Min SINR of Cell-Free Massive MIMO Systems," *IEEE Transactions on Wireless Communications*, vol. 18, no. 4, pp. 2021–2036, 2019.

[171] G. Interdonato, M. Karlsson, E. Björnson, and E. G. Larsson, "Local Partial Zero-Forcing Precoding for Cell-Free Massive MIMO," *IEEE Transactions on Wireless Communications*, vol. 19, no. 7, pp. 4758–4774, 2020.

[172] C. D'Andrea, A. Zappone, S. Buzzi, and M. Debbah, "Uplink Power Control in Cell-Free Massive MIMO via Deep Learning," in *2019 IEEE 8th International Workshop on Computational Advances in Multi-Sensor Adaptive Processing (CAMSAP)*, 2019, pp. 554–558.

[173] M. Bashar, A. Akbari, K. Cumanan, H. Q. Ngo, A. G. Burr, P. Xiao, M. Debbah, and J. Kittler, "Exploiting Deep Learning in Limited-Fronthaul Cell-Free Massive MIMO Uplink," *IEEE Journal on Selected Areas in Communications*, vol. 38, no. 8, pp. 1678–1697, 2020.

[174] F. Liang, C. Shen, W. Yu, and F. Wu, "Towards optimal power control via ensembling deep neural networks," *IEEE Transactions on Communications*, vol. 68, no. 3, pp. 1760–1776, 2020.

[175] H. Yin, L. Cottatellucci, D. Gesbert, R. R. Müller, and G. He, "Robust Pilot Decontamination Based on Joint Angle and Power Domain Discrimination," *IEEE Transactions on Signal Processing*, vol. 64, no. 11, pp. 2990–3003, 2016.

[176] E. Björnson, J. Hoydis, and L. Sanguinetti, "Massive MIMO Has Unlimited Capacity," *IEEE Transactions on Wireless Communications*, vol. 17, no. 1, pp. 574–590, 2018.

[177] R. Van Rompaey and M. Moonen, "Scalable and distributed MMSE algorithms for uplink receive combining in cell-free massive MIMO systems," in *2021 IEEE International Conference on Acoustics, Speech and Signal Processing (ICASSP)*, 2021, pp. 4445–4449.

[178] D. Neumann, M. Joham, and W. Utschick, "Covariance Matrix Estimation in Massive MIMO," *IEEE Signal Processing Letters*, vol. 25, no. 6, pp. 863–867, 2018.

[179] E. Björnson, L. Sanguinetti, and M. Debbah, "Massive MIMO with imperfect channel covariance information," in *2016 50th Asilomar Conference on Signals, Systems and Computers*, 2016, pp. 974–978.

[180] J. Zhang, Y. Wei, E. Björnson, Y. Han, and S. Jin, "Performance Analysis and Power Control of Cell-Free Massive MIMO Systems With Hardware Impairments," *IEEE Access*, vol. 6, pp. 55 302–55 314, 2018.

[181] C. B. Peel, B. M. Hochwald, and A. L. Swindlehurst, "A Vector-Perturbation Technique for Near-Capacity Multiantenna Multiuser Communication — Part I : Channel Inversion and Regularization," *IEEE Transactions on Communications*, vol. 53, no. 1, pp. 195–202, 2005.

[182] E. Biglieri, J. Proakis, and S. Shlomo, "Fading Channels : Information-Theoretic and Communications Aspects," *IEEE Transactions on Information Theory*, vol. 44, no. 6, pp. 2619–2692, 1998.

[183] T. Van Chien, E. Björnson, and E. G. Larsson, "Joint Pilot Design and Uplink Power Allocation in Multi-Cell Massive MIMO Systems," *IEEE Transactions on Wireless Communications*, vol. 17, no. 3, pp. 2000–2015, 2018.

[184] T. C. Mai, H. Q. Ngo, M. Egan, and T. Q. Duong, "Pilot Power Control for Cell-Free Massive MIMO," *IEEE Transactions on Vehicular Technology*, vol. 67, no. 11, pp. 11 264–11 268, 2018.

[185] J. Hoydis, S. Ten Brink, and M. Debbah, "Massive MIMO in the UL/DL of cellular networks: How many antennas do we need?" *IEEE Journal on Selected Areas in Communications*, vol. 31, no. 2, pp. 160–171, 2013.

[186] D. P. Bertsekas, W. W. Hager, and O. L. Mangasarian, *Nonlinear Programming*. Athena Scientific Belmont, 1998.

[187] W. Yu and T. Lan, "Transmitter optimization for the multi-antenna downlink with per-antenna power constraints," *IEEE Transactions on Signal Processing*, vol. 55, no. 6 I, pp. 2646–2660, 2007.

[188] V. Le Nir, M. Moonen, M. Guenach, and J. Verlinden, "Broadcast channel optimal spectrum balancing (BC-OSB) with per-modem total power constraints for downstream DSL," in *2007 15th European Signal Processing Conference (EUCIPCO)*, 2007, pp. 2189–2193.

[189] R. J. Plemmons, "M-matrix characterizations.I-nonsingular M-matrices," *Linear Algebra and Its Applications*, vol. 18, no. 2, pp. 175–188, jan 1977.

[190] Z.-Q. Luo and S. Zhang, "Dynamic spectrum management: Complexity and duality," *IEEE Journal on Selected Topics in Signal Processing*, vol. 2, no. 1, pp. 57–73, 2008.

[191] E. Björnson and E. Jorswieck, *Optimal resource allocation in coordinated multi-cell systems*. Now Publishers, 2012, vol. 9, no. 2-3.

[192] H. Tuy, "Monotonic Optimization: Problems and Solution Approaches," *SIAM Journal on Optimization*, vol. 11, no. 2, pp. 464–494, 2000.

[193] Q. Shi, M. Razaviyayn, Z.-Q. Luo, and C. He, "An iteratively weighted MMSE approach to distributed sum-utility maximization for a MIMO interfering broadcast channel," *IEEE Transactions on Signal Processing*, vol. 59, no. 9, pp. 4331–4340, 2011.

[194] S. Buzzi, C. D'Andrea, and A. Zappone, "User-centric 5G cellular networks: Resource allocation and comparison with the cell-free massive MIMO Approach," *IEEE Transactions on Wireless Communications*, vol. 19, no. 2, pp. 1250–1264, 2020.

[195] M. Bashar, K. Cumanan, A. G. Burr, M. Debbah, and H. Q. Ngo, "Enhanced Max-Min SINR for Uplink Cell-Free Massive MIMO Systems," in *2018 IEEE International Conference on Communications (ICC)*, 2018, pp. 1–6.

[196] Y.-W. P. Hong, C. W. Tan, L. Zheng, C. L. Hsieh, and C. H. Lee, "A unified framework for wireless max-min utility optimization with general monotonic constraints," in *2014 IEEE Conference on Computer Communications (INFOCOM)*, 2014, pp. 2076–2084.

[197] G. Interdonato, E. Björnson, H. Q. Ngo, P. Frenger, and E. G. Larsson, "Ubiquitous cell-free massive MIMO communications," *EURASIP Journal on Wireless Communications and Networking*, vol. 197, pp. 1–13, 2019.

[198] O. Mart, E. D. Carvalho, and J. Ø. Nielsen, "Towards Very Large Aperture Massive MIMO : a measurement based study," in *2014 IEEE Globecom Workshops (GC Wkshps)*, 2014, pp. 281–286.

[199] U. Madhow, D. R. Brown, S. Dasgupta, and R. Mudumbai, "Distributed massive MIMO: Algorithms, architectures and concept systems," in *2014 Information Theory and Applications Workshop (ITA)*, 2014, pp. 1–7.

[200] V. Jungnickel, K. Manolakis, W. Zirwas, B. Panzner, V. Braun, M. Lossow, M. Sternad, R. Apelfröjd, and T. Svensson, "The role of small cells, coordinated multipoint, and massive MIMO in 5G," *IEEE Communications Magazine*, vol. 52, no. 5, pp. 44–51, 2014.

[201] M. Attarifar, A. Abbasfar, and A. Lozano, "Random vs structured pilot assignment in cell-free massive MIMO wireless networks," in *2018 IEEE International Conference on Communications (ICC)*, 2018, pp. 1–6.

[202] S. Haghighatshoar and G. Caire, "Massive MIMO pilot decontamination and channel interpolation via wideband sparse channel estimation," *IEEE Transactions on Wireless Communications*, vol. 16, no. 12, pp. 8316–8332, 2017.

[203] Z. Wang, J. Zhang, E. Björnson, and B. Ai, "Uplink Performance of Cell-Free Massive MIMO over Spatially Correlated Rician Fading Channels," *IEEE Communications Letters*, vol. 25, no. 4, pp. 1348–1352, apr 2021.

[204] S. N. Jin, D. W. Yue, and H. H. Nguyen, "Spectral and Energy Efficiency in Cell-Free Massive MIMO Systems over Correlated Rician Fading," *IEEE Systems Journal*, vol. 15, no. 2, pp. 2822–2833, jun 2021.

[205] N. Shariati, E. Björnson, M. Bengtsson, and M. Debbah, "Low-complexity polynomial channel estimation in large-scale MIMO with arbitrary statistics," *IEEE Journal on Selected Topics in Signal Processing*, vol. 8, no. 5, pp. 815–830, oct 2014.

[206] A. Almamori and S. Mohan, "Estimation of Channel State Information (CSI) in Cell-Free Massive MIMO Based on Time of Arrival (ToA)," *Wireless Personal Communications*, vol. 114, no. 2, pp. 1825–1831, sep 2020.

[207] Y. Jin, J. Zhang, B. Ai, and X. Zhang, "Channel Estimation for mmWave Massive MIMO with Convolutional Blind Denoising Network," *IEEE Communications Letters*, vol. 24, no. 1, pp. 95–98, jan 2020.

[208] Y. Jin, J. Zhang, S. Jin, and B. Ai, "Channel Estimation for Cell-Free mmWave Massive MIMO through Deep Learning," *IEEE Transactions on Vehicular Technology*, vol. 68, no. 10, pp. 10 325–10 329, oct 2019.

[209] E. Björnson and P. Giselsson, "Two Applications of Deep Learning in the Physical Layer of Communication Systems [Lecture Notes]," *IEEE Signal Processing Magazine*, vol. 37, no. 5, pp. 134–140, sep 2020.

[210] J. Zhang, J. Zhang, E. Björnson, and B. Ai, "Local Partial Zero-Forcing Combining for Cell-Free Massive MIMO Systems," *IEEE Transactions on Communications*, vol. 69, no. 12, pp. 8459–8473, 2021.

[211] D. Maryopi, M. Bashar, and A. G. Burr, "On the Uplink Throughput of Zero Forcing in Cell-Free Massive MIMO With Coarse Quantization," *IEEE Transactions on Vehicular Technology*, vol. 68, no. 7, pp. 7220–7224, jul 2019.

[212] R. Van Rompaey and M. Moonen, "Distributed adaptive node-specific signal estimation in a wireless sensor network with partial prior knowledge of the desired source steering matrix," *IEEE Transactions on Signal and Information Processing over Networks*, vol. 7, pp. 478–492, jul 2021.

[213] R. Zhang and J. T. Kwok, "Asynchronous distributed ADMM for consensus optimization," in *2014 31st International Conference on Machine Learning (ICML)*, 2014, pp. 3689–3697.

[214] Z. Wang, Y. Mou, and L. Vandendorpe, "ADMM-based Subcarrier Allocation and Power Control for Uplink OFDMA Channels," in *2019 IEEE Wireless Communications and Networking Conference (WCNC)*, 2019, pp. 1–7.

[215] C. Shen, T. H. Chang, K. Y. Wang, Z. Qiu, and C. Y. Chi, "Distributed robust multicell coordinated beamforming with imperfect CSI: An ADMM approach," *IEEE Transactions on Signal Processing*, vol. 60, no. 6, pp. 2988–3003, jun 2012.

[216] G. Zhang and R. Heusdens, "Distributed Optimization Using the Primal-Dual Method of Multipliers," *IEEE Transactions on Signal and Information Processing over Networks*, vol. 4, no. 1, pp. 173–187, 2018.

[217] M. Boldi, A. Tölli, M. Olsson, E. Hardouin, T. Svensson, F. Boccardi, L. Thiele, and V. Jungnickel, "Coordinated MultiPoint (CoMP) Systems," *Mobile and Wireless Communications for IMT-Advanced and Beyond*, pp. 121–155, aug 2011.

[218] H. V. Balan, R. Rogalin, A. Michaloliakos, K. Psounis, and G. Caire, "AirSync: Enabling distributed multiuser MIMO with full spatial multiplexing," *IEEE/ACM Transactions on Networking*, vol. 21, no. 6, pp. 1681–1695, dec 2013.

[219] D. Wang, C. Zhang, Y. Du, J. Zhao, M. Jiang, and X. You, "Implementation of a Cloud-Based Cell-Free Distributed Massive MIMO System," *IEEE Communications Magazine*, vol. 58, no. 8, pp. 61–67, aug 2020.

[220] M. H. Bahari, A. Bertrand, and M. Moonen, "Blind sampling rate offset estimation for wireless acoustic sensor networks through weighted least-squares coherence drift estimation," *IEEE/ACM Transactions on Audio, Speech and Language Processing*, vol. 25, no. 3, pp. 674–686, 2017.

[221] A. Chinaev, G. Enzner, T. Gburrek, and J. Schmalenstroeer, "Online Estimation of Sampling Rate Offsets in Wireless Acoustic Sensor Networks with Packet Loss," *2021 29th European Signal Processing Conference (EUSIPCO)*, pp. 1110–1114, 2021.

[222] T. Gburrek, J. Schmalenstroeer, and R. Haeb-Umbach, "On Synchronization of Wireless Acoustic Sensor Networks in the Presence of Time-Varying Sampling Rate Offsets and Speaker Changes," in *2022 IEEE International Conference on Acoustics, Speech and Signal Processing (ICASSP)*, 2022, pp. 916–920.

[223] A. Chinaev, P. Thüne, and G. Enzner, "Double-Cross-Correlation Processing for Blind Sampling-Rate and Time-Offset Estimation," *IEEE/ACM Transactions on Audio, Speech and Language Processing*, vol. 29, pp. 1881–1896, 2021.

[224] B. Sundararaman, U. Buy, and A. D. Kshemkalyani, "Clock synchronization for wireless sensor networks: a survey," *Ad Hoc Networks*, vol. 3, no. 3, pp. 281–323, may 2005.

[225] K. Skiadopoulos, A. Tsipis, K. Giannakis, G. Koufoudakis, E. Christopoulou, K. Oikonomou, G. Kormentzas, and I. Stavrakakis, "Synchronization of data measurements in wireless sensor networks for IoT applications," *Ad Hoc Networks*, vol. 89, pp. 47–57, jun 2019.

[226] S. Niknam, H. S. Dhillon, and J. H. Reed, "Federated Learning for Wireless Communications: Motivation, Opportunities, and Challenges," *IEEE Communications Magazine*, vol. 58, no. 6, pp. 46–51, jun 2020.

[227] T. T. Vu, D. T. Ngo, N. H. Tran, H. Q. Ngo, M. N. Dao, and R. H. Middleton, "Cell-Free Massive MIMO for Wireless Federated Learning," *IEEE Transactions on Wireless Communications*, vol. 19, no. 10, pp. 6377–6392, oct 2020.

[228] Y. Zeng and R. C. Hendriks, "Distributed estimation of the inverse of the correlation matrix for privacy preserving beamforming," *Signal Processing*, vol. 107, pp. 109–122, feb 2015.

[229] R. C. Hendriks, Z. Erkin, and T. Gerkmann, "Privacy-preserving distributed speech enhancement forwireless sensor networks by processing in the encrypted domain," *2013 IEEE International Conference on Acoustics, Speech and Signal Processing (ICASSP)*, pp. 7005–7009, 2013.

[230] A. S. Behbahani, A. M. Eltawil, and H. Jafarkhani, "Linear Decentralized Estimation of Correlated Data for Power-Constrained Wireless Sensor Networks," *IEEE Transactions on Signal Processing*, vol. 60, no. 11, pp. 6003–6016, 2012.

[231] A. Hassani and M. Moonen, "Cooperative integrated noise reduction and node-specific direction-of-arrival estimation in a fully connected wireless acoustic sensor network," *Signal Processing*, vol. 107, pp. 68–81, feb 2015.

[232] J. R. Magnus, "On Differentiating Eigenvalues and Eigenvectors," *Econometric Theory*, vol. 1, no. 2, pp. 179–191, 1985.

[233] A. Hjørungnes and D. Gesbert, "Complex-valued matrix differentiation: Techniques and Key results," *IEEE Transactions on Signal Processing*, vol. 55, no. 6 I, pp. 2740–2746, jun 2007.

[234] A.-J. van der Veen, "Joint diagonalization via subspace fitting techniques," in *2001 IEEE International Conference on Acoustics, Speech, and Signal Processing (ICASSP)*. IEEE, 2001, pp. 2773–2776.

[235] A. Ziehe, P. Laskov, G. Nolte, and K.-R. Müller, "A Fast Algorithm for Joint Diagonalization with Non-orthogonal Transformations and its Application to Blind Source Separation," *Journal of Machine Learning Research*, vol. 5, pp. 777–800, 2004.

[236] A. Hassani, A. Bertrand, and M. Moonen, "Distributed signal subspace estimation based on local generalized eigenvector matrix inversion," in *2015 23rd European Signal Processing Conference (EUSIPCO)*, 2015, pp. 1386–1390.

[237] F. Rusek, D. Persson, B. K. Lau, E. G. Larsson, T. L. Marzetta, O. Edfors, and F. Tufvesson, "Scaling up MIMO : Opportunities and challenges with very large arrays," *IEEE Signal Processing Magazine*, vol. 30, no. 1, pp. 40–60, 2013.

[238] I. Viering, H. Hofstetter, and W. Utschick, "Spatial Long-term Variantions in Urban, Rural and Indoor Enviroments," in *Proceedings of the 5th Meeting of COST*, 2002, pp. 1–9.

[239] O. Ledoit and M. Wolf, "A well-conditioned estimator for large-dimensional covariance matrices," *Journal of Multivariate Analysis*, vol. 88, no. 2, pp. 365–411, 2004.

[240] A. Adhikary, J. Nam, J. Y. Ahn, and G. Caire, "Joint spatial division and multiplexing-The large-scale array regime," *IEEE Transactions on Information Theory*, vol. 59, no. 10, pp. 6441–6463, 2013.

Curriculum Vitae



Robbe Van Rompaey was born in Bonheiden, Belgium, in 1994. He received the M.Sc. degree in electrical engineering from KU Leuven, Leuven, Belgium, in 2017 (magna cum laude), where he pursued the Ph.D. degree with the Electrical Engineering Department, under the supervision of Prof. M. Moonen. He is a Fellow of the Research Foundation – Flanders (FWO) and was also involved in a joint project with KU Leuven and Nokia Bell Labs, Antwerp, Belgium.

His research interests include multi-channel signal processing, wireless sensor networks, distributed optimization and distributed signal processing with application in speech/audio processing and MIMO communications.

List of publications

International Journal Papers

1. **Van Rompaey, R.**, Moonen, M., "Distributed MMSE-Based Uplink Receive Combining, Downlink Transmit Precoding and Optimal Power Allocation in Cell-Free Massive MIMO Systems", accepted for publication in EURASIP Journal on Wireless Communications and Networking.
2. **Van Rompaey, R.**, Moonen, M., "Distributed Adaptive Signal Estimation in Wireless Sensor Networks with Partial Prior Knowledge of the Desired Sources Steering Matrix", IEEE Transactions on Signal and Information Processing over Networks, vol. 7, 2021, pp. 478-492.

Journal Papers submitted for publication

1. **Van Rompaey, R.**, Moonen, M., "Distributed Combined Channel Estimation and Optimal Uplink Receive Combining for User-centric Cell-free Massive MIMO systems", submitted for publication.

International Conference Papers

1. **Van Rompaey, R.**, Moonen, M., "GEVD-based Low-Rank Channel Covariance Matrix Estimation and MMSE Channel Estimation for Uplink Cellular Massive MIMO Systems", Proceedings of 2020 30th European Signal Processing Conference (EUSIPCO), Belgrade, Serbia, 2022, pp. 1-5.
2. **Van Rompaey, R.**, Moonen, M., "Sound Zoning in an Ad-hoc Wireless Acoustic Sensor and Actuator Network", Proceedings of 2021 29th

European Signal Processing Conference (EUSIPCO), Dublin, Ireland, 2021, pp. 101-105.

3. **Van Rompaey, R.**, Moonen, M., "Scalable and Distributed MMSE algorithms for Uplink Receive Combining in Cell-free Massive MIMO Systems", Proceedings of 2021 IEEE International Conference on Acoustics, Speech and Signal Processing (ICASSP), Toronto, Canada, 2021, pp. 4445-4449.

4. **Van Rompaey, R.**, Moonen, M., "Distributed Adaptive Acoustic Contrast Control for Node-specific Sound Zoning in a Wireless Acoustic Sensor and Actuator Network", Proceedings of 2020 28th European Signal Processing Conference (EUSIPCO), Amsterdam, The Netherlands, 2021, pp. 481-485.

5. **Van Rompaey, R.**, Moonen, M., "Distributed Adaptive Node-specific signal estimation in a wireless sensor network with partial prior knowledge of the desired source steering vector", Proceedings of 2019 27th European Signal Processing Conference (EUSIPCO), A Coruna, Spain, 2019, pp. 1-5.

6. **Van Rompaey R.**, Moonen M., "GEVD Based Speech and Noise Correlation Matrix Estimation for Multichannel Wiener Filter Based Noise Reduction", Proceedings of 2018 26th European Signal Processing Conference (EUSIPCO), Rome, Italy, 2018, pp. 2544-2548.



FACULTY OF ENGINEERING SCIENCE
DEPARTMENT OF ELECTRICAL ENGINEERING
Stadius Center for Dynamical Systems,
Signal Processing and Data Analytics
Kasteelpark Arenberg 10, bus 2446
B-3001 Leuven
robbe.vanrompaey@esat.kuleuven.be